On optimal control simulations for mechanical systems

vom Fachbereich Maschinenbau und Verfahrenstechnik
der Technischen Universität Kaiserslautern
zur Verleihung der venia legendi für das Fach
Mechanik
angenommene Habilitationsschrift

von
Dr.-Ing. Sigrid Leyendecker
aus Kaiserslautern

Referenten	Prof. Dr.-Ing. R. Müller
	Prof. Dr.-Ing. P. Betsch
	Prof. Dr. M. Ortiz
Tag der Einreichung	30. August 2010
Vollzug des Habilitationsverfahrens	12. Januar 2011

Kaiserslautern, September 2011

D 386

Herausgeber

Lehrstuhl für Technische Mechanik
Technische Universität Kaiserslautern
Gottlieb-Daimler-Strasse
Postfach 3049
67653 Kaiserslautern

Ich danke der “Prof. Dr. Hans Georg und Liselotte Hahn Stiftung” für die finanzielle Unterstützung bei der Drucklegung.

Druck

Technische Universität Kaiserslautern
ZBT – Abteilung Foto-Repro-Druck

ISBN-Nr. 978-3-942695-04-6

Preface

The research presented in this thesis has been carried out during the period 2006-2010, first being a Feodor Lynen postdoctoral scholar of the Alexander von Humboldt-Foundation (AvH) for two years in Control and Dynamical Systems and the Computational Solid Mechanics Group at the California Institute of Technology, then during six months as a substitute professor of the Berlin Mathematical School (BMS) at the Free University of Berlin and finally being the head of Independent Junior Research Group Computational Dynamics and Control in the Emmy Noether Programme of the Deutsche Forschungsgemeinschaft (DFG, LE 1841/2-1) at the Technical University of Kaiserslautern. All support is gratefully acknowledged.

My sincere gratefulness is dedicated to the late Professor Jerry Marsden for the invaluable guidance and inspiration I was allowed to receive. I am especially thankful to Professor Ralf Müller, Professor Peter Betsch and Professor Michael Ortiz for accepting to be referees and for their constant support, many valuable remarks and inspiring discussions.

The exceptionally pleasant and open working atmospheres at Caltech, FU Berlin and TU Kaiserslautern have had a great impact on the motivation for the present work, wherefore all colleagues are sincerely thanked. In particular I would like to thank Sina Ober-Blöbaum for being part of the dream-team, my collaborators Carsten Hartmann, Gwen Johnson, Eva Kanso, Joachim Linn, Lenny Lucas, Houman Owhadi, David Pekarek, Bernd Schmidt and the members of the Emmy Noether Group Ramona Maas, Michael Koch and Pascal Jung.

Most of all I would like to express my deep gratitude to my family, friends and Manus for the strong support and continuous encouragement I enjoyed.

Kaiserslautern, Januar 2011 Sigrid Leyendecker

Abstract

The primary objective of this work is the development of robust, accurate and efficient simulation methods for the optimal control of mechanical systems, in particular of constrained mechanical systems as they appear in the context of multibody dynamics. The focus is on the development of new numerical methods that meet the demand of structure preservation, i.e. the approximate numerical solution inherits certain characteristic properties from the real dynamical process.

This task includes three main challenges. First of all, a kinematic description of multibody systems is required that treats rigid bodies and spatially discretised elastic structures in a uniform way and takes their interconnection by joints into account. This kinematic description must not be subject to singularities when the system performs large nonlinear dynamics. Here, a holonomically constrained formulation that completely circumvents the use of rotational parameters has proved to perform very well. The arising constrained equations of motion are suitable for an easy temporal discretisation in a structure preserving way. In the temporal discrete setting, the equations can be reduced to minimal dimension by elimination of the constraint forces. Structure preserving integration is the second important ingredient. Computational methods that are designed to inherit system specific characteristics – like consistency in energy, momentum maps or symplecticity – often show superior numerical performance regarding stability and accuracy compared to standard methods. In addition to that, they provide a more meaningful picture of the behaviour of the systems they approximate. The third step is to take the previously addressed points into the context of optimal control, where differential equation and inequality constrained optimisation problems with boundary values arise. To obtain meaningful results from optimal control simulations, wherein energy expenditure or the control effort of a motion are often part of the optimisation goal, it is crucial to approximate the underlying dynamics in a structure preserving way, i.e. in a way that does not numerically, thus artificially, dissipate energy and in which momentum maps change only and exactly according to the applied loads.

The excellent numerical performance of the newly developed simulation method for optimal control problems is demonstrated by various examples dealing with robotic systems and a biomotion problem. Furthermore, the method is extended to uncertain systems where the goal is to minimise a probability of failure upper bound and to problems with contacts arising for example in bipedal walking.

Zusammenfassung

Ziel der vorliegenden Arbeit ist die Bereitstellung von stabilen, genauen und effizienten Simulationsmethoden für Optimalsteuerungsprobleme in der Mechanik. Insbesondere werden mechanische Systeme mit Zwangsbedingungen, wie sie zum Beispiel in der Mehrkörperdynamik vorkommen, betrachtet. Ein besonderer Anspruch an die neu entwickelten numerischen Methoden ist die so genannte Strukturerhaltung, d.h. die Vererbung spezieller charakteristischer Eigenschaften des tatsächlichen dynamischen Prozesses an die numerische Approximation der Lösung.

Diese Aufgabe beinhaltet drei hauptsächliche Herausforderungen. Zum einen wird eine kinematische Beschreibung der Mehrkörpersysteme gebraucht, die starre Körper sowie räumlich diskretisierte elastische Strukturen gleichermaßen behandeln und deren Verbindung durch Gelenke mit einbeziehen kann. Diese kinematische Beschreibung darf auch bei großen, nichtlinearen dynamischen Bewegungen keine Singularitäten aufweisen. Hier hat sich eine Beschreibung mit holonomen Zwangsbedingungen bewährt, die Rotationsparameter komplett vermeidet. Die daraus entstehenden Bewegungsgleichungen mit Zwangsbedingungen sind besonders gut für eine einfache strukturerhaltende Zeitdiskretisierung geeignet. Durch Elimination der Zwangskräfte im zeitlich Diskreten kann das Gleichungssystem auf minimale Dimension reduziert werden. Die strukturerhaltende Zeitdiskretisierung ist der zweite wichtige Bestandteil. Numerische Methoden, welche die strukturellen Charakteristika des dynamischen Systems – wie Konsistenz von Energie, Impulsabbildungen und Symplektizität – erben, zeigen im Bezug auf Stabilität und Genauigkeit oft ein wesentlich besseres Verhalten als Standardmethoden. Außerdem liefern sie aussagekräftigere Simulationsergebnisse. Der dritte Schritt setzt die bisher angesprochenen Punkte in Zusammenhang mit Optimalsteuerungsproblemen, in denen Differentialgleichungen und Ungleichungsbedingungen ein Optimierungsproblem mit Randbedingungen restringieren. Bei der Simulation von Optimalsteuerungsproblemen werden oft Energieaufwand oder Steuerungskosten optimiert. Um aussagekräftige Resultate zu erhalten, ist es entscheidend, die zu Grunde liegende Dynamik strukturerhaltend zu approximieren, d.h. in einer Art und Weise, in der nicht numerisch, und damit künstlich, Energie dissipiert wird und in der sich Impulsabbildungen nur und exakt auf Grund der aufgebrachten Lasten ändern.

Die hervorragenden Eigenschaften der neu entwickelten Simulationsverfahren für Optimalsteuerungsprobleme werden anhand von zahlreichen numerischen Beispielen aus dem Bereich der Robotik und biomechanischen Bewegungsproblemen demonstriert. Außerdem wird die Methode für Systeme mit Unsicherheiten erweitert, mit dem Ziel, eine obere Schranke für die Fehlerwahrscheinlichkeit zu minimieren, sowie auf Kontaktprobleme, die zum Beispiel beim zweibeinigen Gehen vorkommen.

Contents

1 Introduction

When planning or predicting motion of mechanical systems, one can pursue quite different strategies, see Figure 1.1. One can rely purely on kinematic considerations, e.g. by capturing motion with a camera or by simply prescribing certain desired positions for the motion. In particular, one could request the end-effector of a robot to stay on a prescribed path, or the hand or feet of an animated character to have certain positions. This information is used as input for inverse kinematics, where a trajectory meeting the prescribed conditions is reconstructed, see e.g. [Zhao 94, Simo 07, Shin 01]. If closed form solutions are not feasible, numerical approaches like least square fits are used to minimise the difference between the desired and possible trajectories (see e.g. [Tola 00] for an overview). This procedure is illustrated in the left branch of the diagram in Figure 1.1. However, thereby no forcing or dynamics is taken into account.

If one is interested in the forces (or controls) that cause real dynamics, then one is faced with a control problem. When the complete trajectory is prescribed – e.g. from a previous inverse kinematic consideration – it is the input for inverse dynamics, whereby the equations of motion are solved for the right hand side, the necessary forces implying this particular motion, see e.g. [Stry 98, Blaj 03, Blaj 07, Nagu 90, Acke 07]. This is in contrast to forward dynamic simulations, where the trajectory in response to the forces is determined. When only certain positions or parts of the trajectory are prescribed, these can be included into the equations of motion as rheonomic, i.e. time dependent, constraints, see e.g. [Bets 07, Uhla 09, Blaj 04, De S 06, Ast 06]. In this case, no optimality criterion is imposed and the force and state trajectories are obtained by forward constrained dynamic simulation.

Dynamic optimisation predicts both the state as well as the force trajectory such that the equations of motion are fulfilled, while at the same time, an objective functional (representing e.g. the required energy or time) is optimised. This procedure is more general than the previously described approaches and can be formulated independent of experimental data. When it is used for optimal control, it yields the optimal force and state trajectory for a particular system, see e.g. [Bull 04, Sten 94, Allg 99, Bind 01, Momb 05, Momb 10, Gerd 08a, Gerd 08b, Gerd 09]. A more detailed overview on literature about specific solution methods for optimal control problems is given in Section 2.3. Dynamic optimisation can also be used for trend optimisation, where the design of dynamics is optimised. Assuming that certain parameters in the model have fixed values, the corresponding best possible motion – in the sense of extremising an objective functional – can be determined. This procedure is also called estimation see e.g. [Sten 94, Bind 01, Allg 99] and the references cited therein.

For the optimal control simulations of mechanical systems in this work, dynamic optimi-

sation methods in the form of optimal control, i.e. the very right branch in Figure 1.1, is used.

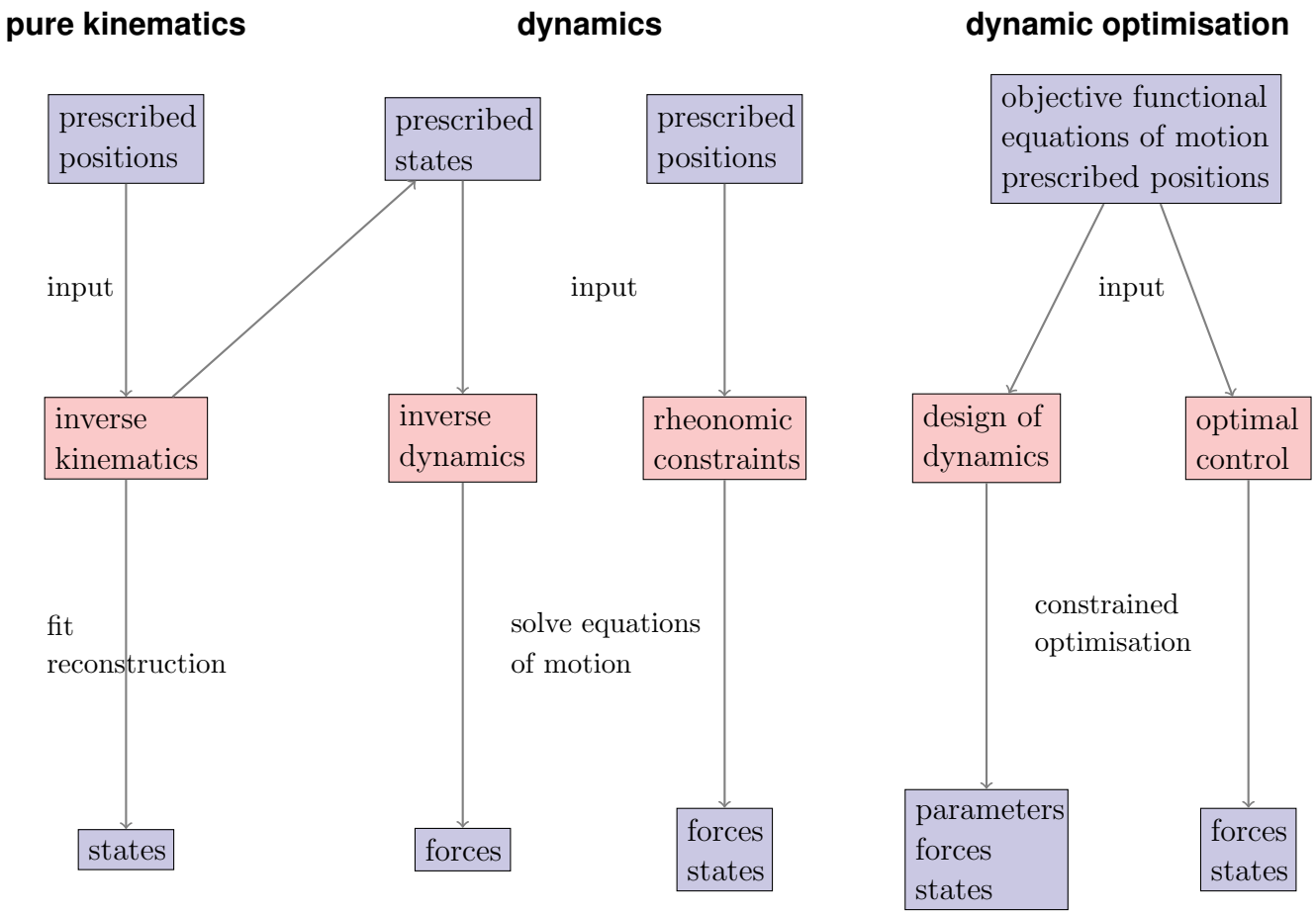

Figure 1.1: Overview over different motion planning strategies.

Simulation techniques for optimal control tasks of mechanical systems are investigated in this work. The focus is on the development of new numerical methods that meet the demand of structure preservation, i.e. the approximate numerical solution inherits certain characteristic properties from the real dynamical process.

Computational methods that are designed to inherit system specific characteristics often show superior numerical performance regarding stability and accuracy compared to standard methods. In addition to that, they provide a more meaningful picture of the behaviour of the systems they approximate. In the last two decades, a lot of research has been devoted to structure preserving time stepping schemes, like e.g. variational integrators in space and time (see e.g. [Lew 03a, Lew 04, Reic 94, Mars 99, Mars 98, Mars 01]), energy-momentum schemes (see e.g. [Gros 09, Uhla 10, Rome 09, Bets 00a, Bets 00b, Bets 01a, Ibra 99, Ibra 02, Arme 01, Cris 96, Gonz 00, Hugh 78, LaBu 76a, LaBu 76b, Noel 04, Reic 95, Simo 91a, Simo 91b, Simo 92, Simo 94, Simo 95]), symplectic-momentum schemes (see e.g. [Bart 98, Hair 04, Jay 96, Leim 94, Leim 96]) or Lie group integrators (see e.g. [Cell 03, Ge 88, McLa 93, Toum 94]). Their extension to the optimal control regime is

both challenging and promising.

While the research documented in the PhD-thesis [Leye 06a] restricts itself to the simulation of initial value problems in flexible multibody dynamics using energy-momentum conserving forward integration methods, the class of problems considered in this work is far more general. It consists of boundary value problems for which an optimal solution (with respect to an objective functional) needs to be approximated in a structure preserving way. The considered multibody systems consist of rigid and flexible parts that are interconnected by joints giving rise to holonomic constraints in the equations of motion. On the one hand, typical applications are all kinds of robot manipulators including industrial manufacturing robots or conveying machinery, as well as deployable structures such as space satellites. On the other hand, such multibody systems can also be used to model (parts of) the human body such that biomechanical problems of human motion like human gait, grasping processes or athletic motion in sports can be addressed. Furthermore, optimal control processes may support the development of prostheses and implants in modern medical surgery.

The simulation of forward dynamics of multibody systems combines several issues. First of all, flexible parts must be discretised in space and a material model for their (elastic) behaviour has to be identified. Secondly, the interconnections have to be taken into account. Typically they give rise to constraints restricting the possible states of the system. The choice of a method to enforce the constraints completes the formulation of the evolution equations and side conditions in the mathematical model. Finally, these semi-discrete equations have to be discretised in time resulting in forward time integration algorithms. An extensive introduction to these topics including a summary of the state of the art literature has been given in [Leye 06a]. An overview on existing simulation techniques for optimal control problems is given in Section 2.3, where also relevant literature is mentioned and the proposed approach to simulate optimal control problems for constrained mechanical systems is classified within the framework of existing methods.

1.1 Main issues and outline of this work

The primary object of this work is the development of robust, accurate and efficient simulation methods for the optimal control of mechanical systems, in particular of constrained mechanical systems as they appear in the context of multibody dynamics. To this end, Chapter 2 places the considered optimal control problems in a general mathematical framework and revisits theoretical results on the existence of optimal solutions. In particular, necessary conditions for optimal solutions are presented together with numerical methods for the approximation of optimal solutions.

Chapter 3 extends the results of the PhD-thesis [Leye 06a] based on an energy-momentum conserving time stepping method to another class of structure preserving integrators, namely to the class of symplectic-momentum schemes based on variational integrators, see [Leye 08b]. A variational formulation of constrained dynamics is presented in the

continuous and in the discrete setting. The existing theory on variational integration of constrained problems is extended by aspects on the initialisation of simulations, the discrete Legendre transform and certain postprocessing steps. Furthermore, the discrete null space method which has been introduced in the framework of energy-momentum conserving integration of constrained systems is adapted to the framework of variational integrators. It eliminates the constraint forces (including the Lagrange multipliers) from the time stepping scheme and subsequently reduces its dimension to the minimum. While retaining the structure preserving properties of the specific integrator, the solution of the smaller dimensional system saves computational costs and does not suffer from conditioning problems. The performance of the variational discrete null space method is illustrated by numerical examples dealing with mass point systems, a closed kinematic chain of rigid bodies and flexible multibody dynamics. The solutions are compared to those obtained by an energy-momentum scheme.

A convergence result for variational integration of constrained systems is shown in Chapter 4 by means of an analytical proof and of illustrating numerical examples, see [Schm 09]. For a physical system described by a motion in an energy landscape under holonomic constraints, we study the Γ-convergence of variational integrators to the corresponding continuum action functional and the convergence properties of solutions of the discrete Euler-Lagrange equations to stationary points of the continuum problem. This extends the results in [Mull 04] to constrained systems. The analytical convergence result (which has been proofed by Bernd Schmidt in [Schm 09]) is illustrated with numerical examples of mass point systems and flexible multibody dynamics.

The most important piece of work, the contribution which takes all previously addressed structure preserving simulations of forward dynamical processes into a completely different problem setting, namely that of optimal control, where differential equation and inequality constrained optimisation problems with boundary values arise, is presented in Chapter 5, see [Leye 09b]. The equations of motion of a controlled mechanical system subject to holonomic constraints may be formulated in terms of the states and controls by applying a constrained version of the Lagrange-d'Alembert principle. This chapter derives a structure preserving scheme for the optimal control of such systems using, as one of the key ingredients, a discrete analogue of that principle. This property is inherited when the system is reduced to its minimal dimension by the discrete null space method. Together with initial and final conditions on the configuration and conjugate momentum, the reduced discrete equations serve as nonlinear equality constraints for the minimisation of a given objective functional. The algorithm yields a sequence of discrete configurations together with a sequence of actuating forces, optimally guiding the system from the initial to the desired final state. In particular, for the optimal control of multibody systems, a force formulation consistent with the joint constraints is introduced. This enables one to prove the consistency of the evolution of momentum maps. Using a two-link pendulum, the method is compared to existing methods. Further, it is applied to a satellite reorientation manoeuvre and a biomotion problem.

In Chapter 6, uncertainty is added into the picture. We present an optimal control

methodology, which we refer to as concentration-of-measure optimal control (COMOC), that seeks to minimise a concentration-of-measure upper bound on the probability of failure of a system, see [Leye 10]. The systems under consideration are characterised by a single performance measure that depends on random inputs through a known response function. For these systems, a concentration-of-measure upper bound on the probability of failure of a system can be formulated in terms of the mean performance measure and a system diameter that measures the uncertainty in the operation of the system. COMOC then seeks to determine optimal controls that maximise the confidence in the safe operation of the system, defined as the ratio of design margin, measured by the difference between the mean performance and the design threshold, to the system uncertainty, measured by the system diameter. This strategy has been assessed in the case of a robot-arm manoeuvre for which the performance measure of interest is assumed to be the placement accuracy of the arm tip. The ability of COMOC to significantly increase design confidence in that particular example of application is demonstrated.

The discrete mechanics approach to the computation of static equilibria for Cosserat rods in Chapter 7 constitutes an exception in this thesis, in the sense that it is the only contribution that does not consider dynamical problems but static equilibria, see [Jung 10]. However, work that addresses the multisymplectic discretisation of the partial differential equations arising in Cosserat beam dynamics is in progress. A theory of discrete Cosserat rods is formulated in the language of discrete Lagrangian mechanics. By exploiting Kirchhoff's kinetic analogy, the potential energy density of a rod is a function on the tangent bundle of the configuration manifold and thus formally corresponds to the Lagrangian function of a dynamical system. The equilibrium equations are derived from a variational principle using a formulation that involves null space matrices. In this formulation, no Lagrange multipliers are necessary to enforce orthonormality of the directors. Noether's theorem relates first integrals of the equilibrium equations to Lie group actions on the configuration bundle, so called symmetries. The symmetries relevant for rod mechanics are frame-indifference, isotropy and uniformity. We show that a completely analogous and self-contained theory of discrete rods can be formulated in which the arc-length is a discrete variable *ab initio*. In this formulation, the potential energy density is defined directly on pairs of points along the arc-length of the rod, in analogy to Veselov's discrete reformulation of Lagrangian mechanics. A discrete version of Noether's theorem then identifies exact first integrals of the discrete equilibrium equations. These exact conservation properties confer the discrete solutions accuracy and robustness, as demonstrated by selected examples of application.

A particular optimal control problem is investigated in Chapter 8, namely that of bipedal walking, see [Leye 09c]. This adds the treatment of contact (between the foot and the ground) to the problem setting. This work considers the optimal control of a bipedal compass gait by modelling the double stance configuration as a transfer of contact constraints between the feet and the ground. A structure preserving simulation method is developed for this context and applied to a periodic gait.

2 Optimal control

2.1 Optimal control theory

The theory of optimal control problems can be examined on quite different levels of mathematical abstraction. The following chapter intends to present an existence result and necessary conditions for optimal solutions in a form that covers the case relevant for this thesis. These results are related to the formulation of optimal control problems for mechanical systems. Most of the presented results can be found in [Hinz 09] but also [Wirt 10, Ober 08] and [Gerd 10] have been consulted extensively. Background on the functional analytical aspects can be found e.g. in [Heus 92, Yosi 06].

Consider the following nonlinear optimal control problem.

Problem 2.1.1 (Optimal control problem)

$$\min_{(y,u)\in Y\times U} J(y,u) \qquad \textit{subject to} \qquad e(y,u)=0, \qquad c(y)\in\mathcal{K}, \qquad u\in U_{ad}$$

where $(y,u)\in Y\times U$ are the state and control variable respectively, the objective functional $J: Y\times U\to\mathbb{R}$, the state equation $e: Y\times U\to Z$ and the state constraints $c: Y\to R$ are continuously Fréchet differentiable, Y, U, R, Z are Banach spaces, $\mathcal{K}\subset R$ is a closed convex cone and $U_{ad}\subset U$ is a non-empty closed convex set.

The optimal control Problem 2.1.1 is a special case of the more general optimisation problem $\min_{w\in W} J(w)$ subject to conditions on w, where one explicitly distinguishes between the state y and the control u in $w=(y,u)$, (where the continuously Fréchet differentiable objective functional $J: W\to\mathbb{R}$ is defined on a Banach space W).

Definition 2.1.2 *A point $(y,u)\in Y\times U$ is called feasible or admissible, if it belongs to the admissible set*

$$F_{ad}=\{(y,u)\in Y\times U | c(y)\in\mathcal{K}, u\in U_{ad}\}$$

The following theorem states the existence of optimal solutions for the case of linear state constraints, i.e. instead of $c(y)\in\mathcal{K}$, here $y\in Y_{ad}$ is requested (see Theorem 1.45 in [Hinz 09] and its proof).

Theorem 2.1.3 (Existence of an optimal solution) *Let $R=Y$ and let $c: Y\to Y$ be the identity, let $\mathcal{K}=Y_{ad}\subset Y$ and let U, Y be reflexive. Further, assume that*

1. *$U_{ad}\subset U$ is convex, bounded and closed.*
2. *$Y_{ad}\subset Y$ is convex and closed, such that Problem (2.1.1) has a feasible point.*

3. *the state equation $e(y,u) \in Z$ has a bounded solution operator $u \in U_{ad} \mapsto y(u) \in Y$.*

4. *$(y,u) \in Y \times U \mapsto e(y,u) \in Z$ is continuous under weak convergence.*

5. *J is sequentially weakly lower semicontinuous.*

Then Problem 2.1.1 has an optimal solution $(\bar{y}, \bar{u})$.

In the case of general nonlinear state constraints $c(y) \in \mathcal{K}$, Robinson's regularity condition

$$0 \in \operatorname{int}\left(\begin{bmatrix} 0 \\ c(\bar{y}) \end{bmatrix} + \begin{bmatrix} e_y(\bar{y},\bar{u}) & e_u(\bar{y},\bar{u}) \\ c'(\bar{y}) & 0 \end{bmatrix} \begin{bmatrix} Y \\ U_{ad} - \bar{u} \end{bmatrix} - \begin{bmatrix} 0 \\ \mathcal{K} \end{bmatrix} \right) \tag{2.1}$$

has to be fulfilled for a feasible point $(\bar{y}, \bar{u})$ to enable the derivation of necessary conditions for an optimal solution. Here, $\operatorname{int}(M)$ denotes the interior of a set M, $c'(y)$ is the Jacobian matrix of c at y, and e_y and e_u denote the matrices of partial derivatives with respect to the components of y and u, respectively.
The following necessary conditions for an optimal solution of Problem 2.1.1 are formulated as a special case of Theorem 1.56 in [Hinz 09], where also a proof can be found.

Theorem 2.1.4 (Necessary optimality conditions) *Let the Lagrangian function $J^\star : Y \times U \times Z^* \times R^* \to \mathbb{R}$ be given by*

$$J^\star(y,u,\lambda,\mu) = J(y,u) + \langle \gamma, e(y,u) \rangle_{Z^*,Z} + \langle \mu, c(y) \rangle_{R^*,R} \tag{2.2}$$

where $\langle \cdot, \cdot \rangle_{V^*,V}$ denotes the pairing between a space V and its dual V^*. For any local solution $(\bar{y}, \bar{u})$ of the optimal control Problem 2.1.1 at which Robinson's regularity condition (2.1) *is fulfilled, the following optimality conditions hold. There exists a Lagrange multiplier $\bar{\vartheta} = (\bar{\gamma}, \bar{\mu}) \in Z^* \times R^*$ with*

$$\begin{aligned} & e(\bar{y},\bar{u}) = 0, && c(\bar{y}) \in \mathcal{K}, \\ & \langle \bar{\mu}, v \rangle_{R^*,R} \le 0 \quad \forall v \in \mathcal{K}, && \langle \bar{\mu}, c(\bar{y}) \rangle_{R^*,R} = 0, \\ & \langle J^\star_y(\bar{y},\bar{u},\bar{\gamma},\bar{\mu}), y - \bar{y} \rangle_{Y^*,Y} \ge 0 \quad \forall y \in Y, \\ & \langle J^\star_u(\bar{y},\bar{u},\bar{\gamma},\bar{\mu}), u - \bar{u} \rangle_{U^*,U} \ge 0 \quad \forall u \in U_{ad}, \quad \bar{u} \in U_{ad} \end{aligned} \tag{2.3}$$

The necessary conditions for $(\bar{y}, \bar{u})$ to be an optimal solution of the optimal control Problem 2.1.1 consist of the state and constraint equations $(2.3)_1$, the complementarity conditions $(2.3)_2$, the adjoint equations $(2.3)_3$ and the optimality conditions $(2.3)_4$. They are known as minimum or maximum principles and fall in the general class of variational principles. If the underlying Banach spaces are finite dimensional, they are called Karush-Kuhn-Tucker conditions. The Lagrange multiplier ϑ is called costate or adjoint variable of the system. The question whether a local optimal solution is also globally optimal depends on the convexity of the admissible set and on convexity of all functions in Problem 2.1.1. Furthermore, stating sufficient conditions for local solutions is an actual research topic, see e.g. [Gerd 10] for details and references.

Remark 2.1.5 *Without the state constraint $c(y) \in \mathcal{K}$ (i.e. $c(y) = y, R = Y, \mathcal{K} = Y$, the constraint is trivial and therefore $\bar{\mu} = 0$), the necessary optimality conditions read*

$$\begin{aligned} & e(\bar{y}, \bar{u}) = 0, \\ & J_y^\star(\bar{y}, \bar{u}, \bar{\gamma}) = 0, \\ & \langle J_u^\star(\bar{y}, \bar{u}, \bar{\gamma}), u - \bar{u} \rangle_{U^*, U} \geq 0 \quad \forall u \in U_{ad}, \quad \bar{u} \in U_{ad} \end{aligned} \tag{2.4}$$

If further $U_{ad} = U$, then $(2.4)_3$ becomes

$$J_u^\star(\bar{y}, \bar{u}, \bar{\gamma}) = 0 \tag{2.5}$$

(Note that a slight abuse of notation is present here, since the same symbol $J^\star$ is used for the Lagrangian depending on three and on four independent variables.)

2.2 Optimal control of mechanical systems

Consider an n-dimensional mechanical system with the time dependent configuration vector $\boldsymbol{q}(t) \in Q$ and velocity vector $\dot{\boldsymbol{q}}(t) \in T_{\boldsymbol{q}(t)}Q$, where $t \in [t_0, t_N] \subset \mathbb{R}$ denotes the time, $n, N \in \mathbb{N}$, further $Q \subseteq \mathbb{R}^n$ is the configuration manifold and TQ its tangent bundle. See e.g. [Mars 94] for the differential geometric background on geometric mechanics. Denote the Lagrangian of the mechanical system by $L : TQ \to \mathbb{R}$. It usually represents the difference between kinetic and potential energy and must not be confused with the Lagrangian of the optimal control problem $J^\star$ defined in (2.2). Let the configuration be influenced by the non-conservative force field $\boldsymbol{f} \in T^*Q$. Then, the general Problem 2.1.1 reads for a mechanical system as follows.

Problem 2.2.1 (Mechanical optimal control problem) *Find $(\boldsymbol{q}, \dot{\boldsymbol{q}}) \in W^{1,\infty}([t_0, t_N], TQ)$ and $\boldsymbol{f} \in L^\infty([t_0, t_N], T^*Q)$ such that*

$$\min_{\boldsymbol{q}, \dot{\boldsymbol{q}}, \boldsymbol{f}} J(\boldsymbol{q}, \dot{\boldsymbol{q}}, \boldsymbol{f}) = \int_{t_0}^{t_N} B(\boldsymbol{q}, \dot{\boldsymbol{q}}, \boldsymbol{f})\, dt + \phi((\boldsymbol{q}(t_0), \dot{\boldsymbol{q}}(t_0)), (\boldsymbol{q}(t_N), \dot{\boldsymbol{q}}(t_N)))$$

subject to

$$\begin{aligned} & \frac{\partial L(\boldsymbol{q}, \dot{\boldsymbol{q}})}{\partial \boldsymbol{q}} - \frac{d}{dt}\left(\frac{\partial L(\boldsymbol{q}, \dot{\boldsymbol{q}})}{\partial \dot{\boldsymbol{q}}}\right) + \boldsymbol{f} = \boldsymbol{0} \\ & \boldsymbol{\psi}((\boldsymbol{q}(t_0), \dot{\boldsymbol{q}}(t_0)), (\boldsymbol{q}(t_N), \dot{\boldsymbol{q}}(t_N))) = \boldsymbol{0} \\ & \boldsymbol{c}(\boldsymbol{q}, \dot{\boldsymbol{q}}) \leq \boldsymbol{0} \\ & \boldsymbol{f} \in U_{ad} \subseteq T^*Q \end{aligned}$$

Here, $B(\boldsymbol{q}, \dot{\boldsymbol{q}}, \boldsymbol{f}) : TQ \times T^*Q \to \mathbb{R}$ is a given cost functional, $\phi : TQ \times TQ \to \mathbb{R}$ depends on the boundary values of the states, $\boldsymbol{\psi} : TQ \times TQ \to \mathbb{R}^{n_\psi}$ with $n_\psi \in \mathbb{N}$ fixes state boundary values and $\boldsymbol{c} : TQ \to \mathbb{R}^{n_c}$ with $n_c \in \mathbb{N}$ represents state constraints (also called path constraints).

Note that the problem as it is specified in Problem 2.2.1 with both $B \not\equiv 0$ and $\phi \not\equiv 0$ is in so called Bolza form. In Mayer form, $B \equiv 0$ and $\phi \not\equiv 0$. The optimal control problems

considered later in this work are of so called Lagrange form, i.e. $B \not\equiv 0$ and $\phi \equiv 0$.

For optimal control problems in Bolza form (not necessarily mechanical optimal control problems, where the state equation is given by the equations of motion as in Problem 2.2.1) without state constraints $\boldsymbol{c}$, the optimal solution can be associated with a saddle point of the Lagrangian $J^\star$ and the classical way to derive necessary optimality conditions is the Pontryagin maximum principle. Early works are due to [Pont 62, Isaa 65, Hest 66]. Necessary conditions for problems with state constraints are discussed in [Jaco 71, Krei 82], see also [Hart 95] for a survey, while the more general case of mixed state and control path constraints is treated in [Neus 76, Zeid 94]. See also [Gerd 10] for a more detailed survey of the literature on necessary conditions for optimal control problems.

2.2.1 Optimal control of constrained mechanical systems

In this thesis, we are mostly concerned with mechanical systems that are subject to holonomic constraints $\boldsymbol{g} : Q \to \mathbb{R}^m$ with $\boldsymbol{g}(\boldsymbol{q}) = \boldsymbol{0}$. This reduces the admissible set of states from TQ to TC where $C = \{\boldsymbol{q} \in Q | \boldsymbol{g}(\boldsymbol{q}) = \boldsymbol{0}\}$ is the constraint manifold. In this case, one could use the constrained equations of motion (5.3) as state equations and add the corresponding Lagrange multiplier $\boldsymbol{\lambda} \in \mathbb{R}^m$ to the unknown optimisation variables. Work on DAE constrained optimisation can be found e.g. in [Cerv 98, Pytl 99, Busk 00]. However, an elegant way that avoids the enlargement of the system is to use a null space matrix (see Chapters 3 and 5 for details on the null space method in the time continuous setting). Then, the state equations in Problem 2.2.1 consist of (3.7) and $(5.3)_2$ and the theory presented in Section 2.1 applies. The derivation of necessary conditions for state equations in terms of a reparametrisation of the redundant configuration and force, as proposed (3.8) in Chapter 3, is not discussed in this theoretical chapter, since we use a direct approach for the solution of the optimal control problems that circumvents the treatment of the necessary conditions in the time continuous case.

2.3 Simulation of optimal control problems

One distinguishes between two fundamentally different approaches to the numerical solution of optimal control problems, namely direct and indirect methods. Essentially, they differ in the point of time when the temporal discretisation takes place, see Figure 2.1 (which is a slightly modified version of Figure 1.3 in [Ober 08]). Both approaches are sketched briefly here, see [Bind 01, Ober 08, Gerd 10] for a more detailed introduction and references. In Section 2.3.3, the method developed in this work is classified within the framework of existing methods.

2.3.1 Indirect methods

Indirect methods are based on the numerical solution of the necessary conditions (2.3), i.e. they follow the steps 'first optimise, then discretise' represented on the very left branch in Figure 2.1. In general, this leads to a fully coupled system of discrete equations which has to be solved for the discrete states, controls and adjoints. However, depending on the

extent to which the state boundary values and the state and control constraints are specified, the necessary conditions might decouple to a certain degree which can be exploited for a more efficient numerical solution.

Consider the case of an optimal control problem for which the final state condition is not specified strongly (it might still appear weakly in the objective functional in the Mayer term) and no state and control constraints are present. In the mechanical optimal control Problem 2.2.1, this means that $\boldsymbol{\psi} = \boldsymbol{\psi}(\boldsymbol{q}(t_0), \dot{\boldsymbol{q}}(t_0))$ and $\boldsymbol{c}$ is trivial. In that particular case, the necessary conditions reduce to a multipoint boundary value problem where the state equations can be regarded as an initial value problem for the state variables and the adjoint equations as a final value problem for the adjoint variables. Furthermore, the objective functional is reformulated as a so called reduced objective functional $\hat{J}(u) = J(y(u), u)$ depending only on the controls (the dependence on the states is implicitly contained through the state equations $e(y, u)$ yielding $y = y(u)$). Then e.g. gradient methods (see e.g. [Cauc 47] and the survey paper [Cher 82]) can be used to iteratively improve an approximation of the reduced objective functional with respect to the controls, while in each iterations step, the multipoint boundary value problem is integrated forward for the states and backward for the controls, respectively. In order to avoid the expensive explicit computation of the gradient of the reduced objective function with respect to the controls (in the so called sensitivity approach), this is often paired with an adjoint approach. This circumvents the computation of the gradient of y with respect to u and with a BFGS approximation of the reduced objective function's Hessian in the iteration, see e.g. [Hinz 09]. On the other hand, multiple shooting and collocation methods can be used to solve the multipoint boundary value problem derived from the necessary conditions of a constrained nonlinear optimal control problem numerically. An introduction to multiple shooting can be found in [Asch 88, Stoe 02], collocation methods are treated e.g. in [Asch 79], see also [Bind 01] for more references.

In practice, the exploitation of the necessary conditions' structure in the multipoint boundary value problem is a benefit that might also reduce computational costs. In spite of that, significant knowledge about the considered optimal control problem and experience in optimal control simulations is necessary to use indirect methods. One reason is that they are sensitive to initial guesses for the iterations, and in particular, initial guesses for the adjoint variables are required. Furthermore, modifications in the model equations are difficult to include in the solution procedure, since they lead to changes in the necessary conditions.

2.3.2 Direct methods

Direct methods are also called direct transcription methods since they transcribe the infinite dimensional optimal control Problem 2.1.1, or the mechanical optimal control Problem 2.2.1 into a finite dimensional nonlinear programming problem [Kraf 85, Bett 98, Stry 92]. State and control variables are discretised directly following the steps 'first discretise, then optimise' illustrated on the middle branch in Figure 2.1. As an approximation to the continuous objective functional, one obtains a discrete objective function.

It has to be optimised while at the same time the discretised state equations as well as discrete versions of all other equations present in Problem 2.1.1 or Problem 2.2.1 must be fulfilled. The resulting finite dimensional nonlinear constrained optimisation problem can be solved by standard nonlinear optimisation techniques such as sequential quadratic programming (see e.g. [Gill 97, Schi 80, Powe 78, Bogg 95, Barc 98]). Sequential quadratic programming is an iterative method, where in each iteration the optimisation variables are improved by the solution of a quadratic subproblem. This subproblem is again solved iteratively, whereby interior point or active set strategies are used to handle the (currently active or inactive) inequality constraints, see e.g. [Rene 01].
As an alternative, analogous to the Lagrangian $J^\star$ of the optimal control problem in (2.2), a discrete Lagrangian can be defined in terms of discrete states, controls and adjoints. The corresponding necessary Karush-Kuhn-Tucker conditions yield a nonlinear algebraic system of equations that can be solved iteratively using e.g. a Newton-Raphson method, see [Wirt 10, Lee 09a, Lee 09b].

In direct shooting methods, the control variable is approximated by a finite dimensional parametrisation. Using this discrete control sequence, the state equations are integrated forward in time (using one's favourite time stepping method). Substituting the obtained discrete states into the objective function, one obtains an objective function that depends only on the discrete control parameters. Discrete versions of the path constraints and the state boundary values then serve as constraints for the optimisation of the discrete objective functional. Direct shooting methods can be split into direct single shooting (see e.g. [Stoe 02, Kraf 85, Hick 71]) and direct multiple shooting methods (see e.g. [Deuf 74, Bock 84]). Direct multiple shooting methods are similar to direct single shooting, however in addition, the time interval is split into subintervals and matching conditions are imposed on the interior boundaries for the states in terms of so called node values. While the set of optimisation variables in single shooting consists of the control parameters only, in multiple shooting the node values also belong to the optimisation variables and the matching conditions restrict the optimisation procedure together with the discretised path constraints and the state boundary values. In direct single shooting, the nonlinear programming problem remains relatively small, however, for highly unstable systems, where solutions of the initial value problem depend strongly on the initial value, the direct shooting optimisation algorithm inherits this ill-conditioning, even if the optimisation problem is well-conditioned. In contrast to that, multiple shooting methods enable the optimisation of highly unstable or even chaotic problems.

Other examples of direct approaches use discrete approximation techniques like collocation methods (see e.g. [Stry 91, Bieg 84]), Runge-Kutta discretisations [Hage 00], finite differences [Maed 81] or Galerkin methods [Flet 84]. See also [Bett 98] and [Bind 01] for an overview of the current state of the art. In [Bott 05], the idea to use a structure preserving scheme in a direct transcription method for the optimal control of multibody systems appears. There, an energy conserving scheme is used and applied to two-dimensional examples. Note that in contrast to DMOCC which reduces the unknown states and controls to the minimal possible number, in [Bott 04] the constraint forces arising from the joint coupling between the bodies are included in the set of unknowns.

2.3.3 DMOC and DMOCC

A recently developed method, DMOC (discrete mechanics and optimal control, see [Ober 08, Jung 05a]), is used in this work and developed further into DMOCC for constrained mechanical systems in Chapter 5 and [Leye 09b]. It is based on the discretisation of the variational structure of the mechanical system directly. In the context of variational integrators, as described in [Mars 01], the discretisation of the Lagrange-d'Alembert principle leads to structure preserving time stepping equations which (together with discretised path constraints and boundary values) serve as equality constraints for the resulting finite dimensional nonlinear optimisation problem. This procedure is illustrated on the right branch in Figure 2.1. Here, discretisation takes place at the earliest possible level. To obtain meaningful results from optimal control simulations, wherein energy expenditure or the control effort of a motion are often part of the optimisation goal, it is crucial to approximate the underlying dynamics in a structure preserving way, i.e. in a way that does not numerically, thus artificially, dissipate energy and in which momentum maps change only and exactly according to the applied loads.

Another important ingredient of DMOCC is the employed formulation of constrained multibody dynamics where the constrained equations of motion are discretised in a structure preserving way and then reduced to the minimum possible dimension via the discrete null space method, see [Leye 06a, Bets 06, Leye 08a] as well as Chapter 3 (see also [Leye 08b]). Since the complete state and control trajectories are computed in dynamic optimisation procedure (in contrast to forward dynamic simulations where the unknowns are determined at one time node only) it is particularly important that the discrete time stepping equations' dimension is minimal. This reduces the number of unknowns and constraints in the optimisation procedure and therefore the computational effort substantially, see Chapter 5 (see also [Leye 09b]). The constrained formulation of rigid multibody dynamics enables the use of three-dimensional models consisting of many bodies coupled by different type of joints while circumventing completely the difficulties associated with rotational motion. The kinematics is straight forward and closed loops can be dealt with on an equal footing as chains or tree-structured systems. The continuous equations of motion are formulated entirely in the inertial frame, thus they contain a constant mass matrix and no Coriolis terms, simplifying temporal discretisation. Furthermore, the treatment of momentum arms is facilitated substantially.

In [Jung 05a, Jung 05b, Jung 06] DMOC is applied to low orbital thrust transfers and the optimal control of formation flying satellites including an algorithm that exploits a hierarchical structure of that problem. An analysis of the convergence properties can be found in [Ober 10]. Other works using DMOC can be found in the context of (nonholonomicaly constrained) robotics [Kobi 07a, Kobi 07b], two-dimensional compass biped gait [Peka 07, Peka 08, Peka 10], space mission design [Moor 09] and articulated submerged bodies [Kans 05, Ross 06].

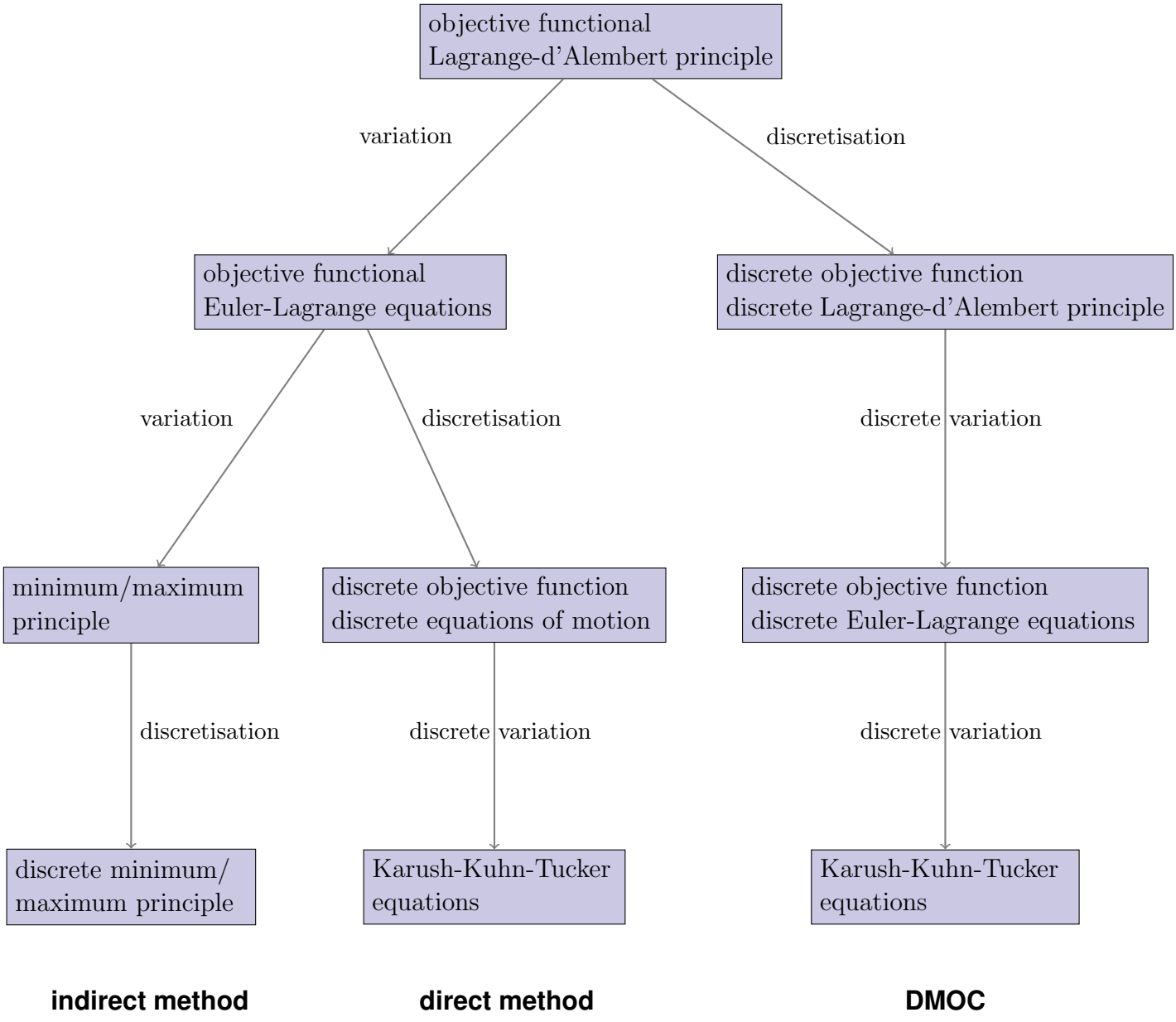

Figure 2.1: Overview over different solution methods for optimal control problems (slightly modified version of Figure 1.3 in [Ober 08]).

3 Variational integrators for constrained dynamical systems

3.1 Introduction

The distinguishing feature of variational integrators is that time stepping schemes are derived from a discrete variational principle based on a discrete action functional that approximates the continuous one. This is opposed to the standard derivation of integration methods that start with a continuous equation of motion (which itself might have been derived from a continuous variational principle) and replace the continuous quantities, in particular the derivatives with respect to time, by discrete approximations. The variational theory of discrete mechanics provides a theoretical framework that parallels continuous variational dynamics. Discrete analogues to the Euler-Lagrange equations, Noether's theorem and the Legendre transform are derived from a discrete Lagrangian by performing similar steps as in the continuous theory. The resulting time stepping schemes are structure preserving, i.e. they are symplectic-momentum conserving and exhibit good energy behaviour, meaning that no artificial dissipation is present and the energy error stays bounded over long time simulations. There exist many works on symplectic integrators like [Hair 04, Leim 94, Leim 96, Reic 94, McLa 06b, Kane 00, Lew 03b] to mention just a view. A detailed introduction plus a survey on the history and literature on the variational view of discrete mechanics is given in [Mars 01].
That work introduces also the theoretical background to deal with holonomically constrained systems in the framework of discrete variational mechanics by enforcing constraints using Lagrange multipliers or formulating the problem in generalised coordinates directly in the constraint manifold. A more applied approach to the variational integration of constrained problems, that already involves the idea of formulating the discrete Lagrangian in terms of a reparametrised redundant configuration variable, is given in [Wend 97]. However, many issues that are important from a practical point of view when using variational integrators for the simulation of constrained dynamics, like a consistent initialisation or postprocessing steps necessary to evaluate the obtained discrete trajectory, have not been addressed yet.

The first purpose of the work in this chapter, see also [Leye 08b], is to fill this gap by providing details on the discrete Lagrangian, the discrete Legendre transform, the calculation of energy along a discrete trajectory for constrained problems and the fulfilment of constraints on configuration and on momentum level. Secondly the recently in the context of energy-momentum conserving time stepping schemes developed discrete null space method [Bets 05] is adapted to the framework of variational integrators, in particular it is shown that the resulting scheme is not only equivalent to the corresponding scheme using Lagrange multipliers, but that it can be derived itself via a discrete variational principle.

Using the discrete null space method, the constraint forces are eliminated from the system and its dimension is reduced to the minimal possible number by the introduction of a discrete reparametrisation in one time interval only. Besides leading to lower computational costs for many applications, this procedure removes the well known conditioning problems associated with the use of Lagrange multipliers [Petz 86, Hair 89] while fulfilling constraints exactly. Thus it combines a number of advantageous properties compared to many other possibilities to handle constraints [Leye 04].
The discrete null space method has been applied successfully to the energy-momentum conserving integration of the dynamics of multibody systems consisting of rigid bodies connected by joints [Bets 06, Leye 06a] and to flexible multibody systems being composed of geometrically exact beams and shells [Leye 08a, Leye 06a]. Symplectic-momentum conserving integration of examples from both fields are presented in this work and the performance is compared to that using an energy-momentum scheme. For constrained problems, the energy-momentum conserving time stepping equations involve the evaluation of more terms at the unknown configuration, wherefore the linearisation is more complicated and the iterative solution is computationally more expensive.
No attempt to place the employed constrained formulation of rigid body and beam dynamics in the existing literature is made in this introduction since such surveys can be found in the introductions of the works cited in the corresponding sections.

This chapter starts with a presentation of continuous constrained Lagrangian dynamics in Section 3.2. Then, the discrete counterparts are shown in Section 3.3. In particular, the discrete null space method with nodal reparametrisation is introduced in the variational framework and the questions of consistent initialisation, constrained discrete Legendre transforms and hidden constraints are addressed. The developed theoretical aspects are illustrated by the simple example of a mathematical pendulum in Section 3.3.1. Section 3.4 recalls the formulation of rigid body dynamics in terms of a constrained configuration variable and presents the null space matrix and nodal reparametrisation required for the integration using the discrete null space method. The procedure is extended to rigid multibody systems in Section 3.5 and an example of a closed kinematic chain is investigated in detail. Finally, aspects of geometrically exact beam dynamics in the framework of variational integration are discussed in Section 3.6, an example of a multibody system, consisting of a beam and rigid bodies is investigated and the results are compared to the those obtained using an energy-momentum scheme.

3.2 Constrained Lagrangian dynamics

Consider an n-dimensional mechanical system in a configuration manifold $Q \subseteq \mathbb{R}^n$ with configuration vector $\boldsymbol{q}(t) \in Q$ and velocity vector $\dot{\boldsymbol{q}}(t) \in T_{\boldsymbol{q}(t)}Q$, where t denotes the time variable in the bounded interval $[t_0, t_N] \subset \mathbb{R}$ and $n, N \in \mathbb{N}$. In general, the Lagrangian of a mechanical system consists of the difference of the kinetic energy $T(\dot{\boldsymbol{q}})$ and a potential $V(\boldsymbol{q})$ accounting for elastic deformation and for external loading (if present). Let the motion be constrained by the vector valued function of holonomic, scleronomic constraints requiring $\boldsymbol{g}(\boldsymbol{q}) = \boldsymbol{0} \in \mathbb{R}^m$. It is assumed that $\boldsymbol{0} \in \mathbb{R}^m$ is a regular value of the constraints,

such that

$$C = \boldsymbol{g}^{-1}(\mathbf{0}) = \{\boldsymbol{q} | \boldsymbol{q} \in Q, \boldsymbol{g}(\boldsymbol{q}) = \mathbf{0}\} \subset Q$$

is an $(n-m)$-dimensional submanifold, called constraint manifold. Just as C can be embedded in Q via $i : C \to Q$, its $2(n-m)$-dimensional tangent bundle

$$TC = \{(\boldsymbol{q}, \dot{\boldsymbol{q}}) | (\boldsymbol{q}, \dot{\boldsymbol{q}}) \in T_{\boldsymbol{q}}Q, \boldsymbol{g}(\boldsymbol{q}) = \mathbf{0}, \boldsymbol{G}(\boldsymbol{q}) \cdot \dot{\boldsymbol{q}} = \mathbf{0}\} \subset TQ \tag{3.1}$$

can be embedded in TQ in a natural way by tangent lift $Ti : TC \to TQ$. Here and in the sequel $\boldsymbol{G}(\boldsymbol{q}) = D\boldsymbol{g}(\boldsymbol{q})$ denotes the $m \times n$ Jacobian of the constraints. Note that admissible velocities are constrained to the null space of the constraint Jacobian.

A Lagrangian $L : TQ \to \mathbb{R}$ can be restricted to $L^C = L_{|TC} : TC \to \mathbb{R}$. To investigate the relation of the dynamics of L^C on TC and the dynamics of L on TQ, the following notation is used. $\mathcal{C}(Q) = \mathcal{C}([t_0, t_N], Q, \boldsymbol{q}_0, \boldsymbol{q}_N)$ denotes the space of smooth functions satisfying $\boldsymbol{q}(t_0) = \boldsymbol{q}_0$ and $\boldsymbol{q}(t_N) = \boldsymbol{q}_N$, where $\boldsymbol{q}_0, \boldsymbol{q}_N \in C \subset Q$ are fixed endpoints. Let $\mathcal{C}(C)$ denote the corresponding space of curves in C and set $\mathcal{C}(\mathbb{R}^m) = \mathcal{C}([t_0, t_N], \mathbb{R}^m)$ to be the space of curves $\boldsymbol{\lambda} : [t_0, t_N] \to \mathbb{R}^m$ with no boundary conditions. This notation has been introduced in [Mars 01], where a large part of the theory presented here can be found.

Theorem 3.2.1 *Suppose that* $\mathbf{0}$ *is a regular value of the scleronomic holonomic constraints* $\boldsymbol{g} : Q \to \mathbb{R}^m$ *and set* $C = \boldsymbol{g}^{-1}(\mathbf{0}) \subset Q$. *Let* $L : TQ \to \mathbb{R}$ *be a Lagrangian and* $L^C = L_{|TC}$ *its restriction to* TC. *Then the following statements are equivalent:*

(i) $\boldsymbol{q} \in \mathcal{C}(C)$ *extremises the action integral* $S^C(\boldsymbol{q}) = \int_{t_0}^{t_N} L^C(\boldsymbol{q}, \dot{\boldsymbol{q}})\, dt$ *and hence solves the Euler-Lagrange equations for* L^C.

(ii) $\boldsymbol{q} \in \mathcal{C}(Q)$ *and* $\boldsymbol{\lambda} \in \mathcal{C}(\mathbb{R}^m)$ *satisfy the constrained Euler-Lagrange equations*

$$\begin{aligned} \frac{\partial L(\boldsymbol{q}, \dot{\boldsymbol{q}})}{\partial \boldsymbol{q}} - \frac{d}{dt}\left(\frac{\partial L(\boldsymbol{q}, \dot{\boldsymbol{q}})}{\partial \dot{\boldsymbol{q}}}\right) - \boldsymbol{G}^T(\boldsymbol{q}) \cdot \boldsymbol{\lambda} &= \mathbf{0} \\ \boldsymbol{g}(\boldsymbol{q}) &= \mathbf{0} \end{aligned} \tag{3.2}$$

(iii) $(\boldsymbol{q}, \boldsymbol{\lambda}) \in \mathcal{C}(Q \times \mathbb{R}^m)$ *extremise* $\bar{S}(\boldsymbol{q}, \boldsymbol{\lambda}) = S(\boldsymbol{q}) - \langle \boldsymbol{\lambda}, \boldsymbol{g}(\boldsymbol{q}) \rangle$ *and hence, solve the Euler-Lagrange equations for the augmented Lagrangian* $\bar{L} : T(Q \times \mathbb{R}^m) \to \mathbb{R}$ *defined by*

$$\bar{L}(\boldsymbol{q}, \boldsymbol{\lambda}, \dot{\boldsymbol{q}}, \dot{\boldsymbol{\lambda}}) = L(\boldsymbol{q}, \dot{\boldsymbol{q}}) - \boldsymbol{g}^T(\boldsymbol{q}) \cdot \boldsymbol{\lambda} \tag{3.3}$$

The proof given in [Mars 01] makes use of the Lagrange multiplier theorem (see e.g. [Abra 88]). The term $-\boldsymbol{G}^T(\boldsymbol{q}) \cdot \boldsymbol{\lambda} \in (TC)^\perp$ in $(3.2)_1$ represents the constraint forces that prevent the system from deviation of the constraint manifold. See Corollary 3.3.5 for further explanation on the space $(TC)^\perp$.

The continuous null space method For every $\boldsymbol{q} \in C$, the basis vectors of $T_{\boldsymbol{q}}C$ form an $n \times (n-m)$ matrix $\boldsymbol{P}(\boldsymbol{q})$ with corresponding linear map $\boldsymbol{P}(\boldsymbol{q}) : \mathbb{R}^{n-m} \to T_{\boldsymbol{q}}C$. This matrix is called null space matrix, since

$$\operatorname{range}(\boldsymbol{P}(\boldsymbol{q})) = \operatorname{null}(\boldsymbol{G}(\boldsymbol{q})) = T_{\boldsymbol{q}}C \tag{3.4}$$

Hence admissible velocities can be expressed as

$$\dot{\boldsymbol{q}}(t) = \boldsymbol{P}(\boldsymbol{q}) \cdot \boldsymbol{\nu}(t) \tag{3.5}$$

with the independent generalised (quasi-) velocities $\boldsymbol{\nu} \in \mathbb{R}^{n-m}$. Thus a premultiplication of the differential equation $(3.2)_1$ by $\boldsymbol{P}^T(\boldsymbol{q})$ eliminates the constraint forces including the Lagrange multipliers from the system. The resulting d'Alembert-type equations of motion read

$$\begin{aligned} \boldsymbol{P}^T(\boldsymbol{q}) \cdot \left[\frac{\partial L(\boldsymbol{q}, \dot{\boldsymbol{q}})}{\partial \boldsymbol{q}} - \frac{d}{dt} \left(\frac{\partial L(\boldsymbol{q}, \dot{\boldsymbol{q}})}{\partial \dot{\boldsymbol{q}}} \right) \right] &= \boldsymbol{0} \\ \boldsymbol{g}(\boldsymbol{q}) &= \boldsymbol{0} \end{aligned} \tag{3.6}$$

They are called d'Alembert-type equations of motion, since the elimination of the constraint forces from the system by premultiplication with the null space matrix is closely related to d'Alembert's principle saying that the virtual work done by constraint forces is zero. Admissible virtual variations in $T_{\boldsymbol{q}}C$ can be expressed as $\delta\boldsymbol{q} = \boldsymbol{P}(\boldsymbol{q}) \cdot \delta\boldsymbol{w}$ with $\delta\boldsymbol{w} \in \mathbb{R}^{n-m}$. With these preliminaries, d'Alembert's principle reads

$$\delta\boldsymbol{q}^T \cdot \boldsymbol{G}^T(\boldsymbol{q}) \cdot \boldsymbol{\lambda} = (\boldsymbol{P}(\boldsymbol{q}) \cdot \delta\boldsymbol{w})^T \cdot \boldsymbol{G}^T(\boldsymbol{q}) \cdot \boldsymbol{\lambda} = 0 \quad \forall \delta\boldsymbol{w} \in \mathbb{R}^{n-m}$$

Remark 3.2.2 (Continuous null space matrix) *Note that the null space matrix is not unique, a necessary and sufficient condition on $\boldsymbol{P}(\boldsymbol{q})$ is* (3.4)*. The null space matrix can be found in different ways, either by velocity analysis (i.e. corresponding to* (3.5)*, the map mapping the independent generalised velocities to the redundant velocities represents a viable null space matrix) or by performing a QR-decomposition of the transposed continuous constraint Jacobian*

$$\boldsymbol{G}^T = \boldsymbol{Q} \cdot \boldsymbol{R} = [\boldsymbol{Q}_1, \boldsymbol{Q}_2] \cdot \begin{bmatrix} \boldsymbol{R}_1 \\ \boldsymbol{0}_{(n-m)\times m} \end{bmatrix}$$

with the nonsingular upper triangular matrix $\boldsymbol{R}_1 \in \mathbb{R}^{m\times m}$ and the orthogonal matrix $\boldsymbol{Q} \in O(n)$, which can be partitioned into the orthogonal matrices $\boldsymbol{Q}_1 \in \mathbb{R}^{n\times m}$ and $\boldsymbol{Q}_2 \in \mathbb{R}^{n\times(n-m)}$. Then $\boldsymbol{P}(\boldsymbol{q}) = \boldsymbol{Q}_2(\boldsymbol{q})$ serves as null space matrix, which is sometimes called 'natural orthogonal complement' (see [Ange 89]). The third way to obtain a continuous null space matrix as the Jacobian of the reparametrisation of the constraint manifold is often possible, but the resulting continuous null space matrix can in general not be used to infer a discrete null space matrix. This is due to the fact that the respective discrete values of the generalised coordinates are not available in the present approach.

Reparametrisation in generalised coordinates For many applications it is possible to find a reparametrisation of the constraint manifold $\boldsymbol{F} : U \subseteq \mathbb{R}^{n-m} \to C$ in terms of independent generalised coordinates $\boldsymbol{u} \in U$. Then the Jacobian $D\boldsymbol{F}(\boldsymbol{u})$ of the coordinate transformation plays the role of a null space matrix. In the sequel, the $(n-m)$-dimensional manifold U will be termed generalised manifold. Since the constraints are fulfilled automatically by the reparametrized configuration variable $\boldsymbol{q} = \boldsymbol{F}(\boldsymbol{u})$, the system is reduced to $n-m$ second order differential equations. The equations of motion of minimal possible dimension for the present mechanical system (which consists of precisely $n-m$ degrees of freedom) then read

$$D\boldsymbol{F}^T(\boldsymbol{u}) \cdot \left[\frac{\partial L(\boldsymbol{q}, \dot{\boldsymbol{q}})}{\partial \boldsymbol{q}} - \frac{d}{dt} \left(\frac{\partial L(\boldsymbol{q}, \dot{\boldsymbol{q}})}{\partial \dot{\boldsymbol{q}}} \right) \right] = \boldsymbol{0} \tag{3.7}$$

Using (3.7), one can write

$$\frac{d}{dt} \left(D\boldsymbol{F}^T(\boldsymbol{u}) \cdot \frac{\partial L(\boldsymbol{q}, \dot{\boldsymbol{q}})}{\partial \dot{\boldsymbol{q}}} \right) = \left(D\left(D\boldsymbol{F}^T(\boldsymbol{u}) \right) \cdot \dot{\boldsymbol{u}} \right) \cdot \frac{\partial L(\boldsymbol{q}, \dot{\boldsymbol{q}})}{\partial \dot{\boldsymbol{q}}} + D\boldsymbol{F}^T(\boldsymbol{u}) \cdot \frac{\partial L(\boldsymbol{q}, \dot{\boldsymbol{q}})}{\partial \boldsymbol{q}}$$

On the other hand, defining a Lagrangian in generalised coordinates $L^U : TU \to \mathbb{R}$ by $L^U(\boldsymbol{u}, \dot{\boldsymbol{u}}) = L(\boldsymbol{F}(\boldsymbol{u}), D\boldsymbol{F}^T(\boldsymbol{u}) \cdot \dot{\boldsymbol{u}})$, its partial derivatives read

$$\begin{aligned} \frac{\partial L^U(\boldsymbol{u}, \dot{\boldsymbol{u}})}{\partial \boldsymbol{u}} &= D\boldsymbol{F}^T(\boldsymbol{u}) \cdot \frac{\partial L(\boldsymbol{q}, \dot{\boldsymbol{q}})}{\partial \boldsymbol{q}} + \left(D\left(D\boldsymbol{F}^T(\boldsymbol{u}) \right) \cdot \dot{\boldsymbol{u}} \right) \cdot \frac{\partial L(\boldsymbol{q}, \dot{\boldsymbol{q}})}{\partial \dot{\boldsymbol{q}}} \\ \frac{\partial L^U(\boldsymbol{u}, \dot{\boldsymbol{u}})}{\partial \dot{\boldsymbol{u}}} &= D\boldsymbol{F}^T(\boldsymbol{u}) \cdot \frac{\partial L(\boldsymbol{q}, \dot{\boldsymbol{q}})}{\partial \dot{\boldsymbol{q}}} \end{aligned}$$

Thus (3.7) is equivalent to the equations of motion in terms of generalised coordinates

$$\frac{\partial L^U(\boldsymbol{u}, \dot{\boldsymbol{u}})}{\partial \boldsymbol{u}} - \frac{d}{dt} \left(\frac{\partial L^U(\boldsymbol{u}, \dot{\boldsymbol{u}})}{\partial \dot{\boldsymbol{u}}} \right) = \boldsymbol{0} \tag{3.8}$$

Corollary 3.2.3 *The equations of motion* (3.2), (3.6), (3.7) *and* (3.8) *are equivalent, they yield the same motion* $\boldsymbol{q}(t)$ *in* $t \in [t_0, t_N]$.

Remark 3.2.4 (Restricted Lagrangian) *It is important to note that even though the restricted Lagrangian* $L^C : TC \to \mathbb{R}$ *can also be written as* $L^C(\boldsymbol{q}, \dot{\boldsymbol{q}}) = L(\boldsymbol{q}, \dot{\boldsymbol{q}})$ *with* $\boldsymbol{q} = \boldsymbol{F}(\boldsymbol{u})$ *and* $\dot{\boldsymbol{q}} = D\boldsymbol{F}(\boldsymbol{u}) \cdot \dot{\boldsymbol{u}}$, *it is different from* L^U *because the two functions are defined on different domains.*

Remark 3.2.5 (Projections) *The premultiplication of the Euler-Lagrange equations by the transposed null space matrix in* (3.6) *can be interpreted as a projection onto the cotangent space of the generalised manifold since* $\boldsymbol{P}^T(\boldsymbol{q}) : T^*_{\boldsymbol{q}}Q \to T^*_{\boldsymbol{u}}U$. *The same holds for the special case in* (3.7) *where the Jacobian of the reparametrisation serves as a null space matrix. Alternatively, one could think of premultiplying* $(3.2)_1$ *by the projection* $\boldsymbol{Q}(\boldsymbol{q}) : T^*_{\boldsymbol{q}}Q \to \eta(T^*_{\boldsymbol{q}}C)$ *where*

$$\eta(T^*_{\boldsymbol{q}}C) = \left\{ (\boldsymbol{q}, \boldsymbol{p}) | (\boldsymbol{q}, \boldsymbol{p}) \in T^*_{\boldsymbol{q}}Q, \boldsymbol{g}(\boldsymbol{q}) = \boldsymbol{0}, \boldsymbol{G}(\boldsymbol{q}) \cdot \boldsymbol{\pi}_{\dot{\boldsymbol{q}}} \left(\mathbb{F}L^{-1}(\boldsymbol{q}, \boldsymbol{p}) \right) = \boldsymbol{0} \right\} \subset T^*Q \tag{3.9}$$

and $\boldsymbol{p} \in T^*_{\boldsymbol{q}}Q$ *denotes the conjugate momentum that can be obtained via the Legendre transform* $\mathbb{F}L : TQ \to T^*Q$ *reading in coordinate form*

$$\mathbb{F}L(\boldsymbol{q}, \dot{\boldsymbol{q}}) = (\boldsymbol{q}, \boldsymbol{p}) = \left(\boldsymbol{q}, \frac{\partial L}{\partial \dot{\boldsymbol{q}}}(\boldsymbol{q}, \dot{\boldsymbol{q}})\right)$$

and $\boldsymbol{\pi}_{\dot{\boldsymbol{q}}} : TQ \to T_{\boldsymbol{q}}Q$ *projects the state* $(\boldsymbol{q}, \dot{\boldsymbol{q}})$ *onto the velocity* $\dot{\boldsymbol{q}}$*. Even though the constraint forces are eliminated by this projection, the resulting equations of motion are redundant, since they have been projected onto a lower dimensional submanifold.* $\eta : T^*C \to T^*Q$ *is the embedding defined by requiring that the following diagram commutes (see [Mars 01] for further details).*

$$\begin{array}{ccc} TQ_{|C} & \xrightarrow{\mathbb{F}L} & T^*Q \\ {\scriptstyle Ti}\uparrow & & \uparrow{\scriptstyle \eta} \\ TC & \xrightarrow[\mathbb{F}L^C]{} & T^*C \end{array}$$

Such a projection can be calculated as

$$\boldsymbol{Q} = \boldsymbol{I}_{n\times n} - \boldsymbol{G}^T \cdot \left[\boldsymbol{G} \cdot \boldsymbol{M}^{-1} \cdot \boldsymbol{G}^T\right]^{-1} \boldsymbol{G} \cdot \boldsymbol{M}^{-1} \tag{3.10}$$

where $\boldsymbol{I}_{n\times n}$ *is the* $n \times n$ *identity matrix and all quantities are evaluated at* $\boldsymbol{q}$*.*

3.3 Constrained discrete variational dynamics

Corresponding to the configuration manifold Q, the discrete state space is defined by $Q \times Q$ which is locally isomorphic to TQ. For a constant time step $h \in \mathbb{R}$, a path $\boldsymbol{q} : [t_0, t_N] \to Q$ is replaced by a discrete path $\boldsymbol{q}_d : \{t_0, t_0 + h, , \ldots, t_0 + Nh = t_N\} \to Q$, $N \in \mathbb{N}$, where $\boldsymbol{q}_n = \boldsymbol{q}_d(t_0 + nh)$ is viewed as an approximation to $\boldsymbol{q}(t_0 + nh)$. Similarly, $\boldsymbol{\lambda}_n = \boldsymbol{\lambda}_d(t_n)$ approximates the Lagrange multiplier at $t_n = t_0 + nh$.
According to the key idea of variational integrators, the variational principle is discretised rather than the resulting equations of motion. The action integral is approximated in a time interval $[t_n, t_{n+1}]$ using the discrete Lagrangian $L_d : Q \times Q \to \mathbb{R}$ via

$$L_d(\boldsymbol{q}_n, \boldsymbol{q}_{n+1}) \approx \int_{t_n}^{t_{n+1}} L(\boldsymbol{q}, \dot{\boldsymbol{q}})\, dt \tag{3.11}$$

In this work, the midpoint approximation

$$L_d(\boldsymbol{q}_n, \boldsymbol{q}_{n+1}) = \frac{1}{2h}(\boldsymbol{q}_{n+1} - \boldsymbol{q}_n)^T \cdot \boldsymbol{M} \cdot (\boldsymbol{q}_{n+1} - \boldsymbol{q}_n) - hV\left(\frac{\boldsymbol{q}_{n+1} + \boldsymbol{q}_n}{2}\right)$$

is used. Variation of the discrete action sum

$$S_d = \sum_{n=0}^{N-1} L_d(\boldsymbol{q}_n, \boldsymbol{q}_{n+1})$$

reads

$$\begin{aligned}\delta S_d =& \delta \boldsymbol{q}_0^T \cdot D_1 L_d(\boldsymbol{q}_0, \boldsymbol{q}_1) + \sum_{n=1}^{N-1} \delta \boldsymbol{q}_n^T \cdot (D_2 L_d(\boldsymbol{q}_{n-1}, \boldsymbol{q}_n) + D_1 L_d(\boldsymbol{q}_n, \boldsymbol{q}_{n+1})) + \\ & \delta \boldsymbol{q}_N^T \cdot D_2 L_d(\boldsymbol{q}_{N-1}, \boldsymbol{q}_N)\end{aligned} \tag{3.12}$$

where $D_\alpha L_d$ denotes partial differentiation of the discrete Lagrangian with respect to the α-th argument. Requiring its stationarity for all $\{\delta \boldsymbol{q}_n\}_{n=1}^{N-1}$ and $\delta \boldsymbol{q}_0 = \delta \boldsymbol{q}_N = \boldsymbol{0}$ yields the discrete (unconstrained) Euler-Lagrange equations

$$D_1 L_d(\boldsymbol{q}_n, \boldsymbol{q}_{n+1}) + D_2 L_d(\boldsymbol{q}_{n-1}, \boldsymbol{q}_n) = \boldsymbol{0}$$

The integral in $[t_n, t_{n+1}]$ of the scalar product of the constraints and the corresponding Lagrange multiplier is approximated by

$$\frac{1}{2} \boldsymbol{g}_d^T(\boldsymbol{q}_n) \cdot \boldsymbol{\lambda}_n + \frac{1}{2} \boldsymbol{g}_d^T(\boldsymbol{q}_{n+1}) \cdot \boldsymbol{\lambda}_{n+1} \approx \int_{t_n}^{t_{n+1}} \boldsymbol{g}^T(\boldsymbol{q}) \cdot \boldsymbol{\lambda} \, dt$$

whereby $\boldsymbol{g}_d^T(\boldsymbol{q}_n) = h \boldsymbol{g}^T(\boldsymbol{q}_n)$ is used and let $\boldsymbol{G}_d^T(\boldsymbol{q}_n) = D \boldsymbol{g}_d^T(\boldsymbol{q}_n)$.
Analogue to Theorem 3.2.1, the relation between the constrained discrete Lagrangian system on $Q \times Q$ and that corresponding to a discrete Lagrangian restricted to $C \times C$ is stated in the following theorem which has again been taken from [Mars 01]. Let $\mathcal{C}_d(Q) = \mathcal{C}(\{t_0, t_0+h, \ldots, t_0+Nh = t_N\}, Q, \boldsymbol{q}_0, \boldsymbol{q}_N)$ denote the space of discrete trajectories satisfying $\boldsymbol{q}_d(t_0) = \boldsymbol{q}_0$ and $\boldsymbol{q}_d(t_N) = \boldsymbol{q}_N$ for given $\boldsymbol{q}_0, \boldsymbol{q}_N \in C$. Let $\mathcal{C}_d(C)$ denote the corresponding set of discrete trajectories in C and set $\mathcal{C}_d(\mathbb{R}^m) = \mathcal{C}(\{t_0, t_0 + h, \ldots, t_0 + (N)h = t_N\}, \mathbb{R}^m)$ to be the set of maps $\boldsymbol{\lambda}_d : \{t_0, t_0 + h, \ldots, t_0 + (N)h = t_N\} \to \mathbb{R}^m$ with no boundary conditions.

Theorem 3.3.1 *Suppose that* $\boldsymbol{0}$ *is a regular value of the scleronomic holonomic constraints* $\boldsymbol{g} : Q \to \mathbb{R}^m$ *and set* $C = \boldsymbol{g}^{-1}(\boldsymbol{0}) \subset Q$. *Let* $L_d : Q \times Q \to \mathbb{R}$ *be a discrete Lagrangian and* $L_d^C = L_{d_{|C \times C}}$ *its restriction to* $C \times C$. *Then the following statements are equivalent:*

(i) $\boldsymbol{q}_d = \{\boldsymbol{q}_n\}_{n=0}^N \in \mathcal{C}_d(C)$ *extremises the discrete action* $S_d^C = S_{d_{|C \times C}}$ *and hence solves the discrete Euler-Lagrange equations for* L_d^C.

(ii) $\{\boldsymbol{q}_n\}_{n=1}^{N-1} \in \mathcal{C}_d(C)$ *and* $\{\boldsymbol{\lambda}_n\}_{n=1}^{N-1} \in \mathcal{C}_d(\mathbb{R}^m)$ *satisfy the constrained discrete Euler-Lagrange equations*

$$\begin{aligned} D_1 L_d(\boldsymbol{q}_n, \boldsymbol{q}_{n+1}) + D_2 L_d(\boldsymbol{q}_{n-1}, \boldsymbol{q}_n) - \boldsymbol{G}_d^T(\boldsymbol{q}_n) \cdot \boldsymbol{\lambda}_n &= \boldsymbol{0} \\ \boldsymbol{g}(\boldsymbol{q}_{n+1}) &= \boldsymbol{0} \end{aligned} \tag{3.13}$$

(iii) $(\boldsymbol{q}_d, \boldsymbol{\lambda}_d) \in \mathcal{C}_d(Q \times \mathbb{R}^m)$ *extremise* $\bar{S}_d(\boldsymbol{q}_d, \boldsymbol{\lambda}_d) = S_d(\boldsymbol{q}_d) - \langle \boldsymbol{\lambda}_d, \boldsymbol{g}_d(\boldsymbol{q}_d) \rangle$ *and hence, solve the Euler-Lagrange equations for the augmented Lagrangian* $\bar{L}_d : (Q \times \mathbb{R}^m) \times (Q \times \mathbb{R}^m) \to \mathbb{R}$ *defined by*

$$\bar{L}_d(\boldsymbol{q}_n, \boldsymbol{\lambda}_n, \boldsymbol{q}_{n+1}, \boldsymbol{\lambda}_{n+1}) = L_d(\boldsymbol{q}_n, \boldsymbol{q}_{n+1}) - \frac{1}{2} \boldsymbol{g}_d^T(\boldsymbol{q}_n) \cdot \boldsymbol{\lambda}_n - \frac{1}{2} \boldsymbol{g}_d^T(\boldsymbol{q}_{n+1}) \cdot \boldsymbol{\lambda}_{n+1} \tag{3.14}$$

Remark 3.3.2 (Augmented discrete Lagrangian) *The particular choice of the augmented discrete Lagrangian* (3.14) *has several consequences that are illustrated by numerical examples in Section 3.3.1. First of all, the negative sign in front of the scalar product of constraints and Lagrange multipliers causes the constraint forces* $-\boldsymbol{G}^T(\boldsymbol{q}_n)\cdot\boldsymbol{\lambda}_n$ *to have the right orientation. Secondly, including the scalar product of the constraints with the Lagrange multiplier at both time nodes yields contributions of the constraint forces in both discrete Legendre transforms* (3.23), (3.24). *One consequence of that is that the first Lagrange multiplier* $\boldsymbol{\lambda}_0$ *which is computed together with* $\boldsymbol{q}_1$ *using* (3.23) *has the correct absolute value. Another consequence is that in the absence of a potential, the discrete Legendre transforms* (3.23), (3.24) *yield conjugate momenta which are consistent with the constraints on momentum level.*

Discrete null space method The reduction of the time stepping scheme (3.13) can be accomplished in analogy to the continuous case according to the discrete null space method. This idea has first been introduced in the context of energy-momentum conserving integration and applied to the constrained dynamics of mass point systems in [Bets 05], then it has been further developed in [Bets 06, Leye 08a, Leye 06a] for rigid and flexible multibody systems. In order to eliminate the discrete constraint forces from the equations, a discrete null space matrix fulfilling

$$\text{range}\,(\boldsymbol{P}(\boldsymbol{q}_n)) = \text{null}\,(\boldsymbol{G}_d(\boldsymbol{q}_n)) \tag{3.15}$$

is employed. Analogue to (3.6), the premultiplication of $(3.13)_1$ by the transposed discrete null space matrix cancels the constraint forces from the system, i.e. the Lagrange multipliers are eliminated from the set of unknowns and the system's dimension is reduced to n.

$$\begin{aligned} \boldsymbol{P}^T(\boldsymbol{q}_n)\cdot[D_2L_d(\boldsymbol{q}_{n-1},\boldsymbol{q}_n)+D_1L_d(\boldsymbol{q}_n,\boldsymbol{q}_{n+1})] &= \boldsymbol{0} \\ \boldsymbol{g}(\boldsymbol{q}_{n+1}) &= \boldsymbol{0} \end{aligned} \tag{3.16}$$

Proposition 3.3.3 *The d'Alembert-type time stepping scheme* (3.16) *is equivalent to the constrained scheme* (3.13).

Proof: Recapitulating the construction procedure of the d'Alembert-type scheme from the constrained scheme, it is obvious that for given values $(\boldsymbol{q}_{n-1},\boldsymbol{q}_n)$, a solution $(\boldsymbol{q}_{n+1},\boldsymbol{\lambda}_n)$ of the constrained scheme (3.13) is also a solution of the d'Alembert-type scheme (3.16). Assume that $\boldsymbol{q}_{n+1}$ solves the d'Alembert-type scheme (3.16) for given $(\boldsymbol{q}_{n-1},\boldsymbol{q}_n)$. Note that condition (3.15) on the discrete null space matrix implies $\text{null}\left(\boldsymbol{P}^T(\boldsymbol{q}_n)\right) = \text{range}\left(\boldsymbol{G}_d^T(\boldsymbol{q}_n)\right)$ (see e.g. [Fisc 97]). Together with (3.16) it follows that

$$[D_2L_d(\boldsymbol{q}_{n-1},\boldsymbol{q}_n)+D_1L_d(\boldsymbol{q}_n,\boldsymbol{q}_{n+1})] \in \text{null}\left(\boldsymbol{P}^T(\boldsymbol{q}_n)\right) = \text{range}\left(\boldsymbol{G}_d^T(\boldsymbol{q}_n)\right)$$

Accordingly, there exists a multiplier $\boldsymbol{\lambda}_n \in \mathbb{R}^m$ such that $(\boldsymbol{q}_{n+1},\boldsymbol{\lambda}_n)$ solve the constrained scheme (3.13). An explicit formula to compute $\boldsymbol{\lambda}_n$ is given in (3.26). ∎
Therefore, the d'Alembert-type scheme has the same conservation properties as the constrained scheme. Symplecticity and momentum maps are conserved along a discrete trajectory $\boldsymbol{q}_d$ of (3.16) and the constraints are fulfilled exactly at the time nodes.

Remark 3.3.4 (Difference to energy-momentum scheme) *It is important to note, that the choice to evaluate the constraints and the Lagrange multipliers at the time nodes in* (3.14) *causes the evaluation of the constraint Jacobian in* (3.13) *at the time nodes. Therefore a discrete null space matrix with the property* (3.15) *can simply be found by evaluation of the continuous null space matrix at the time nodes. Acquaintance of the continuous null space matrix for a specific mechanical system always yields an explicit representation of the discrete null space matrix for the variational time stepping scheme emanating from the discrete variational principle in conjunction with the chosen approximations. This is in contrast to energy-momentum conserving time stepping schemes based on the concept of discrete derivatives [Gonz 96, Bets 05] or on finite elements in time [Bets 02a], where the discrete constraint Jacobian* $\mathbf{G}(\boldsymbol{q}_n, \boldsymbol{q}_{n+1})$ *depends on both the present and the unknown configuration. As a consequence of the more rare appearance of* $\boldsymbol{q}_{n+1}$*, the linearisation of the variational schemes* (3.13) *and* (3.16)*, necessary to solve the nonlinear algebraic system iteratively, is simpler and less computationally cost intensive.*

Nodal reparametrisation Similar to the continuous case, a reduction of the system to the minimal possible dimension can be accomplished by a local reparametrisation of the constraint manifold in the neighbourhood of the discrete configuration variable $\boldsymbol{q}_n \in C$. At the time nodes, $\boldsymbol{q}_n$ is expressed in terms of the discrete generalised coordinates $\boldsymbol{u}_n \in U \subseteq \mathbb{R}^{n-m}$, such that the constraints are fulfilled.

$$\boldsymbol{q}_n = \boldsymbol{F}_d(\boldsymbol{u}_n, \boldsymbol{q}_{n-1}) \quad \text{with} \quad \boldsymbol{g}(\boldsymbol{q}_n) = \boldsymbol{g}(\boldsymbol{F}_d(\boldsymbol{u}_n, \boldsymbol{q}_{n-1})) = \mathbf{0} \tag{3.17}$$

Note that the discrete generalised coordinates $\boldsymbol{u}_n$ are incremental variables that describe the evolution of the configuration variable in one time interval only. This avoids the danger of encountering singularities which are often present in absolute reparametrisations. Insertion of the nodal reparametrisations for the configuration (3.17) into the scheme redundantises $(3.16)_2$. The resulting scheme $n-m$-dimensional scheme

$$\boldsymbol{P}^T(\boldsymbol{q}_n) \cdot [D_2 L_d(\boldsymbol{q}_{n-1}, \boldsymbol{q}_n) + D_1 L_d(\boldsymbol{q}_n, \boldsymbol{F}_d(\boldsymbol{u}_{n+1}, \boldsymbol{q}_n))] = \mathbf{0} \tag{3.18}$$

has to be solved for $\boldsymbol{u}_{n+1}$, then $\boldsymbol{q}_{n+1}$ is obtained by the reparametrisation (3.17). Equation (3.18) is equivalent to the constrained scheme (3.13), thus it also has the key properties of exact constraint fulfilment, symplecticity and momentum conservation. While the constrained scheme becomes increasingly ill-conditioned for decreasing time steps, the condition number of (3.16), (3.18) is independent of the time step.
Starting with the discrete reparametrisation $\boldsymbol{q}_n = \boldsymbol{F}_d(\boldsymbol{u}_n, \boldsymbol{q}_{n-1})$, it is possible to derive (3.18) directly in one step. The variation of a redundant configuration variable can be expressed in terms of variations of the discrete generalised coordinates as

$$\delta\boldsymbol{q}_n = \frac{\partial \boldsymbol{F}_d}{\partial \boldsymbol{u}_n} \cdot \delta\boldsymbol{u}_n + \sum_{k=1}^{n-1} \left[\left(\prod_{i=n-1}^{k} \frac{\partial \boldsymbol{F}_d}{\partial \boldsymbol{q}_i} \right) \cdot \frac{\partial \boldsymbol{F}_d}{\partial \boldsymbol{u}_k} \cdot \delta\boldsymbol{u}_k \right] + \left(\prod_{i=n-1}^{0} \frac{\partial \boldsymbol{F}_d}{\partial \boldsymbol{q}_i} \right) \cdot \delta\boldsymbol{q}_0 \tag{3.19}$$

Here, the discrete variational principle (3.12) requires stationarity for all $\{\delta\boldsymbol{u}_n\}_{n=1}^N$ with $\delta\boldsymbol{q}_0 = \delta\boldsymbol{q}_N = \mathbf{0}$. After inserting (3.19) into (3.12), the variation $\delta\boldsymbol{u}_{N-1}$ appears only in the last term of the sum in (3.12) implying $\left(\dfrac{\partial \boldsymbol{F}_d}{\partial \boldsymbol{u}_{N-1}} \right)^T \cdot [D_2 L_d(\boldsymbol{q}_{N-2}, \boldsymbol{q}_{N-1}) + D_1 L_d(\boldsymbol{q}_{N-1}, \boldsymbol{q}_N)] =$

0. Repeating this argument, one arrives at the variational d'Alembert-type scheme with nodal reparametrisation

$$\left(\frac{\partial \boldsymbol{F}_d}{\partial \boldsymbol{u}_n}\right)^T \cdot [D_2 L_d(\boldsymbol{q}_{n-1}, \boldsymbol{q}_n) + D_1 L_d(\boldsymbol{q}_n, \boldsymbol{F}_d(\boldsymbol{u}_{n+1}, \boldsymbol{q}_n))] = \mathbf{0} \tag{3.20}$$

where $\dfrac{\partial \boldsymbol{F}_d}{\partial \boldsymbol{u}_n}$ is the discrete null space matrix.
A similar procedure is followed in [Wend 97] to derive a reduced variational time stepping scheme for constrained systems. However, an absolute reparametrisation $\boldsymbol{q}_n = \boldsymbol{F}(\boldsymbol{u}_n)$ is used there, thus the variational principle is different and the danger of singularities is not excluded.

Corollary 3.3.5 *The discrete time stepping schemes* (3.13), (3.16), (3.18) *and* (3.20) *are equivalent, they yield the same discrete trajectory* $\boldsymbol{q}_d$ *in* $t \in [t_0, t_N]$. *More specifically,* (3.13), (3.16), (3.18) *and* (3.20) *represent different possibilities to realise the conditions* $\boldsymbol{q}_n \in C$ *and*

$$\delta \boldsymbol{q}_n^T \cdot (D_1 L_d(\boldsymbol{q}_n, \boldsymbol{q}_{n+1}) + D_2 L_d(\boldsymbol{q}_{n-1}, \boldsymbol{q}_n)) = 0 \quad \forall\, \delta \boldsymbol{q}_n \in T_{\boldsymbol{q}_n} C \tag{3.21}$$

Equivalently, one can request $\boldsymbol{q}_n \in C$ *and*

$$D_1 L_d(\boldsymbol{q}_n, \boldsymbol{q}_{n+1}) + D_2 L_d(\boldsymbol{q}_{n-1}, \boldsymbol{q}_n) \quad \perp T_{\boldsymbol{q}_n} C \tag{3.22}$$

whereby the orthogonality condition only makes sense when $D_1 L_d(\boldsymbol{q}_n, \boldsymbol{q}_{n+1}) + D_2 L_d(\boldsymbol{q}_{n-1}, \boldsymbol{q}_n) \in T^*_{\boldsymbol{q}_n} Q$ *is identified with its representing element in* $T_{\boldsymbol{q}_n} Q$ *(using Riez's theorem, see e.g. [Heus 92]). Then* (3.22) *means*

$$D_1 L_d(\boldsymbol{q}_n, \boldsymbol{q}_{n+1}) + D_2 L_d(\boldsymbol{q}_{n-1}, \boldsymbol{q}_n) \quad \in \; ann(T_{\boldsymbol{q}_n} C) = \{\boldsymbol{S} \in T^*_{\boldsymbol{q}_n} Q | \boldsymbol{S}_{|T_{\boldsymbol{q}_n} C} = \mathbf{0}\}$$

Remark 3.3.6 (Projections) *As mentioned for the continuous case in Remark 3.2.5, instead of using the discrete null space matrix* $\boldsymbol{P}^T(\boldsymbol{q}_n) : T^*_{\boldsymbol{q}_n} Q \to T^*U$, *one could realise condition* (3.21) *or* (3.22) *using the projection* $\boldsymbol{Q}(\boldsymbol{q}_n) : T^*_{\boldsymbol{q}_n} Q \to \eta \left(T^*_{\boldsymbol{q}_n} C\right)$ *where* $\boldsymbol{Q}(\boldsymbol{q}_n)$ *is given by formula* (3.10) *and fulfils* $\boldsymbol{Q}(\boldsymbol{q}_n) \cdot \boldsymbol{G}_d^T(\boldsymbol{q}_n) = \mathbf{0}_{n \times m}$. *Thereby the constraint forces (including the Lagrange multipliers) are eliminated from the system while the number of equations is not altered. Thus it can not be employed to determine the trajectory since the projection onto the lower dimensional submanifold yields redundant equations. However, this projection will be useful later for certain postprocessing steps of the discrete trajectory where it is important to know conjugate momenta that are consistent with the hidden constraints.*

Remark 3.3.7 (Γ-convergence) *The* Γ*-convergence of discrete action for constrained systems to the corresponding continuum action functional is proven in [Schm 09] and the convergence properties of solutions of the discrete Euler-Lagrange equations to stationary points of the continuum problem is studied. This extends the results in [Mull 04] to constrained systems. In [Schm 09], the convergence result is illustrated with examples of mass point systems and flexible multibody dynamics that make use of the discrete null space method described in detail here in Sections 3.3.1, 3.4, 3.5 and 3.6.1.*

Constrained discrete Legendre transform So far, the derivation of variational time stepping schemes for constrained systems is based solely on the discrete path of configurations, i.e. the discrete trajectory $\boldsymbol{q}_d \in C$. Thereby, the discrete Lagrangian (3.11) involves a finite difference approximation for the velocity in the kinetic energy and an evaluation of the potential energy at some midpoint. Such approximated velocities do not fulfil the temporal differentiated form of the constraints, the so called hidden constraints. However, information on the systems evolution on velocity or momentum level might be of interest. This can be obtained using a discrete constrained Legendre transform.
Based on the augmented discrete Lagrangian (3.14), the constrained discrete Legendre transforms $\mathbb{F}^{c^-}L_d : Q \times Q \to T^*_{\boldsymbol{q}_n}Q$ and $\mathbb{F}^{c^+}L_d : Q \times Q \to T^*_{\boldsymbol{q}_n}Q$ read

$$\begin{aligned} &\mathbb{F}^{c^-}L_d : (\boldsymbol{q}_n, \boldsymbol{q}_{n+1}) \mapsto (\boldsymbol{q}_n, \boldsymbol{p}_n^-) \\ &\quad \boldsymbol{p}_n^- = -D_1 L_d(\boldsymbol{q}_n, \boldsymbol{q}_{n+1}) + \frac{1}{2}\boldsymbol{G}_d^T(\boldsymbol{q}_n) \cdot \boldsymbol{\lambda}_n \end{aligned} \tag{3.23}$$

$$\begin{aligned} &\mathbb{F}^{c^+}L_d : (\boldsymbol{q}_{n-1}, \boldsymbol{q}_n) \mapsto (\boldsymbol{q}_n, \boldsymbol{p}_n^+) \\ &\quad \boldsymbol{p}_n^+ = D_2 L_d(\boldsymbol{q}_{n-1}, \boldsymbol{q}_n) - \frac{1}{2}\boldsymbol{G}_d^T(\boldsymbol{q}_n) \cdot \boldsymbol{\lambda}_n \end{aligned} \tag{3.24}$$

With (3.23), (3.24), the constrained time stepping scheme $(3.13)_1$ can be interpreted as enforcing the matching of momenta $\boldsymbol{p}_n^+ - \boldsymbol{p}_n^- = \boldsymbol{0}$ such that along the discrete trajectory, there is a unique momentum at each time node n which can be denoted by $\boldsymbol{p}_n$. When the discrete null space method is used, the Lagrange multipliers are not at hand as an output of the simulation. They can be recovered easily using the $n \times m$ matrix

$$\boldsymbol{R}_d(\boldsymbol{q}_n) = \boldsymbol{G}_d^T(\boldsymbol{q}_n) \cdot \left(\boldsymbol{G}_d(\boldsymbol{q}_n) \cdot \boldsymbol{G}_d^T(\boldsymbol{q}_n)\right)^{-1}$$

which obviously fulfils

$$\boldsymbol{G}_d(\boldsymbol{q}_n) \cdot \boldsymbol{R}_d(\boldsymbol{q}_n) = \boldsymbol{I}_{m\times m} \tag{3.25}$$

where $I_{m\times m}$ denotes the m-dimensional identity matrix. Then the Lagrange multipliers can be recovered by premultiplying $(3.13)_1$ by $\boldsymbol{R}^T(\boldsymbol{q}_n)$ and accounting for (3.25). In particular, this yields

$$\boldsymbol{\lambda}_n = \boldsymbol{R}_d^T(\boldsymbol{q}_n) \cdot [D_1 L_d(\boldsymbol{q}_n, \boldsymbol{q}_{n+1}) + D_2 L_d(\boldsymbol{q}_{n-1}, \boldsymbol{q}_n)] \tag{3.26}$$

whereupon the constrained Legendre transforms can be used. On the other hand, if no information on the constraint forces is needed, one can avoid to recover the Lagrange multipliers and use the projected discrete Legendre transforms ${}^{Q}\mathbb{F}^{c^-}L_d : Q \times Q \to \eta\left(T^*_{\boldsymbol{q}_n}C\right)$ and ${}^{Q}\mathbb{F}^{c^+}L_d : Q \times Q \to \eta\left(T^*_{\boldsymbol{q}_n}C\right)$ reading

$${}^{Q}\boldsymbol{p}_n^- = -\boldsymbol{Q}(\boldsymbol{q}_n) \cdot D_1 L_d(\boldsymbol{q}_n, \boldsymbol{q}_{n+1}) \tag{3.27}$$

$${}^{Q}\boldsymbol{p}_n^+ = \boldsymbol{Q}(\boldsymbol{q}_n) \cdot D_2 L_d(\boldsymbol{q}_{n-1}, \boldsymbol{q}_n) \tag{3.28}$$

where $\boldsymbol{Q}(\boldsymbol{q}_n)$ is given by formula (3.10) and fulfils $\boldsymbol{Q}(\boldsymbol{q}_n) \cdot \boldsymbol{G}_d^T(\boldsymbol{q}_n) = \boldsymbol{0}_{n\times m}$. Both projected discrete Legendre transforms yield the same momentum vector denoted by ${}^{Q}\boldsymbol{p}_n$. Note that

for the constrained discrete Legendre transforms and for the projected discrete Legendre transforms, the output is an n-dimensional momentum vector. In the projected case, it lies in the $(n-m)$-dimensional submanifold $\eta\left(T^*_{\boldsymbol{q}_n}C\right)$. Yet another possibility is to compute an $(n-m)$-dimensional momentum vector by projecting with the discrete null space matrix. The reduced discrete Legendre transforms ${}^{P}\mathbb{F}^{c^-}L_d : Q \times Q \to T^*U$ and ${}^{P}\mathbb{F}^{c^+}L_d : Q \times Q \to T^*U$ are given by

$${}^{P}\boldsymbol{p}_n^- = -\boldsymbol{P}^T(\boldsymbol{q}_n) \cdot D_1 L_d(\boldsymbol{q}_n, \boldsymbol{q}_{n+1}) \tag{3.29}$$

$${}^{P}\boldsymbol{p}_n^+ = \boldsymbol{P}^T(\boldsymbol{q}_n) \cdot D_2 L_d(\boldsymbol{q}_{n-1}, \boldsymbol{q}_n) \tag{3.30}$$

Hidden constraints The temporary differentiated form of the configuration constraints yields the so called secondary or hidden constraints, which have been introduced already without mentioning in (3.1) and (3.9)

$$\begin{aligned} \boldsymbol{f}(\boldsymbol{q}, \dot{\boldsymbol{q}}) &= \frac{d\,\boldsymbol{g}(\boldsymbol{q})}{dt} = \boldsymbol{G}(\boldsymbol{q}) \cdot \dot{\boldsymbol{q}} = \boldsymbol{0} \\ \boldsymbol{h}(\boldsymbol{q}, \boldsymbol{p}) &= \frac{d\,\boldsymbol{g}(\boldsymbol{q})}{dt} = \boldsymbol{G}(\boldsymbol{q}) \cdot (\mathbb{F}L(\boldsymbol{p}))^{-1} = \boldsymbol{0} \end{aligned} \tag{3.31}$$

Similar to (3.3), in a continuous augmented Lagrangian they could be included as follows

$$\bar{L}(\boldsymbol{q}, \boldsymbol{\lambda}, \dot{\boldsymbol{q}}, \dot{\boldsymbol{\lambda}}, \boldsymbol{\mu}, \dot{\boldsymbol{\mu}}) = L(\boldsymbol{q}, \dot{\boldsymbol{q}}) - \boldsymbol{g}^T(\boldsymbol{q}) \cdot \boldsymbol{\lambda} - \boldsymbol{f}^T(\boldsymbol{q}, \dot{\boldsymbol{q}}) \cdot \boldsymbol{\mu}$$

Their discrete form could be enforced during the simulation by inclusion of discrete versions in the augmented discrete Lagrangian. However, the investigation of several numerical examples dealing with the energy-momentum conserving integration of point mass systems, rigid bodies and geometrically exact beams (e.g. in [Bets 02b], [Bets 03]) has brought forward that the incorporation of the temporally differentiated form of the constraints has not lead to crucial advantages (besides the fulfilment of the secondary constraints themselves). This fact is also reported in [Gonz 99] and references therein. The discrete trajectory has not been influenced considerably by their fulfilment. Thus, their inclusion in the trajectory based approach of variational integrators seems an exaggeration – besides, they are fulfilled to some extent by the discrete trajectory. On velocity level, one possibility is to write the discrete hidden constraints in the form

$$\boldsymbol{f}_d(\boldsymbol{q}_n, \boldsymbol{q}_{n+1}) = \boldsymbol{G}\left(\frac{\boldsymbol{q}_{n+1} + \boldsymbol{q}_n}{2}\right) \cdot \frac{\boldsymbol{q}_{n+1} - \boldsymbol{q}_n}{h} = \boldsymbol{0} \tag{3.32}$$

In the example of the mathematical pendulum where the constraint manifold is an equicurved circle, they are fulfilled exactly in presence and in absence of the potential energy. However, for general constraint manifolds, they need not be fulfilled. For Lagrangians of the form $L(\boldsymbol{q}, \dot{\boldsymbol{q}}) = \frac{1}{2}\dot{\boldsymbol{q}}^T \cdot \boldsymbol{M} \cdot \dot{\boldsymbol{q}} - V(\boldsymbol{q})$, where the conjugate momenta computed by the continuous Legendre transform are given by $\boldsymbol{p} = \boldsymbol{M} \cdot \dot{\boldsymbol{q}}$, it can be inferred from $(3.31)_2$ that the discrete hidden constraints on momentum level read

$$\boldsymbol{h}_d(\boldsymbol{q}_n, \boldsymbol{p}_n) = \boldsymbol{G}\,(\boldsymbol{q}_n) \cdot \boldsymbol{M}^{-1} \cdot \boldsymbol{p}_n = \boldsymbol{0} \tag{3.33}$$

Of course, $\boldsymbol{h}_d(\boldsymbol{q}_n, {}^{Q}\boldsymbol{p}_n) = \boldsymbol{0}$ holds exactly, since $\operatorname{null}(\boldsymbol{G}(\boldsymbol{q}_n)) = T_{\boldsymbol{q}_n}C$ and elements in $\eta\left(T^*_{\boldsymbol{q}_n}C\right)$ can be identified with their representing element in $T_{\boldsymbol{q}_n}C$ (using Riez's theorem, see e.g. [Heus 92]). To date, experience shows that $\boldsymbol{h}_d(\boldsymbol{q}_n, \boldsymbol{p}_n) = \boldsymbol{0}$ is fulfilled in the absence of a potential but not when a potential is present (see Section 3.3.1).

Initialisation of the simulation Another reason for which a discrete constrained Legendre transform is required is the initialisation of the simulation. To simulate the motion of a constrained dynamical system with one of the equivalent time stepping schemes, it is necessary to specify an initial configuration $\boldsymbol{q}_0 \in C$ and a second configuration $\boldsymbol{q}_1 \in C$. Together with the time step h, their difference quotient represents the velocity of the system in the first time interval $[0, h]$. For non-trivial mechanical systems, it might be difficult or even impossible to come up with a reasonable $\boldsymbol{q}_1$ that fulfils the constraints. Since the purpose of numerical time integration schemes is to approximate a continuous trajectory, it seems appropriate to initialise the simulation by prescribing $\boldsymbol{q}(0) \in C$ and $\dot{\boldsymbol{q}}(0) \in T_{\boldsymbol{q}(0)}C$. The latter can e.g. be found by choosing generalised velocities $\boldsymbol{\nu}(0)$ and employing formula (3.5). Obviously, an Euler step $\boldsymbol{q}_1 = h\dot{\boldsymbol{q}}(0)$ does not yield a second configuration that fulfils the constraints. On the other hand, consistent initial momenta can be calculated via the continuous Legendre transform $\boldsymbol{p}(0) = \dfrac{\partial L}{\partial \dot{\boldsymbol{q}}} \in T^*_{\boldsymbol{q}(0)}C$. Finally, setting $\boldsymbol{p}_0^- = \boldsymbol{p}(0)$, one can solve (3.23) together with $\boldsymbol{g}(\boldsymbol{q}_1) = \boldsymbol{0}$ for $\boldsymbol{q}_1 \in C$ and $\boldsymbol{\lambda}_0$. Alternatively, using the discrete null space method, the reduced continuous momenta are given by ${}^{P}\boldsymbol{p}_0^- = \boldsymbol{P}^T(\boldsymbol{q}(0)) \cdot \boldsymbol{p}(0)$. After inserting ${}^{P}\boldsymbol{p}_0^-$ and $\boldsymbol{q}_1 = \boldsymbol{F}_d(\boldsymbol{u}_1, \boldsymbol{q}(0))$ into (3.29), the latter can be solved for $\boldsymbol{u}_1$, then $\boldsymbol{q}_1$ follows by nodal reparametrisation. In this case, the corresponding Lagrange multiplier can be recovered as

$$\boldsymbol{\lambda}_0 = 2\,\boldsymbol{R}_d^T(\boldsymbol{q}(0)) \cdot [\boldsymbol{p}(0) + D_1 L_d(\boldsymbol{q}(0), \boldsymbol{q}_1)]$$

Remark 3.3.8 (Unconstrained systems) *For unconstrained systems, one can simply choose $\boldsymbol{q}_1 \in Q$. Nevertheless, one has to keep in mind that the difference quotient $\dfrac{\boldsymbol{q}_1 - \boldsymbol{q}_0}{h}$ determines the initial kinetic energy of the system. Also here, one can use the continuous initial state to compute $\boldsymbol{q}_1$ from $\boldsymbol{p}_n^- = -D_1 L_d(\boldsymbol{q}_n, \boldsymbol{q}_{n+1})$. Only when no potential is present and the motion is rectilinear, an Euler steps coincides with the calculation of $\boldsymbol{q}_1$ from the discrete Legendre transform.*

3.3.1 Numerical example: mathematical pendulum

As an easy but illustrative example, a two-dimensional ($n = 2$) mathematical pendulum with mass $M = 1$, yielding the 2×2 mass matrix $\boldsymbol{M} = M\boldsymbol{I}_{2\times 2}$, and rod length $l = 1$ is studied. The configuration space is $Q = \mathbb{R}^2$ and the constraint manifold is $C = S^1_l$. First of all, the gravitation is set to zero such that the mass point moves on the unit circle with constant angular velocity. The initial position is $\boldsymbol{q}(0) = [1, 0]^T$ and the initial generalised velocity is $\nu(0) = 1$, thus the total energy of the system is 0.5. The $m = 1$ constraint function, the constraint Jacobian and the null space matrix read

$$g(\boldsymbol{q}) = \frac{1}{2}\left(\boldsymbol{q}^T \cdot \boldsymbol{q} - l^2\right) = 0 \qquad \boldsymbol{G}(\boldsymbol{q}) = \boldsymbol{q}^T \qquad \boldsymbol{P}(\boldsymbol{q}) = \begin{bmatrix} -q_y \\ q_x \end{bmatrix}$$

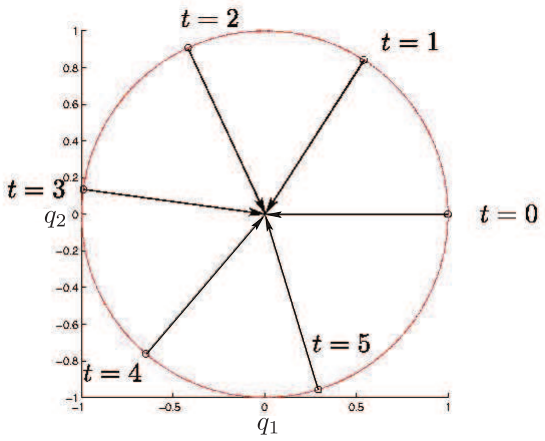

Figure 3.1: Mass point on unit circle: snapshots of the motion and constraint forces ($h = 10^{-1}$).

During the time stepping scheme, they are evaluated at $\boldsymbol{q}_n$. In the time interval $[t_n, t_{n+1}]$, the mass points rotates about the out of plane axis by the angle $u_{n+1} \in \mathbb{R}$, therefore the discrete reparametrisation is given by

$$\boldsymbol{q}_{n+1} = \boldsymbol{F}_d(\boldsymbol{u}_{n+1}, \boldsymbol{q}_n) = \begin{bmatrix} \cos(u_{n+1}) & -\sin(u_{n+1}) \\ \sin(u_{n+1}) & \cos(u_{n+1}) \end{bmatrix} \cdot \boldsymbol{q}_n$$

Using the constrained time stepping scheme (3.13), $n+m = 3$ equations have to be solved for $\boldsymbol{q}_{n+1}$ and λ_n while the number of equations is reduced to one if the discrete null space method with nodal reparametrisation (3.18) is used. Figure 3.1 shows configurations of the motion and the corresponding constraint forces $\boldsymbol{G}^T(\boldsymbol{q}_n) \cdot \boldsymbol{\lambda}_n$ that point towards the centre of the unit circle. The diagram on the left in Figure 3.2 shows the evolution of the discrete energy E_d in the upper graph, calculated in terms of subsequent configurations

$$E_d(\boldsymbol{q}_n, \boldsymbol{q}_{n+1}) = \frac{1}{2} \left(\frac{\boldsymbol{q}_{n+1} - \boldsymbol{q}_n}{h} \right)^T \cdot \boldsymbol{M} \cdot \left(\frac{\boldsymbol{q}_{n+1} - \boldsymbol{q}_n}{h} \right)$$

and the lower graph depicts the discrete Hamiltonian H_d in terms of the momenta as

$$H_d(\boldsymbol{q}_n, \boldsymbol{p}_n) = \frac{1}{2} \boldsymbol{p}_n^T \cdot \boldsymbol{M}^{-1} \cdot \boldsymbol{p}_n$$

Note that the expression for the energy in terms of the momenta exactly preserves the initial energy while that in terms of velocity preserves a value which is slightly different, see Figure 3.2. This indicates that in the presence of constraints, postprocessing steps should involve the momenta obtained by the discrete Legendre transform rather than the velocities.
Furthermore, one can see in Figure 3.1 that besides pointing into the correct direction, the constraint forces do all have the same value $\lambda_n = -1.00251257867$, in particular, λ_0 makes no exception. This is a consequence of the discrete Legendre transform (3.23) being based in the augmented discrete Lagrangian (3.14) (see also Remark 3.3.2).
The right hand diagram in Figure 3.2 reveals that the primary as well as the secondary constraints (3.32), (3.33) are fulfilled exactly in the absence of a potential.

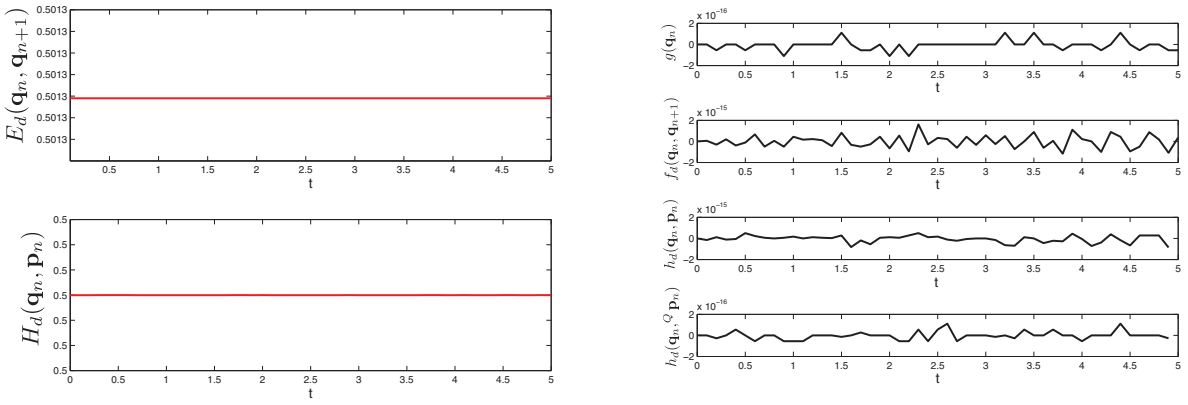

Figure 3.2: Mass point on unit circle: total energy and fulfilment of the constraints on configuration level, on velocity level and on momentum level ($h = 10^{-1}$).

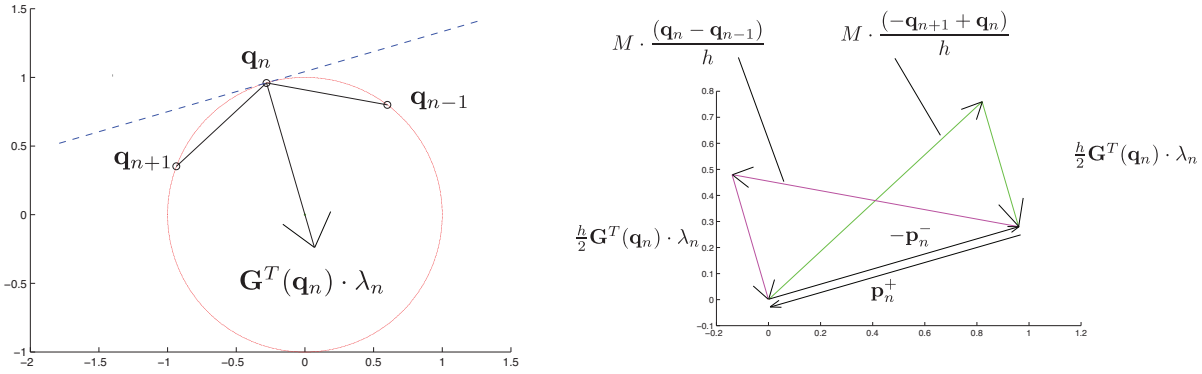

Figure 3.3: Mass point on unit circle: illustration of the discrete Legendre transform and the matching of momenta ($h = 8 \cdot 10^{-1}$).

This is no surprise since one can observe from Figure 3.3 that velocities are tangential at the midpoints and momenta are tangential to the constraint manifold at the configurations themselves. The results obtained using the constrained scheme are indistinguishable from those using the d'Alembert type scheme with nodal reparametrisation.
Secondly, the motion is influenced by the potential $V(\boldsymbol{q}) = (\boldsymbol{M} \cdot \boldsymbol{g})^T \cdot \boldsymbol{q}$ whereby $\boldsymbol{g} = [0, -9.81]^T$. The pendulum is released with no initial velocity from the position $\boldsymbol{q}(0) = [1, 0]^T$. Figure 3.4 shows that the constraint forces again point towards the pendulum's suspension point and their absolute value varies according to the actual configuration.
The energies

$$E_d(\boldsymbol{q}_n, \boldsymbol{q}_{n+1}) = \frac{1}{2}\left(\frac{\boldsymbol{q}_{n+1} - \boldsymbol{q}_n}{h}\right)^T \cdot \boldsymbol{M} \cdot \left(\frac{\boldsymbol{q}_{n+1} - \boldsymbol{q}_n}{h}\right) + V\left(\frac{\boldsymbol{q}_{n+1} + \boldsymbol{q}_n}{2}\right)$$

depicted in the upper graph and

$$H_d(\boldsymbol{q}_n, \boldsymbol{p}_n) = \frac{1}{2}\boldsymbol{p}_n^T \cdot \boldsymbol{M}^{-1} \cdot \boldsymbol{p}_n + V(\boldsymbol{q}_n)$$

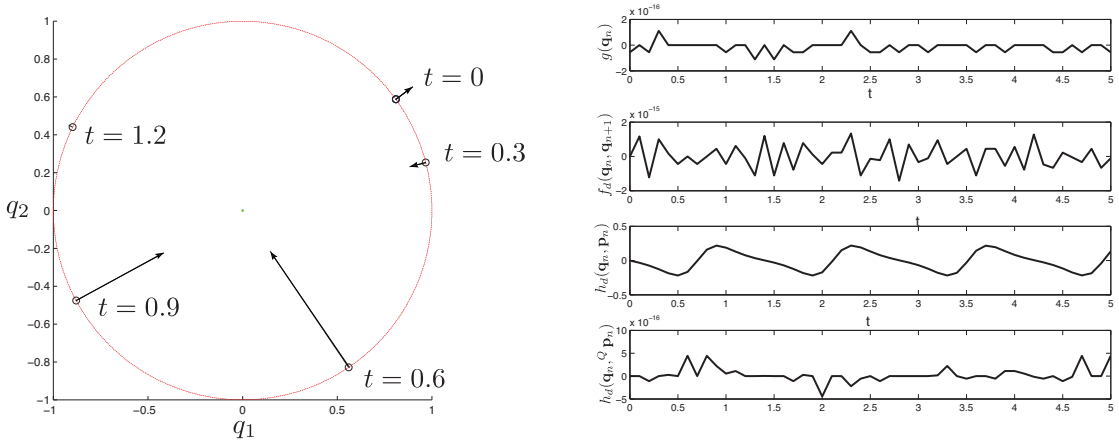

Figure 3.4: Pendulum: snapshots of the motion and constraint forces and fulfilment of constraints on configuration level, on velocity level and on momentum level ($h = 10^{-1}$).

depicted in the lower graph of Figure 3.5 on the left look very much alike, however, the plot of the total energy on a finer scale on the right reveals that H_d oscillates with smaller amplitude than E_d and that deviations occur with a different sign.

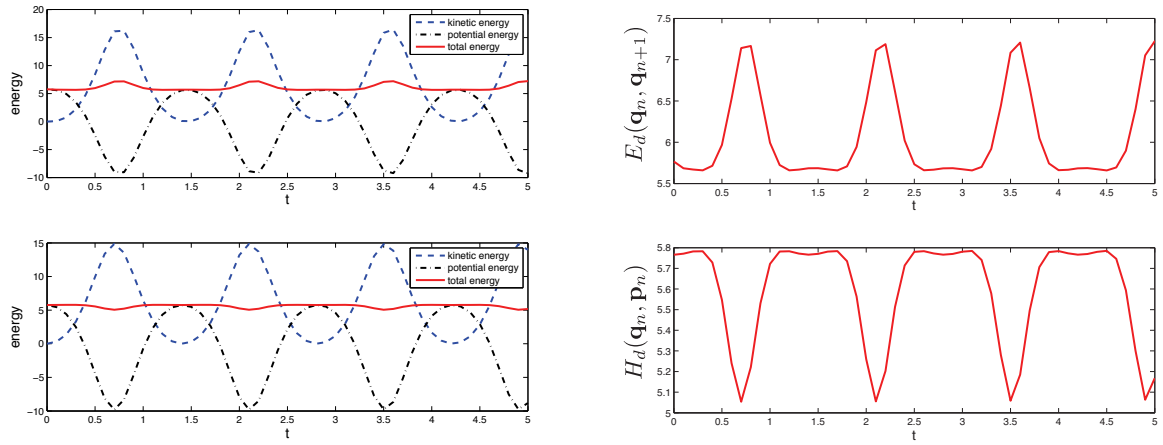

Figure 3.5: Pendulum: energy in terms of $(\boldsymbol{q}_n, \boldsymbol{q}_{n+1})$ and $(\boldsymbol{q}_n, \boldsymbol{p}_n)$ ($h = 10^{-1}$).

In the presence of a potential, the distances between two subsequent configurations are not equal as can be observed from Figure 3.4 and 3.6. It is observable from these pictures that $\boldsymbol{q}_{n+1} - \boldsymbol{q}_n$ is always tangential to the constraint manifold at the midpoint wherefore the constraints on velocity level are fulfilled exactly (see Figure 3.4). However, the momentum vector $\boldsymbol{p}_n$ is not in the direction of the tangent (see Figure 3.6), thus it is not in the null space of the constraint Jacobian and the hidden constraints are not fulfilled. Of course, the projected momenta fulfill them. Despite being not exactly equal, the plots of the evolution of total energy being computed from $\boldsymbol{p}_n$ and ${}^Q\boldsymbol{p}_n$ are indistinguishable, wherefore only one of them is shown in Figure 3.5.

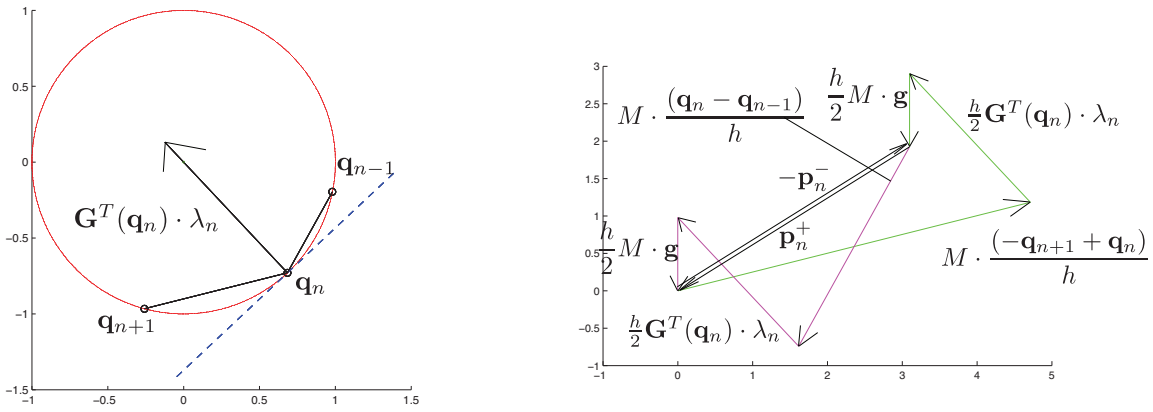

Figure 3.6: Pendulum: illustration of the discrete Legendre transform and the matching of momenta.

3.4 Rigid body dynamics

This work makes use of a constrained formulation of rigid body dynamics [Bets 01b], that directly fits in the framework of DAEs. It circumvents the need to deal with rotational parameters, angular velocities and accelerations in the Lagrangian. This formulation is explained in detail in [Bets 06, Leye 06a] where it is also shown that the reduced equations of motion $(3.6)_1$ represent the well known Newton-Euler equations for the rigid body dynamics. The treatment of rigid bodies as structural elements relies on the kinematic assumptions is illustrated in Figure 3.7 (see [Antm 95]).

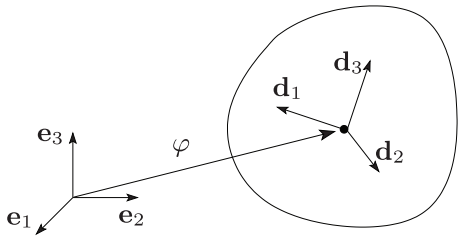

Figure 3.7: Configuration of a rigid body with respect to an orthonormal frame $\{\boldsymbol{e}_I\}$ fixed in space.

The fact that the placement of a material point in the body's configuration $\boldsymbol{X} = X_I \boldsymbol{d}_I \in \mathcal{B} \subset \mathbb{R}^3$ relative to an orthonormal basis $\{\boldsymbol{e}_I\}$ fixed in space can be described as

$$\boldsymbol{x}(\boldsymbol{X}, t) = \boldsymbol{\varphi}(t) + X_I \boldsymbol{d}_I(t) \tag{3.34}$$

is used. Here $X_I \in \mathbb{R}$, $I = 1, 2, 3$ represent coordinates in the body fixed director triad $\{\boldsymbol{d}_I\}$. The time dependent configuration variable of a rigid body

$$\boldsymbol{q}(t) = \begin{bmatrix} \boldsymbol{\varphi}(t) \\ \boldsymbol{d}_1(t) \\ \boldsymbol{d}_2(t) \\ \boldsymbol{d}_3(t) \end{bmatrix} \in \mathbb{R}^{12} \tag{3.35}$$

consists of the placement of the centre of mass $\boldsymbol{\varphi} \in \mathbb{R}^3$ and the directors $\boldsymbol{d}_I \in \mathbb{R}^3, I = 1, 2, 3$ representing the orientation of the rigid body. Due to the body's rigidity, the directors are constrained to stay orthonormal during the motion. Thus one works with the embedding of the constraint manifold $C = \mathbb{R}^3 \times SO(3)$ into the configuration manifold $Q = \mathbb{R}^{12}$. These orthonormality conditions pertaining to the kinematic assumptions of the underlying theory are termed internal constraints. There are $m_{int} = 6$ independent internal constraints for the rigid body with associated constraint functions

$$\boldsymbol{g}_{int}(\boldsymbol{q}) = \begin{bmatrix} \frac{1}{2}[\boldsymbol{d}_1^T \cdot \boldsymbol{d}_1 - 1] \\ \frac{1}{2}[\boldsymbol{d}_2^T \cdot \boldsymbol{d}_2 - 1] \\ \frac{1}{2}[\boldsymbol{d}_3^T \cdot \boldsymbol{d}_3 - 1] \\ \boldsymbol{d}_1^T \cdot \boldsymbol{d}_2 \\ \boldsymbol{d}_2^T \cdot \boldsymbol{d}_3 \\ \boldsymbol{d}_3^T \cdot \boldsymbol{d}_1 \end{bmatrix} \tag{3.36}$$

For simplicity, it is assumed that the axes of the body frame, i.e. the directors, coincide with the principal axes of inertia of the rigid body. Then the body's Euler tensor with respect to the centre of mass can be related to the inertia tensor $\boldsymbol{J}$ via

$$\boldsymbol{E} = \frac{1}{2}(\mathrm{tr}\boldsymbol{J})\boldsymbol{I} - \boldsymbol{J}$$

where $\boldsymbol{I}$ denotes the 3×3 identity matrix. The principal values of the Euler tensor E_I together with the body's total mass M_φ build the rigid body's constant symmetric positive definite mass matrix

$$\boldsymbol{M} = \begin{bmatrix} M_\varphi \boldsymbol{I} & \boldsymbol{0} & \boldsymbol{0} & \boldsymbol{0} \\ \boldsymbol{0} & E_1 \boldsymbol{I} & \boldsymbol{0} & \boldsymbol{0} \\ \boldsymbol{0} & \boldsymbol{0} & E_2 \boldsymbol{I} & \boldsymbol{0} \\ \boldsymbol{0} & \boldsymbol{0} & \boldsymbol{0} & E_3 \boldsymbol{I} \end{bmatrix} \tag{3.37}$$

where $\boldsymbol{0}$ denotes the 3×3 zero matrix. This description of rigid body dynamics has been expatiated in [Bets 06] where also the null space matrix

$$\boldsymbol{P}_{int}(\boldsymbol{q}) = \begin{bmatrix} \boldsymbol{I} & \boldsymbol{0} \\ \boldsymbol{0} & -\widehat{\boldsymbol{d}_1} \\ \boldsymbol{0} & -\widehat{\boldsymbol{d}_2} \\ \boldsymbol{0} & -\widehat{\boldsymbol{d}_3} \end{bmatrix} \tag{3.38}$$

corresponding to the constraints (3.36) has been derived. Here $\widehat{\boldsymbol{a}}$ denotes the skew-symmetric 3×3 matrix with corresponding axial vector $\boldsymbol{a} \in \mathbb{R}^3$. The derivation of the null space matrix in (3.38) makes use of (3.5) and the fact that the independent generalised velocities of a rigid body are the translational velocity $\dot{\boldsymbol{\varphi}} \in \mathbb{R}^3$ and the angular velocity $\boldsymbol{\omega} \in \mathbb{R}^3$. They can be comprised into the twist of the rigid body

$$\boldsymbol{t} = \begin{bmatrix} \dot{\boldsymbol{\varphi}} \\ \boldsymbol{\omega} \end{bmatrix} \tag{3.39}$$

whereupon (3.5) yields the director velocities $\dot{\boldsymbol{d}}_I = \boldsymbol{\omega} \times \boldsymbol{d}_I$ for $I = 1, 2, 3$. When the nodal reparametrisation of unknowns is applied, the configuration of the free rigid body is specified by six unknowns $\boldsymbol{u} = (\boldsymbol{u}_{\varphi_{n+1}}, \boldsymbol{\theta}_{n+1}) \in U \subset \mathbb{R}^3 \times \mathbb{R}^3$, characterising the incremental displacement and incremental rotation, respectively. Accordingly, in the present case the nodal reparametrisation $\boldsymbol{F}_d : U \to C$ introduced in (3.17) assumes the form

$$\boldsymbol{q}_{n+1} = \boldsymbol{F}_d(\boldsymbol{u}_{n+1}, \boldsymbol{q}_n) = \begin{bmatrix} \boldsymbol{\varphi}_n + \boldsymbol{u}_{\varphi_{n+1}} \\ \exp(\widehat{\boldsymbol{\theta}_{n+1}}) \cdot (\boldsymbol{d}_1)_n \\ \exp(\widehat{\boldsymbol{\theta}_{n+1}}) \cdot (\boldsymbol{d}_2)_n \\ \exp(\widehat{\boldsymbol{\theta}_{n+1}}) \cdot (\boldsymbol{d}_3)_n \end{bmatrix} \tag{3.40}$$

where Rodrigues' formula is used to obtain a closed form expression of the exponential map, see e.g. [Mars 94].

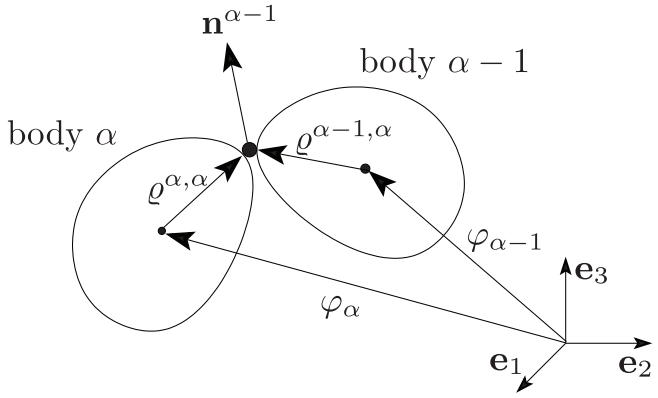

Figure 3.8: α-th pair in a kinematic chain.

3.5 Rigid multibody system dynamics

The constrained description of rigid bodies in terms of directors is exceptionally well suited for the coupling of several bodies in a multibody system. The body fixed directors offer the possibility to specify the coupling of neighbouring bodies by joints constraining their relative motion in a straightforward way. These couplings are termed external constraints. As mentioned in Remark 3.3.4, using a variational integrator based on the augmented Lagrangian (3.14) simplifies the elimination of the constraint forces from the system (compared to the use of certain energy-momentum methods), since a discrete null space matrix can directly be inferred from a continuous one by evaluation at $\boldsymbol{q}_n$. Therefore, this section summarises in a concise way the necessary ingredients for the variational integration of the dynamics of kinematic pairs. The idea of this procedure has been presented already in the framework of energy-momentum conserving time integration in [Bets 06, Leye 06a].
Simple kinematic chains as well as tree structured multibody systems that can be composed by lower kinematic pairs are considered in the sequel. Let a multibody system consist of $N+1$ rigid bodies numbered by $\alpha = 0, \ldots, N$ and N axes $\boldsymbol{n}^0, \ldots \boldsymbol{n}^{N-1}$, where $\boldsymbol{n}^\alpha$ is specified in the α-th body frame by

$$\boldsymbol{n}^\alpha = n_I^\alpha \boldsymbol{d}_I^\alpha$$

The N joints connecting the bodies are numbered by $\alpha = 1, \ldots, N$ and the location of the α-th joint in the $(\alpha-1)$-st and α-th body is characterised by

$$\boldsymbol{\varrho}^{\alpha-1,\alpha} = \varrho_I^{\alpha-1,\alpha} \boldsymbol{d}_I^{\alpha-1} \qquad \boldsymbol{\varrho}^{\alpha,\alpha} = \varrho_I^{\alpha,\alpha} \boldsymbol{d}_I^{\alpha}$$

as depicted schematically for two neighboring links in Figure 3.8. Note that for tree structured multibody systems, the two bodies forming a kinematic pair are not necessarily numbered consecutively.
Assuming that none of the links is fixed in space, the multibody system can be described in terms of $n = 12(N+1)$ redundant coordinates

$$\boldsymbol{q}(t) = \begin{bmatrix} \boldsymbol{q}^0(t) \\ \vdots \\ \boldsymbol{q}^N(t) \end{bmatrix} \tag{3.41}$$

generalising (3.35). The corresponding constant mass matrix is given by

$$\boldsymbol{M} = \begin{bmatrix} \boldsymbol{M}^0 & \boldsymbol{0} & \cdots & \boldsymbol{0} \\ \boldsymbol{0} & \boldsymbol{M}^1 & \cdots & \boldsymbol{0} \\ \vdots & \vdots & \ddots & \vdots \\ \boldsymbol{0} & \boldsymbol{0} & \cdots & \boldsymbol{M}^N \end{bmatrix}$$

where each submatrix $\boldsymbol{M}^\alpha \in \mathbb{R}^{12\times 12}$ coincides with (3.37). The rigidity of each link gives rise to six internal constraints $\boldsymbol{g}^\alpha_{int}(\boldsymbol{q}^\alpha) \in \mathbb{R}^6$ of the form (3.36) for $\alpha = 0, \ldots, N$. They can be combined to the $m_{int} = 6(N+1)$-dimensional vector of internal constraints $\boldsymbol{g}_{int}(\boldsymbol{q})$ and the $m_{int} \times n$ internal constraint Jacobian matrix $\boldsymbol{G}_{int}(\boldsymbol{q})$.
Similar to the case of a single rigid body treated in Section 3.4, the twist of a $N+1$ free rigid bodies reads

$$\boldsymbol{t} = \begin{bmatrix} \boldsymbol{t}^0 \\ \boldsymbol{t}^1 \\ \vdots \\ \boldsymbol{t}^N \end{bmatrix}$$

where, analogous to (3.39), the twist of the α-th body $\boldsymbol{t}^\alpha \in \mathbb{R}^6$, is given by

$$\boldsymbol{t}^\alpha = \begin{bmatrix} \dot{\boldsymbol{\varphi}}^\alpha \\ \boldsymbol{\omega}^\alpha \end{bmatrix} \tag{3.42}$$

Now the redundant velocities $\dot{\boldsymbol{q}} \in \mathbb{R}^{12(N+1)}$ of the multibody system may be expressed as $\dot{\boldsymbol{q}} = \boldsymbol{P}_{int}(\boldsymbol{q}) \cdot \boldsymbol{t}$ where the $12(N+1) \times 6(N+1)$ matrix $\boldsymbol{P}_{int}(\boldsymbol{q})$ is given by

$$\boldsymbol{P}_{int}(\boldsymbol{q}) = \begin{bmatrix} \boldsymbol{P}^0_{int}(\boldsymbol{q}^0) & \boldsymbol{0} & \cdots & \boldsymbol{0} \\ \boldsymbol{0} & \boldsymbol{P}^1_{int}(\boldsymbol{q}^1) & \cdots & \boldsymbol{0} \\ \vdots & \vdots & \ddots & \vdots \\ \boldsymbol{0} & \boldsymbol{0} & \cdots & \boldsymbol{P}^N_{int}(\boldsymbol{q}^N) \end{bmatrix} \tag{3.43}$$

and $\boldsymbol{P}^\alpha_{int}(\boldsymbol{q}^\alpha)$ is the null space matrix associated with the α-th free body, which with regard to (3.38) reads

$$\boldsymbol{P}^\alpha_{int}(\boldsymbol{q}^\alpha) = \begin{bmatrix} \boldsymbol{I} & \boldsymbol{0} \\ \boldsymbol{0} & -\widehat{\boldsymbol{d}^\alpha_1} \\ \boldsymbol{0} & -\widehat{\boldsymbol{d}^\alpha_2} \\ \boldsymbol{0} & -\widehat{\boldsymbol{d}^\alpha_3} \end{bmatrix} \tag{3.44}$$

Note that by design $\boldsymbol{G}_{int}(\boldsymbol{q}) \cdot \boldsymbol{P}_{int}(\boldsymbol{q}) = \boldsymbol{0}$, the $6(N+1) \times 6(N+1)$ zero matrix.

3.5.1 Kinematic pairs

The coupling of two neighbouring links in Figure 3.8 by a specific joint J yields $m^{(J)}_{ext}$ external constraints $\boldsymbol{g}^\alpha_{ext}([\boldsymbol{q}^{\alpha-1}, \boldsymbol{q}^\alpha]^T) \in \mathbb{R}^{m^{(J)}_{ext}}$. In [Bets 06, Leye 06a], lower kinematic pairs $J \in \{R, P, C, S, E\}$, i.e. revolute, prismatic, cylindrical, spherical and planar pairs

have been investigated. Depending on the number of external constraints $m_{ext}^{(J)}$ they give rise to, the degrees of freedom of the relative motion of one body with respect to the other is decreased from 6 to $r^{(J)} = 6 - m_{ext}^{(J)}$. After recalling the derivation of the null space method and nodal reparametrisation for kinematic pairs briefly, details are given for the spherical and the revolute pair only, since these are used in the numerical examples presented in Section 3.5.5 and 3.6.2.
Altogether, $m = m_{int} + m_{ext}$ constraints pertaining to the multibody system and the corresponding constraint Jacobians can be combined to

$$\boldsymbol{g}(\boldsymbol{q}) = \begin{bmatrix} \boldsymbol{g}_{int}(\boldsymbol{q}) \\ \boldsymbol{g}_{ext}(\boldsymbol{q}) \end{bmatrix} \in \mathbb{R}^m \qquad \boldsymbol{G}(\boldsymbol{q}) = \begin{bmatrix} \boldsymbol{G}_{int}(\boldsymbol{q}) \\ \boldsymbol{G}_{ext}(\boldsymbol{q}) \end{bmatrix} \in \mathbb{R}^{m \times n}$$

The remainder of this section presents details of the external constraints caused by lower kinematic pairs (composed of body 1 and body 2) and their treatment in the framework of the discrete null space method. With the null space matrices for kinematic pairs at hand, a generalisation to multibody systems being composed by pairs can be performed easily by respecting formula (3.5).

Null space matrix In a kinematic pair, the motion of the second body with respect to an axis fixed in the first body (or with respect to a plane for the planar pair) can be accounted for by introducing $r^{(J)}$ joint velocities $\boldsymbol{\tau}^{(J)}$. Thus the motion of the kinematic pair can be characterised by the independent generalised velocities $\boldsymbol{\nu}^{(J)} \in \mathbb{R}^{6+r^{(J)}}$ with

$$\boldsymbol{\nu}^{(J)} = \begin{bmatrix} \boldsymbol{t}^1 \\ \boldsymbol{\tau}^{(J)} \end{bmatrix} \tag{3.45}$$

In particular, introducing the $6 \times (6 + r^{(J)})$ matrix $\boldsymbol{P}_{ext}^{2,(J)}(\boldsymbol{q})$, the twist of the second body $\boldsymbol{t}^2 \in \mathbb{R}^6$ can be expressed as

$$\boldsymbol{t}^{2,(J)} = \boldsymbol{P}_{ext}^{2,(J)}(\boldsymbol{q}) \cdot \boldsymbol{\nu}^{(J)}$$

Accordingly, the twist of the kinematic pair can be written in the form

$$\boldsymbol{t}^{(J)} = \boldsymbol{P}_{ext}^{(J)}(\boldsymbol{q}) \cdot \boldsymbol{\nu}^{(J)}$$

with the $12 \times (6 + r^{(J)})$ matrix $\boldsymbol{P}_{ext}^{(J)}(\boldsymbol{q})$, which may be partitioned according to

$$\boldsymbol{P}_{ext}^{(J)}(\boldsymbol{q}) = \begin{bmatrix} \boldsymbol{I}_{6\times 6} & \boldsymbol{0}_{6\times r^{(J)}} \\ \boldsymbol{P}_{ext}^{2,(J)}(\boldsymbol{q}) & \end{bmatrix}$$

Once $\boldsymbol{P}_{ext}^{(J)}(\boldsymbol{q})$ has been established, the total null space matrix pertaining the kinematic pair under consideration can be calculated from

$$\boldsymbol{P}^{(J)}(\boldsymbol{q}) = \boldsymbol{P}_{int}(\boldsymbol{q}) \cdot \boldsymbol{P}_{ext}^{(J)}(\boldsymbol{q}) = \begin{bmatrix} \boldsymbol{P}_{int}^1(\boldsymbol{q}^1) & \boldsymbol{0}_{12\times r^{(J)}} \\ \boldsymbol{P}_{int}^2(\boldsymbol{q}^2) \cdot \boldsymbol{P}_{ext}^{2,(J)}(\boldsymbol{q}) & \end{bmatrix}$$

Remark 3.5.1 (Natural orthogonal complement) *Similar to the procedure for the design of appropriate null space matrices outlined above, the relationship between rigid body twists and joint velocities is used in [Ange 89] to deduce the 'natural orthogonal complement' in the context of simple kinematic chains comprised of elementary kinematic pairs.*

Nodal reparametrisation Corresponding to the independent generalised velocities $\boldsymbol{\nu}^{(J)} \in \mathbb{R}^{6+r^{(J)}}$ introduced in (3.45), the redundant coordinates $\boldsymbol{q} \in \mathbb{R}^{24}$ of each kinematic pair $J \in \{R, P, C, S, E\}$ may be expressed in terms of $6 + r^{(J)}$ independent generalised coordinates. Concerning the reparametrisation of unknowns in the discrete null space method, relationships of the form

$$\boldsymbol{q}_{n+1} = \boldsymbol{F}_d^{(J)}(\boldsymbol{\mu}_{n+1}^{(J)}, \boldsymbol{q}_n) \tag{3.46}$$

are required, where

$$\boldsymbol{\mu}_{n+1}^{(J)} = (\boldsymbol{u}_{\varphi_{n+1}}^1, \boldsymbol{\theta}_{n+1}^1, \boldsymbol{\vartheta}_{n+1}^{(J)}) \in \mathbb{R}^{6+r^{(J)}} \tag{3.47}$$

consists of a minimal number of incremental unknowns in $[t_n, t_{n+1}]$ for a specific kinematic pair. In (3.47), $(\boldsymbol{u}_{\varphi_{n+1}}^1, \boldsymbol{\theta}_{n+1}^1) \in \mathbb{R}^3 \times \mathbb{R}^3$ are incremental displacements and rotations, respectively, associated with the first body (see Section 3.4). Furthermore, $\boldsymbol{\vartheta}_{n+1}^{(J)} \in \mathbb{R}^{r^{(J)}}$ denote incremental unknowns which characterise the configuration of the second body relative to the axis (or plane in case of the E pair) of relative motion fixed in the first body. In view of (3.41), the mapping in (3.46) may be partitioned according to

$$\begin{aligned}
\boldsymbol{q}_{n+1}^1 &= \boldsymbol{F}_d^1(\boldsymbol{u}_{\varphi_{n+1}}^1, \boldsymbol{\theta}_{n+1}^1, \boldsymbol{q}_n^1) \\
\boldsymbol{q}_{n+1}^2 &= \boldsymbol{F}_d^{2,(J)}(\boldsymbol{\mu}_{n+1}^{(J)}, \boldsymbol{q}_n)
\end{aligned}$$

Here, $\boldsymbol{F}_d^1(\boldsymbol{u}_{\varphi_{n+1}}^1, \boldsymbol{\theta}_{n+1}^1, \boldsymbol{q}_n^1)$ is given by (3.40). It thus remains to specify the mapping $\boldsymbol{F}_d^{2,(J)}(\boldsymbol{\mu}_{n+1}^{(J)}, \boldsymbol{q}_n)$ for each kinematic pair under consideration.

3.5.2 Spherical pair

The S pair, shown in Figure 3.9, prevents all relative translation between the two bodies, and thus it gives rise to $m_{ext}^{(S)} = 3$ external constraints of the form

$$\boldsymbol{g}_{ext}^{(S)}(\boldsymbol{q}) = \boldsymbol{\varphi}^2 - \boldsymbol{\varphi}^1 + \boldsymbol{\varrho}^2 - \boldsymbol{\varrho}^1 = \boldsymbol{0} \tag{3.48}$$

While the translational motion of the pair can be accounted for by the velocity of one body's centre of mass, say by $\dot{\boldsymbol{\varphi}}_1$, both bodies can rotate independently. Thus the rotational motion of body 2 is characterised by $r^{(S)} = 3$ degrees of freedom. Specifically, with regard to (3.45) $\boldsymbol{\tau}^{(S)} = \boldsymbol{\omega}^2$, the angular velocity of the second body. Accordingly, in the present case, the vector of independent generalised velocities reads

$$\boldsymbol{\nu}^{(S)} = \begin{bmatrix} \boldsymbol{t}^1 \\ \boldsymbol{\omega}^2 \end{bmatrix} \tag{3.49}$$

Recall that the twist of the first rigid body given in (3.42) consists of its translational velocity $\dot{\boldsymbol{\varphi}}^1$ and its angular velocity $\boldsymbol{\omega}^1$. Taking the time derivative of the external constraints (3.48) and expressing the redundant velocities in terms of the independent generalised velocities (3.49) yields

$$\dot{\boldsymbol{\varphi}}^2 = \dot{\boldsymbol{\varphi}}^1 + \boldsymbol{\omega}^1 \times \boldsymbol{\varrho}^1 - \boldsymbol{\omega}^2 \times \boldsymbol{\varrho}^2$$

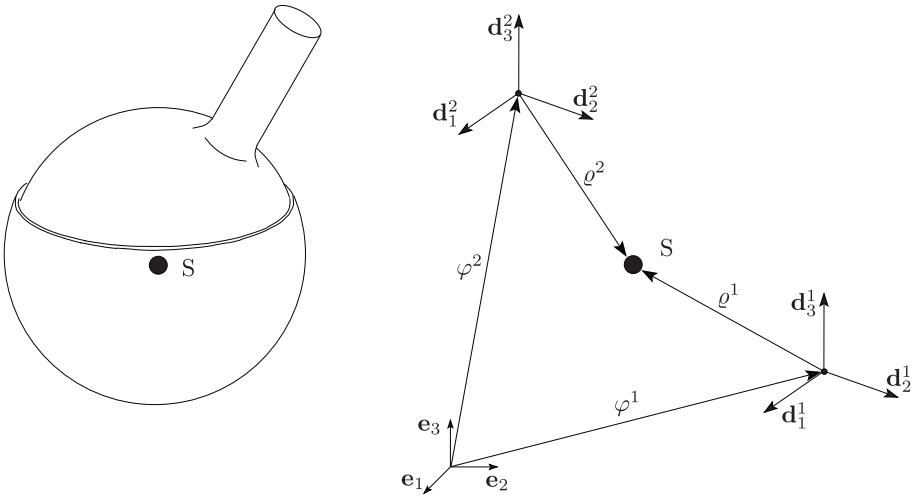

Figure 3.9: Spherical pair.

Now it can be easily deduced from the relationship $\boldsymbol{t}^{2,(S)} = \boldsymbol{P}_{ext}^{2,(S)}(\boldsymbol{q}) \cdot \boldsymbol{\nu}^{(S)}$, that

$$\boldsymbol{P}_{ext}^{2,(S)}(\boldsymbol{q}) = \begin{bmatrix} \boldsymbol{I} & -\widehat{\boldsymbol{\varrho}^1} & \widehat{\boldsymbol{\varrho}^2} \\ \boldsymbol{0} & \boldsymbol{0} & \boldsymbol{I} \end{bmatrix}$$

and finally

$$\boldsymbol{P}_{int}^{2}(\boldsymbol{q}^2) \cdot \boldsymbol{P}_{ext}^{2,(S)}(\boldsymbol{q}) = \begin{bmatrix} \boldsymbol{I} & -\widehat{\boldsymbol{\varrho}^1} & \widehat{\boldsymbol{\varrho}^2} \\ \boldsymbol{0} & \boldsymbol{0} & -\widehat{\boldsymbol{d}_1^2} \\ \boldsymbol{0} & \boldsymbol{0} & -\widehat{\boldsymbol{d}_2^2} \\ \boldsymbol{0} & \boldsymbol{0} & -\widehat{\boldsymbol{d}_3^2} \end{bmatrix}$$

To specify the reduced set of incremental unknowns (3.47) for the S pair, (3.49) induces $\boldsymbol{\vartheta}_{n+1}^{(S)} = \boldsymbol{\theta}_{n+1}^2 \in \mathbb{R}^3$, the incremental rotation vector pertaining to the second body. Then the rotational update of the body frame associated with the second body can be performed according to

$$(\boldsymbol{d}_I^2)_{n+1} = \exp(\widehat{\boldsymbol{\theta}_{n+1}^2}) \cdot (\boldsymbol{d}_I^2)_n$$

Enforcing the external constraints (3.48) at the end of the time step implies

$$\boldsymbol{\varphi}_{n+1}^2 = \boldsymbol{\varphi}_{n+1}^1 + \boldsymbol{\varrho}_{n+1}^1 - \boldsymbol{\varrho}_{n+1}^2 \tag{3.50}$$

Eventually, the last two equations can be used to determine the mapping

$$\boldsymbol{q}_{n+1}^2 = \boldsymbol{F}_d^{2,(S)}(\boldsymbol{\mu}_{n+1}^{(S)}, \boldsymbol{q}_n) = \begin{bmatrix} \boldsymbol{\varphi}_n^1 + \boldsymbol{u}_{\varphi_{n+1}}^1 + \exp(\widehat{\boldsymbol{\theta}_{n+1}^1}) \cdot \boldsymbol{\varrho}_n^1 - \exp(\widehat{\boldsymbol{\theta}_{n+1}^2}) \cdot \boldsymbol{\varrho}_n^2 \\ \exp(\widehat{\boldsymbol{\theta}_{n+1}^2}) \cdot (\boldsymbol{d}_1^2)_n \\ \exp(\widehat{\boldsymbol{\theta}_{n+1}^2}) \cdot (\boldsymbol{d}_2^2)_n \\ \exp(\widehat{\boldsymbol{\theta}_{n+1}^2}) \cdot (\boldsymbol{d}_3^2)_n \end{bmatrix}$$

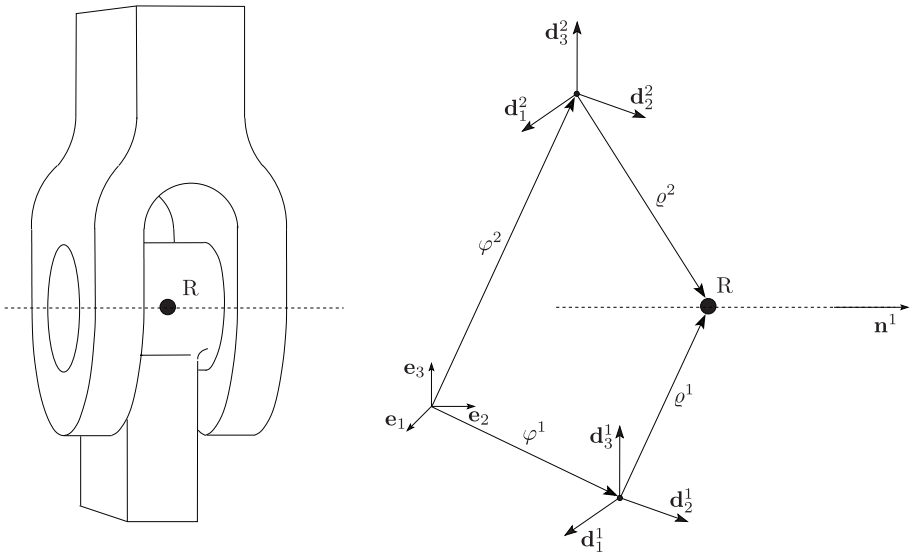

Figure 3.10: Revolute pair.

3.5.3 Revolute pair

For the R pair, shown in Figure 3.10, a unit vector $\boldsymbol{n}^1$ is introduced which is fixed in the first body and specified by constant components n_I^1 with respect to the body frame $\{\boldsymbol{d}_I^1\}$

$$\boldsymbol{n}^1 = n_I^1 \boldsymbol{d}_I^1$$

The R pair entails $m_{ext}^{(R)} = 5$ external constraint functions which may be written in the form

$$\boldsymbol{g}_{ext}^{(R)}(\boldsymbol{q}) = \begin{bmatrix} \boldsymbol{\varphi}^2 - \boldsymbol{\varphi}^1 + \boldsymbol{\varrho}^2 - \boldsymbol{\varrho}^1 \\ (\boldsymbol{n}^1)^T \cdot \boldsymbol{d}_1^2 - \eta_1 \\ (\boldsymbol{n}^1)^T \cdot \boldsymbol{d}_2^2 - \eta_2 \end{bmatrix} \tag{3.51}$$

where $\eta_1, \eta_2 \in \mathbb{R}$ are constant and need be consistent with the initial conditions.

Remark 3.5.2 (Singularities in the constrained formulation) *It is possible that the constraint Jacobian is singular, when the rotation axis $\boldsymbol{n}^1$ is collinear with either of the directors $\boldsymbol{d}_1^2$ or $\boldsymbol{d}_2^2$ used to check the fulfilment of the constraints* (3.51)*. A remedy can be always found in choosing those two directors of $\{\boldsymbol{d}_I^2\}$ that are not collinear with $\boldsymbol{n}^1$, which is always possible.*

The R pair has only one ($r^{(R)} = 1$) relative degree of freedom which characterises the rotational motion of the second body relative to the first one. In particular, the kinematic relationship

$$\boldsymbol{\omega}^2 = \boldsymbol{\omega}^1 + \dot{\theta}^2 \boldsymbol{n}^1$$

holds. The translational velocity of the second body can be expressed as

$$\dot{\boldsymbol{\varphi}}^2 = \dot{\boldsymbol{\varphi}}^1 + \boldsymbol{\omega}^1 \times (\boldsymbol{\varrho}^1 - \boldsymbol{\varrho}^2) + \dot{\theta}^2 \boldsymbol{\varrho}^2 \times \boldsymbol{n}^1$$

giving rise to

$$\boldsymbol{P}_{ext}^{2,(R)}(\boldsymbol{q}) = \begin{bmatrix} \boldsymbol{I} & \widehat{\boldsymbol{\varrho}^2 - \boldsymbol{\varrho}^1} & \boldsymbol{\varrho}^2 \times \boldsymbol{n}^1 \\ \boldsymbol{0} & \boldsymbol{I} & \boldsymbol{n}^1 \end{bmatrix}$$

and

$$\boldsymbol{P}_{int}^{2}(\boldsymbol{q}) \cdot \boldsymbol{P}_{ext}^{2,(R)}(\boldsymbol{q}) = \begin{bmatrix} \boldsymbol{I} & \widehat{\boldsymbol{\varrho}^2 - \boldsymbol{\varrho}^1} & \boldsymbol{\varrho}^2 \times \boldsymbol{n}^1 \\ \boldsymbol{0} & -\widehat{\boldsymbol{d}_1^2} & \boldsymbol{n}^1 \times \boldsymbol{d}_1^2 \\ \boldsymbol{0} & -\widehat{\boldsymbol{d}_2^2} & \boldsymbol{n}^1 \times \boldsymbol{d}_2^2 \\ \boldsymbol{0} & -\widehat{\boldsymbol{d}_3^2} & \boldsymbol{n}^1 \times \boldsymbol{d}_3^2 \end{bmatrix}$$

The incremental rotational motion of the second body relative to the axis $\boldsymbol{n}^1$ is specified by $\vartheta_{n+1}^{(R)} = \theta_{n+1}^2 \in \mathbb{R}$. The mapping $\boldsymbol{F}_d^{2,(R)}(\boldsymbol{\mu}_{n+1}^{(R)}, \boldsymbol{q}_n)$ reads

$$\boldsymbol{q}_{n+1}^2 = \boldsymbol{F}_d^{2,(R)}(\boldsymbol{\mu}_{n+1}^{(R)}, \boldsymbol{q}_n) = \begin{bmatrix} \boldsymbol{\varphi}_n^1 + \boldsymbol{u}_{\varphi_{n+1}}^1 + \exp(\widehat{\boldsymbol{\theta}_{n+1}^1}) \cdot [\boldsymbol{\varrho}_n^1 - \exp\left(\theta_{n+1}^2 \widehat{\boldsymbol{n}_n^1}\right) \cdot \boldsymbol{\varrho}_n^2] \\ \exp(\widehat{\boldsymbol{\theta}_{n+1}^1}) \cdot \exp\left(\theta_{n+1}^2 \widehat{\boldsymbol{n}_n^1}\right) \cdot (\boldsymbol{d}_1^2)_n \\ \exp(\widehat{\boldsymbol{\theta}_{n+1}^1}) \cdot \exp\left(\theta_{n+1}^2 \widehat{\boldsymbol{n}_n^1}\right) \cdot (\boldsymbol{d}_2^2)_n \\ \exp(\widehat{\boldsymbol{\theta}_{n+1}^1}) \cdot \exp\left(\theta_{n+1}^2 \widehat{\boldsymbol{n}_n^1}\right) \cdot (\boldsymbol{d}_3^2)_n \end{bmatrix}$$

3.5.4 Kinematic chains

Combinations of kinematic pairs constitute kinematic chains. Open kinematic chains can be described as a direct extension of lower kinematic pairs. Thereby the null space matrix pertaining to the coupling joints of the open chain $\boldsymbol{P}_{ext}^{o}$ consists of blocks that can be inferred from the null space matrices given for the specific joint connections in [Bets 06, Leye 06a]. The $n \times (n - m^o)$ null space matrix of the open chain is given by

$$\boldsymbol{P}^o(\boldsymbol{q}) = \boldsymbol{P}_{int}(\boldsymbol{q}) \cdot \boldsymbol{P}_{ext}^{o}(\boldsymbol{q})$$

where $\boldsymbol{P}_{int}(\boldsymbol{q})$ is given in (3.43) and $m^o = m_{int} + m_{ext}^o$ is the sum of the number of internal and external constraints.
Unlike for open kinematic chains, where any combination of the lower kinematic pairs can be combined to a movable kinematic chain, the question how many degrees of freedom a closed kinematic chain has, is much more challenging. Generally, it cannot be determined by investigation of the topology of the chain alone (see e.g. [Ange 88]). The investigation of closed kinematic chains usually starts with the associated open kinematic chain, which is subject to m_{ext}^c loop closure conditions

$$\boldsymbol{g}_{ext}^{c}(\boldsymbol{q}) = \boldsymbol{0}$$

connecting the first body with the last one in the open chain. It is reasonable to make use of the null space matrix of the open chain by introduction of the multiplicative decomposition

$$\boldsymbol{P}^c(\boldsymbol{q}) = \boldsymbol{P}^o(\boldsymbol{q}) \cdot \boldsymbol{P}_{ext}^{c}(\boldsymbol{q})$$

For general closed loop systems, it is often hard or even impossible to find an explicit representation of a continuous null space matrix $\boldsymbol{P}^c_{ext}(\boldsymbol{q})$ by analysis of the independent generalised velocities or in terms of a reparametrisation of the constraint manifold. If one succeeds in finding an explicit representation, it can be used in the time stepping schemes (3.16), (3.18). This is in contrast to the treatment of closed kinematic chains in the framework of certain energy-momentum schemes, where highly nonlinear entries in $\boldsymbol{P}^c_{ext}$ make it difficult to infer an explicit representation of a viable discrete null space matrix. In that case one can revert to an implicit representation that has been introduced in [Bets 05] and is also described in detail in [Leye 06a]. According to the procedure described there, an implicit representation of the $(n - m^o) \times (n - m^o - m^c_{ext})$ discrete null space matrix $\boldsymbol{P}^c_{ext}$ can be found using the QR-decomposition of $\left(\boldsymbol{G}^c_{ext}(\boldsymbol{q}_n) \cdot \boldsymbol{P}^o(\boldsymbol{q}_n)\right)^T$ (see also Remark 3.2.2).

Remark 3.5.3 (Computational costs) *The complexity of the QR-decomposition of an $n \times m$ matrix is of the order nm^2. Since the number of constraints in the open kinematic chain $m^o = m_{int} + m^o_{ext}$ is usually higher than the number of closure conditions m^c_{ext}, i.e. $m^o \gg m^c_{ext}$, the decomposition of $\mathbb{R}^{n-m^o}$ relying on the QR-decomposition of the $(n - m^o) \times m^c_{ext}$ matrix $\left(\boldsymbol{G}^c_{ext}(\boldsymbol{q}_n) \cdot \boldsymbol{P}^o(\boldsymbol{q}_n)\right)^T$ is substantially cheaper, than the decomposition of $\mathbb{R}^n$ based on the QR-decomposition of the $n \times m = n \times (m^o + m^c_{ext})$ matrix $\boldsymbol{G}^T(\boldsymbol{q}_n)$.*

3.5.5 Six-body linkage

As an example of a closed loop system, the simple closed kinematic chain consisting of six rigid bodies interconnected by revolute joints in Figure 3.11 is considered.

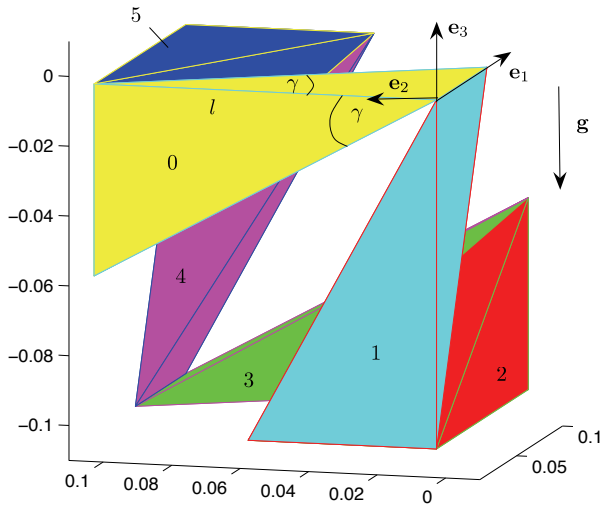

Figure 3.11: Initial configuration of the six-body linkage.

This example has been analysed kinematically in [Witt 77, Lerb 05]. Simulations of the oscillation of the six-body linkage have been reported by [Fuhr 88, Kim 86]. In [Kreu 79], the reduced equation of motion is deduced symbolically and its section wise integration is

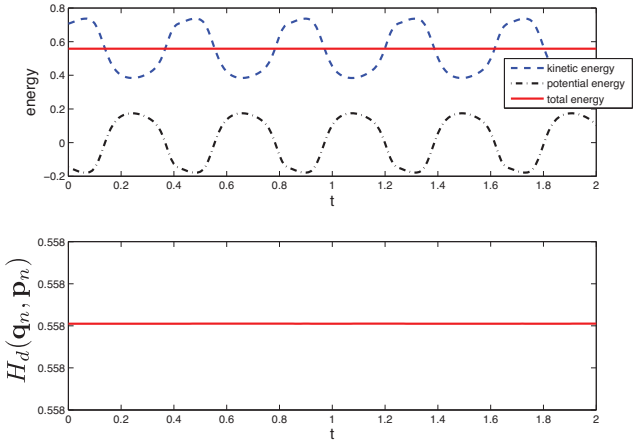

Figure 3.12: Six-body linkage: energy in terms of $(\boldsymbol{q}_n, \boldsymbol{p}_n)$ (energy-momentum scheme, $h = 10^{-2}$).

proposed. Furthermore, the example has been investigated in [Bets 06] in the context of an energy-momentum conserving time-stepping scheme. Note that in contrast to [Bets 06], an explicit representation of $\boldsymbol{P}^c_{ext}$ could be found for the variational integrator. The performance of the variational scheme using Lagrange multipliers (3.13) and that using the discrete null space method (3.18) are compared to the corresponding results from the energy-momentum scheme. The initial configuration of the six-body linkage forms a cube of edge length l (see Figure 3.11).

Numerical results Consistent initial velocities $\dot{\boldsymbol{q}} \in \mathbb{R}^{72}$ follow from $\dot{\boldsymbol{q}} = \boldsymbol{P}^c \dot{\theta}^1$ using the continuous null space matrix. In the numerical example $\dot{\theta}^1 = 30$ has been chosen. Gravity is acting on the system with $g = -9.81$.

Exact algorithmic conservation of the total energy $H_d(\boldsymbol{q}_n, \boldsymbol{p}_n)$ using the energy-momentum scheme in conjunction with the discrete null space method in [Bets 06, Leye 06a] is corroborated in Figure 3.12. In contrast to that, the evolution of the total energies $E_d(\boldsymbol{q}_n, \boldsymbol{q}_{n+1})$ and $H_d(\boldsymbol{q}_n, \boldsymbol{p}_n)$ produced by the variational scheme with the discrete null space method in Figure 3.13 are not exactly conserved. They oscillate whereby the amplitude of the node based discrete Hamiltonian $H_d(\boldsymbol{q}_n, \boldsymbol{p}_n)$ is smaller than that of the interval based discrete energy $E_d(\boldsymbol{q}_n, \boldsymbol{q}_{n+1})$. Both amplitudes get smaller as the time step decreases, see Figure 3.14.

Table 3.1 shows a comparison of the simulations of the motion of the six-body linkage using the constrained scheme and the d'Alembert-type scheme with nodal reparametrisation, respectively for the energy-momentum conserving time-stepping scheme as well as for the variational integrators (3.13) and (3.18). Although a 143-dimensional system of equations has to be solved using the constrained scheme, approximately the same computational time is needed for the setup and solution of the one equation in the d'Alembert-type scheme with nodal reparametrisation for both integrators. The reason is that the computation of the null space matrix at each time step is computational expensive, since it involves the derivative of the relations between the angels. However, the fact that the constraint Jacobian and the null space matrix are evaluated at given configurations $\boldsymbol{q}_n$ only

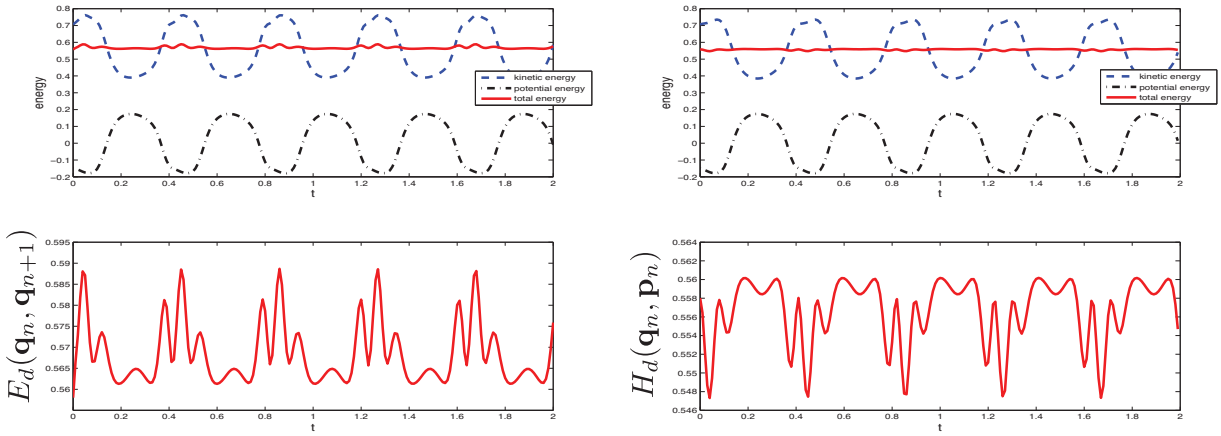

Figure 3.13: Six-body linkage: energy in terms of $(\boldsymbol{q}_n, \boldsymbol{q}_{n+1})$ and $(\boldsymbol{q}_n, \boldsymbol{p}_n)$ (symplectic-momentum scheme, $h = 10^{-2}$).

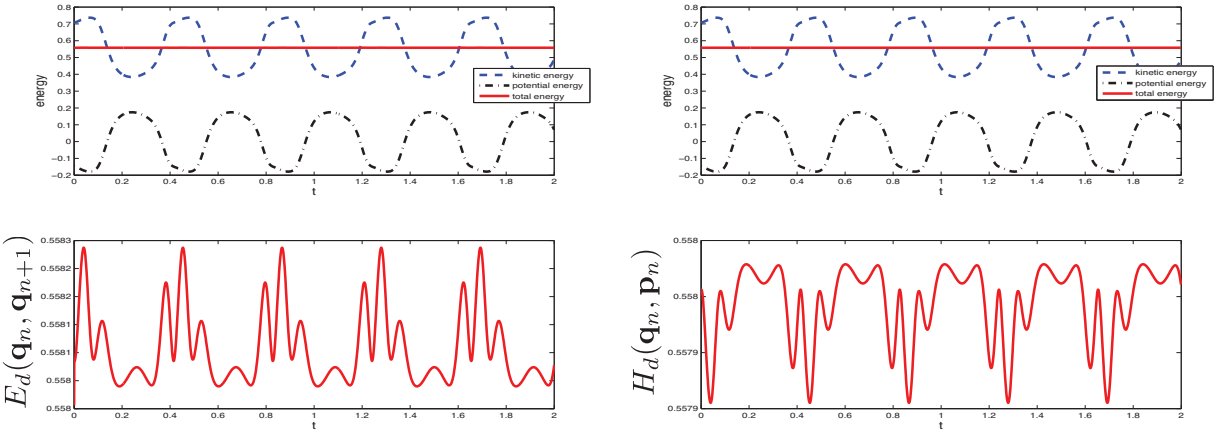

Figure 3.14: Six-body linkage: energy in terms of $(\boldsymbol{q}_n, \boldsymbol{q}_{n+1})$ and $(\boldsymbol{q}_n, \boldsymbol{p}_n)$ (symplectic-momentum scheme, $h = 10^{-3}$).

in the variational scheme causes the linearisation of its nonlinear time stepping equation to involve less terms, wherefore it is about two times faster than the energy-momentum scheme. Concerning the conditioning issue, the advantageous properties of the advocated discrete null space method are obvious in view of Table 3.1.

Table 3.1: Six-body linkage: comparison of energy-momentum scheme and symplectic-momentum scheme in combination with Lagrange multipliers and the discrete null space method with nodal reparametrisation respectively.

	energy-momentum		symplectic-momentum	
	constrained	d'Alembert	constrained	d'Alembert
number of unknowns $n = 72 \quad \tilde{m} = 71$	143	1	143	1
CPU-time	2	2	1	1
condition number				
$h = 10^{-2}$	$1 \cdot 10^{5}$	1	$5 \cdot 10^{4}$	1
$h = 10^{-3}$	$1 \cdot 10^{8}$	1	$3 \cdot 10^{7}$	1
$h = 10^{-4}$	$1 \cdot 10^{11}$	1	$3 \cdot 10^{10}$	1

3.6 Flexible multibody system dynamics

In the context of structural mechanics, rigid bodies can be considered as a special case of geometrically exact beams, for which the spatial distribution is degenerated to a single point. In modelling the sequel, the treatment of beam dynamics in the framework of the discrete null space method and its extension to flexible multibody systems presented in [Leye 08a] will be described briefly.

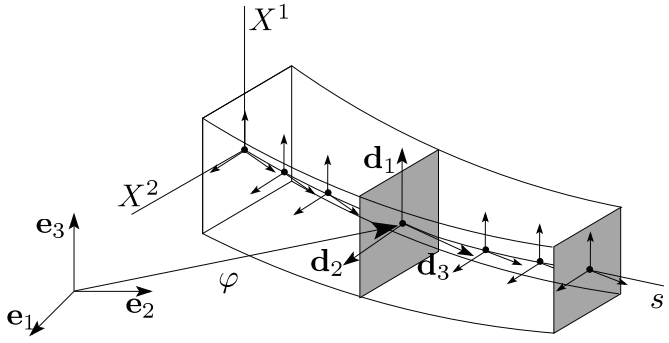

Figure 3.15: Configuration of a spatially discretised beam

3.6.1 Geometrically exact beam dynamics

This description of a 'one-node structure' can be extended easily to the modelling of geometrically exact beams as special Cosserat continuum (see [Antm 95]). The placement of a material point of the beam reads

$$\boldsymbol{x}(X^\kappa, s, t) = \boldsymbol{\varphi}(s, t) + X^\kappa \boldsymbol{d}_\kappa(s, t) \tag{3.52}$$

Here $(X^1, X^2, X^3 = s) \in \mathbb{R}^3$ is a triple of curvilinear coordinates with $s \in [0, L] \subset \mathbb{R}$ being the arc length of the line of centroids $\boldsymbol{\varphi}(s, 0) \in \mathbb{R}^3$ in the reference configuration. $\{\boldsymbol{d}_I\}$ represent an orthonormal triad. The directors $\boldsymbol{d}_\kappa(s, t), \kappa = 1, 2$ span a principal basis of the cross section at s and time t which is accordingly assumed to stay planar. In the reference configuration, $\boldsymbol{d}_3(s, 0)$ is tangent to the central line $\boldsymbol{\varphi}(s, 0)$ but this is not necessary in a deformed configuration. This allowance of transverse shear deformation corresponds to the Timoshenko beam theory (see [Warb 76]). In contrast to kinematic assumption for the placement of a material point in a rigid body (3.34), the sum over the repeated index in (3.52) comprises $\kappa = 1, 2$ and the spatial extension of the beam in the longitudinal direction is accounted for by the parametrisation in s. A spatial discretisation of the beams configuration (see Figure 3.15) in terms of isoparametric finite elements as proposed by [Rome 02, Bets 02b], using one-dimensional Lagrange-type nodal shape functions $N_\alpha(s)$ reads

$$\boldsymbol{q}^h(s, t) = \sum_{\alpha=1}^{n_{node}} N_\alpha(s) \boldsymbol{q}^\alpha(t) \in \mathbb{R}^{12} \tag{3.53}$$

where n_{node} denotes the number of nodes on the central line. This leads to the $12n_{node}$-dimensional semi-discrete configuration vector where the configuration $\boldsymbol{q}^\alpha$, $\alpha = 1, \ldots, n_{node}$ at each node takes the form given in (3.35). Apparently, a spatially discretised beam can be interpreted as a chain of rigid bodies for which the interconnections are prescribed by the connectivity of the spatial finite element method, see e.g. [Hugh 00]. In the sequel, a rigid body is considered as a special semi-discrete beam, consisting of only one node, i.e. $n_{node} = 1$. The internal (orthonormality) constraints $\boldsymbol{g}_{int} : \mathbb{R}^{12n_{node}} \to \mathbb{R}^{m_{int}}$ with $m_{int} = 6n_{node}$, pertaining to the underlying continuous theory are of the form (3.36) for $\alpha = 1, \ldots, n_{node}$.
An inherent property of the interpolation (3.53) is that the constraints on the director triads are relaxed to the nodes of the mesh.

Remark 3.6.1 *Many current semi-discrete beam formulations avoid the introduction of internal constraints by using rotational degrees of freedom, see e.g. [Jele 98, Ibra 98]. However it has been shown by Chrisfield & Jelenic [Cris 99], that the interpolation of non-commutative finite rotations bears the risk of destroying the objectivity of the strain measures in the semi-discrete model. This can be circumvented by the spatial interpolation of the director triad in* (3.53) *as proposed independently in [Rome 02] and [Bets 02b].*

The redundant velocities $\dot{\boldsymbol{q}} \in \mathbb{R}^{12n_{node}}$ of the semi-discrete beam may be expressed in terms of the $6n_{node}$-dimensional twist as $\dot{\boldsymbol{q}} = \boldsymbol{P}_{int}(\boldsymbol{q}) \cdot \boldsymbol{t}$ where the $12n_{node} \times 6n_{node}$ internal null space matrix $\boldsymbol{P}_{int}(\boldsymbol{q})$ has the same block structure as (3.43) with nodal internal null space matrices (3.44) and the nodal reparametrisation $\boldsymbol{q}^\alpha_{n+1} = \boldsymbol{F}_d(\boldsymbol{u}^\alpha_{n+1}, \boldsymbol{q}^\alpha_n)$ assumes the form (3.40).

Differentiating the placement of a material point (3.52) in time, one realises the fact that the beam's kinetic energy is independent of $\dot{\boldsymbol{d}}_3$. Due to that property, the Lagrangian is degenerate and it follows that $\boldsymbol{p}_3 = \partial L / \partial \dot{\boldsymbol{d}}_3 = \boldsymbol{0}$. The kinetic energy is computed in terms of the 9-dimensional reduced velocity $\dot{\bar{\boldsymbol{q}}} = [\dot{\boldsymbol{\varphi}}, \dot{\boldsymbol{d}}_1, \dot{\boldsymbol{d}}_2]^T$ or the reduced conjugate momentum vector $\bar{\boldsymbol{p}} = [\boldsymbol{p}_\varphi, \boldsymbol{p}_1, \boldsymbol{p}_2]^T$ and the non-singular reduced 9×9 mass matrix

$$\bar{\boldsymbol{M}} = \begin{bmatrix} A_\rho \boldsymbol{I} & \boldsymbol{0} & \boldsymbol{0} \\ \boldsymbol{0} & M^1_\rho \boldsymbol{I} & \boldsymbol{0} \\ \boldsymbol{0} & \boldsymbol{0} & M^2_\rho \boldsymbol{I} \end{bmatrix}$$

where $\boldsymbol{I}$ and $\boldsymbol{0}$ denote the 3×3 identity and zero matrices respectively, A_ρ is the mass density per reference length and M^1_ρ, M^2_ρ can be interpreted as principal mass moments of inertia of the cross section. See e.g. [Simo 88, Jele 99, Bets 02b, Leye 06b] for the transition to the mass matrix of the spatially discrete beam formulation.
In a temporally discrete Lagrangian $L_d(\boldsymbol{q}_n, \boldsymbol{q}_{n+1})$ that is formulated in terms of the $12n_{node}$-dimensional configuration vector, a $12n_{node} \times 12n_{node}$ singular mass matrix has to be used whose entries corresponding to $\boldsymbol{d}^\alpha_3$ are zero. Note that this does not lead to problems in determining $\boldsymbol{d}^\alpha_3$ from the equations of motion since of course the stored deformation energy function and the resulting internal forces do depend on $\boldsymbol{d}^\alpha_3$. Therefore one has to be careful in computing only $\bar{\boldsymbol{p}}^\alpha_n$ using the discrete Legendre transforms (3.23), (3.24). The hidden constraints on momentum level (3.33) now read

$$\bar{\boldsymbol{h}}_d(\boldsymbol{q}_n, \bar{\boldsymbol{p}}_n) = \bar{\boldsymbol{G}}(\boldsymbol{q}_n) \cdot \bar{\boldsymbol{M}}^{-1} \cdot \bar{\boldsymbol{p}}_n = \boldsymbol{0}$$

where in $\bar{\boldsymbol{G}}(\boldsymbol{q}_n)$ consists of those rows and columns in $\boldsymbol{G}(\boldsymbol{q}_n)$ that are not related to $\boldsymbol{d}_3^{\alpha}$. Accordingly, in the projected discrete Legendre transforms (3.27), (3.28), the projection reads

$$\bar{\boldsymbol{Q}} = \boldsymbol{I}_{9n_{node}\times 9n_{node}} - \bar{\boldsymbol{G}}^T \cdot \left[\bar{\boldsymbol{G}} \cdot \bar{\boldsymbol{M}}^{-1} \cdot \bar{\boldsymbol{G}}^T\right]^{-1} \bar{\boldsymbol{G}} \cdot \bar{\boldsymbol{M}}^{-1}$$

3.6.2 Flexible multibody systems: the three-bar swing

The description of rigid bodies and spatially discretised geometrically exact beams as constrained continua in terms of the configuration variables given in (3.35) allows their coupling to a multibody system consisting of rigid and elastic components in a systematic way as described in [Leye 08a]. Similar to (3.41), the configuration vectors of all components in the multibody system are combined into the general configuration vector $\boldsymbol{q}(t) \in \mathbb{R}^n$ where n is a 12 times the actual number of spatial nodes present in the semi-discrete system. The external constraints can arise e.g. due to the coupling of neighbouring components by joints, a rigid connection representing the intersection of beams or standard Dirichlet boundary conditions.
As a specific example, the three-bar swing shown in Figure 3.16 is considered. It consists of an elastic beam hinged at its ends to rigid bodies by revolute joints. The rigid bodies are fixed in space by spherical joints. An additional point mass is concentrated at the beams midpoint.

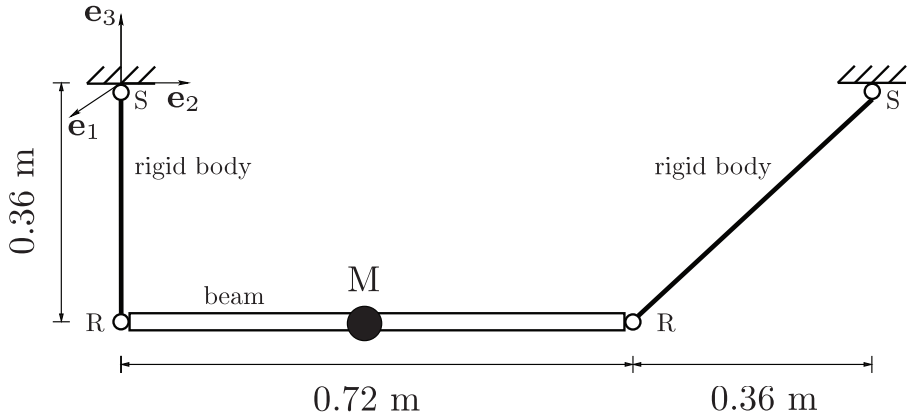

Figure 3.16: Three-bar swing comprising a flexible beam with midspan mass hinged (by revolute joints R) to rigid bodies fixed in space (by spherical joints S).

This example has been investigated previously in [Bauc 95] using an energy-conserving scheme and the generalised-α method. In [Ibra 02] results from an energy-conserving and an energy-decaying scheme are presented. Here, motion and deformation are predicted by the variational integrator and compared to simulations using the energy-momentum scheme based on the discrete derivative [Gonz 96]. Both integrators have been implemented using Lagrange multipliers as well as the discrete null space method to treat the constraints. See [Leye 08a] for a detailed introduction to the energy-momentum conserving integration of flexible multibody dynamics where constraints are treated by the discrete null space method. Besides geometrically exact beams, also shells are treated in [Leye 08a].

A major difference in the performances of the symplectic-momentum conserving variational integrator and the energy-momentum scheme is the capability to simulate stiff problems, i.e. ODEs possessing a wide spectrum of frequencies. While the energy-momentum scheme can reproduce the results in [Bauc 95, Ibra 02] for the set of material parameters used there ($E = 73 \cdot 10^9 \mathrm{N/mm}^2, \nu = 0.3, \rho = 2700 \mathrm{kg/mm}^3$) for a beam of rectangular cross section ($5\mathrm{mm} \times 1\mathrm{mm}$) oriented such that the smaller of the two bending stiffnesses is about the major bending axis, no time step between 10^{-1}s and 10^{-5}s could be found for which the symplectic-momentum scheme was able to simulate a period of motion that includes the 'event X', as it is called in [Bauc 95] in which the rigid link on the right reverses its direction of rotation, causing highly vibratory behaviour of the beam. All attempts resulted in blow up of the total energy at the 'event X'. This indicates in the same direction as the arguments in [Simo 93] saying that temporally unresolved high frequencies are 'seen by the [symplectic] algorithm as infinite sample frequencies leading inevitably to [...] instabilities. In sharp contrast with this result, [...] the energy-momentum conserving scheme remains stable'. However, it is not guaranteed that the energy-momentum scheme distributes the energy over the frequency spectrum correctly. One possibility to deal with a large spectrum of frequencies in a problem is to use asynchronous variational integration [Lew 03a]. The idea is to assign smaller time steps to small elements in the region where high frequency motion is expected. In order not to slow down the overall simulation unnecessarily, larger elements in regions performing slower deformation are integrated using a larger time step. In [Lew 04], this method enables the long term integration of the motion of a long thin helicopter blade for different sets of material parameters ranging from very stiff almost rigid motion to rather soft material behaviour. Another approach to address the capturing of high frequency motion in the overall motion is to approximate the high order modes (e.g. by Fourier transform of the motion of nodes on a fine subgrid as it is done in [Du T 08]) such that one can explicitly calculate a time dependent force that represents the influence of the higher order modes on the main mode.

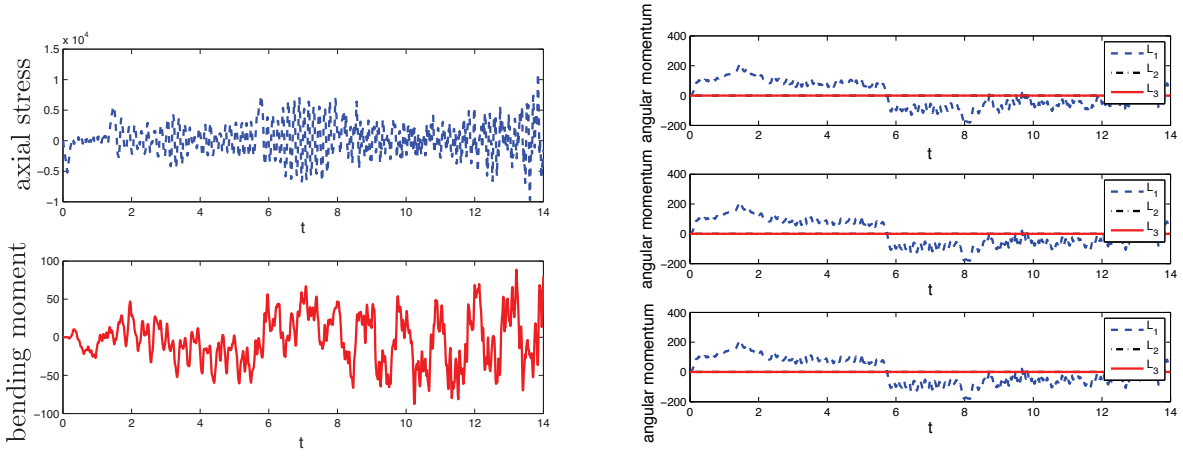

Figure 3.17: Three-bar swing: axial force and bending moment with respect to $\mathbf{e}_1$ in the element to the right of the concentrated mass (left) and components of angular momentum $\boldsymbol{L} = L_I \boldsymbol{e}_I$ in terms of $(\boldsymbol{q}_n, \boldsymbol{q}_{n+1})$, $(\boldsymbol{q}_n, \boldsymbol{p}_n)$ and $(\boldsymbol{q}_n, {}^{Q}\boldsymbol{p}_n)$ (right, top to bottom), (symplectic-momentum scheme, $h = 10^{-2}$).

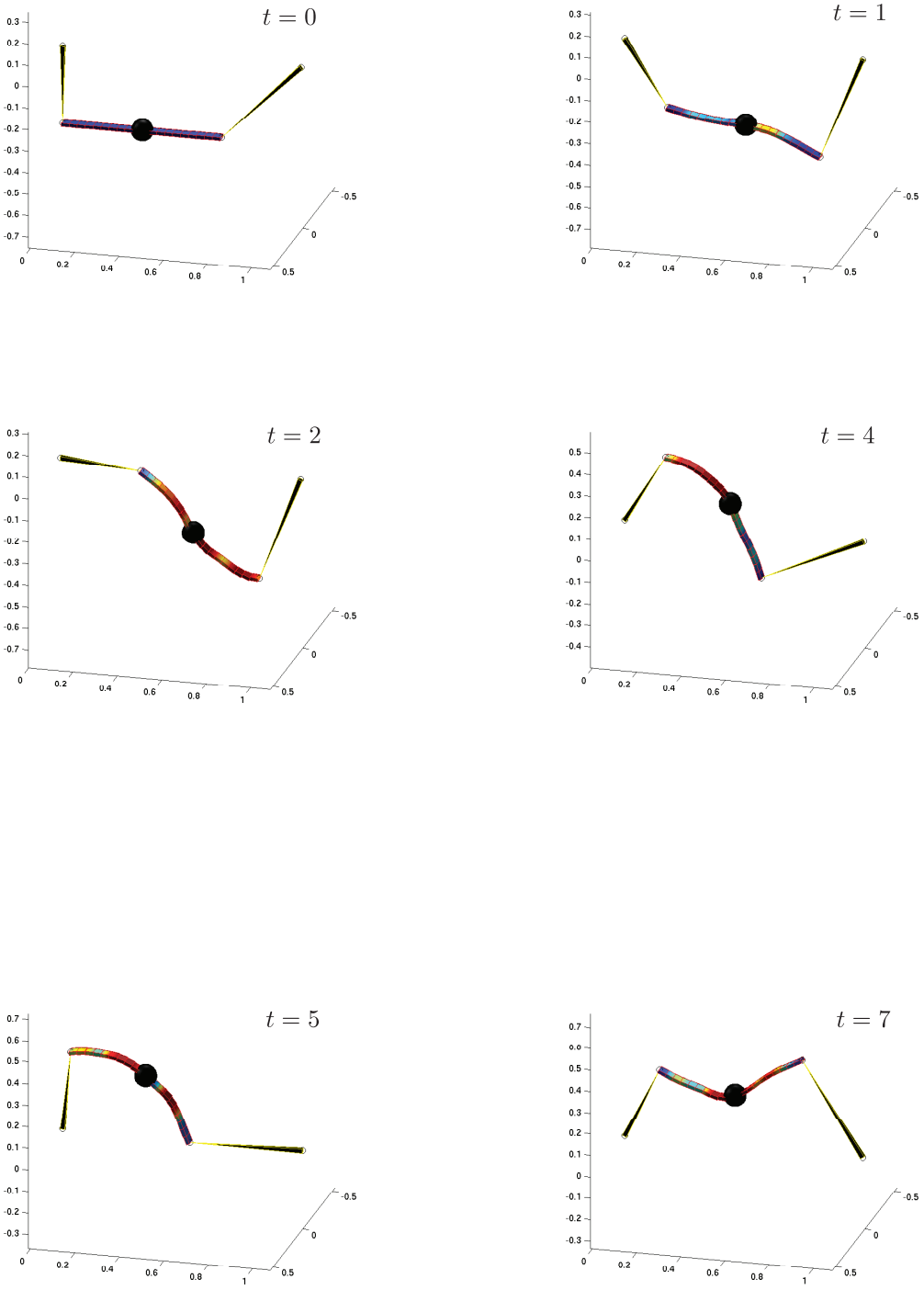

Figure 3.18: Three-bar swing: snapshots of the motion and deformation (symplectic-momentum scheme, $h = 10^{-2}$).

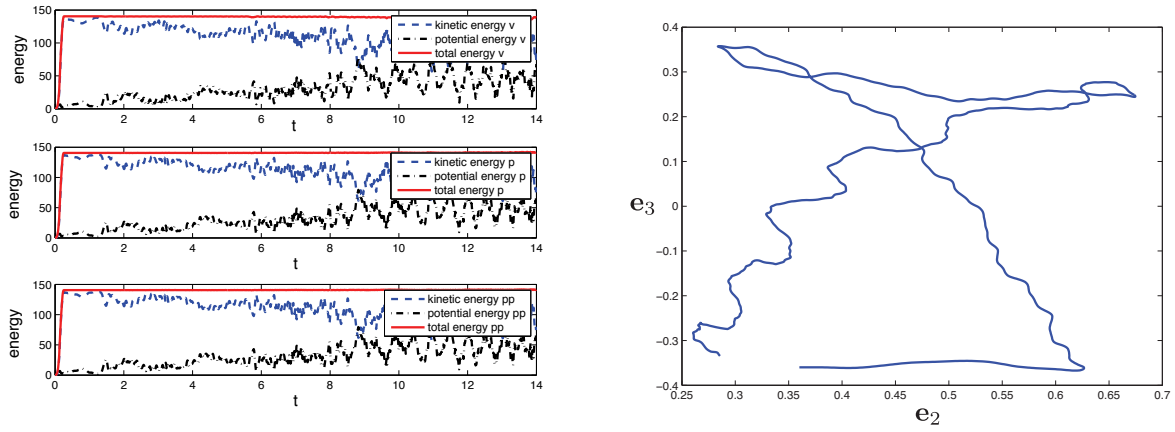

Figure 3.19: Three-bar swing: energy in terms of $(\boldsymbol{q}_n, \boldsymbol{q}_{n+1})$, $(\boldsymbol{q}_n, \boldsymbol{p}_n)$ and $(\boldsymbol{q}_n, {}^{Q}\boldsymbol{p}_n)$ (top to bottom) and orbit of the concentrated mass in the $(\boldsymbol{e}_2, \boldsymbol{e}_3)$-plane (symplectic-momentum scheme, $h = 10^{-2}$).

The simulations described in the sequel use material properties of a less stiff material with higher density. Both rigid bodies' mass is 0.01kg and they have the shape of pyramids with a square ground face of edge length 0.02m and the height of 0.36m and $0.36\sqrt{2}$m, respectively.

A concentrated mass of $M = 5$kg is rigidly connected at the midspan node of the beam, which is discretised by 20 linear finite beam elements. The semi-discrete beam's response to loading is based on hyperelastic Saint Venant-Kirchhoff material with stiffness parameters $GA = 175480.7692$N, $EA = 547500$N, $EI_1 = 114.0625\text{N}\,\text{m}^2$, $EI_2 = 10.2656\text{N}\,\text{m}^2$ and $GJ = 13.7401\text{N}\,\text{m}^2$. The sectional mass properties are $A_\rho = 7500\text{kg/m}$, $M^1_\rho = 1.5625\text{kg}\,\text{m}$ and $M^2_\rho = 0.1406\text{kg}\,\text{m}$. The cross section is oriented such that the smaller of the two bending stiffnesses is with respect to the axis parallel to $\boldsymbol{e}_1$. (Note that the numbering of the bending stiffnesses corresponds to the numbering of the nodal director triads which differ from the inertial frame.) The loading is a triangular pulse in $\boldsymbol{e}_2$-direction which is applied at the midspan mass. It starts with 0N at $t = 0$s, peaks with 10000N at $t = 0.125$s and ends with 0N at $t = 0.25$s.

Snapshots of the motion and deformation are depicted in Figure 3.18. The elements' colours represent a linear interpolation in space of the weighted sum of the resulting axial and shear forces norm and the resulting bending and torsional moments norm. Thereby blue represents zero and red represents 4000. According to the loading in axial direction of the beam, the axial forces dominate the stress resultants therefore the resulting moments have been scaled by a factor of 100.

The evolution of the axial force and bending moments with respect to the axis $\boldsymbol{e}_1$ in the element to the right of the concentrated mass can be observed from the left diagram in Figure 3.17.

This figure shows the high frequency oscillations after the 'event X' at $t \approx 1.4$s. The diagram on the right hand side illustrates that the motion really takes place in the $(\boldsymbol{e}_2, \boldsymbol{e}_3)$-plane (even though a fully three-dimensional model is used) since the only non-zeros component of the angular momentum is that with respect to the out of plane axis $\boldsymbol{e}_1$. The left hand diagram in Figure 3.19 reveals again the good energy behaviour of the

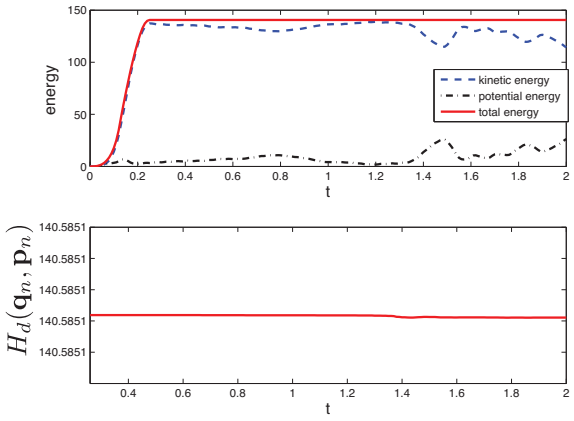

Figure 3.20: Three-bar swing: energy in terms of $(\boldsymbol{q}_n, \boldsymbol{p}_n)$ (energy-momentum scheme, $h = 10^{-2}$).

variational scheme.

The diagram on the right hand side of this figure illustrates the orbit of the concentrated mass in the $(\boldsymbol{e}_2, \boldsymbol{e}_3)$-plane. One can see clearly how the beams deformation superposes the overall rigid motion of the multibody system. Figure 3.20 shows that after the vanishing of the external load, energy is conserved exactly by the energy-momentum scheme.

On the other hand, as expected, the symplectic-momentum scheme shows oscillations with decreasing amplitude for decreasing time steps, see Figure 3.21.

The results presented here have been obtained using the discrete null space method, i.e. (3.16) with reparametrisation has been solved. The Lagrange multiplier method (3.13) has been implemented as well. Since both schemes are equivalent, the resulting diagrams are indistinguishable. However, the constrained scheme (3.13) behaves differently with regard to computational costs and the condition number of the iteration matrix, see Table 3.2. The same problem has also been simulated using the energy-momentum scheme in conjunction with the Lagrange multiplier method and the discrete null space method with

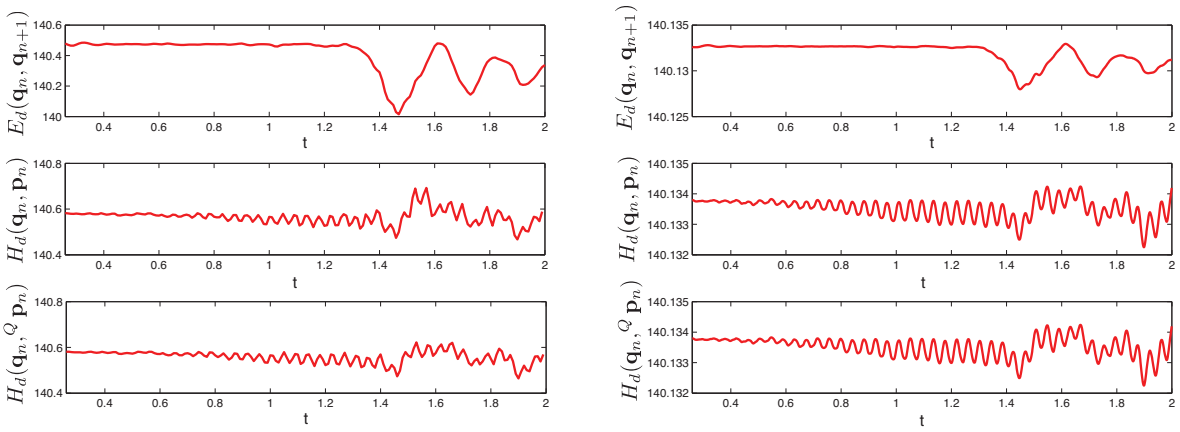

Figure 3.21: Three-bar swing: total energy for $h = 10^{-2}$ (left) and $h = 10^{-3}$ (right), (symplectic-momentum scheme).

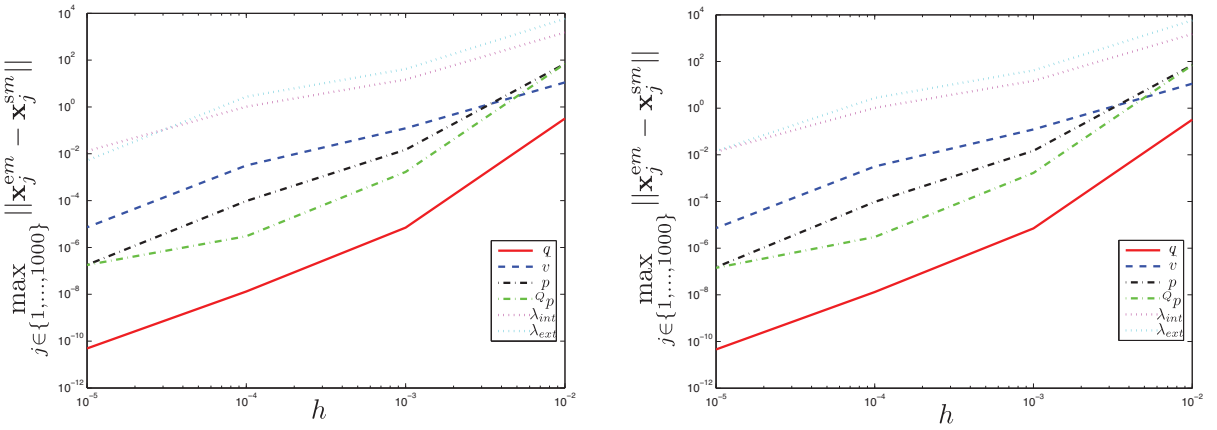

Figure 3.22: Three-bar swing: convergence of trajectories computed by the energy-momentum scheme with Lagrange multipliers (left) and with the discrete null space method with nodal reparametrisation (right) to trajectories obtained by the symplectic-momentum scheme and vice versa.

nodal reparametrisation. Table 3.2 also compares the performance of these simulations to that of the d'Alembert-type symplectic-momentum scheme with reparametrisation based on performing 1000 steps with different time steps. It reveals that the solution of the larger dimensional constrained system takes longer than that of the d'Alembert-type scheme with local reparametrisation with a relatively simple null space matrix. One can also observe that the more complicated linearisation of the energy-momentum scheme requires more computational time. Furthermore, condition numbers increase strongly for decreasing time steps in both Lagrange multiplier schemes while they remain of moderate value in the d'Alembert-type schemes.
Besides the analytical proof of convergence of variational integrators for constrained problems, in Chapter 4 (see also [Schm 09]) the same example is used to verify the second order convergence numerically. A convergence study is not repeated here, however the final Figure 3.22 shows that based on performing 1000 steps with decreasing time steps, the trajectories of the configuration, velocity, conjugate momentum, projected conjugate momentum and Lagrange multipliers corresponding to the internal and external constraints, obtained by the energy-momentum conserving scheme using either Lagrange multipliers or the discrete null space method with nodal reparametrisation, do approach the trajectories predicted by the variational scheme and vice versa.

3.7 Conclusion

The definition of the augmented discrete Lagrangian (3.14) is crucial for the variational integration of constrained systems. It influences the form of the discrete Legendre transform, which is necessary for the consistent initialisation of the simulation as well as for postprocessing steps when evaluating the discrete trajectory.
The discrete null space method, which was originally used with an energy-momentum conserving time stepping scheme, is adapted to the framework of variational integrators.

Table 3.2: Three-bar swing: comparison of energy-momentum scheme and symplectic-momentum scheme in combination with Lagrange multipliers and the discrete null space method with nodal reparametrisation respectively.

	energy-momentum		symplectic-momentum	
	constrained	d'Alembert	constrained	d'Alembert
number of unknowns $n = 276 \quad m = 154$	430	122	430	122
CPU-time	1.5	1.2	1.4	1
condition number				
$h = 10^{-2}$	$2 \cdot 10^{12}$	$4 \cdot 10^{4}$	$6 \cdot 10^{11}$	$5 \cdot 10^{4}$
$h = 10^{-3}$	$2 \cdot 10^{14}$	$9 \cdot 10^{4}$	$5 \cdot 10^{13}$	$9 \cdot 10^{4}$
$h = 10^{-4}$	$2 \cdot 10^{17}$	$2 \cdot 10^{5}$	$5 \cdot 10^{16}$	$2 \cdot 10^{5}$

Specifically, it has been shown that the resulting scheme is not only equivalent to the corresponding scheme using Lagrange multipliers, but that it can be derived itself via a discrete variational principle. The derivation of viable discrete null space matrices is simpler in the variational setting, in fact the discrete null space matrix is simply obtained by evaluating the continuous one at a discrete configuration. This facilitates the solution, in particular the linearisation of the discrete equations leading to reduced computational costs for the example of a closed kinematic chain. On the other hand, for the example of flexible multibody dynamics, the advantageous properties of the smaller dimensional and always well conditioned time stepping scheme emanating from the discrete null space method became obvious for both schemes. However, this example also revealed that the energy-momentum conserving integrator is capable of handling problems with higher stiffness than the variational integrator, although one must say that promising techniques for handling systems with stiff components is still in development in the variational context. Finally it has been demonstrated numerically that the discrete trajectories, velocities, momenta and Lagrange multipliers computed by the energy-momentum scheme approach those of the variational integrator and vice versa for decreasing time steps.
No attempt on comparing the presented constrained formulation of multibody dynamics to other kinematic concepts for tree structured systems as in [Feat 87] or [John 08] is made here. The latter combines a tree representation in generalised coordinates (where parallel linkages and closed loops are handled with holonomic constraints) with a systematic caching technique to reduce computational costs. A comparison is certainly of interest and remains for future work.

4 Γ-convergence of variational integrators for constrained systems

4.1 Introduction

Note that this chapter has been taken from [Schm 09] and the analytical results in Section 4.2 and Section 4.3 have been proofed by the first author Bernd Schmidt.
In this chapter we investigate mechanical systems in an n-dimensional configuration space that can be described by the evolution $t \mapsto u(t) \in \mathbb{R}^n$ with time t subject to the potential $V : \mathbb{R}^n \to \mathbb{R}$ and subject to holonomic constraints. In Lagrangian mechanics the physical trajectories of this motion arise as stationary points of the corresponding action functional I which is the kinetic energy minus the potential energy integrated along the trajectory. In the presence of holonomic constraints, modelled by the so called constraint manifold $M \subset \mathbb{R}^n$, requiring in addition that the trajectories must lie on M gives rise to the constrained functional I_M.
The theory of discrete variational integrators provides approximations of such systems where now time is viewed as a discrete variable. By discretising the action functional I, respectively, I_M, in time, we arrive at discrete action functionals I^h, respectively, I^h_M. (Here we will concentrate on piecewise linear interpolations of trajectories.) A discrete version of Hamilton's principle of stationary action applied to these action sums leads to discrete Euler-Lagrange equations whose solutions should be approximations to the continuum motion. See [Mars 01], and the references therein, for a general introduction to the theory of variational integrators. Many structure preserving integration schemes for ODEs and their properties are investigated extensively in [Hair 04]. Concerning the symplectic integration of constrained systems, work has been done e.g. by [Jay 96, Jay 98, Leim 94, Reic 96] and for nonholonomic systems e.g. by [McLa 06a].
It has been first noticed by Ortiz and Müller that the theory of Γ-convergence is a convenient tool to investigate the convergence properties of the discrete approximations to the continuum trajectories. (For a general introduction to the theory of Γ-convergence see, e.g. [Dal 93].) In [Mull 04] they show that in fact I^h Γ-converges to I and apply this result to prove that discrete stationary points of I^h converge to continuum stationary points of I. Their work as been extended to more general Lagrangians by Maggi and Morini in [Magg 04]. Γ-convergence provides a powerful – albeit as yet not widely used – tool for understanding convergence of dynamical problems. Thus, Γ-convergence establishes convergence of solutions in a global, instead of merely local, sense. In particular, it allows comparing infinite wave trains. This is in contrast to conventional methods of analysis, such as Gronwall's inequality (e. g., [Mars 01]), that merely provide exponentially divergent local bounds on discretisation errors. The global nature of Γ-convergence is in analogy to the traditional phase error analysis of time stepping algorithms for linear systems, which regards convergence in terms of dispersion relations

(e.g. [Bely 76, Bely 81, Hugh 00]). However, Γ-convergence applies to much more general – possibly strongly nonlinear – dynamical systems. The main goal of the present chapter is to extend the results of [Mull 04] to systems with holonomic constraints, i.e. motions confined to lie on some constraint manifold $M \subset \mathbb{R}^n$. (Since our variational integrators will be derived by piecewise linear interpolation of the continuum trajectories, we will assume a linear ambient configuration space $\mathbb{R}^n$ for M.)

In order to describe such constrained systems, it will often be convenient to work in local coordinates for M – at the expense of a more complicated form of the action functional. The resulting Lagrangians are in fact of the form considered in [Magg 04]. However, note carefully that, for the discretised functional I_M^h, the constraint is enforced *only* at the nodal points of the underlying triangulation. As a consequence, our results can not readily be inferred from the corresponding results in [Magg 04].

On the contrary, for constrained systems we will encounter new phenomena which are related to the fact that discrete trajectories are in general non-unique for given initial positions and velocities. The main novelty introduced here for constrained systems is a selection criterion for the physically relevant solutions that firstly guarantees that discrete trajectories do in fact converge to the continuum motion and secondly is satisfied in numerical implementations of the scheme. Analytically, the main difficulty to overcome is to obtain improved regularity for the solutions of the discrete Euler-Lagrange equation. Whereas, e.g. an L^∞-bound on positions implies an L^∞-bound on velocities for unconstrained systems, the corresponding result is no longer true for constrained motions without further assumptions.

We complement our analysis by studying two constrained mechanical system numerically. Holonomic constraints arise naturally in the description of multibody dynamics comprising rigid, elastic or both types of components. As an easy, yet non-trivial, example we will discuss a double spherical pendulum in some detail. In fact, hard configurational constraints are also obtained for systems in the realm of finite elasticity in the limit of singular geometries, e.g. for plates, beams etc. We will also give an example showing that our results apply to (finite element approximations of) multibody dynamical systems comprising rigid and elastic components. Note that in both examples in addition to Theorem 4.3.4 our numerical computations also provide the rate of convergence of the approximating trajectories.

A more precise account of the results in [Mull 04] and of our set up is as follows.

Let $X = L^2_{\mathrm{loc}}(\mathbb{R}, \mathbb{R}^n)$, and by $\mathcal{E}$ denote the collection of all open bounded intervals of $\mathbb{R}$. Note that X is a complete metric space when endowed with the distance function inferred from the seminorms $\|u\|_{L^2((-k,k),\mathbb{R}^n)}$, $k \in \mathbb{N}$.

Let $m > 0$ and $V \in C(\mathbb{R}^n)$. The unconstrained action functional $I : X \times \mathcal{E} \to \mathbb{R} \cup \{\infty\}$ is defined by

$$I(u, A) = \begin{cases} \int_A \frac{m}{2}|\dot{u}(t)|^2 - V(u(t))\,dt, & u \in H^1(A, \mathbb{R}^n), \\ +\infty, & \text{otherwise.} \end{cases}$$

If $V \in C^1$, then the first variation of $I(\cdot, A)$ is given by

$$\begin{aligned}\delta I(u, \varphi, A) &= \left.\frac{d}{dr}\right|_{r=0} I(u + r\varphi) \\ &= \int_A m\dot{u}(t) \cdot \dot{\varphi}(t) - \nabla V(u(t)) \cdot \varphi(t)\, dt\end{aligned}$$

for $u \in H^1(A, \mathbb{R}^n)$, $\varphi \in C_c^\infty(A, \mathbb{R}^n)$. (Note that by the Sobolev embedding theorem $u \in H^1(A, \mathbb{R}^n)$ implies that u – modified on a set of measure zero – lies in $C(\overline{A}, \mathbb{R}^n)$.) We call u a stationary point of I if

$$I(u, A) < \infty \quad \text{and} \quad \delta I(u, \varphi, A) = 0$$

for all $A \in \mathcal{E}$ and $\varphi \in C_c^\infty(A, \mathbb{R}^n)$.
Suppose $\mathcal{T}_h$ is a partition of $\mathbb{R}$ of size h, i.e. $\mathcal{T}_h = \{t_i : i \in \mathbb{Z}\}$ for some $\ldots < t_i < t_{i+1} < \ldots$ such that $|t_{i+1} - t_i| \le h$ and $t_i \to \pm\infty$ if $i \to \pm\infty$. Let X_h be the subspace of X consisting of continuous functions such that $u_{|(t_i, t_{i+1})}$ is affine $\forall t_i \in \mathcal{T}_h$. The unconstrained discrete action functionals $I^h : X \times \mathcal{E} \to \mathbb{R}$ are defined to be

$$I^h(u, A) = \begin{cases} I(u, A), & u \in X_h, \\ +\infty, & \text{otherwise.} \end{cases}$$

The stationary points of I^h are elements u_h of X_h such that

$$I(u_h, A) < \infty \quad \text{and} \quad \delta I(u_h, \varphi_h, A) = 0$$

for all $A \in \mathcal{E}$ and $\varphi_h \in X_h$ with $\varphi_h = 0$ on $\mathbb{R} \setminus A$. Note that if $u_h = 0$ on $\mathbb{R} \setminus A$, then, setting $u_i := u_h(t_i)$, we can write

$$I^h(u_h, A) = \sum_{i=\mu}^{\nu-1} L_d(u_i, u_{i+1})$$

where $(t_\mu, t_\nu) \subset A$ is the maximal subinterval of A compatible with $\mathcal{T}_h$ and

$$L_d(u_i, u_{i+1}) = \frac{m}{2} \frac{(u_{i+1} - u_i)^2}{t_{i+1} - t_i} - \int_{t_i}^{t_{i+1}} V\left(\frac{t_{i+1} - t}{t_{i+1} - t_i} u_i + \frac{t - t_i}{t_{i+1} - t_i} u_{i+1}\right) dt. \tag{4.1}$$

So stationary points of I^h are solutions of the discrete Euler-Lagrange equations

$$\nabla_2 L_d(u_{i-1}, u_i) + \nabla_1 L_d(u_i, u_{i+1}) = 0, \quad i = \mu + 1, \ldots, \nu - 1.$$

The connection between I and its discrete counterpart I^h is studied in detail in [Mull 04], where in particular it is shown that if $V \in C(\mathbb{R}^n)$ with $V(s) \le C(1 + |s|^2)$, then

- for all $A \in \mathcal{E}$, $\Gamma\text{-}\lim_{h\to 0} I^h(\cdot, A) = I(\cdot, A)$ in X. (For the definition of Γ-convergence see below.)
- If in addition $V \in C^2$ with $|\nabla^2 V| \le C$ for some constant C, then sequences of stationary points of I^h that are uniformly bounded converge – up to subsequences – weakly* in $W^{1,\infty}$ to some $u \in W^{2,\infty}$. Moreover the limiting trajectory u is a stationary point of the continuum action functional I.

· If moreover the Fourier transforms $\hat{u}_h$ of u_h are uniformly bounded Radon measures such that no mass leaks to infinity as $h \to 0$, then $\hat{u}_h \to \hat{u}$ as measures in the flat norm.

(Also compare the results in [Magg 04] for more general functionals I.)
Here we are in particular interested in mechanical systems with holonomic constraints. This can be modelled by requiring that $u \in M$ a.e. for some suitable (k-dimensional) sub-manifold M of $\mathbb{R}^n$ (the 'constraint manifold'), which we will assume to be at least of class C^3. Accordingly we define the constrained action functional $I_M : X \times \mathcal{E} \to \mathbb{R} \cup \{\infty\}$ by

$$I_M(u, A) = \begin{cases} I(u, A), & u \in M \text{ a.e. on } A, \\ +\infty, & \text{otherwise.} \end{cases}$$

The constrained discrete action functionals $I_M^h : X \times \mathcal{E} \to \mathbb{R}$ are

$$I_M^h(u, A) = \begin{cases} I^h(u, A), & u(t) \in M \ \forall t \in \mathcal{T}_h \cap A, \\ +\infty, & \text{otherwise.} \end{cases}$$

In view of our examples in the Section 4.4 let us also mention that our results can be extended in a straightforward way to systems with a general positive definite mass matrix $\mathbf{m}$, i.e. whose kinetic energy is given by $\frac{1}{2}\dot{u}^T \mathbf{m}\, \dot{u}$ rather than $\frac{m}{2}|\dot{u}|^2$.
The stationary points for constrained systems are most conveniently defined in terms of local coordinates for M. Suppose $A \in \mathcal{E}$ and u is such that $I_M(u, A)$ is finite. (So in particular u is continuous and takes values in M on A.) Assume that $u(\overline{A})$ is covered by the domain $U \subset M$ of a single coordinate chart, whose inverse is denoted $\psi : \mathbb{R}^k \supset V \to U$. Define the curve $v : A \to V$ by $u_{|A} = \psi \circ v$. Then u is said to be a stationary point of $I_M(\cdot, A)$ if v is a stationary point of

$$\tilde{J}_\psi(v, A) := I(\psi \circ v, A),$$

which means that

$$\delta \tilde{J}_\psi(v, \varphi, A) = \left.\frac{d}{dr}\right|_{r=0} \tilde{J}_\psi(v + r\varphi, A) = 0$$

for all $\varphi \in C_c^\infty(A, \mathbb{R}^k)$. (By density it follows that then in fact $\tilde{J}_\psi(v, \varphi, A) = 0$ for all $\varphi \in H_0^1(A, \mathbb{R}^n)$. It is not hard to see that this, in particular, implies that stationary points of $I_M(\cdot, A)$ are well-defined.) We say that u is a stationary point for I_M if there exists a covering $\mathbb{R} = \bigcup_{i \in I} A_i$ with $A_i \in \mathcal{E}$ such that $u(\overline{A}_i)$ is covered by a single chart and $u_{|A_i}$ is a stationary point of $I(\cdot, A_i)$ for all i. (Using a partition of unity it is again easy to see that this notion is well-defined.)
With the notation introduced above the discrete stationary points of I_M^h are functions in $u_h \in X_h$ such that

$$\nabla_{v_i} \sum_{j=\mu}^{\nu-1} L_d(\psi(v_i), \psi(v_{i+1})) = 0,$$

where $\psi(v_j) = u_j$, or, equivalently,

$$\nabla_2 L_d(u_{i-1}, u_i) + \nabla_1 L_d(u_i, u_{i+1}) \perp T_{u_i} M. \tag{4.2}$$

4.2 Γ-convergence

Our first aim is to obtain a Γ-convergence result for constrained systems. Recall that a sequence of functionals $F^h : Y \to [-\infty, \infty]$ on a metric space Y is said to Γ-converge to the functional F if the following two conditions are satisfied.

(i) ('lim inf-inequality') Whenever $y_h \to y$ in Y then

$$\liminf_{h\to 0} F^h(y_h) \geq F(y).$$

(ii) ('recovery sequence') For each $y \in Y$ there exists a sequence $y_h \to y$ such that

$$\lim_{h\to 0} F^h(y_h) = F(y).$$

Proposition 4.2.1 *Let $V \in C(\mathbb{R}^n)$ with $|V(s)| \leq C(1 + |s|^2)$, $A \in \mathcal{E}$. Then $I_M(\cdot, A)$ Γ-converges in X and*

$$\Gamma - \lim_{h\to 0} I^h_M(\cdot, A) = I_M(\cdot, A).$$

We will first prove two preparatory results. Assume that $V \in C(\mathbb{R}^n)$ with $|V(s)| \leq C(1 + |s|^2)$ throughout this section. Part (i) of the following lemma is contained in [Mull 04].

Lemma 4.2.2 *Let $A \in \mathcal{E}$.*

(i) Then $I(\cdot, A)$ is lower semicontinuous in X and continuous in $H^1(A, \mathbb{R}^n)$.

(ii) If, for a sequence $h_k \to 0$, $u_{h_k} \in X_{h_k}$ converges to u in X such that $I^h_M(u_{h_k}, A)$ is bounded. Then $u \in M$ a.e. on A.

Proof: (i) Due to our assumptions on V, $u \mapsto \int_A V(u)dt$ is continuous on $L^2(A, \mathbb{R}^n)$ and thus on X and on $H^1(A, \mathbb{R}^n)$. Now $u \mapsto \int_A \frac{m}{2}\dot{u}^2 dt$ is clearly continuous on $H^1(A, \mathbb{R}^n)$, which proves the second claim. But it is also lower semicontinuous on $L^2(A, \mathbb{R}^n)$ since it is lower semicontinuous $H^1(A, \mathbb{R}^n)$ with respect to the weak topology and takes the value ∞ outside $H^1(A, \mathbb{R}^n)$.
(ii) $I^h_M(u_{h_k}, A)$ and $\int_A V(u_{h_k})$ being bounded, in fact u_{h_k} converges weakly to u in $H^1(A, \mathbb{R}^n)$. So by the Sobolev embedding theorem we may assume that $u_{h_k} \to u$ uniformly in $C(\overline{A}, \mathbb{R}^n)$. But again because $I^h_M(u_{h_k}, A)$ is bounded, $u_{h_k}(t) \in M$ for all $t \in \mathcal{T}_h \cap A$, and the claim follows. ∎
We will also need the following approximation result extending the corresponding assertion in [Mull 04] to our setting of constrained Lagrangians.

Lemma 4.2.3 *Let $A \in \mathcal{E}$. For every $u \in X$ with $I_M(u, A) < \infty$ there is a sequence $u_h \in X_h$ such that $u_h \to u$ in X and $u_{h|A} \to u_{|A}$ in $H^1(A, \mathbb{R}^n)$ and $u_h(t) \in M$ for all $t \in \mathcal{T}_h \cap A$.*

Proof: Let $A = (a,b)$, $\eta \in C_c^\infty(-1,1)$ be a standard mollifier and define $\eta_h(x) = h^{-1}\eta(x/h)$. Let $N_h w$ denote the nodal interpolation of a function w with respect to the triangulation $\mathcal{T}_h$. By the Sobolev embedding theorem may assume that $u \in C([a,b],\mathbb{R}^n)$. As in [Mull 04] we define approximations of u which are continuous in the slightly larger interval $(a-2h, b+2h)$:

$$v_h(t) = \begin{cases} u(t), & t \le a-2h, \\ u(a), & a-2h < t \le a, \\ u(t), & a < t < b, \\ u(b), & b \le t < b+2h, \\ u(t), & t \ge b+2h. \end{cases}$$

With the help of standard estimates on nodal interpolations and convolutions such as

$$\begin{aligned} &\int_r^s \left|\frac{d}{dt}(N_h w - w)\right|^2 \, dt \le C \int_{r-h}^{s+h} |\dot w|^2 \, dt, \\ &\int_r^s \left|\frac{d}{dt}(N_h w - w)\right|^2 \, dt \le Ch^2 \int_{r-h}^{s+h} |\dot w|^2 \, dt \quad \text{and} \\ &\int_r^s |\eta_h * w|^2 \, dt \le C \int_{r-h}^{s+h} |w|^2 \, dt \end{aligned} \tag{4.3}$$

(which are included here for later reference), in [Mull 04] it is shown that

$$T_h v_h := N_h(\eta_h * v_h) \to u \quad \text{in } X \text{ and in } H^1(A,\mathbb{R}^n). \tag{4.4}$$

Let g, to be specified later, be a positive function on $(0,\infty)$ such that $g(h) \to 0$ as $h \to 0$. Since in a suitable neighbourhood of M the orthogonal projection P of the ambient space $\mathbb{R}^n$ onto M is well defined, smooth and globally Lipschitz, we may choose neighbourhoods U_h of M and $\alpha : M \to (0,\infty)$ such that

$$\{x \in \mathbb{R}^n : \operatorname{dist}(x,M) \le \alpha(Px)g(h)\} \subset U_h \subset \{x \in \mathbb{R}^n : \operatorname{dist}(x,M) < g(h)\},$$

where $\alpha > c(K) > 0$ on compacts $K \subset M$, and functions $p_h \in C^\infty(\mathbb{R}^n,\mathbb{R}^n)$ that are globally Lipschitz continuous with Lipschitz constant independent of h such that $p_h \equiv P$ on U_h and $p_h \equiv \mathrm{id}$ on $\{x \in \mathbb{R}^n : \operatorname{dist}(x,M) \ge g(h)\}$. Set $S_h w := N_h(p_h(\eta_h * w))$. Then $\|T_h v_h - S_h v_h\|_{L^\infty} \le g(h)$ and thus $S_h u \to u$ in X by (4.4).
Since u is uniformly continuous on $[a,b]$, we can choose $g = g(h)$ to be the modulus of continuity of $u_{|\overline{A}}$ such that if $|t-s| \le h$, then $|u(t)-u(s)| \le g(h)$ and $g(h) \to 0$ as $h \to 0$. But then

$$\operatorname{dist}(\eta_h * v_h(t), M) \le Cg^2(h) \tag{4.5}$$

on $[a-2h, b+2h]$. So by construction of p_h we obtain that $p_h(\eta_h * v_h) \in M$ on A, whence indeed $S_h v_h(t) \in M$ for all $t \in \mathcal{T}_h \cap A$.
It remains to estimate

$$\begin{aligned} &\int_a^b \left|\frac{d}{dt}(S_h v_h - T_h v_h)\right|^2 \, dt \le C \int_{a-h}^{b+h} \left|\frac{d}{dt}(p_h(\eta_h * v_h) - \eta_h * v_h\right|^2 \, dt \\ &= C \int_{a-h}^{b+h} |\nabla p_h(\eta_h * v_h) \cdot (\eta_h * \dot v_h) - \eta_h * \dot v_h|^2 \, dt, \end{aligned} \tag{4.6}$$

where the inequality followed from (4.3). Again by (4.5), $\nabla^2 p_h$ is bounded on $[\eta_h * v_h(t), v_h(t)]$ and thus

$$|\nabla p_h(\eta_h * v_h(t)) - \nabla p_h(v_h(t))| \leq Cg(h). \tag{4.7}$$

For $t \in (a-h, b+h)$ we can decompose $\dot{v}_h(s)$ into one part $\dot{v}_h^{\parallel}(s)$ which lies in $T_{v_h(t)}M$ and an orthogonal part $\dot{v}_h^{\perp}(s)$. If $|t-s| \leq h$, then $|\dot{v}_h^{\perp}(s)| \leq Cg(h)|\dot{v}_h^{\parallel}(s)| \leq Cg(h)|\dot{v}_h(s)|$. Noting that $\nabla p_h(v_h(t)) \cdot (\eta_h * \dot{v}_h^{\parallel}(t)) = \eta_h * \dot{v}_h^{\parallel}(t)$ we can estimate

$$\begin{aligned}
&|\nabla p_h(v_h(t)) \cdot (\eta_h * \dot{v}_h(t)) - \eta_h * \dot{v}_h(t)| \\
&= |\nabla p_h(v_h(t)) \cdot (\eta_h * \dot{v}_h^{\perp}(t)) - \eta_h * \dot{v}_h^{\perp}(t)| \leq Cg(h)(\eta_h * |\dot{v}_h|)(t).
\end{aligned}$$

It then follows from (4.3) that

$$\int_{a-h}^{b+h} |\nabla p_h(v_h) \cdot (\eta_h * \dot{v}_h) - \eta_h * \dot{v}_h|^2 \, dt \leq Cg^2(h) \int_{a-2h}^{b+2h} |\dot{v}_h|^2 \, dt. \tag{4.8}$$

Now combine (4.6), (4.7) and (4.8) and apply (4.3) once more to arrive at

$$\begin{aligned}
&\int_a^b \left| \frac{d}{dt}(S_h v_h - T_h v_h) \right|^2 \, dt \\
&\leq Cg^2(h) \int_{a-h}^{b+h} |\eta_h * \dot{v}_h|^2 \, dt + C \int_{a-h}^{b+h} |\nabla p_h(v_h) \cdot (\eta_h * \dot{v}_h) - \eta_h * \dot{v}_h|^2 \, dt \\
&\leq Cg^2(h) \int_{a-2h}^{b+2h} |\dot{v}_h|^2 \, dt \to 0
\end{aligned}$$

as $h \to 0$, whence indeed $S_h v_h \to u$ in $H^1(A, \mathbb{R}^n)$ by (4.4). ∎

Remark 4.2.4 *Note that if $\dot{u}$ is bounded on A, then the above constructed approximations $S_h u_h$ satisfy $\|\frac{d}{dt}(S_h u_h)\|_{L^\infty(A,\mathbb{R}^n)} \leq C\|\dot{u}\|_{L^\infty(A,\mathbb{R}^n)}$.*

With these preparations we can now prove Proposition 4.2.1.

Proof of Proposition 4.2.1: Let $u_h \in X$ be a sequence converging to $u \in X$. We may assume that $I^h(u_h, A)$ is bounded and so $u_h(t) \in M$ for all $t \in \mathcal{T}_h \cap A$ and $u \in M$ on A by Lemma 4.2.2(ii). Since $I^h(\cdot, A) \geq I(\cdot, A)$, we therefore obtain by Lemma 4.2.2(i)

$$\begin{aligned}
\liminf_{h\to 0} I_M^h(u_h, A) &= \liminf_{h\to 0} I^h(u_h, A) \geq \liminf_{h\to 0} I(u_h, A) \\
&\geq I(u, A) = I_M(u, A).
\end{aligned}$$

To provide a recovery sequence for $u \in X$ we may w.l.o.g. assume that $I_M(u, A) < \infty$. By Lemma 4.2.3 there is a sequence $u_h \in X_h$ such that $u_h \to u$ in X, $u_{h|A} \to u_{|A}$ in $H^1(A, \mathbb{R}^n)$ and $u_h(t) \in M$ for all $t \in \mathcal{T}_h \cap A$. So by Lemma 4.2.2(i)

$$I_M^h(u_h, A) = I^h(u_h, A) = I(u_h, A) \to I(u, A) = I_M(u, A).$$

∎

4.3 Stationary points

In this section we will investigate the limiting behaviour of a sequence u_h of stationary points of I_M^h. For the unconstrained case it is shown in [Mull 04] (also compare [Magg 04]) that if u_h is stationary for I^h and $\|u_h\|_{L^\infty}$ is bounded independently of h, then also $\|u\|_{W^{1,\infty}}$ is bounded and in particular – for a subsequence – $u_h \overset{*}{\rightharpoonup} u$ for some u in $W^{1,\infty}$. Furthermore, u is a stationary point of the limiting functional I. We will first see that this does in general not hold for constrained systems. An easy example shows that a sequence of stationary points of I_M^h, although bounded in L^∞, might blow up in $W^{1,\infty}_{\text{loc}}$. However, we will see that this can not happen if the action $I_M^h(u_h, A)$ over bounded intervals A remains bounded. In this case our main result will be that in fact – up to subsequences – u_h converges weakly* in $W^{1,\infty}_{\text{loc}}$ to some stationary point u of I_M.

Example 4.3.1 (Motion on the unit circle.) Suppose $M = S^1 \subset \mathbb{R}^2$. Let $\mathcal{T}_h = h\mathbb{Z}$, $m = 1$ and $V \equiv 0$. Let $u_i = u_h(ih)$. Then u_h is stationary if

$$u_{i+1} + u_{i-1} \in \mathbb{R}u_i.$$

The easiest example is given by $u_i = (\cos(i\alpha), \sin(i\alpha))$ where $\alpha = \alpha(h)$ is fixed. However, if $\alpha \gg h$, then $|\dot{u}| = |2\sin(\frac{\alpha}{2})h^{-1}|$ a.e. diverges.
But even if the trajectory behaves nicely initially, $|\dot{u}|$ does not have to remain bounded. Let, e.g. $u_i = (\cos(ih), \sin(ih))$ if $i \leq 0$. For positive i, set $u_i = (\cos((i-2)h+\pi), \sin((i-2)h+\pi))$ (see Fig. 4.1(b)) or, even worse, $u_i = (-\cos(h), \sin(h)), (-1, 0), (\cos(h), -\sin(h)), (1, 0)$ for $i \equiv 1, 2, 3, 4 \bmod 4$, respectively (see Fig. 4.1(c)). In both cases $\dot{u}$ blows up in $W^{1,\infty}$ (and in H^1).

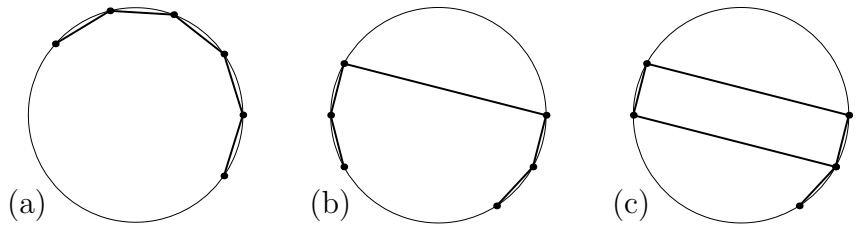

Figure 4.1: Motion on the unit circle.

Lemma 4.3.2 *Suppose $u \in X_h$ is a stationary point of I_M^h, $t^* \in \mathbb{R}$, $c > 0$ is a constant and $V \in C^2$. Let $A = (a, b) \in \mathcal{E}$ be a sufficiently small neighbourhood of t^* and assume that $\|\dot{u}\|_{L^\infty(A,\mathbb{R}^n)} < c$. Then there exists a constant $C > 0$ such that, for all $u' \in X_h$ with $\|\dot{u}'\|_{L^\infty(A,\mathbb{R}^n)} \leq c$, $|u'(a) - u(a)| \leq \varepsilon$ and $|u'(b) - u(b)| \leq \varepsilon$,*

$$I_M^h(u', (a, b)) \geq I_M^h(u, (a, b)) - Ch - C\varepsilon.$$

Proof: For $|b - a|$ small enough, the $c|b - a|$-neighbourhood of $u(A)$ lies in the domain $U \subset M$ of a single chart $\psi^{-1} : U \to V \subset \mathbb{R}^k$, say. For curves v with values in V we define $\tilde{J} = \tilde{J}_\psi = I \circ \psi$ as before and J by

$$J(v) := I(N_h\psi(v)).$$

Note that, for $w \in X_h$ with nodal points $w_i \in M$, the linear interpolation v of $\psi^{-1}(w_i)$ satisfies $J(v) = I^h(w)$ and $\|\dot{v}\|_{L^\infty(A,\mathbb{R}^k)} \le C\|\dot{w}\|_{L^\infty}(A,\mathbb{R}^n)$.
Assume first that $a, b \in \mathcal{T}_h$ and that $u'(a) = u(a)$, $u'(b) = u(b)$. We have to show that, for all piecewise affine functions v' with $\|\dot{v}'\|_{L^\infty} \le c'$ for some constant c',

$$J(v') \ge J(v) - Ch,$$

where $v = N_h\psi^{-1}(u)$.
Let w be a piecewise affine curve with values in V. Then by Taylor expansion

$$\int_a^b |N_h\psi(w) - \psi(w)|^2 \, dt \le Ch^2 \left\| \frac{d}{dt}\psi(w) \right\|^2_{L^\infty(A,\mathbb{R}^k)} \le Ch^2\|\dot{w}\|^2_{L^\infty(A,\mathbb{R}^k)}$$

and

$$\begin{aligned}\int_a^b \left| \frac{d}{dt}\left(N_h\psi(w) - \psi(w)\right)\right|^2 \, dt &\le Ch^2 \left\| \frac{d^2}{dt^2}\psi(w) \right\|^2_{L^\infty(A,\mathbb{R}^k)} \\ = Ch^2 \left\|\nabla^2\psi(w)(\dot{w},\dot{w})\right\|^2_{L^\infty(A,\mathbb{R}^k)} &\le Ch^2\|\dot{w}\|^4_{L^\infty(A,\mathbb{R}^k)},\end{aligned}$$

where $\frac{d^2}{dt^2}\psi(w)$ is the absolute continuous part of the second derivative of $\psi \circ w$. Thus, if $\|\dot{w}\|_{L^\infty(A,\mathbb{R}^k)}$ is bounded,

$$\begin{aligned}|J(w) - \tilde{J}(w)| &= |I(N_h\psi(w)) - I(\psi(w))| \\ &= \left| \int_a^b \left| \frac{d}{dt} N_h\psi(w) \right|^2 - V(N_h\psi(w))\, dt - \int_a^b \left| \frac{d}{dt}\psi(w) \right|^2 - V(\psi(w))\, dt \right| \le Ch.\end{aligned}$$

We also need to compare the first variations of J and $\tilde{J}$. Let φ be a piecewise affine curve such that $w(t) + r\varphi(t) \in V$ for all $t \in [a,b]$, $r \in [0,1]$. Then

$$\begin{aligned}&\frac{d}{dr}\bigg|_{r=0} \tilde{J}(w + r\varphi) \\ &= \int_a^b m\left(\frac{d}{dt}\psi(w)\right) \cdot \left(\frac{d}{dt}(\nabla\psi(w)\varphi)\right) - \nabla V(\psi(w))\nabla\psi(w)\varphi \, dt\end{aligned}$$

and

$$\begin{aligned}&\frac{d}{dr}\bigg|_{r=0} J(w + r\varphi) \\ &= \int_a^b m\left(\frac{d}{dt}N_h\psi(w)\right) \cdot \left(\frac{d}{dt}N_h[\nabla\psi(w)\varphi]\right) - \nabla V(N_h\psi(w))N_h[\nabla\psi(w)\varphi]\, dt.\end{aligned}$$

Now similar estimates as above show that

$$\left| \frac{d}{dr}\bigg|_{r=0} \tilde{J}(w + r\varphi) - \frac{d}{dr}\bigg|_{r=0} J(w + r\varphi) \right| \le Ch.$$

Now choose φ such that $v+\varphi = v'$. Since v is a stationary point of J, the above estimates show that

$$\begin{aligned}
&J(v+\varphi) - J(v) \geq \tilde{J}(v+\varphi) - \tilde{J}(v) - Ch \\
&= \frac{d}{dr}\Big|_{r=0} \tilde{J}(v+r\varphi) + \int_0^1 (1-r)\frac{d^2}{dr^2}\tilde{J}(v+r\varphi)\,dr - Ch \\
&\geq \frac{d}{dr}\Big|_{r=0} J(v+r\varphi) + \int_0^1 (1-r)\frac{d^2}{dr^2}\tilde{J}(v+r\varphi)\,dr - Ch \\
&= \int_0^1 (1-r)\frac{d^2}{dr^2}\tilde{J}(v+r\varphi)\,dr - Ch.
\end{aligned}$$

But

$$\begin{aligned}
&\frac{d^2}{dr^2}\tilde{J}(v+r\varphi) \\
&= \int_a^b m\left|\nabla\psi(v+r\varphi)\cdot\dot{\varphi} + \nabla^2\psi(v+r\varphi)(\dot{v}+r\dot{\varphi},\varphi)\right|^2 \\
&\qquad + m(\nabla\psi(v+r\varphi)\cdot(\dot{v}+r\dot{\varphi}))\cdot \\
&\qquad \cdot(\nabla^3\psi(v+r\varphi)(\dot{v}+r\dot{\varphi},\varphi,\varphi) + 2\nabla^2\psi(v+r\varphi)(\dot{\varphi},\varphi)) \\
&\qquad - \nabla^2 V(\psi(v+r\varphi))(\nabla\psi(v+r\varphi)\cdot\varphi, \nabla\psi(v+r\varphi)\cdot\varphi) \\
&\qquad - \nabla V(\psi(v+r\varphi))\nabla^2\psi(v+r\varphi)(\varphi,\varphi)\,dt \\
&\geq \int_a^b C'|\dot{\varphi}|^2 - C(|\varphi|+|\varphi|^2)|\dot{\varphi}|^2 - C(|\varphi|+|\varphi|^2)|\dot{\varphi}| - C|\varphi|^2\,dt
\end{aligned}$$

for some $C' > 0$.
So if $|b-a|$ and hence $\|\varphi\|_{L^\infty}$ is small enough, we have

$$\begin{aligned}
\frac{d^2}{dr^2}\tilde{J}(v+r\varphi) &\geq \int_a^b \frac{C'}{2}|\dot{\varphi}|^2 - C|\varphi|\cdot|\dot{\varphi}| - C|\varphi|^2\,dt \geq \int_a^b \frac{C'}{4}|\dot{\varphi}|^2 - C|\varphi|^2\,dt \\
&\geq \int_a^b \frac{C'\pi^2}{4|b-a|^2}|\varphi|^2 - C|\varphi|^2\,dt \geq 0
\end{aligned}$$

by Poncaré's inequality, which concludes the first part of the proof.
Now in the general case we can choose a maximal interval $(a_h, b_h) \subset (a,b)$ compatible with $\mathcal{T}_h$ and an affine function l_h such that $v'(a_h) + l_h(a_h) = v(a_h)$, $v'(b_h) + l_h(b_h) = v(b_h)$. Then $\|l_h\|_{W^{1,\infty}} \leq C(\varepsilon + h)$ and so $|J(v'+l_h,(a_h,b_h)) - J(v',(a_h,b_h))| \leq C(\varepsilon+h)$. By our bounds on v' and v we also have

$$|J(v',(a_h,b_h)) - J(v',(a,b))| + |J(v,(a_h,b_h)) - J(v,(a,b))| \leq Ch.$$

So by the first part of the proof we obtain

$$\begin{aligned}
&J(v',(a,b)) \geq J(v',(a_h,b_h)) - Ch \geq J(v'+l_h,(a_h,b_h)) - Ch - C\varepsilon \\
&\geq J(v,(a_h,b_h)) - Ch - C\varepsilon \geq J(v,(a,b) - Ch - C\varepsilon.
\end{aligned}$$

■

We now investigate the limiting behaviour of a sequence u_h of stationary points of I_M^h. Assuming that (u_h) is locally bounded we clearly have that – for a subsequence – $u_h \overset{*}{\rightharpoonup} u$

in $L^\infty_{\rm loc}$ for some u. However, as seen in Example 4.3.1, in general the limit u does not even have to be continuous or to lie on the constraint manifold M. Note that in all these cases the discrete action functional $I^h_M(u_h, A)$ blows up as $h \to 0$ even over bounded intervals A. To avoid such pathological limiting behaviour we will assume that action $I^h_M(u_h, A)$ remains bounded for each $A \in \mathcal{E}$. Then we can in fact prove a positive result:

Lemma 4.3.3 *Let $V \in C^1$ such that $|V(s)| \le C(1+|s|^2)$ and suppose that u_h is a sequence of stationary points for I^h_M such that $|u_h(0)|$ and, for each $A \in \mathcal{E}$, $I^h_M(u_h, A)$ is bounded. Then u_h is bounded in $W^{1,\infty}_{\rm loc}(\mathbb{R}, \mathbb{R}^n)$.*

Proof: Let $a < b$. Using the elementary bounds

$$\|u\|_{L^2((a,b),\mathbb{R}^n)} \le \sqrt{b-a}|u(a)| + (b-a)\|\dot u\|_{L^2((a,b),\mathbb{R}^n)} \quad \text{and}$$
$$|u(t)| \le \sqrt{1+b-a}\sqrt{|u(a)|^2 + \|\dot u\|^2_{L^2((a,b),\mathbb{R}^n)}},\ t \in [a,b],$$

we see that

$$|u(t)| \le 2\sqrt{|u(a)|^2 + \frac{1}{m} I(u,(a,b))}$$

for $t \in [a,b]$, whenever $b-a$ is so small that $8(1+C)(b-a) \le m$ and $(1+b-a)(m + 8(b-a)) \le 4m$. An analogous inequality holds with the roles of a and b interchanged. So inductively we see that (u_h) is bounded in $L^\infty_{\rm loc}(\mathbb{R}, \mathbb{R}^n)$ and hence, by boundedness of the actions, in $H^1_{\rm loc}(\mathbb{R}, \mathbb{R}^n)$. In particular, a suitable subsequence converges to some continuous u uniformly on compact subsets of $\mathbb{R}$.
Let $A = (a,b) \in \mathcal{E}$ and cover a neighbourhood of $u([a,b])$ with finitely many domains $U_1, \dots, U_N \subset M$ such that on each U_j

$$|y-x| \le |P_x(y-x)| + C'|P_x(y-x)|^3 \quad \forall x, y \in U_j,$$

where P_x is the projection onto T_xM. The discrete Euler-Lagrange equations yield

$$P_{u_i}\Bigg[m\left(\frac{u_{i+1}-u_i}{t_{i+1}-t_i} - \frac{u_i - u_{i-1}}{t_i - t_{i-1}}\right) + \int_{t_i}^{t_{i+1}} \nabla V(u_h(t)) \frac{t_{i+1}-t}{t_{i+1}-t_i}\,dt + \int_{t_{i-1}}^{t_i} \nabla V(u_h(t)) \frac{t-t_{i-1}}{t_i - t_{i-1}}\,dt\Bigg] = 0$$

and so

$$\left|P_{u_i}\left(\frac{u_{i+1}-u_i}{t_{i+1}-t_i} - \frac{u_i-u_{i-1}}{t_i-t_{i-1}}\right)\right| \le C|t_{i+1}-t_{i-1}|.$$

Now if h is small enough, then for every i, the points u_{i-1}, u_i and u_{i+1} lie in a single domain U_j, say. But then

$$|u_{i+1}-u_i| \le |P_{u_i}(u_{i+1}-u_i)| + C'|P_{u_i}(u_{i+1}-u_i)|^3$$

and thus

$$\begin{aligned}\left|\frac{u_{i+1}-u_i}{t_{i+1}-t_i}\right| \le{}& \left|\frac{u_i-u_{i-1}}{t_i-t_{i-1}}\right| + C(t_{i+1}-t_{i-1}) \\ &+ C'(t_{i+1}-t_i)^2\left(\left|\frac{u_i-u_{i-1}}{t_i-t_{i-1}}\right| + C(t_{i+1}-t_{i-1})\right)^3.\end{aligned} \tag{4.9}$$

Since $\|\dot{u}_h\|_{L^2(A,\mathbb{R}^n)}$ is bounded, there is a constant c, independent of h, such that $\left|\frac{u_{i_0}-u_{i_0-1}}{t_{i_0}-t_{i_0-1}}\right| \leq c$ for some $i_0 = i_0(h)$ with $t_{i_0} \in A$. Set $\gamma_i := \left|\frac{u_i-u_{i-1}}{t_i-t_{i-1}}\right|$, $f_i := C(t_i - t_{i-2})$, $g_i := C'(t_i - t_{i-1})^2$. Then (4.9) reads

$$\gamma_{i+1} \leq \gamma_i + f_{i+1} + g_{i+1}(\gamma_i + f_{i+1})^3, \quad \gamma_{i_0} \leq c.$$

For $i \geq i_0$ with $t_i \leq b + h$ we let

$$F_i = \sum_{j=i_0+1}^{i} f_j \quad \text{and} \quad G_i = \sum_{j=i_0+1}^{i} g_j$$

and claim that, for small h,

$$\gamma_i \leq c + F_i + G_i(c + F_i + 1)^3. \tag{4.10}$$

This can be easily seen by induction on i. The case $i = i_0$ is clear. If (4.10) holds for $i \geq i_0$, then

$$\begin{aligned}
\gamma_{i+1} &\leq \gamma_i + f_{i+1} + g_{i+1}(\gamma_i + f_{i+1})^3 \\
&\leq c + F_{i+1} + G_i(c + F_i + 1)^3 + g_{i+1}\Big(c + F_{i+1} + G_i(c + F_i + 1)^3\Big)^3 \\
&\overset{!}{\leq} c + F_{i+1} + G_{i+1}(c + F_{i+1} + 1)^3,
\end{aligned}$$

and the last inequality follows if

$$g_{i+1}\Big(c + F_{i+1} + G_i(c + F_i + 1)^3\Big)^3 \leq g_{i+1}(c + F_{i+1} + 1)^3,$$

i.e. if $G_i(c + F_i + 1)^3 \leq 1$. But this is satisfied for small h because

$$F_i = C \sum_{j=i_0+1}^{i} (t_j - t_{j-2}) = C(t_i + t_{i-1} - t_{i_0} - t_{i_0-1}) \leq C(b - a + 2h) \tag{4.11}$$

and

$$\begin{aligned}
G_i &= C' \sum_{j=i_0+1}^{i} (t_j - t_{j-1})^2 \leq C' \max_{i_0+1 \leq j \leq i} (t_j - t_{j-1}) \cdot \sum_{j=i_0+1}^{i} (t_j - t_{j-1}) \\
&\leq C' h(b - a + h).
\end{aligned} \tag{4.12}$$

Now applying (4.11) and (4.12) to (4.10), we see that in fact $|\dot{u}_h| \leq C$ on $[t_{i_0-1}, b]$. A similar argument yields that $|\dot{u}_h|$ is bounded on $[a, t_{i_0}]$, too, which concludes the proof. ∎
We are now in a position to state and prove our main result on the limiting behaviour of a sequence of discrete trajectories. Note, in particular, that we also have strong convergence of the velocities.

Theorem 4.3.4 *Assume that $V \in C^2$ satisfies $|V(s)| \leq C(1 + |s|^2)$. Suppose u_h is a sequence of stationary points for I_M^h such that $|u_h(0)|$ and $I_M^h(u_h, A)$ are bounded uniformly in h for all $A \in \mathcal{E}$. Then there exists a subsequence such that $u_h \overset{*}{\rightharpoonup} u$ in $W^{1,\infty}_{\mathrm{loc}}(\mathbb{R}, \mathbb{R}^n)$, $u_h \to u$ in $W^{1,p}_{\mathrm{loc}}(\mathbb{R}, \mathbb{R}^n)$ for all $1 \leq p < \infty$ and u is a stationary point of I_M.*

Proof: By Lemma 4.3.3, (u_h) is weak*-precompact in $W^{1,\infty}_{\mathrm{loc}}(\mathbb{R},\mathbb{R}^n)$, so it has a convergent subsequence (not relabelled) $u_h \overset{*}{\rightharpoonup} u$ (and in particular $u_h \to u$ uniformly on compact subsets of $\mathbb{R}$). Let $A \in \mathcal{E}$. By Proposition 4.2.1

$$\infty > \liminf_{h\to 0} I^h_M(u_h, A) \geq I_M(u, A).$$

In order to prove that u is a stationary point of I_M we will show that, for every $t^* \in \mathbb{R}$, u is in fact a $W^{1,\infty}$-local minimiser of $I_M(\cdot, A)$ with respect to its own boundary values on A whenever $A = (a, b)$ is a sufficiently small neighbourhood of t^*. By density this implies that u is a stationary point of $I_M(\cdot, A)$.
Let $\tilde{u}$ be a curve with $\tilde{u}(a) = u(a)$, $\tilde{u}(b) = u(b)$ and $\|\tilde{u} - u\|_{W^{1,\infty}(A)}$ sufficiently small. Choose a recovery sequence $\tilde{u}_h$ for $\tilde{u}$ as in the proof of Proposition 4.2.1 such that $\tilde{u}_h \to \tilde{u}$ uniformly on $\overline{A}$. Note that by Remark 4.2.4 we may assume that $\|\dot{\tilde{u}}_h\|_{L^\infty(A,\mathbb{R}^n)}$ is bounded independently of h. Since $u_h \to u$ and $\tilde{u}_h \to \tilde{u}$ uniformly on $\overline{A}$,

$$|u(a) - \tilde{u}(a)|, |u(b) - \tilde{u}(b)| \leq \varepsilon(h)$$

for some $\varepsilon(h) \to 0$ as $h \to 0$. But then, if $|b - a|$ is sufficiently small, we obtain from Lemma 4.3.2

$$\begin{aligned} I_M(\tilde{u}, A) &= \lim_{h\to 0} I^h_M(\tilde{u}_h, A) \geq \limsup_{h\to 0} \left(I^h_M(u_h, A) - Ch - C\varepsilon(h)\right) \\ &\geq \liminf_{h\to 0} \left(I^h_M(u_h, A) - Ch - C\varepsilon(h)\right) \geq I_M(u, A), \end{aligned}$$

which proves the local minimality of u.
Setting $\tilde{u} = u$, the above argument shows that $\lim_h I^h_M(u_h, A) = I_M(u, A)$, whence

$$\begin{aligned} I_M(u, A) &= \lim_{h\to 0} \int_A \frac{m}{2} \left(|\dot{u}|^2 + 2\dot{u} \cdot (\dot{u}_h - \dot{u}) + |\dot{u}_h - \dot{u}|^2\right) - V(u_h)\, dt \\ &= I_M(u, A) + 0 + \lim_{h\to 0} \|\dot{u}_h - \dot{u}\|^2_{L^2}. \end{aligned}$$

But then $\dot{u}_h \to \dot{u}$ in $L^2(A,\mathbb{R}^n)$ and so, $\dot{u}_h$ being bounded in $L^\infty(A,\mathbb{R}^n)$, $\dot{u}_h \to \dot{u}$ in $L^p(A,\mathbb{R}^n)$ for all $1 \leq p < \infty$. ∎

4.4 Numerical examples

In this section, the statements of Theorem 4.3.4 will be illustrated by means of numerical examples. The discrete path $\{u_i\}_{i=0}^N \subset X_h$ of a mechanical system is determined as a stationary point of the constrained discrete action functional I^h_M. According to (4.2), the stationary points are characterised by

$$\nabla_2 L_d(u_{i-1}, u_i) + \nabla_1 L_d(u_i, u_{i+1}) \perp T_{u_i} M. \tag{4.13}$$

In the sequel it is assumed that the triangulation $\mathcal{T}_h$ is equispaced, and the constant time step is denoted by $h = t_{i+1} - t_i$. There are several methods for the implementation of an algorithm that finds discrete paths matching condition (4.13). Assume that the constraint manifold is specified by the holonomic constraint functions $g(u) = 0 \in \mathbb{R}^m$,

$m = n - k$, in particular if zero is a regular value of the constraints, then $= g^{-1}(0) = M$ is a k-dimensional submanifold of $\mathbb{R}^n$. Let $G(u) = \nabla g(u)$ denote the Jacobian of the constraints, then $\mathbb{R}^n = T_{u_i}M \oplus (T_{u_i}M)^\perp = \text{null}(G(u)) \oplus \text{range}(G^T(u))$. Thus it is possible to use the Lagrange multiplier method to find appropriate paths. The corresponding discrete Euler-Lagrange equations then read

$$\begin{aligned} \nabla_2 L_d(u_{i-1}, u_i) + \nabla_1 L_d(u_i, u_{i+1}) + hG^T(u_i) \cdot \lambda_i &= 0, \\ g(u_{i+1}) &= 0. \end{aligned} \tag{4.14}$$

Since the vector of Lagrange multipliers $\lambda_i \in \mathbb{R}^m$ has to be determined as a variable by the algorithm, the system has to be augmented by the constraint equations $(4.14)_2$ and is then $n + m$-dimensional. Being a two-step method, the algorithm (4.14) is not self-starting. From given initial configuration u_0 and initial conjugate momentum p_0, the configuration u_1 (and the Lagrange multiplier λ_0) can be calculated via the constrained discrete Legendre transform

$$\begin{aligned} p_0 + \nabla_1 L_d(u_0, u_1) + \tfrac{h}{2} G^T(u_0) \cdot \lambda_0 &= 0, \\ g(u_1) &= 0. \end{aligned}$$

in a way that is consistent with the constrained dynamics.
Alternatively, the discrete null space method can be used. Besides leading to a k-dimensional system of equations, it also bears the advantage of removing the conditioning problems associated with the use of the Lagrange multiplier method. The discrete null space method relies on a transformation of (4.14) in two steps. First of all, $(4.14)_1$ is premultiplied with the transpose of the null space matrix $P(u) : \mathbb{R}^k \to T_u M$, having the property $\text{range}(P(u)) = \text{null}(G(u))$. Secondly, $(4.14)_2$ is redundantised introducing the nodal reparametrisation $u_{i+1} = F_d(w_{i+1}, u_i) \in M$. The resulting time-stepping scheme

$$P^T(u_i) \cdot [\nabla_2 L_d(u_{i-1}, u_i) + \nabla_1 L_d(u_i, F_d(w_{i+1}, u_i))] = 0 \tag{4.15}$$

has to be solved for w_{i+1} whereupon the redundant configuration variable can be updated using the nodal reparametrisation F_d. A consistent configuration u_1 can be found from the equation

$$P^T(u_0) \cdot [p_0 + \nabla_1 L_d(u_0, F_d(w_1, u_0))] = 0.$$

It is important to note that (4.15) and (4.14) are equivalent and both schemes are variational. See [Leye 08b] for a detailed investigation of the discrete null space method for the variational integration of constrained dynamical systems. Previous works on the discrete null space method in conjunction with an energy-momentum conserving scheme are [Bets 05, Bets 06, Leye 08a].
In the following examples, the midpoint rule has been used to approximate the integral of the potential energy over one time step in the discrete Lagrangian given in (4.1), thus the discrete Lagrangian reads

$$L_d(u_i, u_{i+1}) = \frac{m}{2} \frac{(u_{i+1} - u_i)^2}{h} - hV\left(\frac{u_{i+1} + u_i}{2}\right). \tag{4.16}$$

Using the variational integrator with Lagrange multipliers for constraint enforcement (4.14), the resulting implicit scheme is similar to the SHAKE algorithm. However, SHAKE is based on a trapezoidal rule (instead of the midpoint rule) yielding the evaluation of the potential gradient at one given configuration only, which can have unfavourable consequences on the robustness of simulations, in particular in the context of stiff nonlinear elasticity problems as beam dynamics. In contrast to the so far mentioned algorithms that enforce configuration constraints only, the velocity Verlet integrator RATTLE enforces the temporally differentiated form of the constraints on velocity level as well, see [Ande 83].

4.4.1 Double spherical pendulum

The motion of a double spherical pendulum in three dimensional space has been simulated using the discrete null space method, i.e. (4.15) is solved to determine the stationary points of the constrained discrete action functional I_M^h. The double spherical pendulum in Figure 4.2 is suspended at the origin of the inertial frame $\{e_I\}$. Massless rigid rods of lengths $l_1, l_2 \in \mathbb{R}$ connect the masses $m_1, m_2 \in \mathbb{R}$ to each other and to the origin, respectively. The gravitational acceleration with value g points in the negative e_3-direction. The configuration variable $u \in \mathbb{R}^6$ is composed of the placement in space $u^1 \in \mathbb{R}^3$ of the first mass and the placement $u^2 \in \mathbb{R}^3$ of the second mass $m^2 \in \mathbb{R}$ relative to the first one. The constraints represent the constancy of the lengths of the rigid rods. They restrict possible configurations to the constraint manifold $M = S_{l_1}^2 \times S_{l_2}^2$ consisting of two spheres, one about the origin with radius l_1 and one about the first mass with radius l_2.

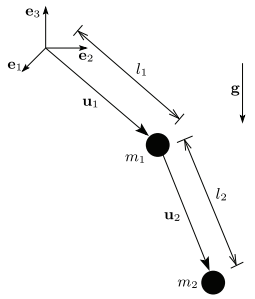

Figure 4.2: Double spherical pendulum.

In the simulation of the double spherical pendulum's motion, the following parameters have been used. The masses are $m_1 = 10$ and $m_2 = 5$ and the rigid rods have the lengths $l_1 = 1$ and $l_2 = 1.5$. The gravitational acceleration is given by $g = 9.81$. The initial positions of the point masses are $u^1(0) = l_1 e_1$ and $u^2(0) = l_2 e_1$ and initial velocities are given by $\dot{u}^1(0) = e_2$ and $\dot{u}^2(0) = e_3$. These initial velocities are consistent with the constraints, i.e. they lie in the tangent space $T_{u_0}M$. The considered motion takes place in the time interval $\bar{A} = [0, 10]$.
Snapshots of the motion of the double spherical pendulum are shown in Figure 4.3 on the left. The diagram on the right confirms the algorithmic conservation of the component L_3 of the angular momentum corresponding to the gravitational direction. Furthermore, the good energy behaviour of the variational integrator is revealed by the evolution of the total energy which appears to be conserved. In fact, the total energy oscillates around the correct value with amplitudes in the range of 10^{-3}.

Table 4.1 shows that for the considered example, velocities are indeed bounded independently of h.

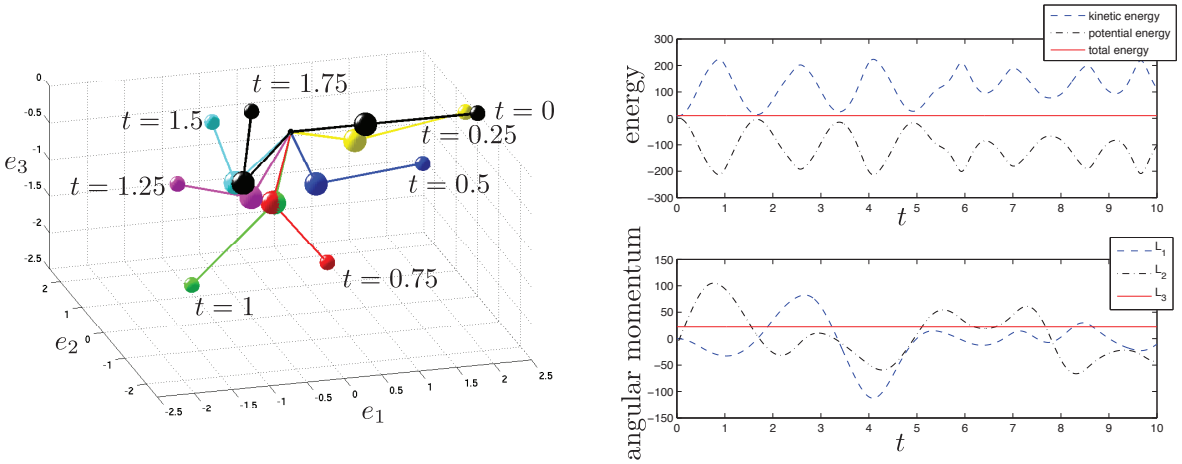

Figure 4.3: Double spherical pendulum: snapshots of the motion and energy and components of angular momentum $L = L_i e_i$ ($h = 10^{-5}$).

h	$\max_{t_j \in \{t_i\}_{i=0}^{N}} \|\|\dot{u}_h(t_j)\|\|$
10^{-1}	14.437579674951671
10^{-2}	11.992045771547241
10^{-3}	11.979460050283279
10^{-4}	11.979355188823591
10^{-5}	11.979353929835233

Table 4.1: Double spherical pendulum: boundedness of velocity.

A reference solution $u_{h_{ref}}$ has been calculated using the time step $h_{ref} = 10^{-5}$. The convergence statement of Theorem 4.3.4 is illustrated by Figure 4.4. It reveals the well known fact that variational integrators based on a discrete Lagrangian given in (4.16) are second order convergent also holds for constrained problems.

4.4.2 Three-bar swing

The second example deals again with the swing from Chapter 3 shown in Fig. 3.16. Here, the example illustrates that Theorem 4.3.4 is applicable in the presence of highly nonlinear elastic behaviour where, despite the fact that the elastic energy is given by a fourth order term in the configuration variables, V satisfies the quadratic energy bound $|V(s)| \leq C(1 + |s|^2)$ in a neighbourhood of the constraint manifold M.

Convergence of configuration and velocity to reference solution is visible in Fig. 4.5. Furthermore, boundedness of the velocities can be observed from Table 4.2.

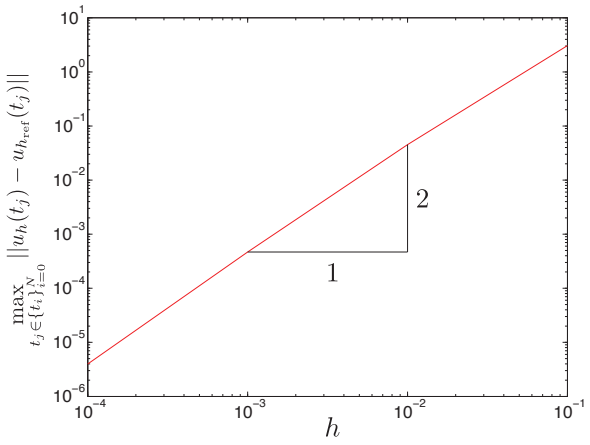

Figure 4.4: Double spherical pendulum: second order convergence to reference solution for $h \in [10^{-1}, \ldots, 10^{-4}]$.

h	$\max_{t_j \in \{t_i\}_{i=0}^N} ||\dot{u}_h(t_j)||$
10^{-2}	21.264358970618083
$5 \cdot 10^{-3}$	21.502895414634740
10^{-3}	29.211974341839312
$5 \cdot 10^{-4}$	29.414409469970764
10^{-4}	28.986258982641335
$5 \cdot 10^{-5}$	28.970130936433204
10^{-5}	28.964966706946093

Table 4.2: Three-bar swing: boundedness of velocity.

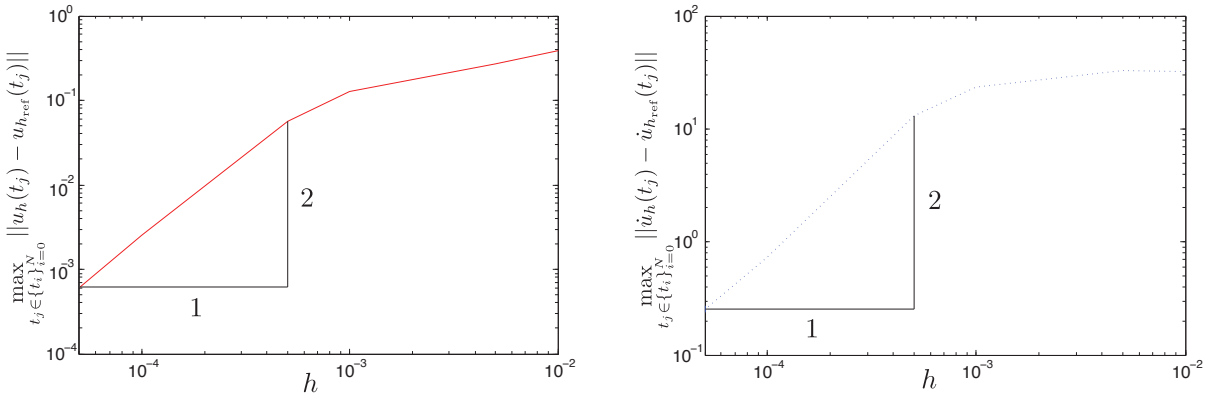

Figure 4.5: Three-bar swing: convergence of configuration and velocity to reference solution for $h \in [10^{-2} \ldots, 5 \cdot 10^{-5}]$.

5 Discrete mechanics and optimal control for constrained systems

5.1 Introduction

This work combines two recently developed methods, namely the discrete null space method which is suitable for the accurate, robust and efficient time integration of constrained dynamical systems (in particular for multibody dynamics) and an approach to discrete mechanics and optimal control (DMOC) based on a discretisation of the Lagrange-d'Alembert principle, see also [Leye 09b]. The new method's acronym is DMOCC. The idea of this combination has been introduced briefly in [Leye 07] and is investigated in detail for three-dimensional multibody systems consisting of rigid bodies interconnected by joints in this work.

From various available methods used to enforce holonomic constraints in the framework of the Hamiltonian or Lagrangian formalism (see e.g. [Bert 95, Luen 84] and for a computational approach [Leye 04]), the focus in this chapter is on two methods yielding exact constraint fulfilment, the Lagrange multiplier method and a null space method, described in, for example, [Benz 05].

Because of the relatively simple structure of the evolution equations derived from the Lagrange multiplier method, their temporal discrete form can be derived easily using mechanical integrators as demonstrated among others in [Bets 02a, Gonz 99, Wend 97]. However, the presence of Lagrange multipliers amongst the set of unknowns enlarges the number of equations and causes the discrete system to be ill-conditioned for small time steps as reported (amongst others) by [Petz 86, Hair 89]. In contrast to this undesirable situation, the use of a specific null space method, especially in conjunction with a reparametrisation in generalised coordinates, has the advantageous property of a small dimensional system of equations. On the other hand, these evolution equations have a highly complicated structure, causing the derivation of their temporal discrete form to be expensive and therefore, in most cases, not recommended [Leim 04, Rhei 97].

A remedy for these difficulties is found in the discrete null space method introduced in [Bets 05], which proposes a reversal of two of the main steps when designing a specific numerical method. In the first step, the discrete form of the simple structured DAEs resulting from the use of the Lagrange multiplier method is derived using a mechanical integrator, e.g. an energy-momentum conserving integrator [Bets 02a, Gonz 99] or a variational integrator leading to a symplectic-momentum conserving scheme [Wend 97]. For forced systems, both methods correctly compute the change in momentum maps. Then, in the second step, the transition to the reduced scheme and finally the nodal reparametrisation are performed in the temporal discrete setting in complete analogy to the procedure described in the continuous case according to the discrete null space method. The resulting time stepping scheme performs excellently in all relevant categories. First of all, it

yields the smallest possible dimension for the system of equations, promising lower computational costs than other schemes. Secondly, it is second order accurate and inherits the conservation properties from the constrained scheme and thirdly, the condition number of the scheme is independent of the time step. Summarising, the discrete null space method is especially suited for the accurate simulation of large dimensional systems subject to a large number of constraints. In particular the resulting equations lend themselves as dynamic constraints in an optimisation algorithm since their dimension is minimal, thus only the exactly required number of unknowns has to be determined.

To find local solutions of nonlinear optimal control problems consisting of a given objective functional and equations describing the underlying dynamics of the system, a numerical method falling into the class of direct methods is used here. Thereby, the state and control variables are discretised directly in order to transform the optimal control problem into a finite dimensional nonlinear constrained optimisation problem that can be solved by standard nonlinear optimisation techniques such as sequential quadratic programming (see [Gill 97, Schi 80]). In contrast to other methods like, e.g. shooting [Stoe 02, Kraf 85, Hick 71], multiple shooting [Deuf 74, Bock 84], or collocation methods [Stry 91, Bieg 84], relying on a direct integration of the associated ordinary differential equations parametrised by states and controls or the controls only (see also [Bett 98] and [Bind 01] for an overview of the current state of the art), a recently developed method DMOC (Discrete Mechanics and Optimal Control, see [Ober 08, Jung 05a]) is used here. It is based on the discretisation of the variational structure of the mechanical system directly. In the context of variational integrators, as in [Mars 01], the discretisation of the Lagrange-d'Alembert principle leads to structure preserving time stepping equations which serve as equality constraints for the resulting finite dimensional nonlinear optimisation problem. In [Jung 05a, Jung 05b, Jung 06] DMOC was first applied to low orbital thrust transfers and the optimal control of formation flying satellites including an algorithm that exploits a hierarchical structure of that problem.

In this work, DMOC is used to find optimal trajectories of state and control variables for systems of rigid bodies subject to joint constraints. Each rigid body is viewed as a constrained continuum, i.e. it is described in terms of redundant coordinates subject to holonomic constraints [Bets 01b, Reic 96]. This is in contrast to rotation based approaches taken e.g. in [Krys 06, Bou 09]. Here, the equations of motion assume the form of DAEs with a constant mass matrix. Their temporal discrete form can be derived and reduced according to the discrete null space method. This procedure has the advantage of circumventing the difficulties associated with rotational parameters [Bauc 03] and it can be generalised easily to the modelling of geometrically exact beams and shells and to multibody systems consisting of theses structures as developed in [Leye 06b, Bets 06, Leye 08a].

The combination of the two proposed methods involves several specific benefits. First of all, the discrete dynamics equation constraining the optimal control problem in DMOC can be formulated easily. Using the discrete Lagrange-d'Alembert principle, they are derived as the discrete analogue to the simple structured evolution equations where the configuration constraints are enforced using Lagrange multipliers. Secondly, the discrete null space method reduces the dynamics constraints to the smallest possible number of equations and variables which leads to lower computational costs for the optimisation

algorithm. Thirdly, the benefit of exact constraint fulfilment and correct computation of the change in momentum maps is guaranteed by the optimisation algorithm. These benefits are important, especially for high dimensional rigid body systems with joint constraints.
An outline of the chapter is as follows. Section 5.2 fixes the formulation of the continuous optimal control problem of constrained dynamics which is formulated in the discrete setting in Section 5.3. Techniques for rigid body systems are set up in Section 5.4. The main contribution is contained in Section 5.5 and Section 5.6. In particular, actuating forces being consistent with the specific joint constraints are given in Section 5.5 and structure preservation of the resulting time stepping scheme is proved. Section 5.6 applies the theory developed in the chapter to the optimal control of multibody systems. Numerical examples from the field of satellite reorientation manoeuvres and biomotion as well as a comparison to existing methods are presented in Section 5.7.

5.2 Constrained dynamics and optimal control

This section derives the equations of motion for forced holonomically constrained systems; these equations are to be fulfilled as constraints in the optimisation problem. The transformation of the differential algebraic equations by the null space method with reparametrisation, and in particular the equivalence of the resulting equations of motion, is described in detail in Chapter 3 (see also [Leye 08b]) for conservative systems.
Consider an n-dimensional mechanical system with the time-dependent configuration vector $\boldsymbol{q}(t) \in Q$ and velocity vector $\dot{\boldsymbol{q}}(t) \in T_{\boldsymbol{q}(t)}Q$, where $t \in [t_0, t_N] \subset \mathbb{R}$ denotes the time and $n, N \in \mathbb{N}$. Let the configuration be constrained by the function $\boldsymbol{g}(\boldsymbol{q}) = \boldsymbol{0} \in \mathbb{R}^m$ with constraint manifold $C = \{\boldsymbol{q} \in Q \mid \boldsymbol{g}(\boldsymbol{q}) = \boldsymbol{0}\}$ and influenced by the force field $\boldsymbol{f} : \mathbb{R}^{n-m} \times TQ \to T^*Q$.

The optimisation problem The goal is to determine the optimal trajectory and force field, such that the system is moved from the initial state $(\boldsymbol{q}^0, \dot{\boldsymbol{q}}^0) \in TC$ to the final state $(\boldsymbol{q}^N, \dot{\boldsymbol{q}}^N) \in TC$, obeying the equations of motion and at the same time, the objective functional

$$J(\boldsymbol{q}, \dot{\boldsymbol{q}}, \boldsymbol{f}) = \int_{t_0}^{t_N} B(\boldsymbol{q}, \dot{\boldsymbol{q}}, \boldsymbol{f})\, dt \tag{5.1}$$

is to be minimised. Here, $B(\boldsymbol{q}, \dot{\boldsymbol{q}}, \boldsymbol{f}) : TC \times T^*Q \to \mathbb{R}$ is a given cost function.

The constrained Lagrange-d'Alembert principle As already mentioned, the motion has to obey the equations of motion which, in the present case, are based on a constrained version of the Lagrange-d'Alembert principle (see e.g. [Mars 94]), which requires that

$$\delta \int_{t_0}^{t_N} \left[L(\boldsymbol{q}, \dot{\boldsymbol{q}}) - \boldsymbol{g}^T(\boldsymbol{q}) \cdot \boldsymbol{\lambda} \right] dt + \int_{t_0}^{t_N} \boldsymbol{f} \cdot \delta\boldsymbol{q}\, dt = 0 \tag{5.2}$$

for all variations $\delta\boldsymbol{q} \in TQ$ vanishing at the endpoints and $\delta\boldsymbol{\lambda} \in \mathbb{R}^m$. The Lagrangian $L : TQ \to \mathbb{R}$ equals the kinetic energy $\frac{1}{2}\, \dot{\boldsymbol{q}}^T \cdot \boldsymbol{M} \cdot \dot{\boldsymbol{q}}$ including the consistent mass matrix

$\boldsymbol{M} \in \mathbb{R}^{n\times n}$ minus a potential function $V : Q \to \mathbb{R}$. Furthermore, $\boldsymbol{\lambda}(t) \in \mathbb{R}^m$ represents the vector of time dependent Lagrange multipliers. The last term represents the virtual work resulting from the force field. The constrained Lagrange-d'Alembert principle (5.2) leads to the differential-algebraic system of equations of motion

$$\begin{aligned} \frac{\partial L(\boldsymbol{q},\dot{\boldsymbol{q}})}{\partial \boldsymbol{q}} - \frac{d}{dt}\left(\frac{\partial L(\boldsymbol{q},\dot{\boldsymbol{q}})}{\partial \dot{\boldsymbol{q}}}\right) - \boldsymbol{G}^T(\boldsymbol{q})\cdot\boldsymbol{\lambda} + \boldsymbol{f} &= \boldsymbol{0} \\ \boldsymbol{g}(\boldsymbol{q}) &= \boldsymbol{0}, \end{aligned} \tag{5.3}$$

where $\boldsymbol{G}(\boldsymbol{q}) = D\boldsymbol{g}(\boldsymbol{q})$ denotes the Jacobian of the constraints. The vector $-\boldsymbol{G}^T(\boldsymbol{q})\cdot\boldsymbol{\lambda}$ represents the constraint forces that prevent the system from deviations off the constraint manifold.

The null space method Assuming that the constraints are independent, for every $\boldsymbol{q} \in C$ the basis vectors of $T_{\boldsymbol{q}}C$ form an $n\times(n-m)$ matrix $\boldsymbol{P}(\boldsymbol{q})$ with corresponding linear map $\boldsymbol{P}(\boldsymbol{q}) : \mathbb{R}^{n-m} \to T_{\boldsymbol{q}}C$. This matrix is called null space matrix, since range $(\boldsymbol{P}(\boldsymbol{q})) =$ null $(\boldsymbol{G}(\boldsymbol{q})) = T_{\boldsymbol{q}}C$. Thus, a premultiplication of the differential equation $(5.3)_1$ by $\boldsymbol{P}^T(\boldsymbol{q})$ eliminates the constraint forces including the Lagrange multipliers from the system.

Reparametrisation For many applications, it is possible to find a local parametrisation of the constraint manifold $\boldsymbol{F} : U \subseteq \mathbb{R}^{n-m} \to C$ in terms of independent generalised coordinates $\boldsymbol{u} \in U$. Then the Jacobian $D\boldsymbol{F}(\boldsymbol{u})$ of the coordinate transformation plays the role of a null space matrix. Since the constraints $(5.3)_2$ are fulfilled automatically by the reparametrised configuration variable $\boldsymbol{q} = \boldsymbol{F}(\boldsymbol{u})$, the system is reduced to $n-m$ second order differential equations

$$\boldsymbol{P}^T(\boldsymbol{q})\cdot\left[\frac{\partial L(\boldsymbol{q},\dot{\boldsymbol{q}})}{\partial \boldsymbol{q}} - \frac{d}{dt}\left(\frac{\partial L(\boldsymbol{q},\dot{\boldsymbol{q}})}{\partial \dot{\boldsymbol{q}}}\right) + \boldsymbol{f}\right] = \boldsymbol{0}. \tag{5.4}$$

Due to the presence of constraints, the forces $\boldsymbol{f}$ are not independent. They can be calculated in terms of the time dependent generalised control forces $\boldsymbol{\tau}(t) \in T^*U$. Consequently, there are $n-m$ independent generalised forces acting on the generalised degrees of freedom. These can be calculated as $\boldsymbol{\tau} = \left(\frac{\partial \boldsymbol{F}}{\partial \boldsymbol{u}}\right)^T \cdot \boldsymbol{f}$, see e.g. [Gold 02]. On the other hand, a redundant force vector $\boldsymbol{f} \in T^*Q$ can be computed via

$$\boldsymbol{f} = \boldsymbol{B}^T(\boldsymbol{q})\cdot\boldsymbol{\tau}, \tag{5.5}$$

with the $n\times(n-m)$ configuration dependent input transformation matrix $\boldsymbol{B}^T : T^*U \to T^*Q$. Thereby, the choice of the transformation matrix must ensure consistency of momentum maps in the sense that they change only and exactly according to the generalised force.

Thus, the optimal control of constrained dynamics gives rise to the optimisation problem in Lagrange form consisting of the optimisation of the objective function (5.1) subject to the reduced equations of constrained motion (5.4).

5.3 Constrained discrete dynamics and optimal control

Analogous steps are performed in the temporal discrete variational setting to derive the forced constrained discrete Euler-Lagrange equations and their reduction to minimal dimension. Corresponding to the configuration manifold Q, the discrete phase space is defined by $Q \times Q$ which is locally isomorphic to TQ. For a constant time step $h \in \mathbb{R}$, a path $\boldsymbol{q} : [t_0, t_N] \to Q$ is replaced by a discrete path $\boldsymbol{q}_d : \{t_0, t_0 + h, , \ldots, t_0 + Nh = t_N\} \to Q$, $N \in \mathbb{N}$, where $\boldsymbol{q}_n = \boldsymbol{q}_d(t_n)$ is viewed as an approximation to $\boldsymbol{q}(t_n)$ at $t_n = t_0 + nh$. Similarly, $\boldsymbol{\lambda}_n = \boldsymbol{\lambda}_d(t_n)$ approximates the Lagrange multipliers, while the force field $\boldsymbol{f}$ is approximated by two discrete forces $\boldsymbol{f}_n^-, \boldsymbol{f}_n^+ : T^*U \times Q \to T^*Q$ in a way that respects work, as is explained below.

Discrete constrained Lagrange-d'Alembert principle According to the derivation of variational integrators for constrained dynamics in Chapter 3 (see also [Leye 08b]), the action integral in (5.2) is approximated in a time interval $[t_n, t_{n+1}]$ using the discrete Lagrangian $L_d : Q \times Q \to \mathbb{R}$ and the discrete constraint function $\boldsymbol{g}_d : Q \to \mathbb{R}$ via

$$L_d(\boldsymbol{q}_n, \boldsymbol{q}_{n+1}) - \frac{1}{2}\boldsymbol{g}_d^T(\boldsymbol{q}_n) \cdot \boldsymbol{\lambda}_n - \frac{1}{2}\boldsymbol{g}_d^T(\boldsymbol{q}_{n+1}) \cdot \boldsymbol{\lambda}_{n+1} \approx \int_{t_n}^{t_{n+1}} L(\boldsymbol{q}, \dot{\boldsymbol{q}}) - \boldsymbol{g}^T(\boldsymbol{q}) \cdot \boldsymbol{\lambda}\, dt. \quad (5.6)$$

Among various possible choices to approximate this integral, in this work the midpoint rule is used for the Lagrangian, i.e.

$$L_d(\boldsymbol{q}_n, \boldsymbol{q}_{n+1}) = hL\left(\frac{\boldsymbol{q}_{n+1} + \boldsymbol{q}_n}{2}, \frac{\boldsymbol{q}_{n+1} - \boldsymbol{q}_n}{h}\right) \quad (5.7)$$

and for the constraints $\boldsymbol{g}_d^T(\boldsymbol{q}_n) = h\boldsymbol{g}^T(\boldsymbol{q}_n)$ is used. Likewise, the virtual work is approximated by

$$\boldsymbol{f}_n^- \cdot \delta\boldsymbol{q}_n + \boldsymbol{f}_n^+ \cdot \delta\boldsymbol{q}_{n+1} \approx \int_{t_n}^{t_{n+1}} \boldsymbol{f} \cdot \delta\boldsymbol{q}\, dt, \quad (5.8)$$

where $\boldsymbol{f}_n^+, \boldsymbol{f}_n^-$ are called the left and right discrete forces, respectively. They are specified in (5.11).
The discrete version of the constrained Lagrange-d'Alembert principle (5.2) requires the discrete path $\{\boldsymbol{q}_n\}_{n=0}^N$ and multipliers $\{\boldsymbol{\lambda}_n\}_{n=0}^N$ to fulfil

$$\delta \sum_{n=0}^{N-1} L_d(\boldsymbol{q}_n, \boldsymbol{q}_{n+1}) - \frac{1}{2}\boldsymbol{g}_d^T(\boldsymbol{q}_n) \cdot \boldsymbol{\lambda}_n - \frac{1}{2}\boldsymbol{g}_d^T(\boldsymbol{q}_{n+1}) \cdot \boldsymbol{\lambda}_{n+1} + \sum_{n=0}^{N-1} \boldsymbol{f}_n^- \cdot \delta\boldsymbol{q}_n + \boldsymbol{f}_n^+ \cdot \delta\boldsymbol{q}_{n+1} = 0$$

for all variations $\{\delta\boldsymbol{q}_n\}_{n=0}^N$ and $\{\delta\boldsymbol{\lambda}_n\}_{n=0}^N$ with $\delta\boldsymbol{q}_0 = \delta\boldsymbol{q}_N = \boldsymbol{0}$, which is equivalent to the constrained forced discrete Euler-Lagrange equations

$$\begin{aligned} D_2L_d(\boldsymbol{q}_{n-1}, \boldsymbol{q}_n) + D_1L_d(\boldsymbol{q}_n, \boldsymbol{q}_{n+1}) - \boldsymbol{G}_d^T(\boldsymbol{q}_n) \cdot \boldsymbol{\lambda}_n + \boldsymbol{f}_{n-1}^+ + \boldsymbol{f}_n^- &= \boldsymbol{0} \\ \boldsymbol{g}(\boldsymbol{q}_{n+1}) &= \boldsymbol{0} \end{aligned} \quad (5.9)$$

for $n = 1, \ldots, N-1$, where $\boldsymbol{G}_d(\boldsymbol{q}_n)$ denotes the Jacobian of $\boldsymbol{g}_d(\boldsymbol{q}_n)$. Note that the time stepping scheme (5.9) has not been deduced by discretising (5.3), but rather via a discrete variational principle.

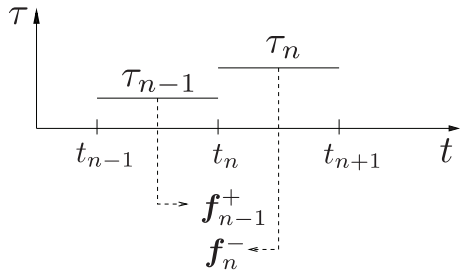

Figure 5.1: Relation of redundant forces $\boldsymbol{f}_{n-1}^+, \boldsymbol{f}_n^-$ to discrete generalised forces $\boldsymbol{\tau}_{n-1}, \boldsymbol{\tau}_n$.

The discrete null space method Analogous to the continuous case, to eliminate the discrete constraint forces from (5.9), a discrete null space matrix fulfilling range $(\boldsymbol{P}(\boldsymbol{q}_n)) = \text{null}\,(\boldsymbol{G}_d(\boldsymbol{q}_n))$ is employed. Premultiplying $(5.9)_1$ by the transposed discrete null space matrix cancels the constraint forces; i.e. the Lagrange multipliers are eliminated from the set of unknowns and the system's dimension is reduced to n.

Nodal reparametrisation As in the continuous case, a reduction of the system to the minimal possible dimension can be accomplished by a local reparametrisation of the constraint manifold in the neighbourhood of the discrete configuration variable. At the time nodes, $\boldsymbol{q}_n$ is expressed in terms of the discrete generalised coordinates $\boldsymbol{u}_n \in U \subseteq \mathbb{R}^{n-m}$ by the map $\boldsymbol{F} : U \subseteq \mathbb{R}^{n-m} \times Q \to C$, such that the constraints are fulfilled.

$$\boldsymbol{q}_n = \boldsymbol{F}(\boldsymbol{u}_n, \boldsymbol{q}_{n-1}) \quad \text{with} \quad \boldsymbol{g}(\boldsymbol{q}_n) = \boldsymbol{g}(\boldsymbol{F}(\boldsymbol{u}_n, \boldsymbol{q}_{n-1})) = \boldsymbol{0} \tag{5.10}$$

The discrete generalised control forces are assumed to be constant in each time interval, see Figure 5.1. First of all, the effect of the generalised forces acting in $[t_{n-1}, t_n]$ and in $[t_n, t_{n+1}]$ is transformed to the time node t_n via $\boldsymbol{\tau}_{n-1}^+ = \dfrac{h}{2}\,\boldsymbol{\tau}_{n-1}$ and $\boldsymbol{\tau}_n^- = \dfrac{h}{2}\,\boldsymbol{\tau}_n$. Secondly, the components of the discrete force vectors $\boldsymbol{f}_{n-1}^+, \boldsymbol{f}_n^- \in T_{\boldsymbol{q}_n}^* Q$ can be calculated similar to (5.5) as

$$\begin{aligned} \boldsymbol{f}_{n-1}^+ &= \boldsymbol{B}^T(\boldsymbol{q}_n) \cdot \boldsymbol{\tau}_{n-1}^+ \qquad \boldsymbol{f}_n^- = \boldsymbol{B}^T(\boldsymbol{q}_n) \cdot \boldsymbol{\tau}_n^- \\ \boldsymbol{f}_n &= \boldsymbol{f}_n^+ + \boldsymbol{f}_n^- \qquad \boldsymbol{f}_d = \{\boldsymbol{f}_n\}_{n=0}^{N-1}\,. \end{aligned} \tag{5.11}$$

Thus $\boldsymbol{f}_{n-1}^+$ denotes the effect of the generalised force $\boldsymbol{\tau}_{n-1}$ acting in $[t_{n-1}, t_n]$ on $\boldsymbol{q}_n$ while $\boldsymbol{f}_n^-$ denotes the effect on $\boldsymbol{q}_n$ of $\boldsymbol{\tau}_n$ acting in $[t_n, t_{n+1}]$.
Insertion of the nodal reparametrisation for the configuration (5.10) into the scheme redundantises $(5.9)_2$. The resulting scheme

$$\boldsymbol{P}^T(\boldsymbol{q}_n) \cdot \left[D_2 L_d(\boldsymbol{q}_{n-1}, \boldsymbol{q}_n) + D_1 L_d(\boldsymbol{q}_n, \boldsymbol{F}(\boldsymbol{u}_{n+1}, \boldsymbol{q}_n)) + \boldsymbol{f}_{n-1}^+ + \boldsymbol{f}_n^- \right] = \boldsymbol{0} \tag{5.12}$$

has to be solved for $\boldsymbol{u}_{n+1}$ whereupon $\boldsymbol{q}_{n+1}$ is obtained from (5.10). (5.12) is equivalent to the constrained scheme (5.9), thus it also has the key properties of exact constraint fulfilment, symplecticity and momentum consistency, i.e. any change in the value of a momentum map reflects exactly the applied forces as will be shown in Section 5.7. When no load is present, momentum maps are conserved exactly. While the constrained scheme (5.9) becomes increasingly ill-conditioned for decreasing time steps, the condition number of (5.12) is independent of the time step.

Boundary conditions In the next step, the boundary conditions $\boldsymbol{q}(t_0) = \boldsymbol{q}^0, \dot{\boldsymbol{q}}(t_0) = \dot{\boldsymbol{q}}^0$ and $\boldsymbol{q}(t_N) = \boldsymbol{q}^N, \dot{\boldsymbol{q}}(t_N) = \dot{\boldsymbol{q}}^N$ have to be formulated in the discrete setting. Let $\boldsymbol{q}_{00} \in C$ be a fixed reference configuration, relative to which the initial configuration is computed as $\boldsymbol{q}_0 = \boldsymbol{F}(\boldsymbol{u}_0, \boldsymbol{q}_{00})$. To prescribe an initial configuration at t_0, one can request $\boldsymbol{u}_0 = \boldsymbol{u}^0$. If an absolute reparametrisation is used, i.e. (5.10) is changed to $\boldsymbol{q}_n = \boldsymbol{F}(\boldsymbol{u}_n, \boldsymbol{q}_{00})$, then $\boldsymbol{u}_N = \boldsymbol{u}^N$ defines the final configuration $\boldsymbol{q}_N$ uniquely (see Sections 5.7.2 and 5.7.3 for examples). However, for the relative reparametrisation (5.10), $n - m$ independent final configuration conditions have to be identified with the function $\boldsymbol{D} : Q \times Q \to \mathbb{R}^{n-m}$ depending on the specific system under consideration. Since in the present formulation of constrained forced discrete variational dynamics on $Q \times Q$, velocities are not properly defined, the velocity conditions have to be transformed into conditions on the conjugate momenta, which are defined at each and every time node using the discrete Legendre transform. Three different versions have been defined in Chapter 3 (see also [Leye 08b]) for the conservative case. Now, the presence of forces at the time nodes has to be incorporated into that transformation leading to the constrained forced discrete Legendre transforms $\mathbb{F}^{cf^-}L_d : Q \times Q \to T^*Q$ and $\mathbb{F}^{cf^+}L_d : Q \times Q \to T^*Q$ reading

$$\begin{aligned} &\mathbb{F}^{cf^-}L_d : (\boldsymbol{q}_n, \boldsymbol{q}_{n+1}) \mapsto (\boldsymbol{q}_n, \boldsymbol{p}_n^-) \qquad \boldsymbol{p}_n^- = -D_1 L_d(\boldsymbol{q}_n, \boldsymbol{q}_{n+1}) + \frac{1}{2}\boldsymbol{G}_d^T(\boldsymbol{q}_n) \cdot \boldsymbol{\lambda}_n - \boldsymbol{f}_n^- \\ &\mathbb{F}^{cf^+}L_d : (\boldsymbol{q}_{n-1}, \boldsymbol{q}_n) \mapsto (\boldsymbol{q}_n, \boldsymbol{p}_n^+) \qquad \boldsymbol{p}_n^+ = D_2 L_d(\boldsymbol{q}_{n-1}, \boldsymbol{q}_n) - \frac{1}{2}\boldsymbol{G}_d^T(\boldsymbol{q}_n) \cdot \boldsymbol{\lambda}_n + \boldsymbol{f}_{n-1}^+. \end{aligned} \tag{5.13}$$

As in the conservative case, the time stepping scheme $(5.9)_1$ can be interpreted as matching of momenta $\boldsymbol{p}_n^+ - \boldsymbol{p}_n^- = \boldsymbol{0}$ such that along the discrete trajectory, there is a unique momentum at each time node n which can be denoted by $\boldsymbol{p}_n$. However, just as the appearance of Lagrange multipliers is avoided in the discrete equations of motion (5.12), their presence in the initial and final momentum conditions complicates matters unnecessarily. A formula to recover the Lagrange multipliers from the discrete trajectory in a post processing step can be found in Chapter 3 (see also [Leye 08b]). The following versions of the discrete Legendre transforms do not use Lagrange multipliers. The projected discrete Legendre transforms ${}^Q\mathbb{F}^{cf^-}L_d : Q \times Q \to \eta\left(T^*_{\boldsymbol{q}_n}C\right)$ and ${}^Q\mathbb{F}^{cf^+}L_d : Q \times Q \to \eta\left(T^*_{\boldsymbol{q}_n}C\right)$ read

$${}^Q\boldsymbol{p}_n^- = \boldsymbol{Q}(\boldsymbol{q}_n) \cdot \left[-D_1 L_d(\boldsymbol{q}_n, \boldsymbol{q}_{n+1}) - \boldsymbol{f}_n^-\right] \qquad {}^Q\boldsymbol{p}_n^+ = \boldsymbol{Q}(\boldsymbol{q}_n) \cdot \left[D_2 L_d(\boldsymbol{q}_{n-1}, \boldsymbol{q}_n) + \boldsymbol{f}_{n-1}^+\right], \tag{5.14}$$

where $\boldsymbol{Q}(\boldsymbol{q}_n)$ is given by $\boldsymbol{Q} = \boldsymbol{I}_{n\times n} - \boldsymbol{G}_d^T \cdot \left[\boldsymbol{G}_d \cdot \boldsymbol{M}^{-1} \cdot \boldsymbol{G}_d^T\right]^{-1} \boldsymbol{G}_d \cdot \boldsymbol{M}^{-1}$ and fulfils $\boldsymbol{Q}(\boldsymbol{q}_n) \cdot \boldsymbol{G}_d^T(\boldsymbol{q}_n) = \boldsymbol{0}_{n\times m}$. Note that for the constrained discrete Legendre transforms and for the projected discrete Legendre transforms, the output is an n-dimensional momentum vector. In the projected case, it lies in the $(n - m)$-dimensional submanifold $\eta\left(T^*_{\boldsymbol{q}_n}C\right)$ being the embedding of $T^*_{\boldsymbol{q}_n}C$ into $T^*_{\boldsymbol{q}_n}Q$. Yet another possibility is to compute an $(n-m)$-dimensional momentum vector by projecting with the discrete null space matrix. The reduced discrete Legendre transforms ${}^P\mathbb{F}^{cf^-}L_d : Q \times Q \to T^*U$ and ${}^P\mathbb{F}^{cf^+}L_d : Q \times Q \to T^*U$ are given by

$${}^P\boldsymbol{p}_n^- = \boldsymbol{P}^T(\boldsymbol{q}_n) \cdot \left[-D_1 L_d(\boldsymbol{q}_n, \boldsymbol{q}_{n+1}) - \boldsymbol{f}_n^-\right] \qquad {}^P\boldsymbol{p}_n^+ = \boldsymbol{P}^T(\boldsymbol{q}_n) \cdot \left[D_2 L_d(\boldsymbol{q}_{n-1}, \boldsymbol{q}_n) + \boldsymbol{f}_{n-1}^+\right].$$

This version is most appropriate to be used as a constraint in the optimisation problem, since it yields the minimal number of independent conditions, while conditions formulated using (5.14) are redundant and (5.13) involves the Lagrange multipliers.
Note that according to the range of the projection, ${}^{Q}\boldsymbol{p}_n$ fulfils the constraints on the momentum level; i.e., $\boldsymbol{h}_d(\boldsymbol{q}_n, {}^{Q}\boldsymbol{p}_n) = \boldsymbol{G}(\boldsymbol{q}_n) \cdot \boldsymbol{M}^{-1} \cdot {}^{Q}\boldsymbol{p}_n = \boldsymbol{0}$ while this is not in general the case for $\boldsymbol{p}_n$. This question is superfluous for ${}^{P}\boldsymbol{p}_n$.
Prescribed initial and final velocities of course should be consistent with the constraints on velocity level. Using the standard continuous Legendre transform $\mathbb{F}L : TC \to T^*C$

$$\mathbb{F}L : (\boldsymbol{q}, \dot{\boldsymbol{q}}) \mapsto (\boldsymbol{q}, \boldsymbol{p}) = (\boldsymbol{q}, D_2L(\boldsymbol{q}, \dot{\boldsymbol{q}}))$$

yields momenta which are consistent with the constraints on momentum level as well. With these preliminaries, the velocity boundary conditions are transformed to the following conditions on momentum level: $\boldsymbol{p}(t_0) = D_2L(\boldsymbol{q}(t_0), \dot{\boldsymbol{q}}(t_0)) = \boldsymbol{p}^0$ and $\boldsymbol{p}(t_N) = D_2L(\boldsymbol{q}(t_N), \dot{\boldsymbol{q}}(t_N)) = \boldsymbol{p}^N$, respectively. Then, $\boldsymbol{p}^0 = \boldsymbol{p}_0^-$ and $\boldsymbol{p}^N = \boldsymbol{p}_N^+$ are the corresponding conditions on the discrete level which read in detail

$$\begin{aligned} \boldsymbol{P}^T(\boldsymbol{q}_0) \cdot \left[D_2L(\boldsymbol{q}_0, \dot{\boldsymbol{q}}_0) + D_1L_d(\boldsymbol{q}_0, \boldsymbol{q}_1) + \boldsymbol{f}_0^- \right] &= \boldsymbol{0} \\ \boldsymbol{P}^T(\boldsymbol{q}_N) \cdot \left[D_2L(\boldsymbol{q}_N, \dot{\boldsymbol{q}}_N) - D_2L_d(\boldsymbol{q}_{N-1}, \boldsymbol{q}_N) - \boldsymbol{f}_{N-1}^+ \right] &= \boldsymbol{0}. \end{aligned} \tag{5.15}$$

The discrete constrained optimisation problem Now the optimal control problem for the constrained discrete motion can be formulated. To begin with, an approximation

$$B_d(\boldsymbol{q}_n, \boldsymbol{q}_{n+1}, \boldsymbol{f}_n) \approx \int_{t_n}^{t_{n+1}} B(\boldsymbol{q}, \dot{\boldsymbol{q}}, \boldsymbol{f})\, dt$$

of the continuous objective functional (5.1) has to be defined. As with the approximations (5.7), the midpoint rule is used:

$$B_d(\boldsymbol{q}_n, \boldsymbol{q}_{n+1}, \boldsymbol{f}_n) = hB\left(\frac{\boldsymbol{q}_{n+1} + \boldsymbol{q}_n}{2}, \frac{\boldsymbol{q}_{n+1} - \boldsymbol{q}_n}{h}, \boldsymbol{f}_n \right).$$

This yields the discrete objective function

$$J_d(\boldsymbol{q}_d, \boldsymbol{f}_d) = \sum_{n=0}^{N-1} B_d(\boldsymbol{q}_n, \boldsymbol{q}_{n+1}, \boldsymbol{f}_n), \tag{5.16}$$

where the discrete configurations and forces are expressed in terms of their corresponding independent generalised quantities $\boldsymbol{u}_d = \{\boldsymbol{u}_n\}_{n=0}^{N}$ and $\boldsymbol{\tau}_d = \{\boldsymbol{\tau}_n\}_{n=0}^{N-1}$, respectively. Alternatively, a new objective function can be formulated directly in the generalised quantities

$$\bar{J}_d(\boldsymbol{u}_d, \boldsymbol{\tau}_d) = \sum_{n=0}^{N-1} \bar{B}_d(\boldsymbol{u}_n, \boldsymbol{u}_{n+1}, \boldsymbol{\tau}_n) \tag{5.17}$$

depending on the desired interpretation of the optimisation problem. In any case, (5.16) or (5.17) has to be minimised with respect to $\boldsymbol{u}_d, \boldsymbol{\tau}_d$ subject to the initial and final configuration constraints $\boldsymbol{u}_0 - \boldsymbol{u}^0 = \boldsymbol{0}$, $\boldsymbol{D}(\boldsymbol{q}_N, \boldsymbol{q}^N) = \boldsymbol{0}$, the initial and final momenta constraints (5.15), and the discretised dynamics (5.12).

Accuracy and efficiency The order of approximation of the discrete Lagrangian and the discrete virtual work given in (5.7) and (5.8), respectively, determines the accuracy and the order of convergence of the optimal control method. In general, one uses polynomial approximations to the trajectories and numerical quadrature to approximate the integrals. Then, the order of the discrete Lagrangian and the discrete virtual work is given by the order of the quadrature rule in use. In [Ober 08, Ober 10] it is shown for DMOC (unconstrained dynamics) that a discrete Lagrangian and discrete virtual work of order κ lead to an optimal control scheme of order κ.[1] That means, the state and control trajectories as well as the Lagrange multipliers resulting from the Pontryagin Maximum Principle are approximated with an accuracy of $\mathcal{O}(h^\kappa)$. This is in contrast to other schemes, e.g. standard Runge-Kutta or collocation methods, where the approximation of the Lagrange multipliers may be of one or more orders less and is a result of the symplectic nature of the underlying discretisation.

When accuracy is improved by increasing the number of discretisation points, an implementation on configuration level $Q \times Q$ only, rather than on configuration-momentum or configuration-velocity level, leads to a smaller number of optimisation parameters and therefore to a smaller number of SQP iterations[2] compared to collocation methods. Thereby, the optimal trajectory for the configuration and the control forces is determined while the corresponding momenta and velocities are reconstructed. Note that the purely configuration based formulation of DMOC leads to equivalent discrete solution as the configuration-momentum based collocation resulting from symplectic Runge-Kutta methods, see [Ober 10].

In the case of constrained dynamics, the use of the discrete null space method with nodal reparametrisation in DMOCC yields a constrained optimisation problem of minimal possible dimension: the optimisation of (5.16) or (5.17) subject to the discretised equations includes $(2N+1)(n-m)$ variables and $(N+3)(n-m)$ constraints. In contrast to that, the optimisation problem resulting from the Lagrange multiplier formulation involves $N(2n+m)+n$ unknowns and $(N-1)(n+m)+4n$ constraints (i.e. $(3N+1)m$ more variables and $(N+1)2m$ more constraints). Certainly, this influences the computational costs of the SQP solver substantially. Both formulations, DMOC in generalised coordinates and DMOCC, converge to the same solution as shown for a simple example in Section 5.7.1.

Of course, the SQP solver provides only local solutions that are strongly dependent on the initial guess. Since the focus of this work is on the structure preserving approximation of the optimal control of constrained motion, the problem of finding global solutions is not pursued here.

[1] Here, smoothness and coercivity of the solution as well as bounded variation of the controls are assumed.

[2] By exploiting the sparse structure of the optimisation problem, the number of SQP iterations grows approximately linearly w.r.t. the number of optimisation variables, see [Ober 10].

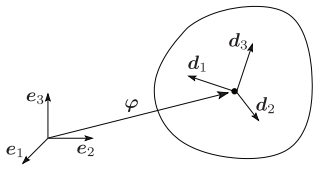

Figure 5.2: Configuration of a rigid body with respect to an orthonormal frame $\{\boldsymbol{e}_I\}$ fixed in space.

5.4 Optimal control for rigid body dynamics

A constrained formulation of rigid body dynamics (see [Antm 95, Bets 01b]) is used in this work. The time dependent configuration variable of a rigid body

$$\boldsymbol{q}(t) = \begin{bmatrix}\boldsymbol{\varphi}(t) & \boldsymbol{d}_1(t) & \boldsymbol{d}_2(t) & \boldsymbol{d}_3(t)\end{bmatrix}^T \in \mathbb{R}^{12} \tag{5.18}$$

consists of the placement of the centre of mass $\boldsymbol{\varphi} \in \mathbb{R}^3$ and the directors $\boldsymbol{d}_I \in \mathbb{R}^3, I = 1, 2, 3$ which are constrained to stay orthonormal during the motion, see Figure 5.2. Of course this is equivalent to specifying that the configuration manifold is the Euclidean group, SE(3), which is common in other treatments, such as [Mars 94]. These constraints on the directors are called internal constraints, since they represent the underlying kinematic assumptions. Then the body's Euler tensor with respect to the centre of mass can be related to the inertia tensor $\boldsymbol{J}$ via $\boldsymbol{E} = \frac{1}{2}(\mathrm{tr}\boldsymbol{J})\boldsymbol{I} - \boldsymbol{J}$, where $\boldsymbol{I}$ denotes the 3×3 identity matrix. The principal values of the Euler tensor E_i together with the body's total mass M_φ are ingredients in the rigid body's constant symmetric positive definite mass matrix

$$\boldsymbol{M} = \mathrm{diag}(M_\varphi \boldsymbol{I} \quad E_1\boldsymbol{I} \quad E_2\boldsymbol{I} \quad E_3\boldsymbol{I}).$$

The angular momentum of the rigid body can be computed as

$$\boldsymbol{L} = \boldsymbol{\varphi} \times \boldsymbol{p}_\varphi + \boldsymbol{d}_I \times \boldsymbol{p}_I, \tag{5.19}$$

where summation convention is used to sum over the repeated index I.

Null space matrix An account of rigid body dynamics is given in [Bets 06, Leye 06a] where also the null space matrix

$$\boldsymbol{P}_{\mathrm{int}}(\boldsymbol{q}) = \begin{bmatrix}\boldsymbol{I} & \boldsymbol{0} \\ \boldsymbol{0} & -\widehat{\boldsymbol{d}_1} \\ \boldsymbol{0} & -\widehat{\boldsymbol{d}_2} \\ \boldsymbol{0} & -\widehat{\boldsymbol{d}_3}\end{bmatrix} \tag{5.20}$$

has been derived. Here $\widehat{\boldsymbol{a}}$ denotes the skew-symmetric 3×3 matrix with corresponding axial vector $\boldsymbol{a} \in \mathbb{R}^3$. For a single rigid body moving free in space, no external constraints are present, therefore $\boldsymbol{P}(\boldsymbol{q}) = \boldsymbol{P}_{\mathrm{int}}(\boldsymbol{q})$.

Nodal reparametrisation When the nodal reparametrisation of unknowns is applied, the configuration of the free rigid body is specified by six unknowns $\boldsymbol{u}_{n+1} = (\boldsymbol{u}_{\varphi_{n+1}}, \boldsymbol{\theta}_{n+1}) \in$

$U \subset \mathbb{R}^3 \times \mathbb{R}^3$, characterising the incremental displacement and incremental rotation, respectively. Accordingly, in the present case the nodal reparametrisation $\boldsymbol{F} : U \times Q \to C$ introduced in (5.10) assumes the form

$$\begin{aligned} \boldsymbol{q}_{n+1} &= \boldsymbol{F}_d(\boldsymbol{u}_{n+1}, \boldsymbol{q}_n) \\ &= \left[\boldsymbol{\varphi}_n + \boldsymbol{u}_{\varphi_{n+1}} \quad \exp(\widehat{\boldsymbol{\theta}_{n+1}}) \cdot (\boldsymbol{d}_1)_n \quad \exp(\widehat{\boldsymbol{\theta}_{n+1}}) \cdot (\boldsymbol{d}_2)_n \quad \exp(\widehat{\boldsymbol{\theta}_{n+1}}) \cdot (\boldsymbol{d}_3)_n\right]^T, \end{aligned} \tag{5.21}$$

where Rodrigues' formula is used to obtain a closed form expression of the exponential map, see e.g. [Mars 94].

Actuation of the rigid body Consider a single rigid body that is actuated by generalised forces $\boldsymbol{\tau}_{rb} = [\boldsymbol{\tau}_\varphi \quad \boldsymbol{\tau}_\theta]^T \in \mathbb{R}^6$ consisting of a translational force $\boldsymbol{\tau}_\varphi \in \mathbb{R}^3$ and a torque $\boldsymbol{\tau}_\theta \in \mathbb{R}^3$. Assume that the force is not applied in the centre of mass, but in material points of the rigid body located at $\boldsymbol{\varrho}^{rb} = \varrho_I^{rb} \boldsymbol{d}_I$ away from the centre of mass. This results in a force $\boldsymbol{\tau}_\varphi$ applied at the centre of mass and a torque $\boldsymbol{\varrho}^{rb} \times \boldsymbol{\tau}_\varphi + \boldsymbol{\tau}_\theta$ that are given by

$$\begin{bmatrix} \boldsymbol{\tau}_\varphi \\ \boldsymbol{\varrho}^{rb} \times \boldsymbol{\tau}_\varphi + \boldsymbol{\tau}_\theta \end{bmatrix} = \boldsymbol{C}_{rb}(\boldsymbol{q}) \cdot \boldsymbol{\tau}_{rb} \qquad \boldsymbol{C}_{rb}(\boldsymbol{q}) = \begin{bmatrix} \boldsymbol{I} & \boldsymbol{0} \\ \widehat{\boldsymbol{\varrho}}^{rb} & \boldsymbol{I} \end{bmatrix} \in \mathbb{R}^{6\times 6}.$$

As with (5.5), the redundant forces can be computed according to

$$\boldsymbol{f} = [\boldsymbol{f}_\varphi \quad \boldsymbol{f}_1 \quad \boldsymbol{f}_2 \quad \boldsymbol{f}_3]^T = \boldsymbol{B}^T(\boldsymbol{q}) \cdot \boldsymbol{\tau}_{rb} \in \mathbb{R}^{12},$$

with

$$\boldsymbol{B}^T(\boldsymbol{q}) = \boldsymbol{P}_{\text{int}}(\boldsymbol{q}) \cdot \begin{bmatrix} \boldsymbol{I} & \boldsymbol{0} \\ \boldsymbol{0} & \frac{1}{2}\boldsymbol{I} \end{bmatrix} \cdot \boldsymbol{C}_{rb}(\boldsymbol{q}) \in \mathbb{R}^{12\times 6}.$$

A straightforward calculation shows

$$\boldsymbol{P}^T(\boldsymbol{q}) \cdot \boldsymbol{f} = \boldsymbol{C}_{rb}(\boldsymbol{q}) \cdot \boldsymbol{\tau}_{rb}. \tag{5.22}$$

The resulting reduced forces in (5.12) represent the effect of the applied forces and torques $\boldsymbol{\tau}_{rb}$ on the generalised degrees of freedom. The same holds in the discrete setting, where the resulting reduced forces in (5.12)

$$\boldsymbol{P}^T(\boldsymbol{q}_n) \cdot (\boldsymbol{f}_{n-1}^+ + \boldsymbol{f}_n^-) = \boldsymbol{C}_{rb}(\boldsymbol{q}_n) \cdot \left(\boldsymbol{\tau}_{rb}{}_{n-1}^+ + \boldsymbol{\tau}_{rb}{}_n^-\right)$$

represent the effect of the applied forces and torques at t_n on the generalised degrees of freedom.

Proposition 5.4.1 *The above definition of the redundant left and right discrete forces guarantees that, in the absence of a potential energy, the change in angular momentum along the solution trajectory $\boldsymbol{q}_d$ of (5.12) is induced only by the effect of the discrete generalised forces.*

Proof: Computation of $\boldsymbol{p}_{n+1}^{+}$ and via $\boldsymbol{p}_{n}^{-}$ the discrete Legendre transforms (5.13) and insertion into the definition of angular momentum (5.19) yields

$$\begin{aligned}
\boldsymbol{L}_{n+1} - \boldsymbol{L}_n &= \boldsymbol{\varphi}_{n+1} \times \boldsymbol{p}_{\varphi_{n+1}}^{+} + \boldsymbol{d}_{I\,n+1} \times \boldsymbol{p}_{I_{n+1}}^{+} - \boldsymbol{\varphi}_n \times \boldsymbol{p}_{\varphi_n}^{-} - \boldsymbol{d}_{I\,n} \times \boldsymbol{p}_{I_n}^{-} \\
&= \boldsymbol{\varphi}_{n+1} \times \left(\boldsymbol{f}_{\varphi_n}^{+}\right) + \boldsymbol{d}_{I\,n+1} \times \left(\boldsymbol{f}_{I_n}^{+}\right) - \boldsymbol{\varphi}_n \times \left(-\boldsymbol{f}_{\varphi_n}^{-}\right) - \boldsymbol{d}_{I\,n} \times \left(-\boldsymbol{f}_{I_n}^{-}\right) \\
&= \boldsymbol{\varphi}_{n+1} \times \boldsymbol{\tau}_{\varphi_n}^{+} + \boldsymbol{d}_{I\,n+1} \times \left(\frac{1}{2}\left(\boldsymbol{\varrho}_{n+1}^{rb} \times \boldsymbol{\tau}_{\varphi_n}^{+} + \boldsymbol{\tau}_{\theta_n}^{+}\right) \times \boldsymbol{d}_{I\,n+1}\right) \\
&\quad + \boldsymbol{\varphi}_n \times \boldsymbol{\tau}_{\varphi_n}^{-} + \boldsymbol{d}_{I\,n} \times \left(\frac{1}{2}\left(\boldsymbol{\varrho}_{n}^{rb} \times \boldsymbol{\tau}_{\varphi_n}^{-} + \boldsymbol{\tau}_{\theta_n}^{-}\right) \times \boldsymbol{d}_{I\,n}\right) \\
&= \boldsymbol{\varphi}_{n+1} \times \boldsymbol{\tau}_{\varphi_n}^{+} + \boldsymbol{\varrho}_{n+1}^{rb} \times \boldsymbol{\tau}_{\varphi_n}^{+} + \boldsymbol{\tau}_{\theta_n}^{+} + \boldsymbol{\varphi}_n \times \boldsymbol{\tau}_{\varphi_n}^{-} + \boldsymbol{\varrho}_{n}^{rb} \times \boldsymbol{\tau}_{\varphi_n}^{-} + \boldsymbol{\tau}_{\theta_n}^{-}.
\end{aligned} \tag{5.23}$$

A straightforward calculation shows that all terms stemming from the kinetic energy and the constraint forces cancel. ∎

Remark 5.4.2 (The presence of gravity) *With an acceleration $g \in \mathbb{R}$ due to gravity in the negative $\boldsymbol{e}_3$-direction, the corresponding potential reads*

$$V(\boldsymbol{q}) = [0 \quad 0 \quad -M_\varphi g \quad 0 \quad \cdots \quad 0] \cdot \boldsymbol{q}.$$

In this case, (5.23) *yields*

$$\begin{aligned}
\boldsymbol{L}_{n+1} - \boldsymbol{L}_n &= \boldsymbol{\varphi}_{n+1} \times \boldsymbol{\tau}_{\varphi_n}^{+} + \boldsymbol{\varrho}_{n+1}^{rb} \times \boldsymbol{\tau}_{\varphi_n}^{+} + \boldsymbol{\tau}_{\theta_n}^{+} + \boldsymbol{\varphi}_n \times \boldsymbol{\tau}_{\varphi_n}^{-} + \boldsymbol{\varrho}_{n}^{rb} \times \boldsymbol{\tau}_{\varphi_n}^{-} + \boldsymbol{\tau}_{\theta_n}^{-} \\
&\quad - \left(\boldsymbol{\varphi}_{n+1} + \boldsymbol{\varphi}_n\right) \times \frac{h}{2} [0 \quad 0 \quad -M_\varphi g]^T,
\end{aligned}$$

meaning that the third component of the angular momentum changes only according to the applied forces while the change in the first and second component is influenced by gravity as well. In particular in the absence of any external forces, this shows that the third component of the angular momentum is conserved exactly.

5.5 Optimal control for kinematic pairs

In the sequel, actuating forces being consistent with the specific joint constraints are given and structure preservation of the resulting time stepping scheme is proved.
The coupling of two neighbouring links (body 1 and body 2) by a specific joint J yields $m_{\text{ext}}^{(J)}$ external constraints on the configuration variable

$$\boldsymbol{q} = \begin{bmatrix} \boldsymbol{q}^1 & \boldsymbol{q}^2 \end{bmatrix}^T \in \mathbb{R}^{24} \tag{5.24}$$

consisting of $\boldsymbol{q}^\alpha, \alpha = 1, 2$ of the form (5.18). The degrees of freedom of the relative motion of one body with respect to the other is decreased from 6 to $r^{(J)} = 6 - m_{\text{ext}}^{(J)}$. The location of a specific joint in the α-th body is characterised by coordinates ϱ_i^α in the body frame $\{\boldsymbol{d}_I^\alpha\}$ as $\boldsymbol{\varrho}^\alpha = \varrho_i^\alpha \boldsymbol{d}_i^\alpha$ for $\alpha = 1, 2$.

Null space matrix The total null space matrix associated with a kinematic pair can be calculated from

$$\boldsymbol{P}^{(J)}(\boldsymbol{q}) = \begin{bmatrix} \boldsymbol{P}_{\text{int}}(\boldsymbol{q}^1) & \boldsymbol{0}_{12\times r^{(J)}} \\ \boldsymbol{P}_{\text{int}}(\boldsymbol{q}^2)\cdot\boldsymbol{P}^{2,(J)}_{\text{ext}}(\boldsymbol{q}) \end{bmatrix}, \tag{5.25}$$

where the internal null space matrix of each body is given in (5.20) and the $6\times(6+r^{(J)})$ matrix $\boldsymbol{P}^{2,(J)}_{\text{ext}}(\boldsymbol{q})$ accounts for the coupling induced by a specific joint.

Nodal reparametrisation The redundant coordinates $\boldsymbol{q}\in\mathbb{R}^{24}$ of each kinematic pair may be expressed in terms of $6+r^{(J)}$ independent generalised coordinates. When using a reparametrisation of unknowns in the discrete null space method, relationships of the form

$$\boldsymbol{q}_{n+1} = \boldsymbol{F}^{(J)}(\boldsymbol{\mu}^{(J)}_{n+1}, \boldsymbol{q}_n) \tag{5.26}$$

are required, where

$$\boldsymbol{\mu}^{(J)}_{n+1} = (\boldsymbol{u}^1_{\varphi_{n+1}}, \boldsymbol{\theta}^1_{n+1}, \boldsymbol{\vartheta}^{(J)}_{n+1}) \in \mathbb{R}^{6+r^{(J)}} \tag{5.27}$$

consists of a minimal number of incremental unknowns in $[t_n, t_{n+1}]$ for a specific kinematic pair. In (5.27), $(\boldsymbol{u}^1_{\varphi_{n+1}}, \boldsymbol{\theta}^1_{n+1})\in\mathbb{R}^3\times\mathbb{R}^3$ are incremental displacements and rotations, respectively, associated with the first body (see Section 5.4). Furthermore, $\boldsymbol{\vartheta}^{(J)}_{n+1}\in\mathbb{R}^{r^{(J)}}$ denotes incremental unknowns which characterise the configuration of the second body relative to the axis (or plane in case of the E pair) of relative motion fixed in the first body. In view of (5.24), the mapping in (5.26) may be partitioned according to

$$\boldsymbol{q}^1_{n+1} = \boldsymbol{F}^1(\boldsymbol{u}^1_{\varphi_{n+1}}, \boldsymbol{\theta}^1_{n+1}, \boldsymbol{q}^1_n), \quad \boldsymbol{q}^2_{n+1} = \boldsymbol{F}^{2,(J)}(\boldsymbol{\mu}^{(J)}_{n+1}, \boldsymbol{q}_n),$$

where $\boldsymbol{F}^1(\boldsymbol{u}^1_{\varphi_{n+1}}, \boldsymbol{\theta}^1_{n+1}, \boldsymbol{q}^1_n)$ is given by (5.21) and $\boldsymbol{F}^{2,(J)}(\boldsymbol{\mu}^{(J)}_{n+1}, \boldsymbol{q}_n)$ remains to be specified for each kinematic pair.

Actuation of a kinematic pair The actuation of kinematic pairs is twofold. First of all, the overall motion of the pair can be influenced by applying translational forces and torques $\boldsymbol{\tau}_{rb}\in\mathbb{R}^6$ to one of the bodies, say body 1. Any resulting change in the first bodies velocities will be transferred to the second body via the constrained equations of motion. Secondly, the relative motion of the pair can be influenced. Actuation of the joint connection itself by joint forces $\boldsymbol{\tau}^{(J)}\in\mathbb{R}^{r^{(J)}}$ effects both bodies, where according to "action equals reaction", the resulting generalised forces on the bodies are equal, but opposite in sign, see e.g. [Bull 04]. The dimension of the joint force $\boldsymbol{\tau}^{(J)}$ is determined by the number of relative degrees of freedom $r^{(J)}$ permitted by the specific joint.
Altogether, the generalised forces

$$\begin{bmatrix}\boldsymbol{\tau}_{rb} & \boldsymbol{\tau}^{(J)}\end{bmatrix}^T \in \mathbb{R}^{6+r^{(J)}} \tag{5.28}$$

act on the kinematic pair. The redundant forces can then be computed similar to (5.5) as

$$\boldsymbol{f} = \begin{bmatrix}\boldsymbol{f}^1 & \boldsymbol{f}^2\end{bmatrix}^T = \boldsymbol{B}^T(\boldsymbol{q})\cdot\begin{bmatrix}\boldsymbol{\tau}_{rb} & \boldsymbol{\tau}^{(J)}\end{bmatrix}^T \in \mathbb{R}^{24}, \tag{5.29}$$

with the $24 \times (6 + r^{(J)})$ matrix

$$\boldsymbol{B}^T(\boldsymbol{q}) = \begin{bmatrix} \boldsymbol{P}_{\text{int}}(\boldsymbol{q}^1) & \boldsymbol{0} \\ \boldsymbol{0} & \boldsymbol{P}_{\text{int}}(\boldsymbol{q}^2) \end{bmatrix} \cdot \begin{bmatrix} \boldsymbol{I} & \boldsymbol{0} & \boldsymbol{0} & \boldsymbol{0} \\ \boldsymbol{0} & \frac{1}{2}\boldsymbol{I} & \boldsymbol{0} & \boldsymbol{0} \\ \boldsymbol{0} & \boldsymbol{0} & \boldsymbol{I} & \boldsymbol{0} \\ \boldsymbol{0} & \boldsymbol{0} & \boldsymbol{0} & \frac{1}{2}\boldsymbol{I} \end{bmatrix} \cdot \begin{bmatrix} \boldsymbol{C}_{rb}(\boldsymbol{q}^1) & \boldsymbol{C}^{1,(J)}(\boldsymbol{q}) \\ \boldsymbol{0} & \boldsymbol{C}^{2,(J)}(\boldsymbol{q}) \end{bmatrix} \tag{5.30}$$

and the $6 \times r^{(J)}$ matrices $\boldsymbol{C}^{\alpha,(J)}(\boldsymbol{q}), \alpha = 1, 2$ being specified according to the specific joint in use.
As with equation (5.22), the product of the transposed null space matrix and the redundant forces yields the effect of the generalised forces on the generalised degrees of freedom of the kinematic pair.

5.5.1 Spherical pair

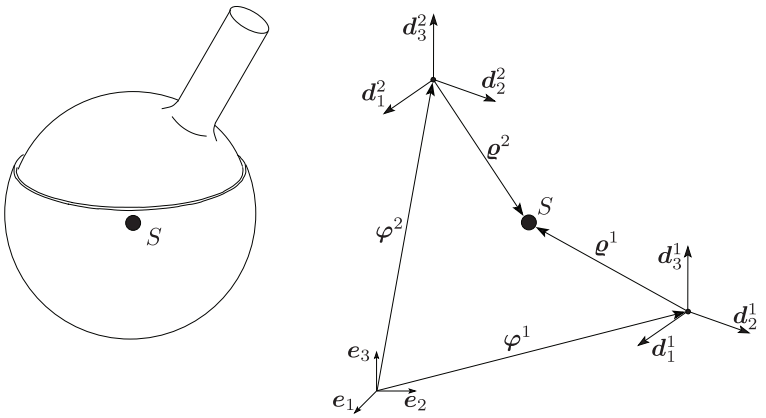

Figure 5.3: Spherical pair.

The S pair (Figure 5.3) prevents all relative translation between the two bodies. The null space matrix and nodal reparametrisation for the S pair do not differ from those given in [Bets 06, Leye 06a].

Actuation of the spherical pair A torque $\boldsymbol{\tau}^{(S)} \in \mathbb{R}^3$ can be applied at the spherical joint. Then the forces on each body are computed according to (5.29) with

$$\boldsymbol{C}^{1,(S)}(\boldsymbol{q}) = [\boldsymbol{0} \quad -\boldsymbol{I}]^T \qquad \boldsymbol{C}^{2,(S)}(\boldsymbol{q}) = [\boldsymbol{0} \quad \boldsymbol{I}]^T .$$

The generalised forces effect the following actuation of the generalised degrees of freedom of the spherical pair. In addition to the rigid body actuation, the first body's rotation is influenced by the joint torque, which also actuates the relative rotation of the second body.

$$\left(\boldsymbol{P}^{(S)}(\boldsymbol{q})\right)^T \cdot \boldsymbol{f} = \left[\boldsymbol{\tau}_\varphi \quad \boldsymbol{\varrho}^{rb} \times \boldsymbol{\tau}_\varphi + \boldsymbol{\tau}_\theta - \boldsymbol{\tau}^{(S)} \quad \boldsymbol{\tau}^{(S)}\right]^T$$

Proposition 5.5.1 *This definition of the redundant left and right discrete forces guarantees that the change of angular momentum along the solution trajectory $\boldsymbol{q}_d$ of* (5.12) *is induced only by the effect of the discrete generalised forces $\boldsymbol{\tau}_{rb}$. In particular, it is conserved exactly, if the motion of the pair is induced by shape changes only.*

Proof: In proving the second statement, it is assumed that only the joint is actuated, i.e. $\boldsymbol{\tau}_{rb} = \mathbf{0}$. Computation of $\boldsymbol{p}_{n+1}^{+}$ and via $\boldsymbol{p}_n^{-}$ the discrete Legendre transform (5.13) and insertion into the definition of angular momentum (5.19) yields

$$\begin{aligned}
\boldsymbol{L}_{n+1} - \boldsymbol{L}_n &= \boldsymbol{\varphi}_{n+1}^1 \times \boldsymbol{p}_{\varphi_{n+1}}^{1\,+} + \boldsymbol{d}_{I\,n+1}^1 \times \boldsymbol{p}_{I\,n+1}^{1+} + \boldsymbol{\varphi}_{n+1}^2 \times \boldsymbol{p}_{\varphi_{n+1}}^{2\,+} + \boldsymbol{d}_{I\,n+1}^2 \times \boldsymbol{p}_{I\,n+1}^{2+} + \\
&\quad - \boldsymbol{\varphi}_n^1 \times \boldsymbol{p}_{\varphi_n}^{1\,-} - \boldsymbol{d}_{I\,n}^1 \times \boldsymbol{p}_{I\,n}^{1-} - \boldsymbol{\varphi}_n^2 \times \boldsymbol{p}_{\varphi_n}^{2\,-} - \boldsymbol{d}_{I\,n}^2 \times \boldsymbol{p}_{I\,n}^{2-} \\
&= \boldsymbol{d}_{I\,n+1}^1 \times \left(-\frac{1}{2} \boldsymbol{\tau}_n^{(S)\,+} \times \boldsymbol{d}_{I\,n+1}^1 \right) + \boldsymbol{d}_{I\,n+1}^2 \times \left(\frac{1}{2} \boldsymbol{\tau}_n^{(S)\,+} \times \boldsymbol{d}_{I\,n+1}^2 \right) + \\
&\quad \boldsymbol{d}_{I\,n}^1 \times \left(-\frac{1}{2} \boldsymbol{\tau}_n^{(S)\,-} \times \boldsymbol{d}_{I\,n}^1 \right) + \boldsymbol{d}_{I\,n}^2 \times \left(\frac{1}{2} \boldsymbol{\tau}_n^{(S)\,-} \times \boldsymbol{d}_{I\,n}^2 \right) \\
&= -\boldsymbol{\tau}_n^{(S)\,+} + \boldsymbol{\tau}_n^{(S)\,+} - \boldsymbol{\tau}_n^{(S)\,-} + \boldsymbol{\tau}_n^{(S)\,-} = \mathbf{0}.
\end{aligned} \tag{5.31}$$

The first statement follows by combining (5.31) and (5.23). ∎

5.5.2 Cylindrical pair

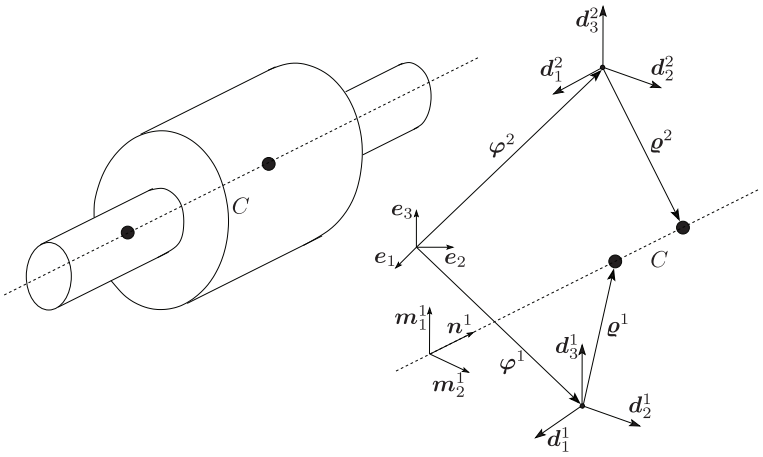

Figure 5.4: Cylindrical pair.

Let $\{\boldsymbol{m}_1^1, \boldsymbol{m}_2^1, \boldsymbol{n}^1\}$ constitute a right-handed orthonormal frame which is fixed in the first body and specified by $\boldsymbol{n}^1 = n_I^1 \boldsymbol{d}_I^1$ and $\boldsymbol{m}_\kappa^1 = (m_\kappa^1)_I \boldsymbol{d}_I^1$ for $\kappa = 1, 2$. The motion of the second body relative to the axis $\boldsymbol{n}^1$ can be described by $r^{(C)} = 2$ degrees of freedom: translation u^2 along $\boldsymbol{n}^1$ and rotation θ^2 about $\boldsymbol{n}^1$.

Remark 5.5.2 (Comparison with [Bets 06, Leye 06a]) *The assumption*

$$\boldsymbol{\omega}^2 = \boldsymbol{\omega}^1 + \dot{\theta}^2 \boldsymbol{n}^1 \tag{5.32}$$

used in [Bets 06, Leye 06a] induces the second body to perform the same rotational motion as the first one and to additionally rotate relative to it about the axis $\boldsymbol{n}^1$. In particular,

the second body follows the first bodies rotation about $\boldsymbol{n}^1$ *if the relative velocity is zero. For example a pure rotation of the first body about* $\boldsymbol{n}^1$ *would affect the second body, but not vice versa according to* (5.32)*. The new kinematic assumptions, to be introduced in* (5.33)*, in combination with the new update formula* (5.35) *completely decouple the bodies with respect to rotations about and translations along* $\boldsymbol{n}^1$*. Therefore it is easier to apply joint actuations that lead to momentum consistent dynamics.*

Null space matrix Specifically, the new relation between the angular velocities reads

$$\boldsymbol{\omega}^2 = \boldsymbol{I}^{11} \cdot \boldsymbol{\omega}^1 + \dot{\theta}^2 \boldsymbol{n}^1. \tag{5.33}$$

It ensures that the translation along and rotation about the axis $\boldsymbol{n}^1$ of one body leaves the other body motionless. With $\boldsymbol{I}^{11} = \boldsymbol{I} - \boldsymbol{n}^1 \otimes \boldsymbol{n}^1$, the null space matrix for the C pair can be inferred from (5.25) with

$$\boldsymbol{P}_{\mathrm{int}}(\boldsymbol{q}^2) \cdot \boldsymbol{P}_{\mathrm{ext}}^{2,(C)}(\boldsymbol{q}) = \begin{bmatrix} \boldsymbol{I}^{11} & \widehat{\boldsymbol{\varrho}^2} \cdot \boldsymbol{I}^{11} - \widehat{\boldsymbol{\varrho}^1} - \widehat{u^2 \boldsymbol{n}^1} & \boldsymbol{n}^1 & \boldsymbol{\varrho}^2 \times \boldsymbol{n}^1 \\ \boldsymbol{0} & -\widehat{\boldsymbol{d}_1^2} \cdot \boldsymbol{I}^{11} & \boldsymbol{0} & \boldsymbol{n}^1 \times \boldsymbol{d}_1^2 \\ \boldsymbol{0} & -\widehat{\boldsymbol{d}_2^2} \cdot \boldsymbol{I}^{11} & \boldsymbol{0} & \boldsymbol{n}^1 \times \boldsymbol{d}_2^2 \\ \boldsymbol{0} & -\widehat{\boldsymbol{d}_3^2} \cdot \boldsymbol{I}^{11} & \boldsymbol{0} & \boldsymbol{n}^1 \times \boldsymbol{d}_3^2 \end{bmatrix}.$$

Nodal reparametrisation For the C pair, the configuration of the second body with respect to the axis $\boldsymbol{n}^1$ can be characterised by $\boldsymbol{\vartheta}_{n+1}^{(C)} = (u_{n+1}^2, \theta_{n+1}^2) \in \mathbb{R}^2$. Here θ_{n+1}^2 accounts for the incremental rotation. The rotation of the second body's directors consist of this rotation and that part of the rotation of body one which is not about the axis $\boldsymbol{n}^1$. Using the notation

$$\boldsymbol{R}^{1,2} = \exp(\widehat{\boldsymbol{\theta}_{n+1}^1}) \cdot \exp(-\widehat{(\boldsymbol{n}_n^1 \otimes \boldsymbol{n}_n^1) \cdot \boldsymbol{\theta}_{n+1}^1}), \tag{5.34}$$

it may be expressed via the product of exponentials formula

$$\boldsymbol{q}_{n+1}^2 = \boldsymbol{F}^{2,(C)}(\boldsymbol{\mu}_{n+1}^{(C)}, \boldsymbol{q}_n) = \begin{bmatrix} \boldsymbol{\varphi}_n^1 + \boldsymbol{I}_n^{11} \cdot \boldsymbol{u}_{\varphi_{n+1}}^1 + \exp(\widehat{\boldsymbol{\theta}_{n+1}^1}) \cdot [\boldsymbol{\varrho}_n^1 + (\bar{u}_n^2 + u_{n+1}^2)\boldsymbol{n}_n^1] - \boldsymbol{R}^{1,2} \cdot \exp\left(\theta_{n+1}^2 \widehat{\boldsymbol{n}_n^1}\right) \cdot \boldsymbol{\varrho}_n^2 \\ \boldsymbol{R}^{1,2} \cdot \exp\left(\theta_{n+1}^2 \widehat{\boldsymbol{n}_n^1}\right) \cdot (\boldsymbol{d}_1^2)_n \\ \boldsymbol{R}^{1,2} \cdot \exp\left(\theta_{n+1}^2 \widehat{\boldsymbol{n}_n^1}\right) \cdot (\boldsymbol{d}_2^2)_n \\ \boldsymbol{R}^{1,2} \cdot \exp\left(\theta_{n+1}^2 \widehat{\boldsymbol{n}_n^1}\right) \cdot (\boldsymbol{d}_3^2)_n \end{bmatrix}, \tag{5.35}$$

where $\bar{u}_n^2 = \boldsymbol{n}_n^1 \cdot (\boldsymbol{\varphi}_n^2 + \boldsymbol{\varrho}_n^2 - \boldsymbol{\varphi}_n^1 - \boldsymbol{\varrho}_n^1)$ denotes the translation of the second body relative to the first one in the direction of the axis $\boldsymbol{n}_n^1$ at time t_n.

Actuation of the cylindrical pair The two relative degrees of freedom allowed by the cylindrical joint can be actuated by a translational force $\tau_\varphi^{(C)} \in \mathbb{R}$ that acts in the direction of the axis $\boldsymbol{n}^1$ and a torque $\tau_\theta^{(C)} \in \mathbb{R}$ about $\boldsymbol{n}^1$. Even if the joint is located away from the centres of mass, translational force along $\boldsymbol{n}^1$ can not cause a relative rotation of the

second body for this pair. However, it causes the pair to rotate according to a torque $(\boldsymbol{\varphi}^1 - \boldsymbol{\varphi}^2) \times \boldsymbol{n}^1$, which is assigned to the first body. Using the matrices

$$\boldsymbol{C}^{1,(C)}(\boldsymbol{q}) = \begin{bmatrix} -\boldsymbol{n}^1 & \boldsymbol{0} \\ (\boldsymbol{\varphi}^1 - \boldsymbol{\varphi}^2) \times \boldsymbol{n}^1 & -\boldsymbol{n}^1 \end{bmatrix} \qquad \boldsymbol{C}^{2,(C)}(\boldsymbol{q}) = \begin{bmatrix} \boldsymbol{n}^1 & \boldsymbol{0} \\ \boldsymbol{0} & \boldsymbol{n}^1 \end{bmatrix},$$

consistent forces can be computed from (5.29). The actuation of the generalised degrees of freedom reads

$$\left(\boldsymbol{P}^{(C)}(\boldsymbol{q})\right)^T \cdot \boldsymbol{f} = \begin{bmatrix} \boldsymbol{\tau}_\varphi - \tau_\varphi^{(C)} \boldsymbol{n}^1 & \boldsymbol{\varrho}^{rb} \times \boldsymbol{\tau}_\varphi + \boldsymbol{\tau}_\theta - \tau_\theta^{(C)} \boldsymbol{n}^1 & \tau_\varphi^{(C)} & \tau_\theta^{(C)} \end{bmatrix}^T. \tag{5.36}$$

Proposition 5.5.1 stating the consistency of angular momentum holds for the C pair and can be proved in exactly the same steps as for the S pair.

5.5.3 Revolute and prismatic pair

The revolute and the prismatic pair are both special cases of the cylindrical pair, having one of the two relative degrees of freedom present in the C pair, respectively. Their null space matrices, nodal reparametrisation and actuation can be inferred from the previous treatment of the C pair by eliminating the translational degree of freedom in case of the R pair and the rotational degree of freedom in case of the P pair.

5.5.4 Planar pair

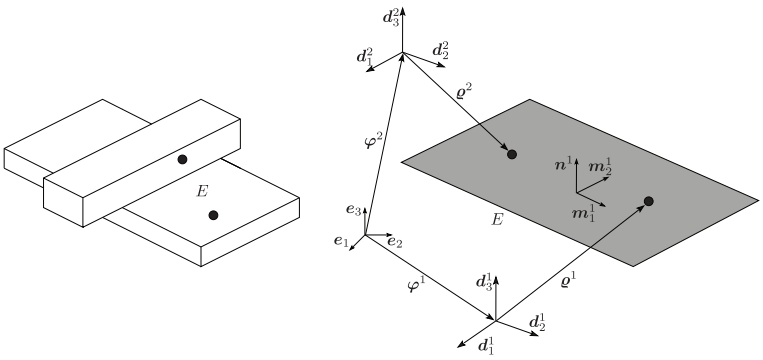

Figure 5.5: Planar pair.

For the E pair (Figure 5.5), the second body may rotate about the axis specified by $\boldsymbol{n}^1$ and translate in the plane spanned by $\boldsymbol{m}_1^1$ and $\boldsymbol{m}_2^1$.

Null space matrix Using $\boldsymbol{I}^{12} = \boldsymbol{I} - \boldsymbol{m}_1^1 \otimes \boldsymbol{m}_1^1 - \boldsymbol{m}_2^1 \otimes \boldsymbol{m}_2^1$, the relation between the angular velocities reads $\boldsymbol{\omega}^2 = \boldsymbol{I}^{11} \cdot \boldsymbol{\omega}^1 + \dot{\theta}^2 \boldsymbol{n}^1$. With regard to (5.25), the null space matrix for the E pair is given by

$$\boldsymbol{P}_{\text{int}}(\boldsymbol{q}^2) \cdot \boldsymbol{P}_{\text{ext}}^{2,(E)}(\boldsymbol{q}) = \begin{bmatrix} \boldsymbol{I}^{12} & \widehat{\boldsymbol{\varrho}^2} \cdot \boldsymbol{I}^{11} - \widehat{\boldsymbol{\varrho}^1} - \widehat{u_\kappa^2 \boldsymbol{m}_\kappa^1} & \boldsymbol{m}_1^1 & \boldsymbol{m}_2^1 & \boldsymbol{\varrho}^2 \times \boldsymbol{n}^1 \\ \boldsymbol{0} & -\widehat{\boldsymbol{d}_1^2} \cdot \boldsymbol{I}^{11} & \boldsymbol{0} & \boldsymbol{0} & \boldsymbol{n}^1 \times \boldsymbol{d}_1^2 \\ \boldsymbol{0} & -\widehat{\boldsymbol{d}_2^2} \cdot \boldsymbol{I}^{11} & \boldsymbol{0} & \boldsymbol{0} & \boldsymbol{n}^1 \times \boldsymbol{d}_2^2 \\ \boldsymbol{0} & -\widehat{\boldsymbol{d}_3^2} \cdot \boldsymbol{I}^{11} & \boldsymbol{0} & \boldsymbol{0} & \boldsymbol{n}^1 \times \boldsymbol{d}_3^2 \end{bmatrix}.$$

Nodal reparametrisation In the present case the configuration of the second body can be characterised by the incremental variables $\boldsymbol{\vartheta}_{n+1}^{(E)} = (u_{1_{n+1}}^2, u_{2_{n+1}}^2, \theta_{n+1}^2) \in \mathbb{R}^3$. Accordingly, the mapping $\boldsymbol{q}_{n+1}^2 = \boldsymbol{F}_{q_n}^{2,(E)}(\boldsymbol{\mu}_{n+1}^{(E)})$ can be written in the form

$$\boldsymbol{F}_{q_n}^{2,(E)}(\boldsymbol{\mu}_{n+1}^{(E)}) = \begin{bmatrix} \boldsymbol{\varphi}_n^1 + (\boldsymbol{I}^{12})_n \cdot \boldsymbol{u}_{\varphi_{n+1}}^1 + \boldsymbol{R}^{1,2} \cdot [\boldsymbol{\varrho}_n^1 + ((\bar{u}_\kappa^2)_n + u_{\kappa_{n+1}}^2)(\boldsymbol{m}_\kappa^1)_n] - \boldsymbol{R}^{1,2} \cdot \exp\left(\theta_{n+1}^2 \widehat{\boldsymbol{n}_n^1}\right) \cdot \boldsymbol{\varrho}_n^2 \\ \boldsymbol{R}^{1,2} \cdot \exp\left(\theta_{n+1}^2 \widehat{\boldsymbol{n}_n^1}\right) \cdot (\boldsymbol{d}_1^2)_n \\ \boldsymbol{R}^{1,2} \cdot \exp\left(\theta_{n+1}^2 \widehat{\boldsymbol{n}_n^1}\right) \cdot (\boldsymbol{d}_2^2)_n \\ \boldsymbol{R}^{1,2} \cdot \exp\left(\theta_{n+1}^2 \widehat{\boldsymbol{n}_n^1}\right) \cdot (\boldsymbol{d}_3^2)_n \end{bmatrix}.$$

Here, $(\bar{u}_\kappa^2)_n = (\boldsymbol{m}_\kappa^1)_n \cdot (\boldsymbol{\varphi}2_n + \boldsymbol{\varrho}2_n - \boldsymbol{\varphi}_n^1 - \boldsymbol{\varrho}_n^1)$ denotes the translation of the second body relative to the first one in the direction of the axis $(\boldsymbol{m}_\kappa^1)_n$ at time t_n.

Actuation of the planar pair The three relative degrees of freedom allowed by the planar joint can be actuated by translational forces $\tau_{\varphi_1}^{(E)}, \tau_{\varphi_2}^{(E)} \in \mathbb{R}$ acting in the directions of $\boldsymbol{m}_1^1, \boldsymbol{m}_2^1$ and a torque $\tau_\theta^{(E)} \in \mathbb{R}$ about $\boldsymbol{n}^1$. In (5.29), they are accounted for using

$$\boldsymbol{C}^{1,(E)}(\boldsymbol{q}) = \begin{bmatrix} -\boldsymbol{m}_1^1 & -\boldsymbol{m}_2^1 & \boldsymbol{0} \\ (\boldsymbol{\varphi}_1 - \boldsymbol{\varphi}_2) \times \boldsymbol{m}^1 & (\boldsymbol{\varphi}_1 - \boldsymbol{\varphi}_2) \times \boldsymbol{m}^2 & -\boldsymbol{n}^1 \end{bmatrix} \quad \boldsymbol{C}^{2,(E)}(\boldsymbol{q}) = \begin{bmatrix} \boldsymbol{m}_1^1 & \boldsymbol{m}_2^1 & \boldsymbol{0} \\ \boldsymbol{0} & \boldsymbol{0} & \boldsymbol{n}^1 \end{bmatrix}.$$

Similar to (5.36), the torque induced by a translational joint force away from the centre of mass effects the generalised rotational degrees of freedom only with respect to the allowed rotation around $\boldsymbol{n}^1$

$$\left(\boldsymbol{P}^{(E)}(\boldsymbol{q})\right)^T \cdot \boldsymbol{f} = \begin{bmatrix} \boldsymbol{\tau}_\varphi - \tau_{\varphi_1}^{(E)} \boldsymbol{m}_1^1 - \tau_{\varphi_2}^{(E)} \boldsymbol{m}_2^1 \\ \boldsymbol{\varrho}^{rb} \times \boldsymbol{\tau}_\varphi + \boldsymbol{\tau}_\theta + \left(\boldsymbol{n}^1\right)^T \cdot \left(\boldsymbol{\varrho}^2 \times \left(\tau_{\varphi_1}^{(E)} \boldsymbol{m}_1^1 + \boldsymbol{\tau}_{\varphi_2}^{(E)} \boldsymbol{m}_2^1\right)\right) \cdot \boldsymbol{n}^1 - \tau_\theta^{(E)} \boldsymbol{n}^1 \\ \tau_{\varphi_1}^{(E)} \\ \tau_{\varphi_2}^{(E)} \\ -\left(\boldsymbol{n}^1\right)^T \cdot \left(\boldsymbol{\varrho}^2 \times \left(\tau_{\varphi_1}^{(E)} \boldsymbol{m}_1^1 + \boldsymbol{\tau}_{\varphi_2}^{(E)} \boldsymbol{m}_2^1\right)\right) + \tau_\theta^{(E)} \end{bmatrix}.$$

Again, Proposition 5.5.1 stating the consistency of angular momentum holds and the proof is straightforward.

5.6 Optimal control for multibody systems

In a kinematic chain or tree structured system, where N bodies are interconnected by $N-1$ joints, the multibody system consists of $N-1$ pairs. The configuration variable

$$\boldsymbol{q} = \begin{bmatrix} \boldsymbol{q}^1 & \cdots & \boldsymbol{q}^N \end{bmatrix}^T \in \mathbb{R}^{12N}$$

is a generalisation of (5.24).

Actuation of a multibody system As a generalisation of (5.28), the forces and torques acting on the multibody system can be collected in

$$\begin{bmatrix} \boldsymbol{\tau}_{rb} & \boldsymbol{\tau}^{(J_1)} & \cdots & \boldsymbol{\tau}^{(J_{N-1})} \end{bmatrix}^T \in \mathbb{R}^{6+\sum_{i=1}^{N-1} r^{(J_i)}}.$$

The redundant forces for each body can be computed as

$$\boldsymbol{f} = \begin{bmatrix} \boldsymbol{f}^1 & \cdots & \boldsymbol{f}^N \end{bmatrix}^T = \boldsymbol{B}^T(\boldsymbol{q}) \cdot \begin{bmatrix} \boldsymbol{\tau}_{rb} \boldsymbol{\tau}^{(J_1)} & \vdots & \boldsymbol{\tau}^{(J_{N-1})} \end{bmatrix}^T \in \mathbb{R}^{12N}, \tag{5.37}$$

with the $12N \times (6 + \sum_{i=1}^{N-1} r^{(J_i)})$ matrix $\boldsymbol{B}^T(\boldsymbol{q})$ being the product of three matrices as in (5.30). The first matrix corresponds to the internal constraints of each body and consists of N blocks $\boldsymbol{P}_{\text{int}}(\boldsymbol{q}^\alpha), \alpha = 1, \ldots, N$. The second $6N \times 6N$ diagonal matrix is an obvious extension of the one given in (5.30) consisting of multiples of the identity matrix. The third matrix is given by concatenating column-wise the matrices $\boldsymbol{C}_{rb}(\boldsymbol{q}^1)$ and $\boldsymbol{C}^{1,(J_i)}, \boldsymbol{C}^{2,(J_i)}$ for each joint $J_i, i = 1, \ldots, N-1$ into a $6N \times (6 + \sum_{i=1}^{N-1} r^{(J_i)})$ matrix. The first $6N \times 6$ column consists of $\boldsymbol{C}_{rb}(\boldsymbol{q}^1)$ and a zero matrix below. In the following $6N \times r^{(J_i)}$ columns, $\boldsymbol{C}^{1,(J_i)}(\boldsymbol{q})$ and $\boldsymbol{C}^{2,(J_i)}(\boldsymbol{q})$ occur in the rows corresponding to the forces $\boldsymbol{f}^\alpha$ and $\boldsymbol{f}^\beta$ (if the α-th and β-th body are connected by the joint J_i), respectively. See Section 5.7.2 and Section 5.7.3 for examples of this matrix in the context of a tree structured multibody system and a kinematic chain.

5.7 Numerical examples

For all numerical examples, we apply the midpoint rule to approximate the relevant integrals leading to second order optimal control schemes. The solution of the resulting restricted optimisation problem is solved using a sparse SQP optimisation algorithm based on SNOPT (see [Gill 97] for details) that is implemented in the routine `nag_opt_nlp_sparse` of the NAG library[3].

5.7.1 Two-link pendulum

As a first numerical example, the optimal control of a two-link pendulum is considered that was already investigated in [Ober 08, Ober 10]. In the mentioned work, the system was directly formulated in generalised coordinates which is easily possible for this two-dimensional problem. For this system, a comparison between DMOC and a collocation method was performed with respect to convergence rates, the consistency of momentum maps, and number of iterations executed by the SQP solver. In this contribution, the numerical example is completed by a comparison with DMOCC.

Set up and problem statement The two-link pendulum in Figure 5.6 consists of two coupled planar rigid bodies, of which one is fixed in space. θ_i, $i = 1, 2$, denotes the orientation of the i-th link measured counterclockwise from the positive horizontal axis. The configuration of the system is specified by $q = (\theta_1, \theta_2)$.
The control torques τ_1, τ_2 are applied at the base of the first link and at the joint between the two links. The two-link pendulum is to be steered from the stable equilibrium point

[3] `www.nag.com`

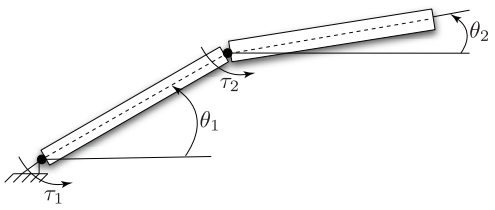

Figure 5.6: Model of a two-link pendulum.

$q^0 = (-\frac{\pi}{2}, -\frac{\pi}{2})$ with zero angular velocity $\dot{q}^0 = (0, 0)$ to the unstable equilibrium point $q^T = (\frac{\pi}{2}, \frac{\pi}{2})$ with velocity $\dot{q}^T = (0, 0)$. For the motion of the pendulum, the control effort

$$J(\tau_1, \tau_2) = \int_0^T \frac{1}{2}(\tau_1^2(t) + \tau_2^2(t))\, dt \tag{5.38}$$

is to be minimised, where the final time $T = 1$ is fixed.

Problem solution Three different methodologies are compared. Firstly, a collocation method of order 2 is applied to two different models: the differential equation systems resulting from the Hamiltonian system with generalised coordinates (q, p) as well as the system formulated on the tangent space with generalised coordinates $(q, \dot{q}) = (q, v)$. Secondly, DMOC in generalised coordinates, and thirdly, DMOCC is performed. To insure that the same local minimum is found by the SQP solver for different numbers of discretisation points, the reference solution with $N = 512$ is computed first, while initial guesses for coarser discretisations are extracted from the reference trajectory. Note, that, as already described in [Ober 10], identical solutions are obtained for DMOC and the equivalent collocation method for the Hamiltonian formulation.
In Figure 5.7 (left) the convergence rates for the configurations u_d and the control torques τ_d are depicted. Here, for each method a reference trajectory has been created with $N = 512$ discretisations points and time step $h = 1.9 \cdot 10^{-3}$, and the maximum norm is used to compute the error. For all methods the convergence rate for the configuration and control trajectory is quadratic. Note, that for the configuration the convergence rate for DMOCC is slightly better as for DMOC in generalised coordinates. For all methods also the objective function value converges quadratically as shown in Figure 5.7 (right).
In Figure 5.8 (left) the convergence of the DMOCC solution to the DMOC solution in generalised coordinates is depicted. Indeed, both methods converge to the same discrete solution.
In Figure 5.8 (right), the consistency in the momentum map for all methods is shown. For the solution resulting from DMOC, the collocation approach applied to the Hamiltonian system and DMOCC, the change in angular momentum exactly equals the sum of the applied control forces (to numerical accuracy). These results are consistent with the well known conservation properties of variational integrators, that provide discretisations that preserve continuous properties such as momentum maps in the discrete setting in a natural way. On the other hand, the collocation method applied to the tangent space system described in velocities fails to capture the change in angular momentum accurately

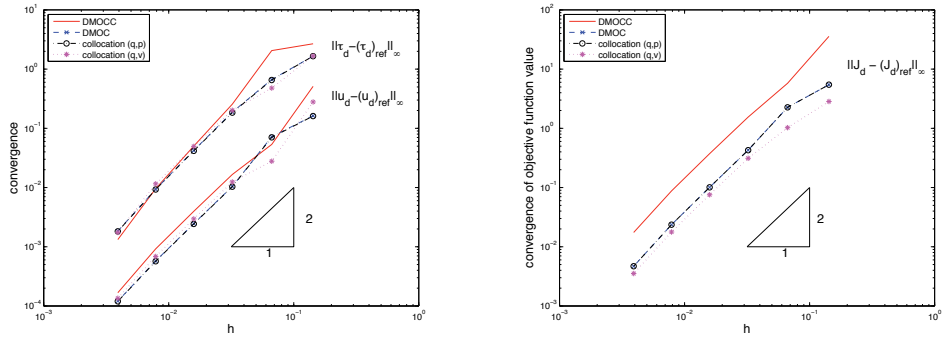

Figure 5.7: Two-link pendulum. Comparison of the convergence rates for DMOCC, DMOC, and a collocation approach. Left: Configuration and control. Right: Objective function value.

because the discrete tangent space formulation destroys the discrete Hamiltonian structure and the resulting scheme is not momentum-preserving anymore.

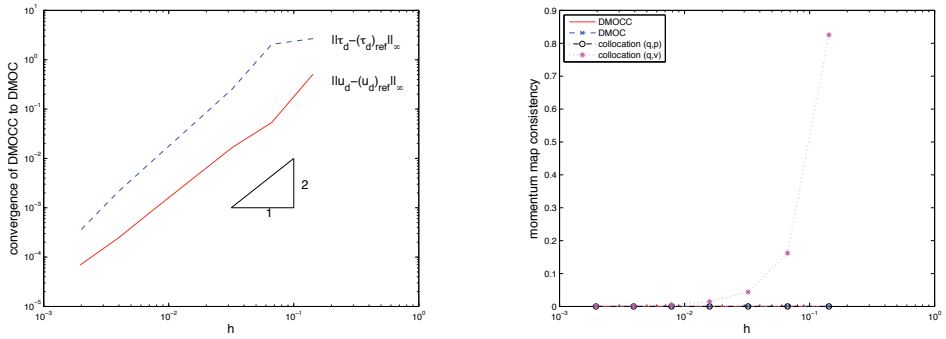

Figure 5.8: Two-link pendulum. Left: Convergence of DMOCC solution to DMOC solution in generalised coordinates. Right: Momentum map consistency.

The methods based on a formulation in generalised coordinates behave equally well compared to DMOCC for the two-dimensional example under consideration. However, for the optimal control of more complex three-dimensional systems as the examples described next, a discrete formulation in generalised coordinates becomes cumbersome and the structure preserving discrete equations of motion are far more complicated.

5.7.2 Optimal control of a rigid body with rotors

Fully actuated case – set up and problem statement Inspired by space telescopes such as the Hubble telescope, whose change in orientation is induced by spinning rotors, a multibody system consisting of a main body to which rotors are connected by revolute joints has been analysed. The revolute joints allow each rotor to rotate relative to the main body around an axis through its centre which is fixed in the main body and are actuated by torques $\tau^{(R_1)}, \tau^{(R_2)}, \tau^{(R_3)} \in \mathbb{R}$. No other force and torque is applied to this

tree structured system, therefore in (5.30), the last matrix reduces to

$$\begin{bmatrix} \boldsymbol{C}^{1,(R_1)}(\boldsymbol{q}) & \boldsymbol{C}^{1,(R_2)}(\boldsymbol{q}) & \boldsymbol{C}^{1,(R_3)}(\boldsymbol{q}) \\ \boldsymbol{C}^{2,(R_1)}(\boldsymbol{q}) & \boldsymbol{0} & \boldsymbol{0} \\ \boldsymbol{0} & \boldsymbol{C}^{2,(R_2)}(\boldsymbol{q}) & \boldsymbol{0} \\ \boldsymbol{0} & \boldsymbol{0} & \boldsymbol{C}^{2,(R_3)}(\boldsymbol{q}) \end{bmatrix},$$

which is then used in (5.37) to compute the redundant forces on each body.
The goal is to determine optimal torques to guide the main body from the initial orientation $\boldsymbol{u}_\theta^0 = [0,0,0]$ into the final position $\boldsymbol{u}_\theta^N = \frac{\pi}{14}[1,2,3]$, where the absolute reparametrisation $\boldsymbol{q}_n = \boldsymbol{F}(\boldsymbol{u}_n, \boldsymbol{q}_{00})$ is used instead of (5.10) here. The motion starts and ends at rest. The manoeuvre time is $T = 5$ and the time step is $h = 0.1$, thus $N = 50$. As in the first example, the objective function represents the control effort which has to be minimised. Due to the presence of three rotors with non-planar axes of rotation, this problem is fully actuated.

Fully actuated case – problem solution The employed initial guess does not fulfil the discrete equations of motion, the main body rotates uniformly into the final orientation while the rotors do not move and the control torques are set to zero. Figure 5.9 shows the configuration of the system at $t = 0, 1, \ldots, 5$. The static frame represents the required final orientation where the axes must coincide with the centres of the rotors as the motion ends (see last picture). The optimal torques which are constant in each time interval are depicted in Figure 5.10. They yield a control effort of $\bar{J}_d = 2.8242 \cdot 10^6$. Finally, Figure 5.10 illustrates the evolution of the kinetic energy and a special attribute of the system under consideration. Due to a geometric phase, the motion occurs although the total angular momentum remains zero at all times. As shown in Proposition 5.5.1, the algorithm is able to represent this correctly.

Remark 5.7.1 (Dimension of the constrained optimisation problem) *Using the advocated method, the problem consists of* 909 *unknowns and* 477 *constraints, rather than* 6798 *variables and* 4555 *constraints using the Lagrange multiplier formulation.*

Underactuated case The same rest to rest manoeuvre is investigated for the underactuated system where one momentum wheel has been removed. The fully actuated manoeuvre serves as an initial guess. The reorientation manoeuvre depicted in Figure 5.11 requires only slightly more control effort $\bar{J}_d = 2.9168 \cdot 10^6$ than the fully actuated case. Here, the optimal solution for the fully actuated system served as initial guess for the optimisation procedure.
Consistency of angular momentum is observable from Figure 5.12. It also shows that the energy does not evolve as symmetrically as for the fully actuated problem. That means that acceleration phase and braking phase are not exactly inverse to each other. This becomes also obvious from Figure 5.12 showing the evolution of the optimal generalised forces.

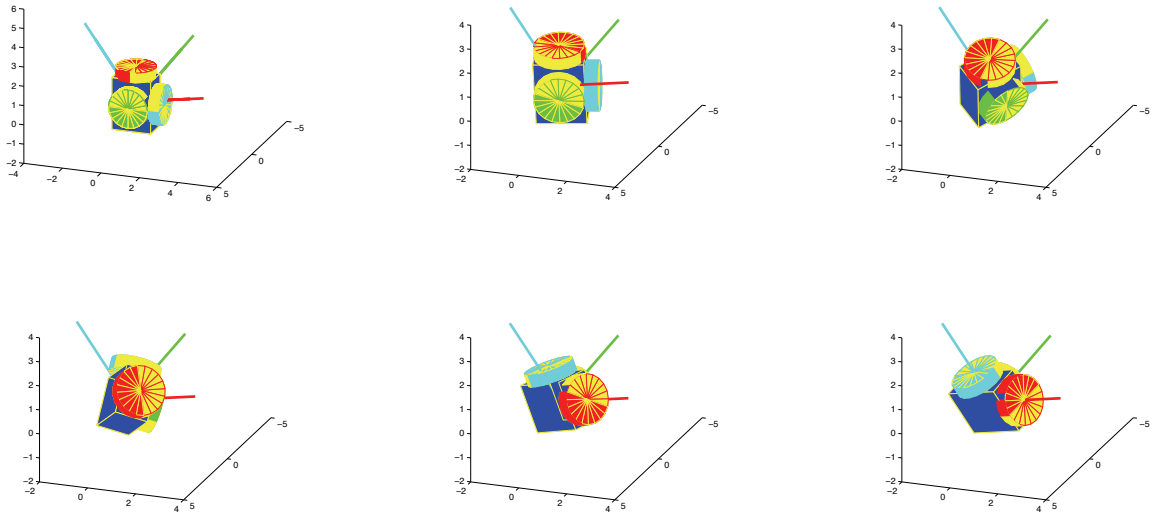

Figure 5.9: Rigid body with three rotors. Configuration at $t = 10nh, n = 0, \ldots, 5$ ($h = 0.1$).

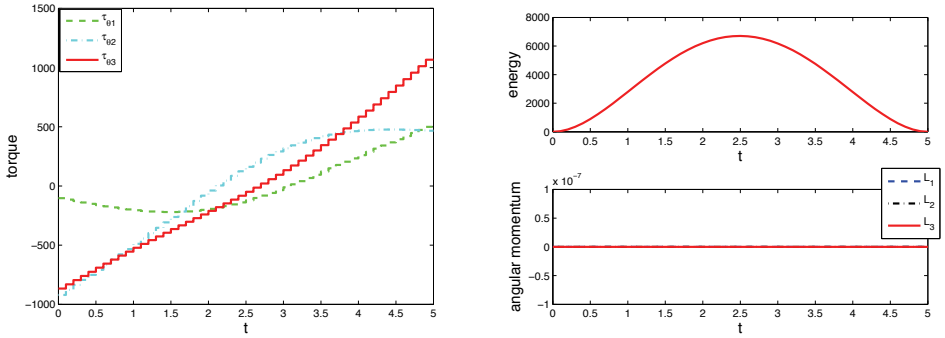

Figure 5.10: Rigid body with three rotors. Left: Torque [Nm]. Right: Energy [J] and components of angular momentum vector $\boldsymbol{L} = L_I \boldsymbol{e}_I$ [Nms] ($h = 0.1$).

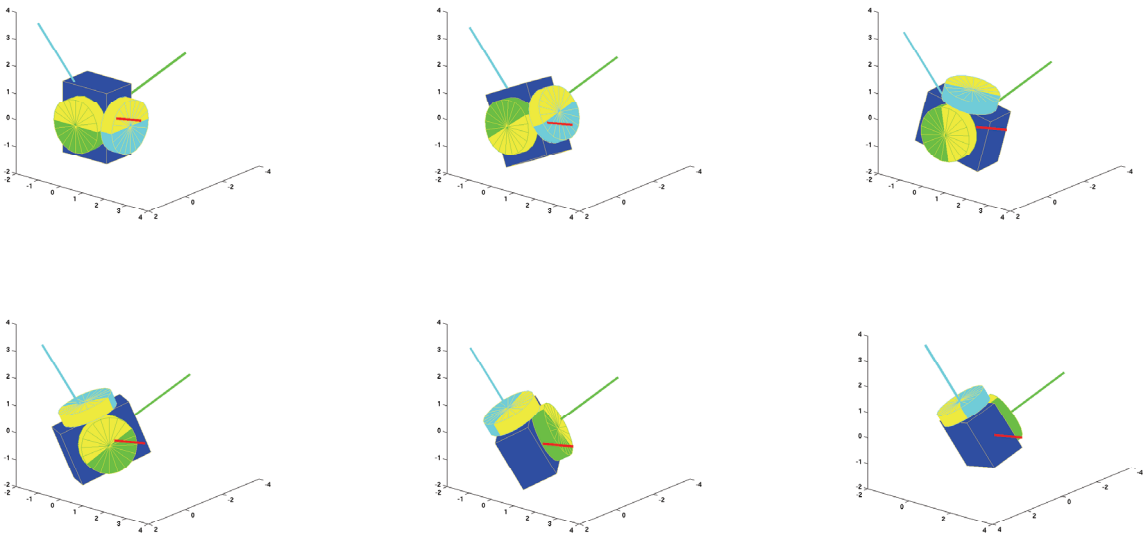

Figure 5.11: Rigid body with two rotors. Configuration at $t = 10nh, n = 0, \ldots, 5$ ($h = 0.1$).

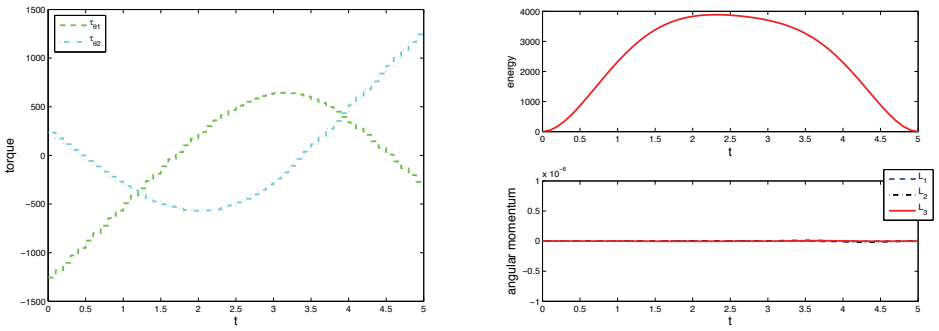

Figure 5.12: Rigid body with two rotors. Left: Torque [Nm]. Right: Energy [J] and components of angular momentum vector $\boldsymbol{L} = L_I \boldsymbol{e}_I$ [Nms] ($h = 0.1$).

5.7.3 Optimal control of a pitcher's motion

As an example of biomotion in sports, the optimal pitch of an athlete is investigated in this section. For simplicity, a kinematic chain representing the pitcher's arm is considered including the collarbone, the upper arm and the forearm (see Figure 5.13). Here, the control torques in the joints represent the muscle activation.

Set up and problem statement The first rigid body, representing the collarbone, is assumed to be fixed in the inertial frame via a revolute joint modelling the rotation of the torso around the $\boldsymbol{e}_3$-axis, thus the axis of the first revolute joint is $\boldsymbol{n}^1 = \boldsymbol{e}_3$. Collarbone and upper arm are connected via a spherical joint, representing the three-dimensional rotation of the shoulder. A revolute joint serves as the elbow between upper and forearm allowing the forearm to rotate around a prescribed axis $\boldsymbol{n}^2$ fixed in the upper arm.
It is assumed that all degrees of freedom, that is the rotations of the collarbone $\theta^1 \in \mathbb{R}$, the shoulder $\theta^2, \theta^3, \theta^4 \in \mathbb{R}$ and the elbow $\theta^5 \in \mathbb{R}$, are directly steerable. There is a rotational torque $\boldsymbol{\tau}^{(S)} \in \mathbb{R}^3$ acting in the shoulder joint and two scalar torques $\tau^{(R_1)}, \tau^{(R_2)} \in \mathbb{R}$ acting in the first revolute joint and the elbow joint, respectively. Since the first body is fixed in space, the last matrix in (5.30) reduces to

$$\begin{bmatrix} \boldsymbol{C}^{2,(R_1)}(\boldsymbol{q}) & \boldsymbol{C}^{1,(S)}(\boldsymbol{q}) & \boldsymbol{0} \\ \boldsymbol{0} & \boldsymbol{C}^{2,(S)}(\boldsymbol{q}) & \boldsymbol{C}^{1,(R_2)}(\boldsymbol{q}) \\ \boldsymbol{0} & \boldsymbol{0} & \boldsymbol{C}^{2,(R_2)}(\boldsymbol{q}) \end{bmatrix}.$$

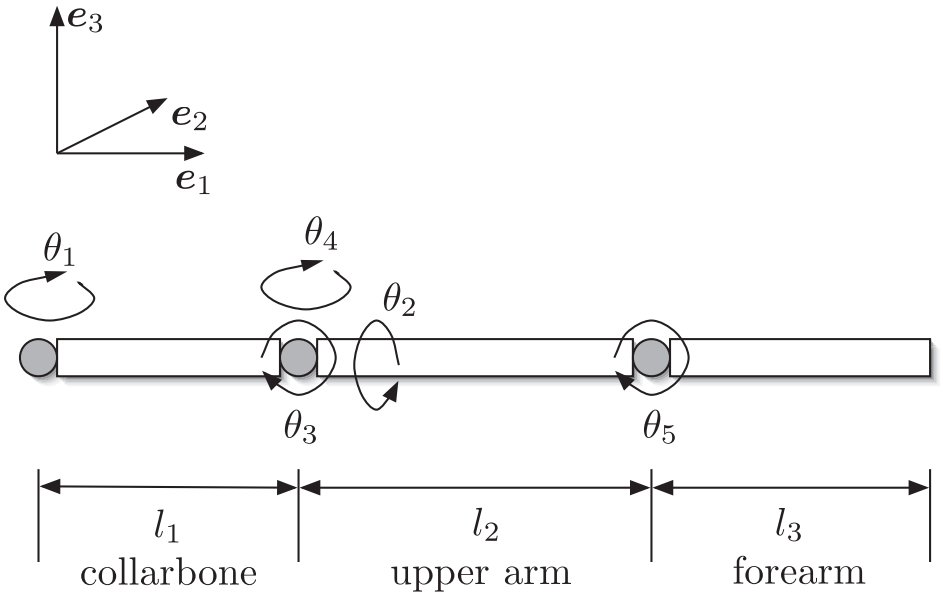

Figure 5.13: The optimal pitch. Model for the arm consisting of collarbone, upper arm, and forearm.

Remark 5.7.2 *For the pitcher, the effect of the actuating torques in the joints on the generalised degrees of freedom takes the form*

$$\boldsymbol{P}^T(\boldsymbol{q}) \cdot \boldsymbol{f} = \left[\tau^{(R_1)} - \left(\boldsymbol{n}^1\right)^T \cdot \boldsymbol{\tau}^{(S)} \qquad \boldsymbol{\tau}^{(S)} - \tau^{(R_2)}\boldsymbol{n}^2 \qquad \tau^{(R_2)}\right]^T.$$

The control torque $\boldsymbol{\tau}^{(S)}$ in the spherical joint acts with different signs on the collarbone and on the upper arm. Only $(\boldsymbol{n}^1)^T \cdot \boldsymbol{\tau}^{(S)}$, the part of $\boldsymbol{\tau}^{(S)}$ in the direction of $\boldsymbol{n}^1$, influences the collarbone's rotation, since the collarbone is constrained to perform rotational motion around $\boldsymbol{n}^1$ only. Similarly, $\tau^{(R_2)}$ acts on the upper and forearm with different signs, therefore it influences the three generalised degrees of freedom in the shoulder by $\tau^{(R_2)}\boldsymbol{n}^2$.

The pitcher is assumed to begin the motion with prescribed initial configuration and zero velocity. Rather than prescribing final configurations for all present bodies, a limited but not fixed final configuration is defined for the hand position[4], for example positive $\boldsymbol{e}_2$- and $\boldsymbol{e}_3$-position. Due to the human body's anatomy, the relative motion in each joint is limited. To obtain a realistic motion, each generalised configuration variable is bounded, for example the forearm is assumed to bend in only one direction. In addition, the incorporation of bounds on the control torques is needed, since the muscles are not able to create an arbitrary amount of strength.
The goal is to maximise the final momentum of the hand in $\boldsymbol{e}_2$-direction. More specifically, the projected discrete Legendre transform (5.14) is used to compute the discrete objective function $J_d(\boldsymbol{q}_d, \boldsymbol{f}_d) = -\boldsymbol{e}_2^T \cdot \left({}^Q\boldsymbol{p}_N^+\right)_{\text{hand}}$. During the optimisation the final time is free, that means also the optimal duration of the pitch is determined as a variable.

Problem solution The number of time nodes has been set to $N = 35$. Starting from an initial position of the joints as $\theta_0^1 = \theta_0^2 = \theta_0^3 = \theta_0^4 = 0$, $\theta_0^5 = -\frac{\pi}{4}$, different local solutions for the optimal motion are obtained, depending on the initial guess in use, where initial guesses were constructed by interpolating coarse pitch sequences and setting the control parameters to zero. In Figure 5.14 snapshots of a particular locally optimal motion are depicted with the optimal final time $T = 0.41545$, i.e. $h = 0.01187$. Starting from the initial configuration shown in the first picture, the pitcher strikes his arm out, moves it rearwards, pulls it above his head, before he finally moves his arm like a whip to obtain the necessary swing to maximise the final momentum $J_d = 24.502$. The evolution of discrete generalised coordinates and torques can be observed from Figure 5.15. Figure 5.16 illustrates the consistency of angular momentum. Due to the presence of gravity and the fixing of the chain in space by a revolute joint with rotation axis $\boldsymbol{e}_3$, the only symmetry of the augmented discrete Lagrangian (5.6) is rotation about $\boldsymbol{e}_3$. Therefore, the corresponding component of the angular momentum L_3 changes exactly according to the torque $\tau^{(R_1)}$, applied in the supporting joint. The kinetic energy, which is increasing substantially towards the end of the movement, is shown in Figure 5.16.

Remark 5.7.3 (Dimension of the constrained optimisation problem) *Including the free final time, the number of variables is* 356 *and the initial conditions and dynamic*

[4]Since the hand is not modelled as a separate rigid body within the system, it is assumed to be located at the endpoint of the forearm.

constraints sum up to 190. *In the Lagrange multiplier formulation, one is faced with* 3641 *variables and* 2422 *constraints.*

The next step is to consider more complex models that behave more realistically. For example, the interaction of the muscles and the resulting muscle force can be included, see [Timm 08]. Due to the constrained formulation of multibody dynamics, model extensions can easily be incorporated by coupling new bodies to the system via constraints.

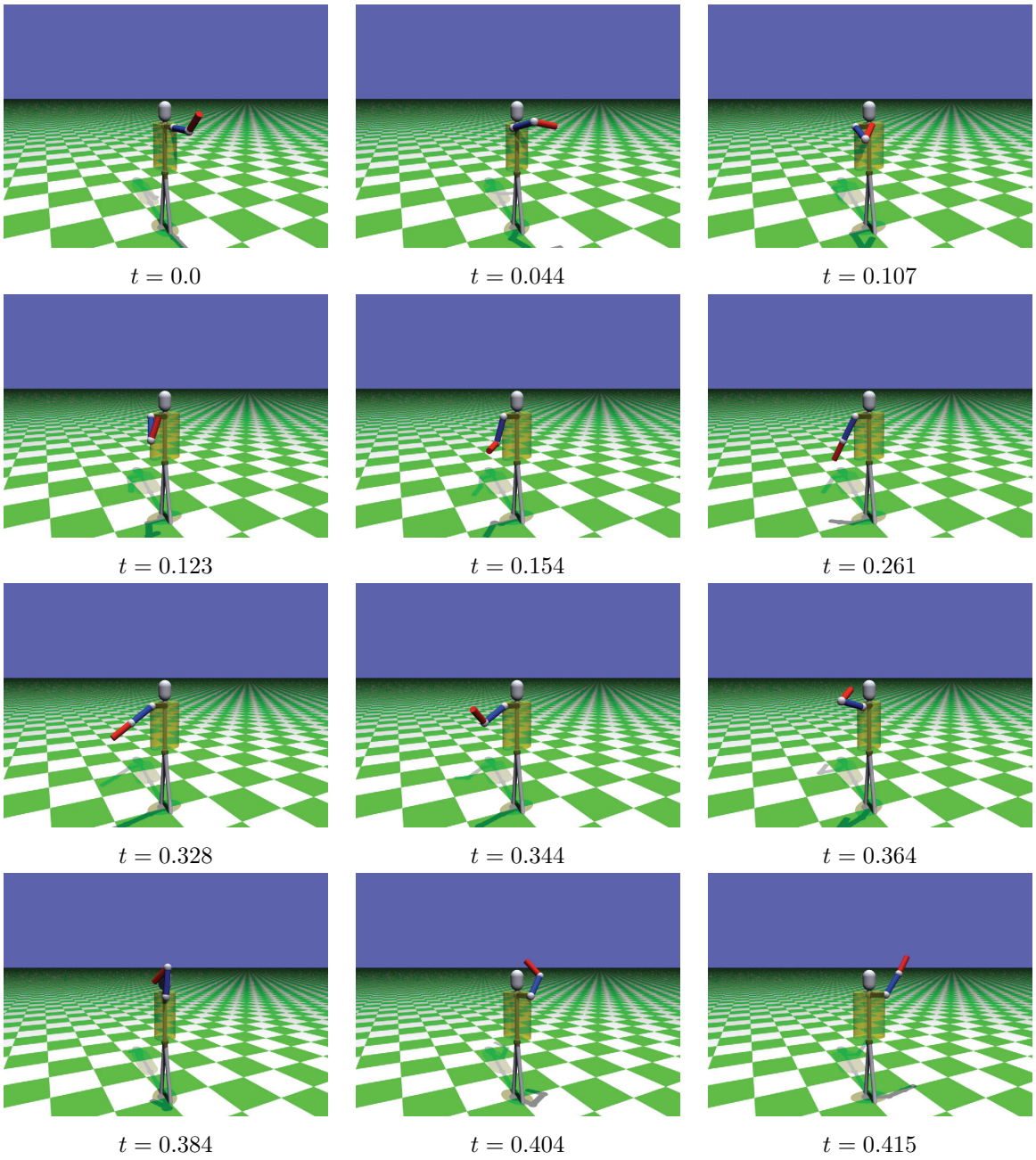

Figure 5.14: The optimal pitch. Snapshots of the motion sequence ($h = 0.01187$).

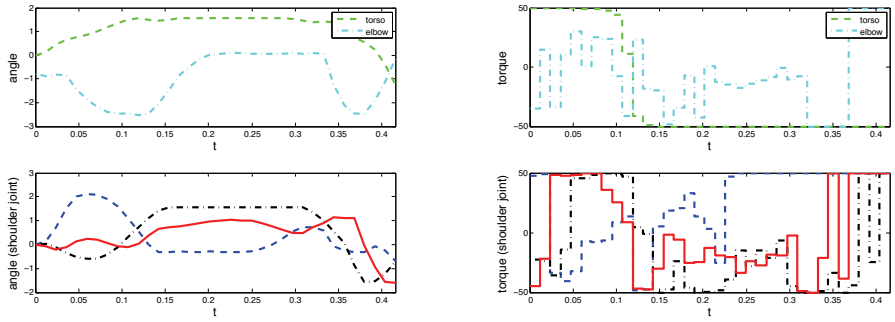

Figure 5.15: The optimal pitch. Left: Evolution of discrete generalised coordinates [rad]. Right: Torque [Nm] ($h = 0.01187$).

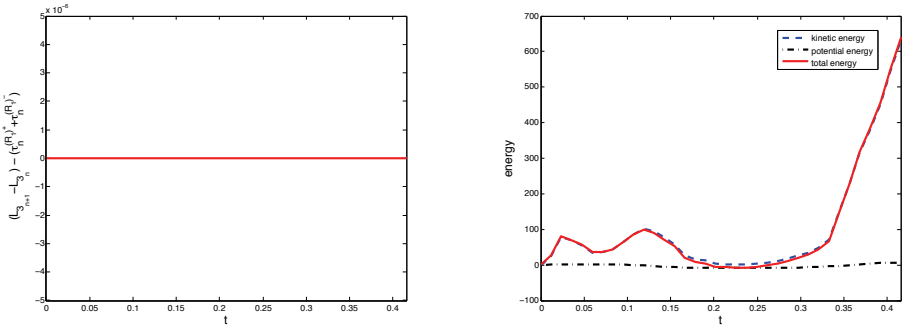

Figure 5.16: The optimal pitch. Left: Consistency of angular momentum [Nms]. Right: Evolution of kinetic, potential and total energy [J] ($h = 0.01187$).

5.8 Conclusion

This chapter proposes a new approach, DMOCC, to the solution of optimal control problems for constrained mechanical systems via the combination of two recently developed methods: the discrete null space method and the optimal control method DMOC.
DMOCC is used to compute trajectories for a mechanical system that is optimally guided from an initial to a final configuration via external forces. The given objective function is extremised subject to the reduced discrete dynamic equations of the constrained mechanical system.
The proposed method benefits from an easy derivation and implementation of the constraint equation for the optimisation algorithm and ensures exact constraint fulfilment and structure preserving properties of the computed solutions. In particular, actuating forces being consistent with the specific joint constraints are given and angular momentum consistency of the resulting time stepping scheme is proved analytically and verified numerically with a satellite reorientation problem and the optimisation of a pitcher's motion.

6 Optimal control strategies for robust certification

6.1 Introduction

The objective of this work is the development of an optimal control methodology for the minimisation of the probability of failure of a system. Thus, we consider systems that are stochastic and whose operation can succeed or fail with a certain probability. In addition, the operation of the system depends on a certain set of control variables. For these systems, the mathematical and computational problem that we address concerns the determination of optimal control laws that result in the least possible probability of failure of the system.

Often, the probability of failure of a system – and its dependence on the control variables – is not known. However, for certain classes of systems, upper bounds of the probability of failure can be formulated – and computed – with some generality. For instance, consider systems that are deterministic except for the randomness of their inputs X. Suppose, in addition, that the safe operation of the system requires that a certain performance measure Y be below a threshold a, and that the performance measure depends on the inputs through a response function $F(X)$. Under these assumptions, concentration-of-measure inequalities (confirm e.g. [Ledo 01,Bouc 04,Luca 08], Section 6.2 of this paper for a brief review) provide convenient upper bounds for the probability of failure of the system. These upper bounds are attractive because they depend solely on two quantities: the mean performance of the system and a system diameter that measures the uncertainty in the operation of the system. The computations of both parameters is straightforward, albeit possibly costly: the mean performance can be computed by Monte Carlo sampling and the diameter by a global optimisation over the space of inputs. In lieu of an exact probability of failure, we may instead seek optimal controls that minimise a probability of failure upper bound, such as supplied by concentration-of-measure inequalities. The proposed methodology, called concentration-of-measure optimal control (COMOC), is introduced in Section 6.3. The resulting optimal controls then maximise the design margin, i.e. the difference between the threshold and the mean performance for safe operation, or reduce the uncertainty in the operation of the system, as measured by the system diameter, or both.

We assess the COMOC in a specific area of application: positioning accuracy in robotic arm manoeuvres, modelled as three-dimensional systems of rigid bodies [Leye 07,Leye 09b]. The system is made stochastic by first assuming that the lengths of the various segments of the arm are random and secondly, that in addition, the system experiences random forcing due to side wind. We investigate a particular robot arm manoeuvre whose successful operation requires a minimum arm tip positioning accuracy, both by deterministic analysis of the nominal geometry of the system without wind forces and by COMOC. For

completeness, a brief account of the discrete mechanics and optimal control for constrained systems (DMOCC) methodology employed in the deterministic calculations is included in Section 6.4. DMOCC is a direct transcription method transforming the optimal control problem into a constrained optimisation problem, where boundary conditions and the discrete equations of motion serve as equality constraints. In particular, DMOCC is designed for mechanical systems whose dynamics itself is holonomically constrained. Results of numerical experiments are collected in Section 6.5. In the particular example under consideration, COMOC reduces the concentration-of-measure probability of failure upper bound by about one order of magnitude with respect to the deterministic optimal control.

6.2 Concentration-of-measure inequalities for uncertainty quantification and certification

The application of concentration-of-measure inequalities for uncertainty quantification and certification of engineering systems is relatively new [Luca 08]. For completeness, we proceed to give a brief account of concentration-of-measure inequalities as they bear on the type of systems and applications under consideration here.
The goal is to certify whether a system is likely to perform safely and reliably within design specifications. Suppose that the system operates safely if its performance measure $Y \in A \subset E$ is in the admissible set A and is considered to fail if $Y \in A^c = E \setminus A$ is in the inadmissible set A^c, where E is an Euclidian space. For systems characterised by a single performance measure, the admissible set often is of the form $A = (-\infty, a]$, where a is the threshold for the safe operation of the system. The system is certified when the probability of failure $\mathbb{P}[Y \in A^c]$ is less than a prespecified tolerance ϵ, i.e. if

$$\mathbb{P}[Y \in A^c] < \epsilon.$$

Often, however, the probability of failure of a system is not known, and its direct computation, e.g. by Monte Carlo sampling is prohibitively expensive. Such is the case, for instance, of systems of large dimensionality for which failure is a rare event. In these cases, rigorous certification can still be achieved if a probability of failure upper bound can be determined, namely, by requiring that the probability of failure upper bound be less than the tolerance ϵ. For systems whose randomness can be characterised by means of random inputs, a convenient class of upper bounds is supplied by concentration-of-measure inequalities, which we briefly summarise in subsequent sections. A rigorous certification methodology can then be formulated based on such concentration-of-measure inequalities, see [Luca 08].
For present purposes, it suffices to assume that a perfect model for the system's response is available, i.e. a mathematical model that describes the system exactly. In particular, errors stemming from numerical approximations are neglected. For simplicity, we restrict attention to the quantification of uncertainty of a single performance measure $Y \in E$ and assume that the relation $Y = F(X)$ describes the system exactly in terms of the the random vector $X : \Omega \to \chi_1 \times \ldots \times \chi_M$, where $(\Omega, \mathcal{U}, \mathbb{P})$ is a probability space, see e.g. [Lawr 04]. Let $\mathbb{E}[Y]$ denote the mean performance of the system and assume that

it belongs to the interior of A. Then, if F is integrable and the input parameters are independent, McDiarmid's inequality (see [McDi 89]) states that

$$\mathbb{P}[Y - \mathbb{E}[Y] \leq -r] \leq \exp\left(-2\frac{r^2}{D_F^2}\right) \tag{6.1}$$

where $r \geq 0$ and the diameter of the system is defined as

$$D_F^2 = \sum_{k=1}^{M} \sup_{X_1,\ldots,X_{k-1},X_{k+1},\ldots,X_M \in \mathcal{X}_1\times\ldots\mathcal{X}_{k-1}\times\mathcal{X}_{k+1},\ldots\times\mathcal{X}_M} \sup_{(A_k,B_k)\in\mathcal{X}_k^2} |F(X_1,\ldots,A_k,\ldots,X_M) - F(X_1,\ldots,B_k,\ldots,X_M)|^2. \tag{6.2}$$

Thus, the diameter is the sum of maximum squared oscillation in response from a random variable pair (independent and identically distributed) varying in turn when all random variables are allowed to vary over their entire ranges, and provides a measure of the uncertainty in the operation of the system. Using $r = (a - \mathbb{E}[Y])_+ = \max(0, a - \mathbb{E}[Y])$, the bound (6.1) can be rewritten as an upper bound on the probability of failure

$$\mathbb{P}[Y \in A^c] \leq \exp\left(-2\frac{(a - \mathbb{E}[Y])_+^2}{D_F^2}\right). \tag{6.3}$$

Often, however, the mean performance $\mathbb{E}[Y]$ is not known a priori and must be estimated. For instance, the mean performance can be estimated by performing m evaluations of the model $F(X)$ based on unbiased Monte Carlo sampling of the input parameters, resulting in predicted performance measures $Y^1, \ldots, Y^m$. The corresponding mean performance estimate is

$$\langle Y \rangle = \frac{1}{m}\sum_{i=1}^{m} Y^i. \tag{6.4}$$

When the mean performance is estimated by sampling, the probability of failure can only be determined to within a predefined estimation tolerance ϵ' reflecting the randomness of $\langle Y \rangle$. Specifically, if

$$\alpha = D_F m^{-\frac{1}{2}} \left(-\log \epsilon'\right)^{\frac{1}{2}},$$

then, with probability $1 - \epsilon'$,

$$\mathbb{P}[Y \in A^c] \leq \exp\left(-2\frac{(a - \langle Y \rangle - \alpha)_+^2}{D_F^2}\right). \tag{6.5}$$

A rigorous certification criterion can now be obtained by requiring that this bound be less than the probability of failure tolerance, with the result

$$\mathrm{CF} \equiv \frac{M}{U} \equiv \frac{(a - \langle Y \rangle - \alpha)_+}{D_F} \geq \sqrt{\log\sqrt{\frac{1}{\epsilon}}} \tag{6.6}$$

Here $M = (a - \langle Y \rangle - \alpha)_+$ may be interpreted as a design margin, $U = D_F$ as a measure of the uncertainty in the operation of the system, and CF as a confidence factor. Certification then requires the confidence factor CF to be in excess of the value $\sqrt{\log \sqrt{\frac{1}{\epsilon}}}$. It is interesting to observe, comparing (6.5) to (6.3), that the estimation of the mean performance reduces the margin by the value α to account for statistical deviations. This margin hit can be reduced to an arbitrary small value by carrying out a sufficiently large number of model evaluations.

It is instructive to compare the probabilities of failure bounds obtained from concentration-of-measure inequalities with those determined directly by random sampling. Consider an empirical probability measure

$$\mu_m = \frac{1}{m} \sum_{i=1}^{m} \delta_{Y^i}$$

obtained via traditional random sampling methods. Here, $\delta_Y = \begin{cases} 1 & \text{for } \mathrm{Y} \in \mathrm{A^c} \\ 0 & \text{for } \mathrm{Y} \in \mathrm{A} \end{cases}$. Then Hoeffding's inequality [Hoef 63] gives

$$\mathbb{P}\left[Y \in A^c\right] \leq \mu_m\left[A^c\right] + \sqrt{\frac{1}{2m} \log \frac{1}{\epsilon'}}$$

with probability $1 - \epsilon'$. This bound reveals that the number of experiments required to certify a system based on statistical sampling alone is of the order of $\frac{1}{2}\epsilon^{-2} \log \frac{1}{\epsilon'}$. For computationally expensive models, the number of function evaluations becomes restrictive and unreasonable as ϵ' decreases. By contrast, the diameter in the concentration-of-measure inequality (6.5) is independent of ϵ, which confers concentration-of-measure inequalities a considerable advantage when failure is a rare event and the required probability of failure is low.

6.3 Concentration-of-measure optimal control

With this concept to compute probability of failure upper bounds at hand, one can design the system such that confidence in its safe operation is improved via concentration-of-measure optimal control (COMOC).
Suppose that the system under consideration is a controlled dynamical system with time dependent states $\boldsymbol{x} : [t_0, t_N] \to \mathbb{R}^{n_x}$ and controls $\boldsymbol{\tau} : [t_0, t_N] \to \mathbb{R}^{n_\tau}$, where $t \in [t_0, t_N] \subset \mathbb{R}$ denotes the time and $N, n_x, n_\tau, n_h \in \mathbb{N}$. Let the dynamical system be specified by

$$\begin{aligned} \dot{\boldsymbol{x}}(t) &= \boldsymbol{\phi}(\boldsymbol{x}(t), \boldsymbol{\tau}(t)) \\ \boldsymbol{x}(t_0) &= \boldsymbol{x}_0 \\ \boldsymbol{h}(\boldsymbol{x}(t)) &= \boldsymbol{0} \end{aligned} \tag{6.7}$$

with the smooth function $\boldsymbol{\phi} : \mathbb{R}^{n_x} \times \mathbb{R}^{n_\tau} \to \mathbb{R}^{n_x}$, the initial value $\boldsymbol{x}_0 \in \mathbb{R}^{n_x}$ and the path constraints $\boldsymbol{h} : \mathbb{R}^{n_x} \to \mathbb{R}^{n_h}$. In general, the quantification of uncertainty of a performance

measure Y and the corresponding confidence factor CF are dependent on the complete system, i.e. on $\boldsymbol{x}_0, \boldsymbol{\phi}, \boldsymbol{h}$ and $\boldsymbol{\tau}$, and one could aim at improving the system such that the probability of failure decreases. However, in many practical situations, one has to deal with given system equations, initial conditions and path constraints, but can manipulate the controls more easily. Therefore, we seek to determine optimal control laws that result in the least possible probability of failure by identifying the objective function for optimal control with the probability of failure $\mathbb{P}[Y > a]$. Often, however, the probability $\mathbb{P}[Y > a]$ is not known explicitly. In these cases, we seek instead to minimize a concentration-of-measure upper bound of the probability of failure such as (6.5).
Indicate the dependence of the performance measure on a given control law by $Y^\tau = F^\tau(X)$. Then one is faced with the following optimal control problem.

$$\begin{aligned} &\min_{\boldsymbol{\tau}(\cdot)} \left(-\mathrm{CF}(\boldsymbol{\tau})\right) \equiv -\frac{M^\tau}{U^\tau} \equiv -\frac{\left(a - \langle Y^\tau \rangle - \alpha^\tau\right)_+}{D_{F^\tau}} \\ &\text{subject to (6.7)} \end{aligned} \tag{6.8}$$

where the system equations, initial conditions and path constraints serve as constraints for the optimisation. Evidently, by this choice of objective function the optimal control $\boldsymbol{\tau}$ seeks to maximise confidence in the safe operation of the systems either by increasing the placement margin M^τ, i.e. by decreasing $a - \langle Y^\tau \rangle$, or by reducing the uncertainty U^τ of the manoeuvre, i.e. by reducing the diameter D_{F^τ}, or both.

6.4 Discrete mechanics and optimal control of constrained multibody dynamics

The equations of motion of a controlled mechanical system subject to holonomic constraints may be formulated in terms of the states and controls by applying a constrained version of the Lagrange-d'Alembert principle. Discrete mechanics and optimal control for constrained systems (DMOCC), a structure preserving scheme for the optimal control of such systems, is derived in [Leye 07,Leye 09b], using a discrete analogue of that principle. Structure preservation is inherited when the system is reduced to its minimal dimension by the discrete null space method. Together with initial and final conditions on the configuration and conjugate momentum, the reduced discrete equations serve as nonlinear equality constraints for the minimisation of a given objective functional. The algorithm yields a sequence of discrete configurations together with a sequence of actuating forces, optimally guiding the system from the initial to the desired final state. In particular, for the optimal control of three-dimensional multibody systems, a force formulation consistent with the joint constraints is introduced in Chapter 5 (see also [Leye 09b]) and consistency of the evolution of momentum maps is proved for different types of joints. [Ober 10] focuses on the analysis of discrete mechanics and optimal control (DMOC in the unconstrained case) and gives a proof of convergence of the DMOC solution to that of the original (continuous) optimal control problem.

In this section, the formulation of discrete mechanics and optimal control for constrained systems (DMOCC) is summarised briefly. Then, it is described how the robot arm is

modeled as a spatially fixed spherical pair and a short overview on the main ingredients for the optimal control of the robot arm is given. Finally, DMOCC will be used to determine a cost minimising robot arm manoeuvre in the deterministic setting.

6.4.1 Discrete mechanics and optimal control for constrained systems (DMOCC)

The equations of motion for forced, holonomically constrained systems can be derived via a variational principle. Quite different strategies for the treatment of the constraints are at the disposal. One possibility described for conservative systems in Chapter 3 (see also [Leye 08b]) is to transform the differential algebraic equations by a null space method with reparametrisation. Analogous steps can be performed in the temporal discrete variational setting to derive the forced constrained discrete Euler-Lagrange equations and their reduction to minimal dimension. Again, these steps have been investigated in detail in Chapter 3 (see also [Leye 08b]) for conservative systems and in Chapter 5 (see also [Leye 09b]) for forced systems and the method is summarised here.

Consider an n-dimensional mechanical system with the time dependent configuration vector $\boldsymbol{q}(t) \in Q$ and velocity vector $\dot{\boldsymbol{q}}(t) \in T_{\boldsymbol{q}(t)}Q$ in the tangent space $T_{\boldsymbol{q}(t)}Q$ to the configuration manifold Q. Let the configuration be constrained by the function $\boldsymbol{g}(\boldsymbol{q}) = \boldsymbol{0} \in \mathbb{R}^m$ with constraint manifold $C = \{\boldsymbol{q} \in Q \mid \boldsymbol{g}(\boldsymbol{q}) = \boldsymbol{0}\}$ and influenced by the force field $\boldsymbol{f} : \mathbb{R}^{n-m} \times TQ \to T^*Q$.

Corresponding to the configuration manifold Q, the discrete phase space is defined by $Q \times Q$ which is locally isomorphic to TQ. For a constant time step $h \in \mathbb{R}$, a path $\boldsymbol{q} : [t_0, t_N] \to Q$ is replaced by a discrete path $\boldsymbol{q}_d : \{t_0, t_0 + h, , \ldots, t_0 + Nh = t_N\} \to Q$, $N \in \mathbb{N}$, where $\boldsymbol{q}_n = \boldsymbol{q}_d(t_n)$ is viewed as an approximation to $\boldsymbol{q}(t_n)$ at $t_n = t_0 + nh$. The action integral is approximated in a time interval $[t_n, t_{n+1}]$ using the discrete Lagrangian $L_d : Q \times Q \to \mathbb{R}$ and the discrete constraint function $\boldsymbol{g}_d : Q \to \mathbb{R}$. Similarly, $\boldsymbol{\lambda}_n = \boldsymbol{\lambda}_d(t_n)$ approximates the Lagrange multiplier, while the force field $\boldsymbol{f}$ is approximated by two discrete forces $\boldsymbol{f}_n^-, \boldsymbol{f}_n^+ : T^*U \times Q \to T^*Q$.

Discrete constrained Lagrange-d'Alembert principle The discrete version of the constrained Lagrange-d'Alembert principle requires the discrete path $\{\boldsymbol{q}_n\}_{n=0}^N$ and multipliers $\{\boldsymbol{\lambda}_n\}_{n=0}^N$ to fulfil

$$\delta \sum_{n=0}^{N-1} \left(L_d(\boldsymbol{q}_n, \boldsymbol{q}_{n+1}) - \frac{1}{2}\boldsymbol{g}_d^T(\boldsymbol{q}_n) \cdot \boldsymbol{\lambda}_n - \frac{1}{2}\boldsymbol{g}_d^T(\boldsymbol{q}_{n+1}) \cdot \boldsymbol{\lambda}_{n+1} \right) + \sum_{n=0}^{N-1} \left(\boldsymbol{f}_n^- \cdot \delta\boldsymbol{q}_n + \boldsymbol{f}_n^+ \cdot \delta\boldsymbol{q}_{n+1} \right) = 0$$

for all variations $\{\delta\boldsymbol{q}_n\}_{n=0}^N$ and $\{\delta\boldsymbol{\lambda}_n\}_{n=0}^N$ with $\delta\boldsymbol{q}_0 = \delta\boldsymbol{q}_N = \boldsymbol{0}$, which is equivalent to the constrained forced discrete Euler-Lagrange equations

$$\begin{aligned} D_2L_d(\boldsymbol{q}_{n-1}, \boldsymbol{q}_n) + D_1L_d(\boldsymbol{q}_n, \boldsymbol{q}_{n+1}) - \boldsymbol{G}_d^T(\boldsymbol{q}_n) \cdot \boldsymbol{\lambda}_n + \boldsymbol{f}_{n-1}^+ + \boldsymbol{f}_n^- &= \boldsymbol{0} \\ \boldsymbol{g}(\boldsymbol{q}_{n+1}) &= \boldsymbol{0} \end{aligned} \tag{6.9}$$

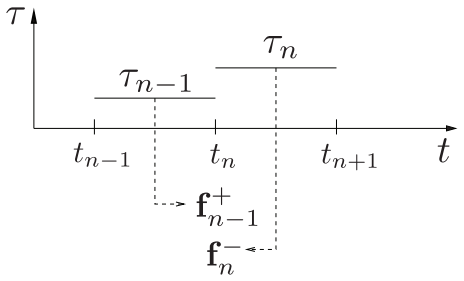

Figure 6.1: Relation of redundant forces $\boldsymbol{f}_{n-1}^{+}, \boldsymbol{f}_{n}^{-}$ at t_n to piecewise constant discrete generalised forces $\boldsymbol{\tau}_{n-1}, \boldsymbol{\tau}_n$.

for $n = 1, \ldots, N-1$ where $\boldsymbol{G}_d(\boldsymbol{q}_n)$ denotes the Jacobian of $\boldsymbol{g}_d(\boldsymbol{q}_n)$ and $D_\alpha L_d$ denotes the derivative of the discrete Lagrangian with respect to the α-th variable. Due to the variational derivation of this scheme, the discrete trajectory conserves a discrete symplectic form and is consistent in momentum maps, i.e. any change in the value of a momentum map reflects exactly the applied forces, see [Mars 01]. Furthermore, the solution shows 'good energy behaviour' in the sense that energy is not gained or dissipated numerically, which is typical for symplectic methods, see [Hair 04].

The discrete null space method To eliminate the discrete constraint forces from the equations, a discrete null space matrix fulfilling $\text{range}\,(\boldsymbol{P}(\boldsymbol{q}_n)) = \text{null}\,(\boldsymbol{G}_d(\boldsymbol{q}_n))$ is employed. Premultiplying $(6.9)_1$ by the transposed discrete null space matrix cancels the constraint forces; i.e. the Lagrange multipliers are eliminated from the set of unknowns and the system's dimension is reduced to n.

Nodal reparametrisation A reduction of the system to the minimal possible dimension can be accomplished by a local reparametrisation of the constraint manifold. At the time nodes, $\boldsymbol{q}_n = \boldsymbol{F}(\boldsymbol{u}_n, \boldsymbol{q}_{n-1})$ is expressed in terms of the discrete generalised coordinates $\boldsymbol{u}_n \in U \subseteq \mathbb{R}^{n-m}$ by the map $\boldsymbol{F} : U \subseteq \mathbb{R}^{n-m} \times Q \to C$, such that the constraints are fulfilled. The discrete generalised control forces are assumed to be constant in each time interval, see Figure 6.1. First of all, the effect of the generalised forces acting in $[t_{n-1}, t_n]$ and in $[t_n, t_{n+1}]$ is transformed to the time node t_n via $\boldsymbol{\tau}_{n-1}^{+} = \dfrac{h}{2}\,\boldsymbol{\tau}_{n-1}$ and $\boldsymbol{\tau}_{n}^{-} = \dfrac{h}{2}\,\boldsymbol{\tau}_{n}$. Secondly, the components of the discrete force vectors $\boldsymbol{f}_{n-1}^{+}, \boldsymbol{f}_{n}^{-} \in T_{\boldsymbol{q}_n}^{*}Q$ can be calculated as

$$\boldsymbol{f}_{n-1}^{+} = \boldsymbol{B}^T\,(\boldsymbol{q}_n) \cdot \boldsymbol{\tau}_{n-1}^{+} \qquad \boldsymbol{f}_{n}^{-} = \boldsymbol{B}^T\,(\boldsymbol{q}_n) \cdot \boldsymbol{\tau}_{n}^{-}$$

with the $n \times (n-m)$ configuration dependent input transformation matrix $\boldsymbol{B}^T : T^*U \to T^*Q$.
Upon insertion of the nodal reparametrisation, the resulting scheme

$$\boldsymbol{P}^T(\boldsymbol{q}_n) \cdot \left[D_2 L_d(\boldsymbol{q}_{n-1}, \boldsymbol{q}_n) + D_1 L_d(\boldsymbol{q}_n, \boldsymbol{F}(\boldsymbol{u}_{n+1}, \boldsymbol{q}_n)) + \boldsymbol{f}_{n-1}^{+} + \boldsymbol{f}_{n}^{-} \right] = \boldsymbol{0} \tag{6.10}$$

has to be solved for $\boldsymbol{u}_{n+1}$ whereupon $\boldsymbol{q}_{n+1}$ is obtained from local reparametrisation $\boldsymbol{F}$ of the constraint manifold. Note that locality of this reparametrisation avoids the danger of singularities which is present in formulations that start with a Lagrangian in generalised

coordinates. The reduced scheme (6.10) is equivalent to the constrained scheme (6.9), thus it also has the key properties of exact constraint fulfilment, symplecticity and momentum consistency. While the constrained scheme (6.9) becomes increasingly ill-conditioned for decreasing time steps, the condition number of (6.10) is independent of the time step.

Boundary conditions In the next step, the boundary conditions $\boldsymbol{q}(t_0) = \boldsymbol{q}^0, \dot{\boldsymbol{q}}(t_0) = \dot{\boldsymbol{q}}^0$ and $\boldsymbol{q}(t_N) = \boldsymbol{q}^N, \dot{\boldsymbol{q}}(t_N) = \dot{\boldsymbol{q}}^N$ are formulated in the discrete setting. Let $\boldsymbol{q}_{00} \in C$ be a fixed reference configuration, relative to which the initial configuration is computed as $\boldsymbol{q}_0 = \boldsymbol{F}(\boldsymbol{u}_0, \boldsymbol{q}_{00})$. To prescribe an initial configuration at t_0, one can request $\boldsymbol{u}_0 = \boldsymbol{u}^0$. However, since the relative reparametrisation computes $\boldsymbol{q}_N$ in terms of $\boldsymbol{u}_N$ and $\boldsymbol{q}_{N-1}$, prescribing $\boldsymbol{u}_N$ does not enforce a unique final configuration. Final configuration conditions have to be formulated in terms of $\boldsymbol{q}^N$ depending on the specific system under consideration (see Section 6.4.2 for an example). Since in the present formulation of constrained forced discrete variational dynamics on $Q \times Q$, velocities are not properly defined, velocity conditions have to be transformed into conditions on the conjugate momentum, which are defined at each and every time node using a discrete Legendre transform. Three different discrete Legendre transforms have been defined in Chapter 5 (see also [Leye 09b]). The reduced discrete Legendre transforms are the most appropriate version to formulate boundary conditions on momentum level as

$$\begin{aligned} \boldsymbol{P}^T(\boldsymbol{q}_0) \cdot \left[D_2 L(\boldsymbol{q}^0, \dot{\boldsymbol{q}}^0) + D_1 L_d(\boldsymbol{q}_0, \boldsymbol{q}_1) + \boldsymbol{f}_0^- \right] &= \boldsymbol{0} \\ \boldsymbol{P}^T(\boldsymbol{q}_N) \cdot \left[D_2 L(\boldsymbol{q}^N, \dot{\boldsymbol{q}}^N) - D_2 L_d(\boldsymbol{q}_{N-1}, \boldsymbol{q}_N) - \boldsymbol{f}_{N-1}^+ \right] &= \boldsymbol{0}. \end{aligned} \tag{6.11}$$

Here, the continuous Legendre transform $\boldsymbol{p}^0 = D_2 L(\boldsymbol{q}^0, \dot{\boldsymbol{q}}^0)$ and $\boldsymbol{p}^N = D_2 L(\boldsymbol{q}^N, \dot{\boldsymbol{q}}^N)$ is applied to the prescribed boundary velocities.

The discrete constrained optimisation problem To formulate the optimal control problem for the constrained discrete motion, an approximation

$$J_d(\boldsymbol{u}_d, \boldsymbol{\tau}_d) = \sum_{n=0}^{N-1} B_d(\boldsymbol{u}_n, \boldsymbol{u}_{n+1}, \boldsymbol{\tau}_n) \tag{6.12}$$

of the continuous objective functional $J(\boldsymbol{q}, \dot{\boldsymbol{q}}, \boldsymbol{f}) = \int_{t_0}^{t_N} B(\boldsymbol{q}, \dot{\boldsymbol{q}}, \boldsymbol{f})\, dt$ has to be defined, where $B(\boldsymbol{q}, \dot{\boldsymbol{q}}, \boldsymbol{f}) : TC \times T^*Q \to \mathbb{R}$ is a given cost function. The objective function (6.12) has to be minimised with respect to $\boldsymbol{u}_d = \{\boldsymbol{u}_n\}_{n=0}^N$ and $\boldsymbol{\tau}_d = \{\boldsymbol{\tau}_n\}_{n=0}^{N-1}$ subject to a minimal set of initial and final configuration constraints, initial and final momentum constraints (6.11) and the discrete equations of motion (6.10) for $n = 1, \ldots, N-1$. Furthermore, time dependent path, constraints prescribing (parts of) the motion, and inequality constraints bounding the optimisation variables can be present.

Remark 6.4.1 (Dimension of the constrained optimisation problem) *The use of the discrete null space method with nodal reparametrisation yields a constrained optimisation problem of minimal possible dimension: the optimisation of* (6.12) *subject to boundary conditions and* (6.10) *includes the* $(2N+1)(n-m)$ *variables* $\boldsymbol{u}_d, \boldsymbol{\tau}_d$ *and* $(N+3)(n-m)$ *constraints. In contrast to that, the constrained optimisation problem resulting from the*

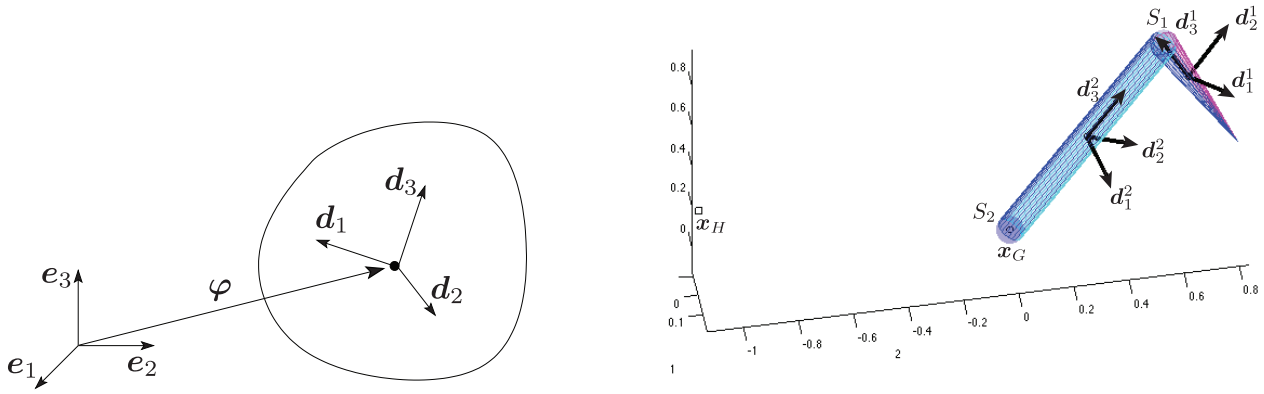

Figure 6.2: Configuration of a rigid body (left) and initial configuration of the robot arm consisting of two rigid bodies combined into a spherical pair by the joint S_1 and fixed in space by the spherical joint S_2 (right).

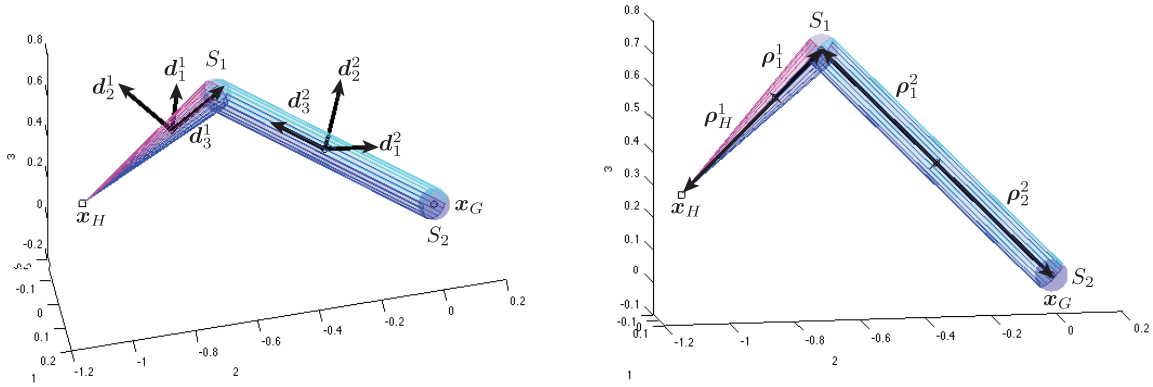

Figure 6.3: Final configuration of the robot arm showing the director triads $\{\boldsymbol{d}_I^\alpha\}$, $\alpha = 1, 2,\ I = 1, 2, 3$ (left) and the joint location vectors $\boldsymbol{\rho}_\beta^\alpha$, $\beta = 1, 2$ (right).

Lagrange multiplier formulation (6.9) *involves the* $N(2n + m) + n$ *unknowns* $\boldsymbol{q}_d, \boldsymbol{f}_d, \boldsymbol{\lambda}_d$ *and* $(N - 1)(n + m) + 4n$ *constraints (this are* $(3N + 1)m$ *more variables and* $(N + 1)2m$ *more constraints). Of course, this influences the computational costs and the spectrum of available methods to solve the problem substantially.*

6.4.2 Deterministic optimal control of the robot arm

This section describes the constrained formulation of the crane-like robot arm and its optimal control using DMOCC to compute the optimal trajectory and control sequence steering the arm form its initial position depicted in Figure 6.2 (right) to the final position, where the tip is located in $\boldsymbol{x}_H$, in Figure 6.3. The objective of this rest to rest manoeuvre is the minimisation of the control effort $J_d(\boldsymbol{u}_d, \boldsymbol{\tau}_d) = \sum_{n=0}^{N-1} \|\boldsymbol{\tau}_n\|^2$. The robot arm model consists of two rigid bodies and two spherical joint connections, the first body being a cone and the second body a cylinder, see Figure 6.2 (right). The first spherical joint S_1

connects the two bodies by preventing relative translation. However, relative rotation of the bodies is not constrained. The second joint S_2 fixes the end of the cylinder in space at $\boldsymbol{x}_G$.
In contrast to rotation based approaches to rigid body dynamics taken e.g. in [Krys 06,Bou 09], here, each rigid body is viewed as a constrained continuum, described in redundant coordinates subject to holonomic constraints, see e.g. [Antm 95, Reic 96]. The α-th rigid body's configuration variable

$$\boldsymbol{q}^\alpha = \begin{bmatrix} \boldsymbol{\varphi}^\alpha \\ \boldsymbol{d}_1^\alpha \\ \boldsymbol{d}_2^\alpha \\ \boldsymbol{d}_3^\alpha \end{bmatrix} \in \mathbb{R}^{12} \quad \alpha = 1, 2 \tag{6.13}$$

consists of the placement of the centre of mass $\boldsymbol{\varphi}^\alpha \in \mathbb{R}^3$ and the directors $\boldsymbol{d}_I^\alpha \in \mathbb{R}^3, I = 1, 2, 3$ which are constrained to stay orthonormal during the motion, see Figure 6.2 (left) and Figure 6.3 (left). The equations of motion assume the from of DAEs with a constant mass matrix. This formulation circumvents many difficulties associated with rotational parameters [Bets 98, Bauc 03] and can be generalised easily to three-dimensional multibody systems consisting of many rigid bodies and also elastic structural elements [Bets 06, Leye 08a]. The location of the β-th joint in the α-th body is characterised by coordinates $\left(\rho_\beta^\alpha\right)_i$ in the body frame $\{\boldsymbol{d}_I^\alpha\}$ for $\alpha, \beta = 1, 2$

$$\boldsymbol{\rho}_\beta^\alpha = \left(\rho_\beta^\alpha\right)_i \boldsymbol{d}_i^\alpha,$$

see Figure 6.3 (right).

Null space matrix The null space matrix associated with the robot arm is given by

$$\boldsymbol{P}(\boldsymbol{q}) = \begin{bmatrix} \widehat{\boldsymbol{\rho}_1^1} & \widehat{\boldsymbol{\rho}_2^2} - \widehat{\boldsymbol{\rho}_2^1} \\ -\widehat{\boldsymbol{d}_1^1} & \boldsymbol{0} \\ -\widehat{\boldsymbol{d}_2^1} & \boldsymbol{0} \\ -\widehat{\boldsymbol{d}_3^1} & \boldsymbol{0} \\ \boldsymbol{0} & \widehat{\boldsymbol{\rho}_2^2} \\ \boldsymbol{0} & -\widehat{\boldsymbol{d}_1^2} \\ \boldsymbol{0} & -\widehat{\boldsymbol{d}_2^2} \\ \boldsymbol{0} & -\widehat{\boldsymbol{d}_3^2} \end{bmatrix},$$

with the hat map $\widehat{\cdot}: \mathbb{R}^3 \to so(3)$ and $\boldsymbol{0}$ denoting the 3×3 zero matrix.

Nodal reparametrisation Let $\boldsymbol{\theta}_{n+1}^1, \boldsymbol{\theta}_{n+1}^2$ represent the incremental rotation vectors pertaining to the two bodies, respectively. In particular, the nodal reparametrisation

reads

$$\boldsymbol{q}_{n+1} = \begin{bmatrix} \boldsymbol{x}_G + \exp(\widehat{\boldsymbol{\theta}^2_{n+1}}) \cdot (-(\boldsymbol{\varrho}^2_2)_n + (\boldsymbol{\varrho}^2_1)_n) - \exp(\widehat{\boldsymbol{\theta}^1_{n+1}}) \cdot (\boldsymbol{\varrho}^1_1)_n \\ \exp(\widehat{\boldsymbol{\theta}^1_{n+1}}) \cdot (\boldsymbol{d}^1_1)_n \\ \exp(\widehat{\boldsymbol{\theta}^1_{n+1}}) \cdot (\boldsymbol{d}^1_2)_n \\ \exp(\widehat{\boldsymbol{\theta}^1_{n+1}}) \cdot (\boldsymbol{d}^1_3)_n \\ \boldsymbol{x}_G - \exp(\widehat{\boldsymbol{\theta}^2_{n+1}}) \cdot (\boldsymbol{\varrho}^2_2)_n \\ \exp(\widehat{\boldsymbol{\theta}^2_{n+1}}) \cdot (\boldsymbol{d}^2_1)_n \\ \exp(\widehat{\boldsymbol{\theta}^2_{n+1}}) \cdot (\boldsymbol{d}^2_2)_n \\ \exp(\widehat{\boldsymbol{\theta}^2_{n+1}}) \cdot (\boldsymbol{d}^2_3)_n \end{bmatrix}.$$

Rodrigues' formula is used to obtain a closed form expression of the exponential map $\exp : so(3) \to SO(3)$ mapping skew-symmetric matrices to proper rotations, see e.g. [Mars 94].

Actuation of the robot arm The actuation of the arm is twofold. First of all, the spherical joint connection S_1 is actuated by the joint torque $\boldsymbol{\tau}_{\theta_1} \in \mathbb{R}^3$. It effects both bodies, where according to 'action equals reaction', the resulting generalised forces on the bodies are equal, but opposite in sign, see e.g. [Bull 04]. Secondly, the torque $\boldsymbol{\tau}_{\theta_2} \in \mathbb{R}^3$ actuates S_2 and effects the second body only.
The redundant forces on the bodies' centre of mass and the directors corresponding to the configuration variable (6.13) can then be computed as

$$\boldsymbol{f} = \begin{bmatrix} \boldsymbol{f}^1 \\ \boldsymbol{f}^2 \end{bmatrix} = \boldsymbol{B}^T(\boldsymbol{q}) \cdot \begin{bmatrix} \boldsymbol{\tau}_{\theta_1} \\ \boldsymbol{\tau}_{\theta_2} \end{bmatrix},$$

with the 24×6 input transformation matrix

$$\boldsymbol{B}^T(\boldsymbol{q}) = \frac{1}{2} \begin{bmatrix} \boldsymbol{0} & \boldsymbol{0} \\ \widehat{\boldsymbol{d}^1_1} & \boldsymbol{0} \\ \widehat{\boldsymbol{d}^1_2} & \boldsymbol{0} \\ \widehat{\boldsymbol{d}^1_3} & \boldsymbol{0} \\ \boldsymbol{0} & \boldsymbol{0} \\ -\widehat{\boldsymbol{d}^2_1} & \widehat{\boldsymbol{d}^2_1} \\ -\widehat{\boldsymbol{d}^2_2} & \widehat{\boldsymbol{d}^2_2} \\ -\widehat{\boldsymbol{d}^2_3} & \widehat{\boldsymbol{d}^2_3} \end{bmatrix}.$$

Angular momentum of the robot arm reads $\boldsymbol{L} = \sum_{\alpha=1}^{2} \boldsymbol{\varphi}^\alpha \times \boldsymbol{p}^\alpha_{\boldsymbol{\varphi}} + \boldsymbol{d}^\alpha_I \times \boldsymbol{p}^\alpha_I$, where the summation convention is used to sum over the repeated index I. In the discrete setting, angular momentum at t_n can be computed in terms of conjugate momenta obtained via the constrained discrete Legendre transform, or equivalently, via the projected discrete Legendre transform, see Chapter 5 (see also [Leye 09b]).

In the present case of the robot arm, change in angular momentum is induced by $\boldsymbol{\tau}_{\theta_2}$ and the force due to the gravitational potential

$$V(\boldsymbol{q}) = [0\ 0\ -M^1_\varphi g\ \boldsymbol{0}_{1\times 9}\ 0\ 0 M^2_\varphi g\ \boldsymbol{0}_{1\times 9}] \cdot \boldsymbol{q}$$

with the acceleration $g \in \mathbb{R}$ and the total masses $M_\varphi^\alpha, \alpha = 1, 2$ of the bodies. In particular, change of angular momentum in one time interval is given by

$$\boldsymbol{L}_{n+1} - \boldsymbol{L}_n = (\boldsymbol{\tau}_{\theta_2})_n^+ + (\boldsymbol{\tau}_{\theta_2})_n^- - (\boldsymbol{\varphi}_{n+1}^1 + \boldsymbol{\varphi}_n^1) \times \frac{h}{2}[0\ 0\ -M_\varphi^1 g] - (\boldsymbol{\varphi}_{n+1}^2 + \boldsymbol{\varphi}_n^2) \times \frac{h}{2}[0\ 0\ -M_\varphi^2 g]. \tag{6.14}$$

The consistency of momentum maps can be proved analytically and is illustrated numerically in Figure 6.4.

Robot arm manoeuvre in the deterministic setting

The particular robot arm we consider consists of a cone of radius $r^1 = 0.05$ length $l^1 = 0.6$ and mass $M_\varphi^1 = 10$ and a cylinder of radius $r^2 = 0.05$, length $l^2 = 0.5$ and mass $M_\varphi^2 = 5$. One end of the cylinder is fixed in space at $\boldsymbol{x}_G = [0\ 0\ 0]$ by the spherical joint S_2, the other end is coupled to the cylinder via S_2. In the reference configuration $\boldsymbol{q}_{00}$ depicted in Figure 6.2 (right), both bodies are tilted from a vertical position by a rotation of $\frac{\pi}{4}$ around the axis $\boldsymbol{e}_1$. The directors are aligned with the bodies' principal axes of inertia such that $\boldsymbol{d}_3^\alpha$ coincides with the longitudinal axis, respectively.
At the start of the manoeuvre, the initial configuration must coincide with the reference configuration, thus $\boldsymbol{q}_0 = \boldsymbol{q}_{00}$ and the initial configuration condition for the optimal control problem reads $\boldsymbol{u}_0 = \boldsymbol{0}_{6\times 1}$. In the final configuration, the tip of the cone must coincide with a prescribed location $\boldsymbol{x}_H = [0\ -1.131\ 0.283]$ in space. Using the vector $\boldsymbol{\rho}_H^1$ specifying the location of the tip in the body frame $\{\boldsymbol{d}_I^1\}$ (see Figure 6.3 (right)), the final configuration condition reads $\boldsymbol{\varphi}_N^1 + (\boldsymbol{\rho}_H^1)_N - \boldsymbol{x}_H = \boldsymbol{0}_{3\times 1}$. The desired motion is a rest to rest manoeuvre, thus $\boldsymbol{p}^0 = \boldsymbol{p}^N = \boldsymbol{0}_{24\times 1}$ in the boundary conditions on momentum level (6.11). In the deterministic setting, the objective function (6.12) represents the control effort, therefore the convex objective function $J_d(\boldsymbol{u}_d, \boldsymbol{\tau}_d) = \sum_{n=0}^{N-1} \|\boldsymbol{\tau}_n\|^2$ is minimised subject to the described boundary conditions and the discrete equations of motion (6.10). Furthermore, bound constraints insure that the components of the applied torques are in the range $-120 \leq ((\tau_{\theta_\alpha})_i)_n \leq 120$ for $\alpha = 1, 2,\ i = 1, 2, 3$ and $n = 0, N-1$. The manoeuvre takes place in $t_N = 1.5$ and $N = 15$ time steps of size $h = 0.1$ are used.
The left hand plot in Figure 6.4 shows the evolution of kinetic, potential and total energy. In particular, the first plot illustrates that the manoeuvre starts and ends at rest. The evolution of the components of angular momentum is shown on the right hand side. The bottom plot verifies equation (6.14) numerically (note that $(\boldsymbol{\tau}_n^+ + \boldsymbol{\tau}_n^-)$ in the plot represents the entire right hand side of (6.14)). The evolution of the components of the torques in each joint can be observed from Figure 6.5 (left). As described before, the torques are constant in each time interval. Finally, the resulting tip trajectory is depicted in Figure 6.5 on the right hand side.

Remark 6.4.2 (Implementation) *The constrained minimisation has been performed by the SQP solver* `fmincon` *in Matlab which can handle bound constraints on the optimisation variables as well as linear and nonlinear equality and inequality constraints. The gradient of the objective function and the Jacobian of the nonlinear equality constraints have been derived analytically and given as user supplied derivatives to Matlab. This sub-*

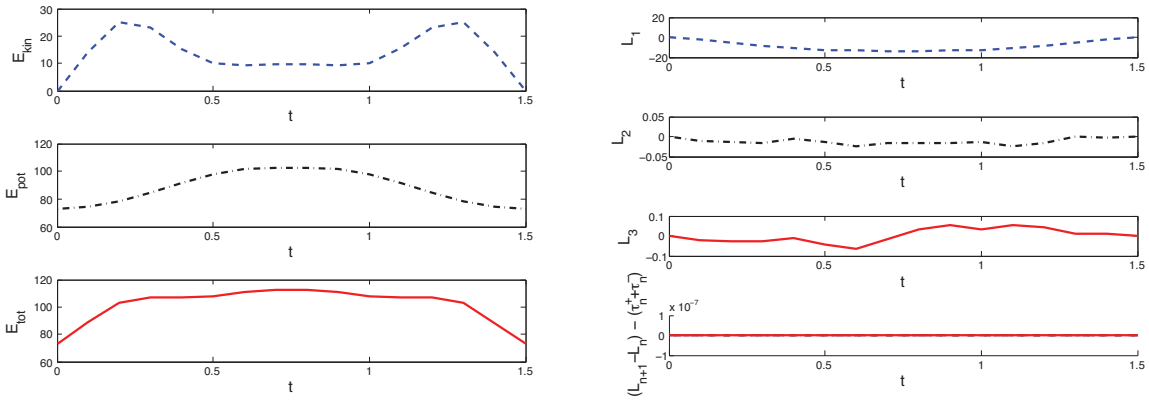

Figure 6.4: Evolution of kinetic, potential and total energy (left) and components of angular momentum (right). The bottom plot on the right shows that momentum maps are represented consistently.

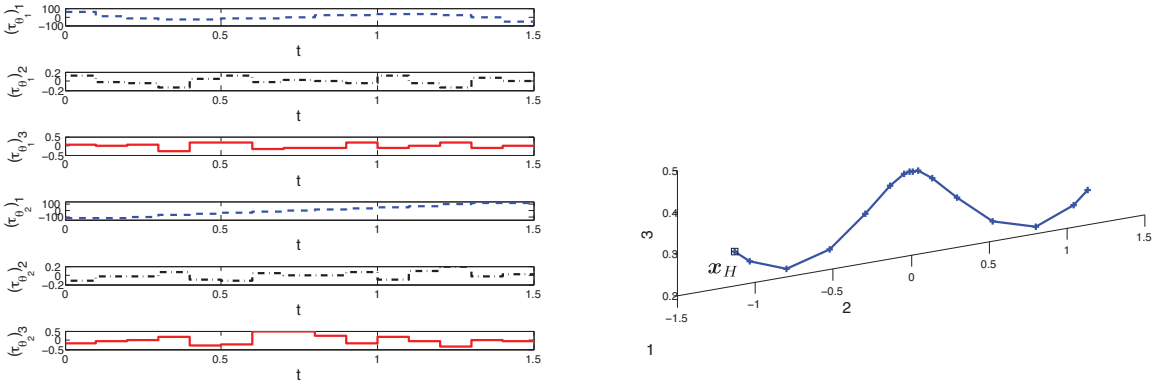

Figure 6.5: Evolution of torques (left) and trajectory of the tip (right).

stantially reduces the computational costs compared to the case when Matlab approximates the derivatives via finite differencing.

Remark 6.4.3 (Inequality constraints) *No inequality constraints have been imposed on the minimisation in this simulation. To obtain more realistic manoeuvres, it is necessary to prevent interpenetration of the two bodies via appropriate inequality constraints. This is left for future work.*

6.5 Test case: minimising the probability of failure for a robot arm manoeuvre

In this section, the deterministic robot arm manoeuvre from Section 6.4.2 is reconsidered in the presence of uncertainty. Specifically, we consider two different uncertainty cases. First, there is uncertainty in the geometry of the robot arm, i.e. the lengths l^1, l^2 are uncertain. Secondly, uncertain operating conditions are represented by the presence

of uncertain wind forces in addition to the uncertain lengths. In all calculations we use the reduced variational time stepping scheme (6.10) obtained via the discrete null space method with nodal reparametrisation. By design, this scheme is symplectic and represents changes in momentum maps exactly. Furthermore, energy is not gained or dissipated numerically. As it is typical for the integration of constrained dynamics, the discrete equations of motion are implicit and need to be solved iteratively, e.g. by means of a Newton-Raphson iteration.

The performance measure Y of interest is assumed to be the placement accuracy of the arm tip, i.e. the distance from the arm tip and its prescribed location $\boldsymbol{x}_H$ at the end of the manoeuvre's duration of $t_N = 1.5$. Thus, in this case $Y^{\tau_d} = \|\boldsymbol{\varphi}_N^1 + (\boldsymbol{\rho}_H^1)_N - \boldsymbol{x}_H\|$ is obtained for a candidate control sequence $\boldsymbol{\tau}_d$ by stepping forward in time using (6.10) and the initial conditions described in Section 6.4.2. From an optimal control point of view, this is similar to a shooting approach to solve the concentration-of-measure optimal control problem (6.8). We additionally suppose that a positioning accuracy a is prescribed, so that the robot arm operates safely if $Y \leq a$ and fails if $Y > a$. The goal is to find a control sequence $\boldsymbol{\tau}_d$ for which the confidence in safe operation is maximal, i.e. the resulting objective function to be minimised is

$$-\mathrm{CF}(\boldsymbol{\tau}_d) \equiv -\frac{M^{\tau_d}}{U^{\tau_d}} \equiv -\frac{(a - \langle Y^{\tau_d} \rangle - \alpha^{\tau_d})_+}{D_{F^{\tau_d}}} \tag{6.15}$$

The evaluation of the objective function (6.15) requires the evaluation of the mean response and the diameter. In all calculations presented here, the mean response (6.4) is computed by random Monte Carlo sampling and the system diameter (6.2) and optimal controls $\boldsymbol{\tau}_d$ are computed by simulated annealing. The basic simulated annealing algorithm is that described in [Kirp 83] and has been enhanced with several user specified options to suit our needs. Details are as given below. The starting controls for the iteration are set to the deterministic controls computed in Section 6.4.2.

Optimisation algorithm The basic simulated annealing algorithm is that described in [Kirp 83] and has been enhanced with several user specified options to suit our needs. Define T as 'temperature' and N as the number of function evaluations. We use a default cooling schedule of $T_{new} = 0.8 \times T^{old}$ with $T_0 = 1.0$. The optimisation stops if $T \leq 1.0e-8$, $N > N_{max} = 2000$, or $N_R > 300$ where N_R is the number of successive rejected states. Temperature decrease happens if $N_T > 30$ or $N_S > 20$, i.e. if 30 function evaluations are made or if there are 20 successive accepted optimal states found at the current temperature. The Boltzmann constant is set to 1.0.

The bound constraints on the random variables need to be satisfied in the optimisation algorithm as well. The neighbour finding routine intelligently seeks out neighbouring states that assert compliance of any permutations of these constraints to find a new neighbour by projecting a randomly generated neighbour into a parametrised point within the constrained design space.

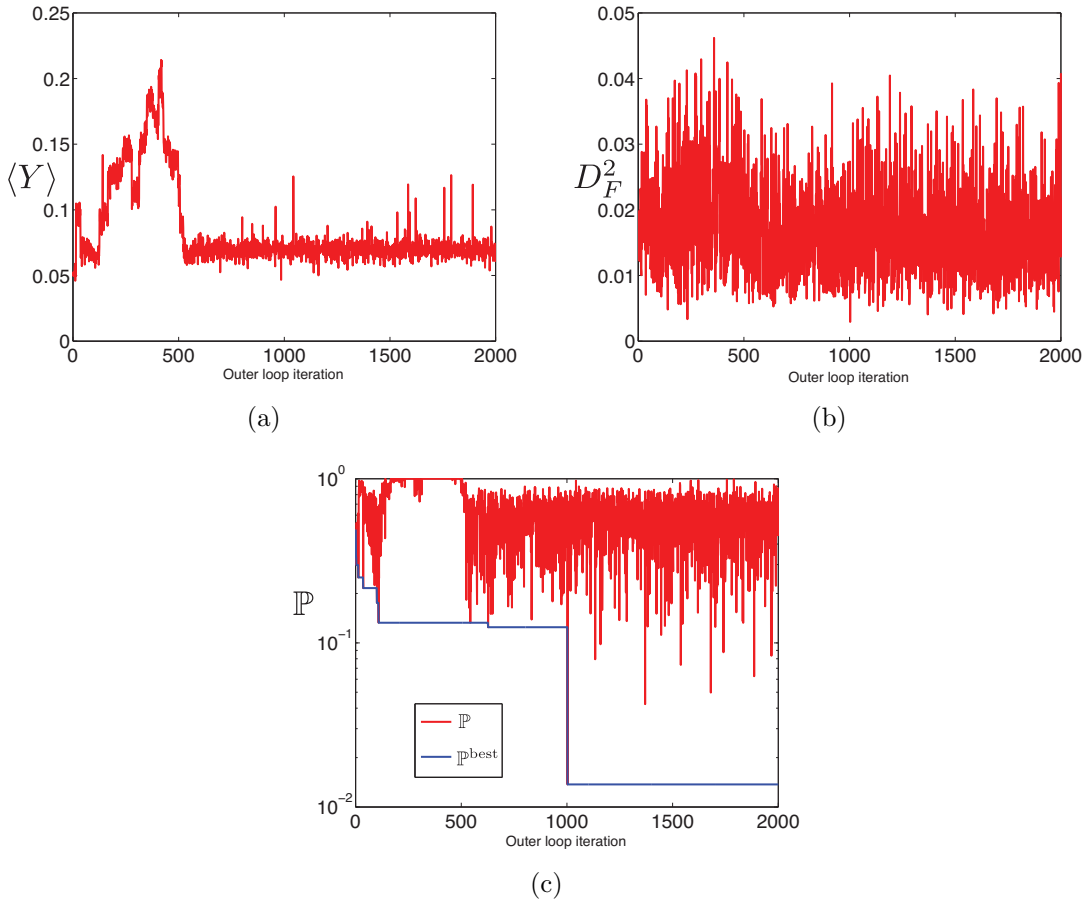

Figure 6.6: Uncertain geometry: Simulated annealing iteration for the determination of the optimal controls. Evolution of: a) mean performance; b) system diameter; and c) concentration-of-measure probability of failure upper bound.

6.5.1 Uncertain geometry

First, there are $M = 2$ uncertain variables. The lengths l^1 can vary randomly in a range of 5% and l^2 varies randomly in the range of 0.1% around the given value, respectively. These values assure that their influence on the system's uncertainty is of the same order of magnitude.

The evolution of the mean performance, system diameter and concentration-of-measure probability of failure upper bound along the simulated annealing iteration for the determination of the optimal controls is shown in Figure 6.6. As expected, both the positioning accuracy of the manoeuvre, measured by the mean response $\langle Y \rangle$ with $m = 100$, and the uncertainty in the operation of the manoeuvre, measured by the diameter D_F, show a decreasing tendency. Correspondingly, the concentration-of-measure probability of failure upper bound decreases from initially $\mathbb{P} = 0.49$ to $\mathbb{P}^{\text{best}} = 0.013722$. This reduction in probability of failure may be alternatively interpreted as an increase in the confidence that may be placed in the safe operation of the manoeuvre, as measured by the confidence factor (6.6). Recall that the right hand side of (6.5) is a random variable and with probability at most ϵ', it may fail to be an upper bound on the probability of failure. This is why, for the optimal control sequence with with $\mathbb{P}_{best} = 0.013722$ computed via (6.5)

(using the empirical mean which is subject to large deviations as rare events), the mean has been recomputed with $m = 10000$. Assuming that the latter empirical mean is an 'accurate' approximation of the exact mean in (6.3) results in the even lower probability of failure bound $\mathbb{P}_{best} = 0.00047207$.

It bears emphasis that high confidence in the safe operation of a system requires achieving a large design margin and a low uncertainty simultaneously. More precisely, confidence requires that the design margin be large in relation to the uncertainty in the operation of the system, which underscores the importance of quantifying – and mitigating by means of optimal control – system uncertainties for purposes of certification. Here, again, the ability of concentration-of-measure optimal control (COMOC) to increase design confidence in the particular example of the robot-arm manoeuvre becomes obvious.

6.5.2 Uncertain wind forces and uncertain geometry

Secondly, in addition to the uncertain lengths, each body is affected by a random wind force in every time step, hitting the body's surface around the centre of mass in a prescribed location. Each component of the two three-dimensional force vectors varies randomly between in $[-0.001, 0.001]$. Altogether, $M = 92$ uncertain variables are present in this simulation. Figure 6.7 shows the evolution of the mean performance with $m = 100$, system diameter and concentration-of-measure probability of failure upper bound along the simulated annealing iteration. The probability of failure upper bound has been improved from $\mathbb{P} = 1$ to $\mathbb{P}^{\text{best}} = 0.11581$. Also here it can be observed that the $\mathbb{P}^{\text{best}}$ has been found for a control sequence that leads to (local) minima in the mean and diameter, respectively. Again, assuming that the mean resulting from $m = 10000$ samples yields exactly the mean performance, (6.3) bounds the probability of failure by $\mathbb{P}^{\text{best}} = 0.0567$.

6.6 Summary and conclusions

We have presented an optimal control methodology, which we refer to as concentration-of-measure optimal control (COMOC), that seeks to minimise a concentration-of-measure upper bound on the probability of failure of a system. The systems under consideration are characterised by a single performance measure that depends on random inputs through a known response function. In addition, the safe operation of the system is characterised by a threshold value of the performance measure. For these systems, a concentration-of-measure upper bound on the probability of failure of a system can be formulated in terms of the mean performance measure and a system diameter that measures the uncertainty in the operation of the system. COMOC then seeks to determine optimal controls that maximise the confidence in the safe operation of the system, defined as the ratio of design margin, measured by the difference between the mean performance and the design threshold, to the system uncertainty, measured by the system diameter. This strategy has been assessed in the case of a robot arm manoeuvre for which the performance measure of interest is assumed to be the placement accuracy of the arm tip. The ability of COMOC to increase design confidence in that particular example of application is remarkable and bodes auspiciously for the approach.

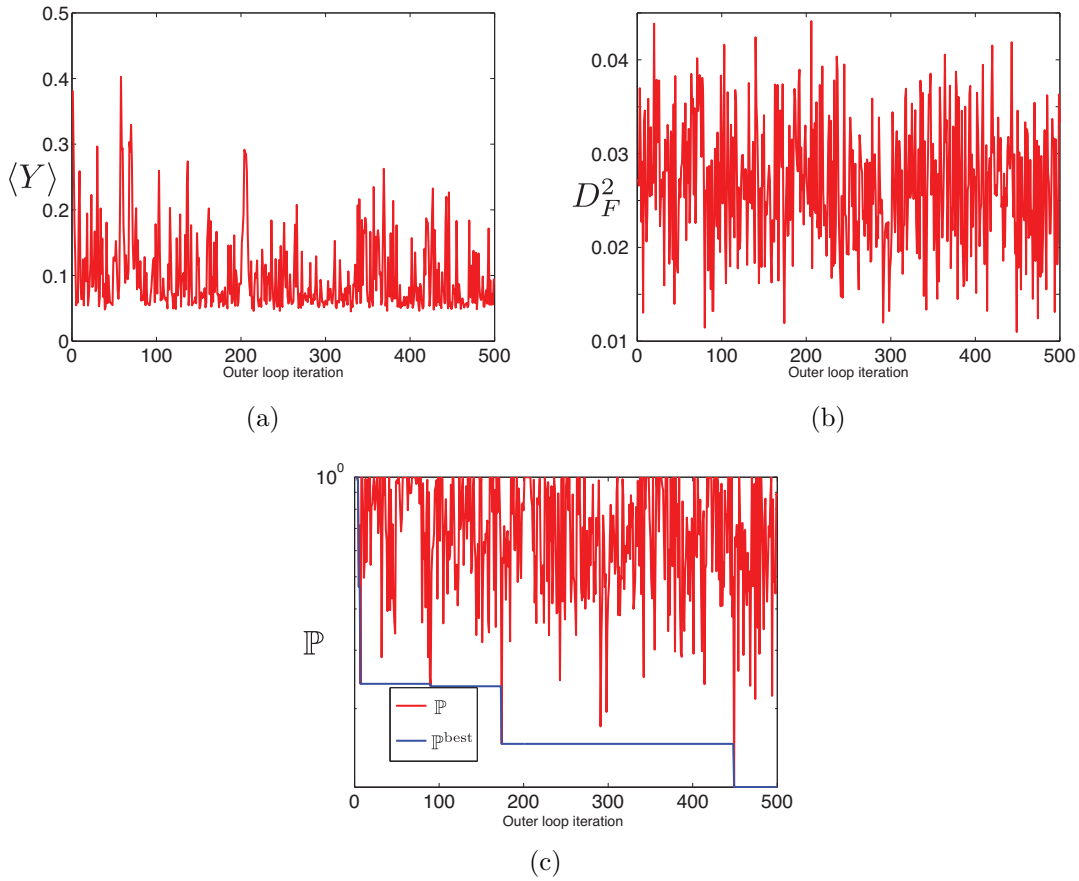

Figure 6.7: Uncertain wind forces and uncertain geometry: Simulated annealing iteration for the determination of the optimal controls. Evolution of: a) mean performance; b) system diameter; and c) concentration-of-measure probability of failure upper bound.

The most severe limitation of the COMOC implementation presented in this paper is its computational expense. Each evaluation of the confidence factor objective function requires the calculation of the mean response and system diameter for a particular control, which in turn requires multiple solutions of the equations of motion of the system. In order to reduce the computational expense to a tractable level, in the calculations presented here the controls have been constrained to remain close to the initial deterministic solution. It is conceivable that further gains in design confidence could be achieved from an unrestricted control optimisation, but the computational resources and infrastructure required for such an optimisation are beyond the scope of this paper. In view of these present limitations, the formulation of efficient COMOC implementations that alleviate its computational expense clearly suggests itself as a subject of further research.

7 A discrete mechanics approach to Cosserat rod theory – static equilibria

7.1 Introduction

Over the past two decades, the theory of discrete mechanics (confirm e.g. [Mars 01] for a review) has received the focus of intense research and attained a considerable degree of development. Numerical integrators that are derived from a discrete variational principle have favourable conservation properties. The aim of this article is the systematic application of concepts that have been developed in the context of discrete mechanics (and also concepts from classical mechanics) to the formulation of a theory of discrete Cosserat rods, analogous in structure and scope to the classical theory of Cosserat rods, in which the arc length is a discrete variable ab initio. Thus, whereas the potential energy density of a rod is a function on the tangent bundle TQ of a one-dimensional manifold Q parametrised by arc length, the discrete rod theory formulated here is predicated on potential energy densities defined over $Q \times Q$, i.e. on pairs of points along the arc length of the rod, in analogy to Veselov's discrete reformulation of Lagrangian mechanics, see [Vese 88]. On this foundation, a complete and selfcontained theory of discrete rods, including the derivation of discrete equations of equilibrium and of exactly conserved arc length wise momentum maps, can be formulated that is in analogy with discrete Lagrangian mechanics.
First steps in this direction were taken by Bobenko and Suris. In their paper [Bobe 99] they derived an integrable discretisation of a Lagrange top as an application case of their general approach to formulate continuous as well as discrete time Lagrangian mechanics on Lie groups. Using a discrete version of Kirchhoff's kinetic analogy (see Love [Love 27], Section 260) they obtained an edge-based, equidistantly discretised version of an inextensible, unshearable and isotropic Kirchhoff rod model which, like its rigid body counterpart, turns out to be a discrete integrable system. In our article we apply the discrete Lagrangian mechanics approach to a more general rod model of Cosserat type. We formulate two discrete models, possibly with non-equidistant step size. In the vertex-based approach, displacements and rotational degrees of freedom are defined on the grid nodes while the edge-based approach associates the rotational degrees of freedom with the edges between the nodes.
As the configuration space SE(3) of a Cosserat rod is a Lie group, it is possible to apply the general approach developed in [Bobe 99] in the continuous as well as in the discrete setting. However, in the context of geometrically exact rod mechanics the spatial or material representation of physical quantities is a more appropriate concept than an equivalent, but rather abstract reformulation of the theory in terms of the right or left trivialisation of a Lagrangian system on a Lie group. We formulate a Cosserat rod model, without explicitly exploiting the Lie group structure, as a Lagrangian system whose configuration space consists of a six-dimensional submanifold of $\mathbb{R}^{12}$. This submanifold structure is

generated by internal holonomic constraints on the rod directors, which we enforce by the method of null space matrices. In the discrete setting we use the corresponding discrete null space method which has been proposed by Betsch in [Bets 05] and developed for multibody systems in [Bets 06] and for flexible multibody systems in [Leye 08a].

The potential energy density (or stored energy function) is an object of central importance in rod theory: it specifies the constitutive properties of the rod and implies the constitutive equations which relate strains to forces and moments. Kirchhoff's kinetic analogy suggests that this energy density function (depending on the curve parameter) is formally equivalent to the Lagrangian function of a time dependent mechanical system, such that the static equilibrium equations of a rod correspond to the Euler-Lagrange equations of the latter. The possibility to generalise Kirchhoff's classical kinetic analogy to Cosserat rods has been utilised in the articles by Kehrbaum and Maddocks [Kehr 97] and Chouaieb and Maddocks [Chou 04] to investigate static equilibrium problems for both Kirchhoff and Cosserat rods as Hamiltonian systems (see also Chouaieb [Chou 03]). Starting from the energy density, which is assumed to be uniform and may be augmented by various constraints to enforce inextensibility or unshearability, they directly proceed to define the respective Hamiltonians via a Legendre transform. In this way, they obtain a variety of Hamiltonian systems whose canonical equations are equivalent to the static equilibrium equations of the respective rod model. However, these authors do not explore the formulation of static equilibrium problems for Cosserat rods as constrained Lagrangian systems on manifolds. We present such a Lagrangian formulation of the continuum theory of Cosserat rods to provide a starting as well as a reference point for our discrete mechanics formulation of the theory.

Like all systems of non-relativistic classical mechanics, the theory of Cosserat rods is formulated on the background of Galilean space-time [Arno 78]. As part of the general requirement of Galilei invariance of all equations this implies that frame-indifference (i.e. invariance under rigid body motions) is a fundamental property for all internal quantities in three-dimensional elasticity as well as in one and two-dimensional theories of structural members (i.e. rods and shells). This holds in particular for the equilibrium equations, any measure of strain as well as the constitutive relations relating the latter to the former (see Truesdell and Noll [True 65] and Antman [Antm 05] for a detailed discussion).

Likewise frame-indifference is required also for corresponding discrete structure models. In the context of finite element discretisations of Cosserat rods this subject is discussed in detail by Crisfield and Jelenić [Cris 99]. We would like to add that frame-indifference already implies a specific form (7.18) of the equilibrium equations and ensures the existence of six first integrals that can be recovered as momentum maps in the context of Noether's theorem. This theorem is a powerful tool to identify first integrals in Lagrangian mechanics due to invariance properties of the Lagrangian function under symmetry transformations (see Marsden and Ratiu [Mars 94]). Two more integrals not depending on space-time symmetries, but rather on the constitutive properties of a rod appear in the special cases of uniform or isotropic material and geometric behaviour. Frame-indifference in the discrete setting requires special attention, as it can be violated by certain interpolations of rotations (see [Cris 99] or [Rome 04]).

Discrete Lagrangian mechanics for Cosserat rods is also a topic in Dixon [Dixo 07]. He

gives a variational formulation of rod dynamics next to and motivated by a comprehensive treatment of rigid bodies in the discrete setting. Our approach is similar, but we restrict ourselves to static rod configurations and spatial momentum maps. Also, we note that our formulation is different in many aspects, as we use different techniques to discrete the Lagrangian function and to handle constraints.
An outline of the article is as follows. In Section 7.2, we define the configuration of a rod and introduce strain measures. Using the tools from variational calculus, we derive the equilibrium equations as constrained Euler-Lagrange equations in Sections 7.3 and 7.4. In Section 7.5, we formulate a theory of discrete rods involving discrete pendants of energy density, stress quantities and equilibrium equations. Numerical examples, including a comparison with a finite-element discretisation, are presented in Section 7.7. The article concludes with a summary in Section 7.8.

7.2 Kinematics of Cosserat rods

We briefly summarise the basic kinematics of the special Cosserat theory of rods using a notation adopted from Antman [Antm 05]. Generally, a rod is a fibre-like elastic body, i.e. it is possible to specify a family of cross sections which have small proportions compared to the length of the rod. This suggests a mathematical model of a rod in terms of a spacecurve corresponding to its centerline and a director frame which defines the orientation of the local cross section plane. For a thorough discussion of the physical aspects of Cosserat rod theory and its relation to three-dimensional, finite deformation elasticity we refer to the seminal article [Simo 85] of Simo and the recent textbook [Gera 01] of Géradin and Cardona.

Notation 7.2.1 *Throughout this work, we denote three-dimensional Euclidean space by* $(\mathbb{E}^3, \langle \cdot, \cdot \rangle)$ *and choose a fixed right-handed orthonormal triple* $(\boldsymbol{e}_1, \boldsymbol{e}_2, \boldsymbol{e}_3)$ *of basis vectors. We denote vectors* $\boldsymbol{w} \in \mathbb{E}^3$ *by boldface roman italic letters. Any vector quantity* $\boldsymbol{w} \in \mathbb{E}^3$ *may be decomposed with respect to the basis* $(\boldsymbol{e}_1, \boldsymbol{e}_2, \boldsymbol{e}_3)$ *in the form* $\boldsymbol{w} = w_1\boldsymbol{e}_1 + w_2\boldsymbol{e}_2 + w_3\boldsymbol{e}_3$. *We denote the triple* $w = (w_1, w_2, w_3)^T \in \mathbb{R}^3$ *of the cartesian components* $w_k = \langle \boldsymbol{w}, \boldsymbol{e}_k \rangle$ *by roman italic letters and isomorphically identify real column vectors* $w \in \mathbb{R}^3$ *with their Euclidean counterparts* $\boldsymbol{w} \in \mathbb{E}^3$. *In the same way, any vector equation in* $\mathbb{E}^3$ *can be isomorphically written in* $\mathbb{R}^3$ *using real column vectors.*

7.2.1 Configuration variables

A configuration of a special Cosserat rod is defined by a regular spacecurve $\boldsymbol{r} : [s_c, s_f] \to \mathbb{E}^3$, which corresponds to the centerline of the rod and continuously connects the position vectors $\boldsymbol{r}(s)$ of the cross section centroids, together with a pair $\boldsymbol{d}^{(1)}, \boldsymbol{d}^{(2)} : [s_c, s_f] \to \mathbb{E}^3$ of director fields spanning the family of cross section planes along the centerline (see Figure 7.1). The directors are required to satisfy the orthonormality conditions

$$\langle \boldsymbol{d}^{(1)}(s), \boldsymbol{d}^{(2)}(s) \rangle = 0, \qquad \|\boldsymbol{d}^{(k)}(s)\| = 1, \qquad k = 1, 2 \tag{7.1}$$

at any $s \in [s_c, s_f]$. The orientation of a cross section is given by its unit normal vector $\boldsymbol{d}^{(3)}(s) = \boldsymbol{d}^{(1)}(s) \times \boldsymbol{d}^{(2)}(s)$ in accordance with the condition $\langle \boldsymbol{d}^{(3)}(s), \boldsymbol{r}'(s) \rangle > 0$

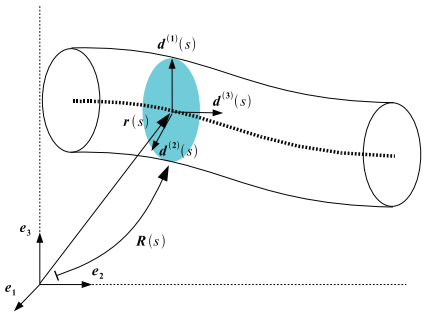

Figure 7.1: Configuration of a Cosserat rod.

which prevents degenerate rod configurations and assures that the cross section normal $\boldsymbol{d}^{(3)}(s)$ and the centerline tangent vector $\boldsymbol{r}'(s)$ point into the same half space. The triple $(\boldsymbol{d}^{(1)}(s), \boldsymbol{d}^{(2)}(s), \boldsymbol{d}^{(3)}(s))$ of orthonormal director fields is related to the fixed basis $(\boldsymbol{e}_1, \boldsymbol{e}_2, \boldsymbol{e}_3)$ by a proper orthogonal linear map $\boldsymbol{R}(s) : \mathbb{E}^3 \to \mathbb{E}^3$ defined by the set of equations

$$\boldsymbol{d}^{(k)}(s) = \boldsymbol{R}(s)\, \boldsymbol{e}_k, \qquad k = 1, 2, 3.$$

The matrix representation of $\boldsymbol{R}(s)$ with respect to the basis $(\boldsymbol{e}_1, \boldsymbol{e}_2, \boldsymbol{e}_3)$ is an element $R(s) \in \mathrm{SO}(3)$ i.e. $R(s)^T = R(s)^{-1}$, $\det(R(s)) = 1$, and the k-th column of $R(s)$ consists of the column vector $d^{(k)}(s) \in \mathbb{R}^3$ corresponding to $\boldsymbol{d}^{(k)}(s)$. In summary, we arrive at a mathematical description of the configurations of a Cosserat rod in terms of a curve within the product manifold $\mathbb{R}^3 \times \mathrm{SO}(3)$, which is completely defined by specifying a pair (r, R) of curves

$$r : [s_c, s_f] \to \mathbb{R}^3 \qquad \text{and} \qquad R : [s_c, s_f] \to \mathrm{SO}(3) \tag{7.2}$$

that are both assumed to be sufficiently smooth.

7.2.2 Submanifolds and nullspace matrices

Disregarding the orthonormality conditions in (7.1), the mapping $s \mapsto (r(s), R(s))$ corresponds to a regular curve in $\mathbb{R}^{12}$. Since there are six independent constraints, the curve is constrained to a differentiable manifold of dimension six.
Let Q be a $(n-k)$-dimensional submanifold of $\mathbb{R}^n$ and let T_qQ denote the tangent space of Q at $q \in Q$. Here, k is the number of independent constraints imposed on $\mathbb{R}^n$. A null space matrix at q is a matrix $P(q) \in \mathbb{R}^{n \times (n-k)}$ such that

$$\mathrm{range}(P(q)) = T_qQ \qquad \text{for all} \qquad q \in Q\,.$$

Clearly, the columns of $P(q)$ for each $q \in Q$ form a basis for T_qQ and, as a consequence, the matrix $P(q)$ induces a linear isomorphism $P(q) : \mathbb{R}^{(n-k)} \to T_qQ$. For the terminology of null space matrices see Betsch [Bets 05], Leyendecker et al. [Leye 08b] and references therein. By the definition of submanifolds of $\mathbb{R}^n$ and the implicit function theorem (see

[Flem 77], Sections 4.7 and 8.2) we may assume the existence of a neighbourhood $U \subset \mathbb{R}^n$, of each $q \in Q$, and a function $g : U \to \mathbb{R}^k$ such that $Q \cap U = g^{-1}(\{0\})$. Then, while $G(q)$ denotes the Jacobi-matrix of g at q, we have

$$\operatorname{range}(P(q)) = \operatorname{null}(G(q)). \tag{7.3}$$

In the setting of Cosserat rods, we have $Q = \mathbb{R}^3 \times \mathrm{SO}(3)$ (confirm (7.2)), and for $q \in Q$ we write

$$q = \begin{bmatrix} r \\ d^{(1)} \\ d^{(2)} \\ d^{(3)} \end{bmatrix} .$$

For each $q \in Q$, there exists a neighbourhood U of q such that $Q \cap U = g^{-1}(\{0\})$ with the constraint function

$$g(q) = \begin{bmatrix} \frac{1}{2}(\|d^{(1)}\|^2 - 1) \\ \frac{1}{2}(\|d^{(2)}\|^2 - 1) \\ \frac{1}{2}(\|d^{(3)}\|^2 - 1) \\ \langle d^{(1)}, d^{(2)} \rangle \\ \langle d^{(1)}, d^{(3)} \rangle \\ \langle d^{(2)}, d^{(3)} \rangle \end{bmatrix}$$

that consists of the six orthonormality conditions $\langle d^{(j)}, d^{(k)} \rangle = \delta_{jk}$ which constitute internal holonomic constraints on the director degrees of freedom. We choose the corresponding null space matrix to be

$$P(q) = \begin{bmatrix} \mathbf{1}_3 & \mathbf{0}_3 \\ \mathbf{0}_3 & -\hat{d}^{(1)} \\ \mathbf{0}_3 & -\hat{d}^{(2)} \\ \mathbf{0}_3 & -\hat{d}^{(3)} \end{bmatrix} \quad \text{for} \quad q \in Q \, . \tag{7.4}$$

Notation 7.2.2 *Let $d \in \mathbb{R}^3$. By $\hat{d} \in \mathfrak{so}(3)$ we denote the skew-symmetric matrix that is uniquely determined by the relation $\hat{d}\, y = d \times y$ for all $y \in \mathbb{R}^3$. In (7.4), $\mathbf{1}_3$ and $\mathbf{0}_3$ denote the 3×3 identity and zero matrices, respectively.*

Obviously, P is a valid null space matrix according to (7.3).

7.2.3 Strain measures

The strain vectors **u** and **v** take values in $\mathbb{R}^3$ and are frame-indifferent quantities which fully describe the internal deformation of the rod as well as its configuration up to a rigid body motion. For a detailed discussion of the strain variables we refer to Chapter 8.6 in Antman [Antm 05].
The local change of the moving frame consisting of the directors $\boldsymbol{d}^{(k)}(s)$ is uniquely determined through the set of evolution equations

$$\frac{\mathrm{d}}{\mathrm{d}s}\, \boldsymbol{d}^{(k)}(s) = \boldsymbol{u}(s) \times \boldsymbol{d}^{(k)}(s), \qquad k = 1, 2, 3 \, . \tag{7.5}$$

The vector function $\boldsymbol{u} : [s_c, s_f] \to \mathbb{E}^3$ is called the Darboux-vector corresponding to the director field. From now, we will drop the argument s as long as there is no danger of confusion. Let us consider the components of $\boldsymbol{u}$ with respect to the basis $(\boldsymbol{d}^{(1)}, \boldsymbol{d}^{(2)}, \boldsymbol{d}^{(3)})$:

$$\boldsymbol{u} = \bar{u}_1\, \boldsymbol{d}^{(1)} + \bar{u}_2\, \boldsymbol{d}^{(2)} + \bar{u}_3\, \boldsymbol{d}^{(3)} \tag{7.6}$$

Notation 7.2.3 *To distinguish between the decompositions of a vector quantity with respect to the fixed basis $(\boldsymbol{e}_1, \boldsymbol{e}_2, \boldsymbol{e}_3)$ and the director basis $(\boldsymbol{d}^{(1)}, \boldsymbol{d}^{(2)}, \boldsymbol{d}^{(3)})$, vector components with respect to the latter are denoted by sans-serif boldface letters, e.g. $\mathbf{u} = (\bar{u}_1, \bar{u}_2, \bar{u}_3)^T$ is called the material description of the Darboux-vector $\boldsymbol{u}$, whereas u (with $u_k = \langle \boldsymbol{u}, \boldsymbol{e}_k \rangle$) is called its spatial description.*

Equations (7.5) and (7.6) imply that the skew-symmetric matrix associated with $\mathbf{u}$ can be expressed by:

$$\hat{\mathbf{u}} = R^T \frac{\mathrm{d}}{\mathrm{d}s} R \tag{7.7}$$

From this expression, we see that the material components $\bar{u}_k$ of $\mathbf{u}$ are invariant under arbitrary rotations of the director field, i.e. they are frame-indifferent quantities. This will become important in the subsequent sections. A second look at (7.7) reveals that the components $(\bar{u}_1, \bar{u}_2)$ of $\mathbf{u}$ describe flexure, as they result from projecting the local change $\frac{\mathrm{d}}{\mathrm{d}s}\boldsymbol{d}^{(3)}$ of the cross section normal onto the cross section plane. Likewise the third component $\bar{u}_3$ of $\mathbf{u}$ measures the local twist of the rod. The material description of the centerline tangent vector

$$\frac{\mathrm{d}}{\mathrm{d}s}\boldsymbol{r} = \bar{v}_1\, \boldsymbol{d}^{(1)} + \bar{v}_2\, \boldsymbol{d}^{(2)} + \bar{v}_3\, \boldsymbol{d}^{(3)}$$

yields the strain variables $\bar{v}_1, \bar{v}_2$, associated with shear, and $\bar{v}_3$ associated with dilatation. A more compact and obviously frame-indifferent expression for $\mathbf{v}$ is

$$\mathbf{v} = R^T \frac{\mathrm{d}}{\mathrm{d}s} r\,. \tag{7.8}$$

The frame-indifferent material vector quantities $\mathbf{u}(s)$ and $\mathbf{v}(s)$ are differential invariants of the framed curve (r, R) which determine the configuration of a Cosserat rod up to an overall rigid body motion, qualifying them as proper strain variables of a Cosserat rod. If the six components of the pair $(\mathbf{u}, \mathbf{v})$ are given as continuous functions of the real variable $s \in [s_c, s_f]$, one may first solve the director frame evolution equation $\frac{\mathrm{d}}{\mathrm{d}s}R = R \cdot \hat{\mathbf{u}}$ with an arbitrarily chosen frame $R_0 = R(s_0)$ fixing the value of $R(s)$ at some particular $s_0 \in [s_c, s_f]$. Using this known frame $R(s; R_0)$ as well as the given material shear strains $\mathbf{v}(s)$ we obtain the centerline curve by means of integrating (7.8) with the final result $r(s) = r_0 + \int_{s_c}^{s} R(s; R_0) \cdot \mathbf{v}(s)\, \mathrm{d}s$, which indicates how the solution $s \mapsto (r(s), R(s))$ depends parametrically on rigid body motions (r_0, R_0) as integration constants. More specifically one can show that for given $(\mathbf{u}, \mathbf{v})$ any two solutions differ by at most a rigid body motion (see [Antm 05], Chapter 8.6 for a detailed proof).

Remark 7.2.4 *One can think of the strain vectors $\mathbf{u}$ and $\mathbf{v}$ as functions on $[s_c, s_f]$ as they describe the deformation along the rod. However, it is also possible to treat them as functions on the tangent bundle TQ since in* (7.7) *and* (7.8) *only elements of Q and their derivatives occur. This is the crucial step that establishes the link to geometric mechanics.*

7.3 Variational formulation: uniform rods

The fact that the equations of motion for a Lagrange top are formally equivalent to the equilibrium equations of an isotropic Kirchhoff rod is known in the literature as Kirchhoff's kinetic analogy (see Love [Love 27]; a modern treatment can be found in Nizette and Goriely [Nize 99]). In the setting for the Lagrange top, the independent variable denotes time whereas for the Kirchhoff rod it denotes arc length. Likewise, the body frame of the top corresponds to the director frame of the rod. It is important to note that the Lagrangian function formally corresponds to the potential energy density of the rod configuration, since this is the starting point for the kinetic analogy. Unlike for the Kirchhoff rod, it is questionable if there exists a dynamical system in the real world which has the same mathematical formulation as a Cosserat rod. However, this does not touch the mathematical theory, so we are going to use mathematical tools from classical mechanics [Mars 94,Mars 01] to derive the equilibrium equations. In summary, we give a variational method to derive the equilibrium equations which is different from the procedure in Antman [Antm 05] or Simo [Simo 85]. In this section, we restrict ourselves to the theory for uniform rods. Some aspects of the non-uniform theory, involving more technicalities, are presented in Section 7.4.

7.3.1 Derivation of the equilibrium equations

First of all, we assume a hyperelastic material behaviour. The potential energy density has the same domain as the strain vectors $\mathbf{u}$ and $\mathbf{v}$, i.e. it is described by a function

$$W : TQ \to \mathbb{R}$$

and the total potential energy is then obtained by

$$V(q) = \int_{s_c}^{s_f} W\left(q(s), \frac{\mathrm{d}}{\mathrm{d}s} q(s)\right) \mathrm{d}s, \qquad q \in C(Q).$$

Generally, the domain $C(Q)$ of V is a subset of $C^2([s_c, s_f], Q)$, the set of twice continuously differentiable curves in Q and depends on the imposed boundary conditions.
Without loss of generality, the energy density $W = W^{\mathrm{int}} + W^{\mathrm{ext}}$ splits into an internal component W^{int}, associated to strain and an external component W^{ext} associated to external loads such as gravity. The internal potential energy is required to be frame-indifferent as it is associated only with elastic deformation. This means that W^{int} remains constant if rigid body transformations

$$\begin{aligned} r &\mapsto y + r, & y &\in \mathbb{R}^3 \\ (r, R) &\mapsto (Yr, YR), & Y &\in \mathrm{SO}(3) \end{aligned}$$

(and compositions thereof) are applied. By an argument analogous to [Antm 05], it can be shown that a frame-indifferent energy density takes the most general form

$$W^{\mathrm{int}}(r, R, r', R') = \overline{W}^{\mathrm{int}}(\mathbf{u}, \mathbf{v}). \tag{7.9}$$

We define internal forces n and moments m as

$$n = \frac{\partial W^{\text{int}}}{\partial r'}, \qquad m = \sum_{k=1}^{3} d^{(k)} \times \frac{\partial W^{\text{int}}}{\partial d^{(k)\prime}} \tag{7.10}$$

and the external forces f and moments l (n, m, f and l are spatial quantities) as

$$f = -\frac{\partial W^{\text{ext}}}{\partial r}, \qquad l = -\sum_{k=1}^{3} d^{(k)} \times \frac{\partial W^{\text{ext}}}{\partial d^{(k)}}. \tag{7.11}$$

It can be shown that the material counterparts of (7.10) respectively take the equivalent form

$$\mathbf{n} = \frac{\partial \overline{W}^{\text{int}}}{\partial \mathbf{v}}, \qquad \mathbf{m} = \frac{\partial \overline{W}^{\text{int}}}{\partial \mathbf{u}}$$

which are possibly more familiar expressions.

Lemma 7.3.1 *Frame-indifference of W^{int} implies the relations*

$$\begin{aligned} \frac{\partial W^{int}}{\partial r} &= 0 \\ \sum_{k=1}^{3} d^{(k)} \times \frac{\partial W^{int}}{\partial d^{(k)}} + \sum_{k=1}^{3} d^{(k)\prime} \times \frac{\partial W^{int}}{\partial d^{(k)\prime}} + r' \times n &= 0 \end{aligned} \tag{7.12}$$

that become useful when analysing the equilibrium equations.

Proof: Let $t \in \mathbb{R}$, $\xi \in \mathbb{R}^3$ then

$$W^{\text{int}}(r, R, r', R') = W^{\text{int}}(r + t\xi, R, r', R') \tag{7.13}$$

due to frame-indifference. Differentiating (7.13) with respect to t and setting $t = 0$ yields

$$0 = \left\langle \frac{\partial W^{\text{int}}}{\partial r}, \xi \right\rangle.$$

Since ξ can be chosen arbitrarily, $(7.12)_1$ follows. Next, set $Y(t) = \exp(t\hat{\xi})$, and again due to frame-indifference we have

$$W^{\text{int}}(r, R, r', R') = W^{\text{int}}(Y(t)r, Y(t)R, Y(t)r', Y(t)R'). \tag{7.14}$$

Differentiating (7.14) with respect to t and setting $t = 0$ yields

$$0 = \left\langle \frac{\partial W^{\text{int}}}{\partial r}, \hat{\xi} r \right\rangle + \sum_{k=1}^{3} \left\langle \frac{\partial W^{\text{int}}}{\partial d^{(k)}}, \hat{\xi} d^{(k)} \right\rangle + \left\langle \frac{\partial W^{\text{int}}}{\partial r'}, \hat{\xi} r' \right\rangle + \sum_{k=1}^{3} \left\langle \frac{\partial W^{\text{int}}}{\partial d^{(k)\prime}}, \hat{\xi} d^{(k)\prime} \right\rangle$$

By cyclic permutation, this computes to

$$0 = \left\langle \xi, \hat{r} \frac{\partial W^{\text{int}}}{\partial r} \right\rangle + \sum_{k=1}^{3} \left\langle \xi, \hat{d}^{(k)} \frac{\partial W^{\text{int}}}{\partial d^{(k)}} \right\rangle + \left\langle \xi, \hat{r'} \frac{\partial W^{\text{int}}}{\partial r'} \right\rangle + \sum_{k=1}^{3} \left\langle \xi, \hat{d}^{(k)\prime} \frac{\partial W^{\text{int}}}{\partial d^{(k)\prime}} \right\rangle$$

Now we use $\frac{\partial W^{\text{int}}}{\partial r} = 0$ and $\frac{\partial W^{\text{int}}}{\partial r'} = n$ to obtain $(7.12)_2$. ∎

The equilibrium configurations of any static system coincide with the critical points of the potential energy. This means, for hyperelastic rods, a (stable or unstable) equilibrium configuration satisfies

$$\mathbf{d}V(q)\,\delta q = 0 \qquad \text{in any direction } \delta q \in T_q C(Q) \tag{7.15}$$

where $\mathbf{d}V(q) \in T_q C(Q)^*$ denotes the derivative of V at q. Equation (7.15) formally corresponds to Hamilton's principle of critical action, yet the physical dimension of the integral is energy and integration is taken with respect to the curve parameter s. For simplicity, we assume fixed endpoints q_c, q_f and set

$$C(Q) = \{q \in C^2([s_c, s_f], Q) \,|\, q(s_c) = q_c, q(s_f) = q_f\}.$$

For (7.15), the following are necessary and sufficient:

$$\begin{aligned} P(q)^T \left(\frac{\mathrm{d}}{\mathrm{d}s} \frac{\partial W}{\partial q'} - \frac{\partial W}{\partial q} \right) = 0, \\ g(q) = 0 \end{aligned} \tag{7.16}$$

with P given in (7.4). The details of the derivation are omitted and can be found in [Jung 09] and in [Leye 08b]. Equations (7.16) are the Euler-Lagrange equations corresponding to the variational principle (7.15) with respect to the boundary conditions specified in $C(Q)$. There is another set of equations which is also equivalent to (7.15) and possibly more familiar reading

$$\begin{aligned} \frac{\mathrm{d}}{\mathrm{d}s} \frac{\partial W}{\partial q'} - \frac{\partial W}{\partial q} + G(q)^T \lambda = 0, \\ g(q) = 0. \end{aligned} \tag{7.17}$$

Here, $\lambda : [s_c, s_f] \to \mathbb{R}^6$ is a Lagrange multiplier associated to the orthonomality constraints in Q.

Remark 7.3.2 *The equivalence of* (7.15), (7.16) *and* (7.17) *holds for arbitrary submanifolds Q. However, in the setting for special Cosserat rods, $Q = \mathbb{R}^3 \times \mathrm{SO}(3)$ is the case of interest.*

As s denotes the curve parameter, we will call (7.16) or (7.17) spatial Euler-Lagrange or equilibrium equations. It is interesting to see that, as a consequence of frame-indifference, the Euler-Lagrange equations attain a specific form (see also [Jung 09]).

Lemma 7.3.3 *Consider a hyperelastic rod with $W^{ext} = W^{ext}(r, R)$. Using the definitions* (7.10) *and* (7.11)*, the spatial Euler-Lagrange equations* (7.16) *can be rewritten in the form*

$$\begin{aligned} \frac{\mathrm{d}}{\mathrm{d}s} n + f = 0 \\ \frac{\mathrm{d}}{\mathrm{d}s} m + \left(\frac{\mathrm{d}}{\mathrm{d}s} r \right) \times n + l = 0. \end{aligned} \tag{7.18}$$

Proof: The spatial Euler-Lagrange equations on $Q = \mathbb{R}^3 \times \mathrm{SO}(3)$ can be split in two components:

$$\frac{\mathrm{d}}{\mathrm{d}s}\frac{\partial W}{\partial r'} - \frac{\partial W}{\partial r} = 0$$
$$\sum_{k=1}^{3} d^{(k)} \times \left(\frac{\mathrm{d}}{\mathrm{d}s}\frac{\partial W}{\partial d^{(k)\prime}} - \frac{\partial W}{\partial d^{(k)}} \right) = 0$$

Using (7.10), (7.11) and (7.12), the first equation becomes

$$\frac{\mathrm{d}}{\mathrm{d}s}\frac{\partial W^{\mathrm{int}}}{\partial r'} - \frac{\partial W^{\mathrm{int}}}{\partial r} - \frac{\partial W^{\mathrm{ext}}}{\partial r} = \frac{\mathrm{d}}{\mathrm{d}s}n + f = 0$$

and the second equation becomes

$$\sum_{k=1}^{3} d^{(k)} \times \frac{\mathrm{d}}{\mathrm{d}s}\frac{\partial W^{\mathrm{int}}}{\partial d^{(k)\prime}} - \sum_{k=1}^{3} d^{(k)} \times \frac{\partial W^{\mathrm{int}}}{\partial d^{(k)}} - \sum_{k=1}^{3} d^{(k)} \times \frac{\partial W^{\mathrm{ext}}}{\partial d^{(k)}}$$
$$= \sum_{k=1}^{3} d^{(k)} \times \frac{\mathrm{d}}{\mathrm{d}s}\frac{\partial W^{\mathrm{int}}}{\partial d^{(k)\prime}} + \sum_{k=1}^{3} \left(\frac{\mathrm{d}}{\mathrm{d}s} d^{(k)} \right) \times \frac{\partial W^{\mathrm{int}}}{\partial d^{(k)\prime}} + \left(\frac{\mathrm{d}}{\mathrm{d}s} r \right) \times n + l = \frac{\mathrm{d}}{\mathrm{d}s} m + \left(\frac{\mathrm{d}}{\mathrm{d}s} r \right) \times n + l = 0.$$

■

Remark 7.3.4 *The equilibrium equations* (7.18) *can be rewritten, in the equivalent form*

$$\frac{\mathrm{d}}{\mathrm{d}s}\mathbf{n} + \mathbf{u} \times \mathbf{n} + \mathbf{f} = 0$$
$$\frac{\mathrm{d}}{\mathrm{d}s}\mathbf{m} + \mathbf{u} \times \mathbf{m} + \mathbf{v} \times \mathbf{n} + \mathbf{l} = 0$$

in which only material quantities appear. This can be seen by using the chain rule on $m = R\,\mathbf{m}$ *and* $n = R\,\mathbf{n}$ *and then applying* (7.7).

7.3.2 Spatial symmetries and momentum maps

It is well known that the static equilibrium equations (7.18) feature various first integrals due to frame-indifference as well as further, constitutively determined, symmetries. In the absence of external forces and moments, (7.18) immediately imply the conservation of both the spatial force n as well as the total momentum $m + r' \times n$. Two additional integrals, namely the twist moment $\langle m, d^{(3)} \rangle$ and the quantity $\langle n, v \rangle + \langle m, u \rangle - W$ arise in the isotropic and in the uniform case, respectively. A comprehensive analysis within the framework of rod dynamics is given in Maddocks and Dichmann [Madd 94]. The conservation of the corresponding static integrals follows immediately from the vanishing time derivatives (see also Dichmann, Li and Maddocks [Dich 96], Section 4.4). In the following we explicitly show how these integrals may be derived in a constructive way via Noether's theorem.

Noether's theorem, as first formulated by E. Noether [Noet 18], provides a systematic framework that recovers conserved quantities as a result of Lie group symmetries. We now give a few definitions that are needed to formulate Noether's theorem in a version

similar to the one given in Marsden and West [Mars 01]. Let G be a Lie group acting on the configuration manifold Q and let

$$\Phi : G \times Q \to Q$$

denote the group action of G on Q. The tangent lift

$$\Phi^{TQ} : G \times TQ \to TQ$$

of Φ is defined by $\Phi_g^{TQ}(\delta q) = \frac{\mathrm{d}}{\mathrm{d}t}\Phi_g(c(t))\big|_{t=0}$ for $g \in G$, $\delta q \in TQ$ and c being a curve in Q such that $c(0) = q$ and $\frac{\mathrm{d}}{\mathrm{d}t}c(t)\big|_{t=0} = \delta q$.
Let $\mathfrak{g}$ denote the Lie algebra corresponding to G and $\mathfrak{g}^*$ its dual space. Given an energy density W and a group action Φ, the corresponding momentum map $J : TQ \to \mathfrak{g}^*$ is given by

$$J(q, q')\,\xi = \left\langle \frac{\partial W}{\partial q'}, \xi_Q(q) \right\rangle, \qquad \xi \in \mathfrak{g} \tag{7.19}$$

where

$$\xi_Q(q) = \frac{\mathrm{d}}{\mathrm{d}\varepsilon}\Phi(\exp(\varepsilon\xi), q)\bigg|_{\varepsilon=0} \qquad \in T_qQ$$

denotes the infinitesimal generator.
An energy density $W : TQ \to \mathbb{R}$ is said to be invariant under Φ if

$$W \circ \Phi_g^{TQ} = W \qquad \text{for all} \qquad g \in G$$

which implies that the potential energy integral is invariant under pointwise transformation by Φ_g. If W is Φ-invariant then Φ is called a symmetry and by Noether's theorem, there exists a momentum map (first integral of the equilibrium equations) associated with this symmetry.

Theorem 7.3.5 (Noether's theorem) *Consider a hyperelastic rod in equilibrium, W denoting the potential energy density and q denoting the corresponding configuration map. If W is invariant under the action $\Phi : G \times Q \to Q$ then*

$$\frac{\mathrm{d}}{\mathrm{d}s}J(q(s), q'(s)) = 0$$

i.e. the momentum map J of Φ is conserved.

A proof can be found e.g. in [Mars 01]. In the following, we list symmetries for the Cosserat rod ($Q = \mathbb{R}^3 \times \mathrm{SO}(3)$) and construct the associated integrals via Noether's theorem.

Frame-indifference Recall from Section 7.3.1 that spatial quantities (e.g. strains, forces, moments and energy density) are frame-indifferent, or objective, if they are invariant under rigid motions. i.e. under the group actions

$$\Phi_y^{\mathrm{trans}} : (r, R) \mapsto (y + r, R), \qquad y \in \mathbb{R}^3$$
$$\Phi_Y^{\mathrm{rot}} : (r, R) \mapsto (Yr, YR), \qquad Y \in \mathrm{SO}(3)$$

on the configuration manifold Q. What could eventually be seen from the fact that (7.16) and (7.18) are equivalent can also be derived in a more formal way via Noether's theorem. Assume $W = W^{\text{int}}$ that is no external loads act on the rod. First, we consider translational invariance: Let $\xi \in \mathbb{R}^3$, then the infinitesimal generator reads $\xi_Q(q) = (\xi, 0)$ and

$$J^{\text{trans}}(q, q')\xi = \left\langle \frac{\partial W}{\partial q'}, (\xi, 0) \right\rangle = \langle n, \xi \rangle$$

i.e. the stress force n is a momentum map of the Cosserat rod. Secondly, rotational invariance is considered. Let $\hat{\xi} \in \mathfrak{so}(3)$, then $\xi_Q(q) = (\hat{\xi}r, \hat{\xi}R)$ and

$$\begin{aligned} J^{\text{rot}}(q, q')\,\hat{\xi} &= \left\langle \frac{\partial W}{\partial q'}, (\hat{\xi}r, \hat{\xi}R) \right\rangle \\ &= \langle n, \hat{\xi}r \rangle + \sum_{k=1}^{3} \left\langle \frac{\partial W}{\partial (d^{(k)\prime})}, \hat{\xi} d^{(k)} \right\rangle = \langle r \times n + m, \xi \rangle \end{aligned}$$

where the last equality follows by cyclic permutation. The duality on $\mathfrak{so}(3)$ is as follows: $\langle \hat{\psi}, \hat{\xi} \rangle_{\mathfrak{so}(3)} = \frac{1}{2}(\hat{\psi}\hat{\xi}^T) = \langle \psi, \xi \rangle_{\mathbb{R}^3}$ for $\hat{\psi}, \hat{\xi} \in \mathfrak{so}(3)$. Thus, the total momentum $m + r \times n$ is another momentum map of the Cosserat rod.

Isotropy A rod is called isotropic, if its energy density W is invariant under the action

$$\Phi_\alpha^{\text{iso}} : (r, R) \mapsto (r, R\,Q(\alpha))$$

where

$$Q(\alpha) = \begin{bmatrix} \cos(\alpha) & -\sin(\alpha) & 0 \\ \sin(\alpha) & \cos(\alpha) & 0 \\ 0 & 0 & 1 \end{bmatrix}$$

rotates the cross section around $d^{(3)}$ by the angle α. Let $\xi \in \mathbb{R}$ then $\frac{\mathrm{d}}{\mathrm{d}t}\cos(t\xi)\big|_{t=0} = 0$, $\frac{\mathrm{d}}{\mathrm{d}t}\sin(t\xi)\big|_{t=0} = \xi$ and consequently $\xi_Q(q) = (0, d^{(2)}\xi, -d^{(1)}\xi, 0)$. Thus,

$$J^{\text{iso}}(q, q')\,\xi = \left\langle \frac{\partial W}{\partial q'}, \xi_Q(q, s) \right\rangle = \left\langle d^{(2)}, \frac{\partial W}{\partial (d^{(1)\prime})} \right\rangle \xi - \left\langle d^{(1)}, \frac{\partial W}{\partial (d^{(2)\prime})} \right\rangle \xi = \langle m, d^{(3)} \rangle \xi$$

where the last equality follows with (7.10). Hence the third momentum map is the twist moment $\langle m, d^{(3)} \rangle$.

Remark 7.3.6 *From* (7.7) *and* (7.8)*, we see that the strain vectors are compatible with the action of* Φ^{iso} *in the following sense:*

$$\begin{aligned} \mathbf{u} \circ \Phi_\alpha^{iso^{TQ}} &= Q(\alpha)^T \mathbf{u} \\ \mathbf{v} \circ \Phi_\alpha^{iso^{TQ}} &= Q(\alpha)^T \mathbf{v} \end{aligned} \tag{7.20}$$

which are helpful relations when testing isotropy.

Example 7.3.7 *In the range of small strains one expects – in analogy to linear beam theory – the energy density to be quadratic in the strains. The most frequently encountered example of a frame-indifferent energy density of this type is given by the function*

$$W(q,q') = W^{int}(q,q') = \frac{1}{2}\big\langle \mathbf{u}-\mathbf{u}^0, C_1(\mathbf{u}-\mathbf{u}^0)\big\rangle + \frac{1}{2}\big\langle \mathbf{v}-\mathbf{v}^0, C_2(\mathbf{v}-\mathbf{v}^0)\big\rangle\,, \qquad (7.21)$$

where

$$C_1 = \begin{bmatrix} EI_1 & 0 & 0 \\ 0 & EI_2 & 0 \\ 0 & 0 & GJ \end{bmatrix} \quad \textit{and} \quad C_2 = \begin{bmatrix} GA & 0 & 0 \\ 0 & GA & 0 \\ 0 & 0 & EA \end{bmatrix}$$

are the positive definite stiffness matrices of a pre-deformed prismatic rod with a constant cross section area A and geometric area moments I_1, I_2 and $J = I_1 + I_2$, consisting of an isotropic, elastic material characterised by the shear modulus G and Young's modulus E. The pre-deformed geometry is given by its strain measures $\mathbf{v}^0 = (0,0,1)^T$, corresponding to centerline parametrized by arc length and cross sections orthogonal to its tangent, and $\mathbf{u}^0$, describing the initial curvature and twist of the rod. The constitutive equations

$$\mathbf{m} = C_1(\mathbf{u}-\mathbf{u}^0), \qquad \mathbf{n} = C_2(\mathbf{v}-\mathbf{v}^0)$$

derived from this energy density provide a linear relation of the forces and moments to the strains. The energy density (7.21) *is obviously frame-indifferent. Note that despite the spatial isotropy of the rod material, the effective constitutive behaviour of the rod is anisotropic unless the shape of the cross section displays kinetic symmetry ($I_1 = I_2 = I$).*

One may consider more general rod geometries with cross sections varying smoothly along the centerline, which yields variable geometry parameters $A(s)$ and $I_1(s), I_2(s)$ and effectively leads to an explicit dependence of the energy density on the curve parameter. This likewise happens if the curvature and twist of the undeformed rod are not constant. More general rod models of this type are treated in the following section.

7.4 Variational formulation: non-uniform rods

Until now we only considered uniform rods but we did not define the actual concept of uniformity. In order to do this properly, we have to refine the theory presented so far by choosing a different domain for W. In the dynamical setting, the theory from this section corresponds to non-autonomous systems, such as considered in [Mars 01], Part 4.

7.4.1 Derivation of the equilibrium equations

Generally, the potential energy density may depend on the curve parameter s. It is therefore described by a function

$$W : \mathbb{R} \times TQ \to \mathbb{R}$$

and the total potential energy is obtained by

$$V(q) = \int_{s_c}^{s_f} W\left(s, q(s), \frac{\mathrm{d}}{\mathrm{d}s}q(s)\right) \mathrm{d}s, \qquad q \in C(Q).$$

$C(Q)$ denotes the set of admissible curves. It is again a subset of $C^2([s_c, s_f], Q)$ corresponding to the problem setup.
Before we proceed, we define the configuration bundle $Y = \mathbb{R} \times Q$, which is needed for discussing the variations and for formally defining uniformity. For a configuration map $q \in C(Q)$ we choose a representation defined in the following way: let $c : [a_c, a_f] \to Y$ be a map, its components denoted by $c(a) = (c_s(a), c_q(a))$. The first component $c_s : [a_c, a_f] \to \mathbb{R}$ is strictly increasing and maps $[a_c, a_f]$ diffeomorphically to $[s_c, s_f]$. The curve c is required to satisfy $q = c_q \circ c_s^{-1}$. Recall that $q = \{(s, q(s)) \,|\, s \in [s_c, s_f]\}$ is a subset of Y, thus variations of q involve both variations of $q(s)$ and variations of s. In the following, q is identified with a class of curves c that are associated with the same configuration map $q = c_q \circ c_s^{-1}$. Using the chain rule on $q(s) = c_q(c_s^{-1}(s))$ gives $q'(s) = \frac{c_q'(c_s^{-1}(s))}{c_s'(c_s^{-1}(s))}$. Accordingly, $V(q)$ can be written as

$$V(q) = \int_{a_c}^{a_f} W\left(c_s(a), c_q(a), \frac{c_q'(a)}{c_s'(a)}\right) c_s'(a)\,\mathrm{d}a \tag{7.22}$$

where integration is now taken over $[a_c, a_f]$. This formulation reveals that the full expression for the derivative $\mathbf{d}V$ contains derivatives with respect to s, and that further the tangent space $T_qC(q)$ includes variations δc_s of the s-parameter. For uniform rods, these terms can be neglected.
In the extended setting, consider again the variational principle

$$\mathbf{d}V(q)\delta q = 0, \qquad \delta q \in T_qC(Q)$$

Computing the derivative $\mathbf{d}V$ using the expression in (7.22), we obtain exactly the same result as for uniform rods: If the endpoints of the rod are considered fixed, then (7.15), (7.16) and (7.17) are equivalent.
Consequently, the equilibrium equations (7.18) apply both to uniform and to non-uniform rods, which is little surprising, but proved once more in a formal way. However, the details of the computation are somewhat different (see [Mars 01]). The variational principle now yields two equations, (7.16) being the first and

$$\frac{\partial W}{\partial s} + \frac{\mathrm{d}}{\mathrm{d}s}\left(\left\langle \frac{\partial W}{\partial q'}, q' \right\rangle - W\right) = 0 \tag{7.23}$$

being the second, but it turns out that (7.23) is implied by (7.16).

7.4.2 Spatial symmetries and momentum maps

Symmetry transformations may act on Y, rather than on Q. This is crucial to define uniformity.

Uniformity A Cosserat rod is called uniform if its energy density W is invariant under the action

$$\Phi_y^{\mathrm{uni}} : (s, r, R) \to (s + y, r, R), \qquad y \in \mathbb{R}$$

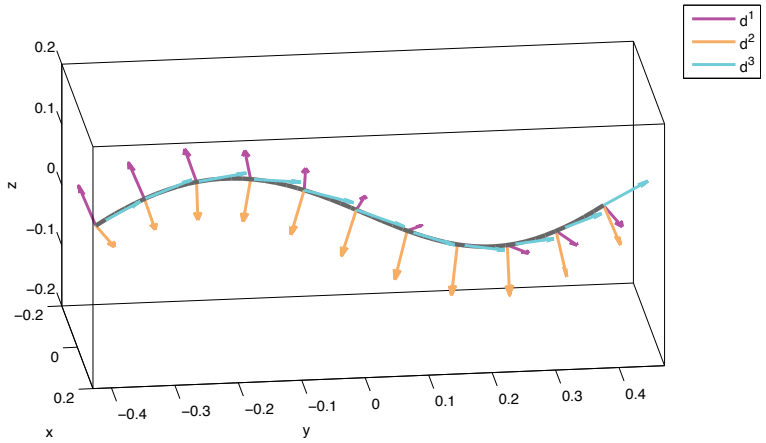

Figure 7.2: Deformed configuration with 11 vertices.

i.e. in the case of translational invariance with respect to the curve parameter s. From equation (7.23) we see that

$$J^{\text{uni}} = \left\langle \frac{\partial W}{\partial q'}, q' \right\rangle - W = \langle m, u \rangle + \langle n, v \rangle - W$$

is the associated momentum map.

Remark 7.4.1 *The formal definition for a momentum map* $J : \mathbb{R} \times TQ \to \mathfrak{g}^*$ *in the general case reads*

$$J(s, q, q')\,\xi = \left\langle \frac{\partial W}{\partial q'}, \xi_Y^q(s, q) \right\rangle - \left(\left\langle \frac{\partial W}{\partial q'}, q' \right\rangle - W \right) \xi_Y^s(s) \qquad \textit{for} \quad \xi \in \mathfrak{g}$$

and reduces to (7.19) *if* $\xi_Y^s(s) = 0$.

7.5 Discrete rod theory

In this section, we convey continuous rod theory to the discrete setting. We apply the concepts of variational calculus and the discrete null space method which allow us to formulate a discrete version of the equilibrium equations that can be solved numerically. In the discrete setting, we lose the pushforward operation ($m = R\mathbf{m}$) between spatial and material quantities. Also, we have to deal with the fact that discrete mechanics confines the admissible functional form of discrete strain measures, but does not provide a canonical choice.

7.5.1 Discrete rods

Consider a predefined grid $s_1 \dots s_N$ (with $s_i < s_{i+1}$) and define increments $h_i = s_{i+1} - s_i$. A discrete configuration map is given by a sequence $q_1 \dots q_N \in Q$ and we write $q_i = q_i(s_i)$,

which we denote as a vertex-based discretisation approach (see also Section 7.6.3). The energy integral is approximated by $N-1$ discrete energy density functions

$$W_i : Q \times Q \to \mathbb{R}, \qquad i = 1 \dots N-1$$

where $Q \times Q$ is the usual (in discrete mechanics) discrete replacement for TQ. These energy functions should be chosen such that W_i is a consistent approximation of the energy integral over the i-th rod segment, i.e.

$$W_i(q_i, q_{i+1}) = \int_{s_i}^{s_{i+1}} W\left(q(s), \frac{\mathrm{d}}{\mathrm{d}s} q(s)\right) \mathrm{d}s + \mathcal{O}(h_i^{\alpha+1}) \tag{7.24}$$

for some $\alpha \in \mathbb{N}$. Moreover, it is crucial that the W_i inherit all symmetries from the continuous model. In Section 7.6.1 we will make suggestions based on the formulation of discrete strain measures. The potential energy sum reads

$$V^d(q^d) = \sum_{i=1}^{N-1} W_i(q_i, q_{i+1}), \qquad q^d \in S(Q).$$

Here, $\mathcal{S}(Q)$ denotes the set of discrete configuration maps and must be a subset of $Q^{\{s_1 \dots s_N\}}$ which accounts for certain boundary conditions. As for continuous rods, we assume that each W_i is of the form $W_i = W_i^{\mathrm{int}} + W_i^{\mathrm{ext}}$ with W_i^{int} being frame-indifferent.
Now, we define the discrete elastic forces n_i and moments m_i and the discrete external forces f_i and moments l_i.

$$n_i = \frac{\partial W_i^{\mathrm{int}}}{\partial r_{i+1}}, \qquad m_i^- = -\sum_{k=1}^{3} d_i^{(k)} \times \frac{\partial W_i^{\mathrm{int}}}{\partial d_i^{(k)}}, \qquad m_i^+ = \sum_{k=1}^{3} d_{i+1}^{(k)} \times \frac{\partial W_i^{\mathrm{int}}}{\partial d_{i+1}^{(k)}} \tag{7.25}$$

$$f_{i+1} = -\left(\frac{\partial W_i^{\mathrm{ext}}}{\partial r_{i+1}} + \frac{\partial W_{i+1}^{\mathrm{ext}}}{\partial r_{i+1}}\right), \qquad l_{i+1} = -\sum_{k=1}^{3} d_{i+1}^{(k)} \times \left(\frac{\partial W_i^{\mathrm{ext}}}{\partial d_{i+1}^{(k)}} + \frac{\partial W_{i+1}^{\mathrm{ext}}}{\partial d_{i+1}^{(k)}}\right). \tag{7.26}$$

Lemma 7.5.1 *As a consequence of frame-indifference, the following hold.*

$$n_i = \frac{\partial W_i^{int}}{\partial r_{i+1}} = -\frac{\partial W_i^{int}}{\partial r_i} \tag{7.27}$$

$$m_i^- + r_i \times n_i = m_i^+ + r_{i+1} \times n_i \tag{7.28}$$

Proof: Let $t \in \mathbb{R}$, $\xi \in \mathbb{R}^3$ then

$$W_i^{\mathrm{int}}(r_i, R_i, r_{i+1}, R_{i+1}) = W_i^{\mathrm{int}}(r_i + t\xi, R_i, r_{i+1} + t\xi, R_{i+1}) \tag{7.29}$$

due to frame-indifference. Differentiating (7.29) with respect to t and setting $t = 0$ yields

$$0 = \left\langle \frac{\partial W_i^{\mathrm{int}}}{\partial r_i}, \xi \right\rangle + \left\langle \frac{\partial W_i^{\mathrm{int}}}{\partial r_{i+1}}, \xi \right\rangle.$$

Since ξ can be chosen arbitrarily, (7.27) follows. Next, set $Y(t) = \exp(t\hat{\xi}) \in \mathrm{SO}(3)$ and, again due to frame-indifference, we have

$$W_i^{\mathrm{int}}(r_i, R_i, r_{i+1}, R_{i+1}) = W_i^{\mathrm{int}}(Y(t)r_i, Y(t)R_i, Y(t)r_{i+1}, Y(t)R_{i+1}). \tag{7.30}$$

Differentiating (7.30) with respect to t and setting $t = 0$ yields

$$0 = \left\langle \frac{\partial W_i^{\text{int}}}{\partial r_i}, \hat{\xi} r_i \right\rangle + \sum_{k=1}^{3} \left\langle \frac{\partial W_i^{\text{int}}}{\partial d_i^{(k)}}, \hat{\xi} d_i^{(k)} \right\rangle + \left\langle \frac{\partial W_i^{\text{int}}}{\partial r_{i+1}}, \hat{\xi} r_{i+1} \right\rangle + \sum_{k=1}^{3} \left\langle \frac{\partial W_i^{\text{int}}}{\partial d_{i+1}^{(k)}}, \hat{\xi} d_{i+1}^{(k)} \right\rangle.$$

By cyclic permutation, this computes to

$$0 = \left\langle \xi, \hat{r}_i \frac{\partial W_i^{\text{int}}}{\partial r_i} \right\rangle + \sum_{k=1}^{3} \left\langle \xi, \hat{d}_i^{(k)} \frac{\partial W_i^{\text{int}}}{\partial d_i^{(k)}} \right\rangle + \left\langle \xi, \hat{r}_{i+1} \frac{\partial W_i^{\text{int}}}{\partial r_{i+1}} \right\rangle + \sum_{k=1}^{3} \left\langle \xi, \hat{d}_{i+1}^{(k)} \frac{\partial W_i^{\text{int}}}{\partial d_{i+1}^{(k)}} \right\rangle.$$

Using the definitions (7.25) and, since ξ can be chosen arbitrarily, (7.28) follows. ∎

Remark 7.5.2 *The definitions* (7.25) *are again motivated by the discrete momentum maps and they are precisely those which permit a formulation of the equilibrium equations surprisingly similar to the continuous case.*

In complete analogy to the continuous setting a variational principle characterises equilibrium configurations.

$$\mathbf{d}V^d(q^d)\,\delta q = 0 \qquad \text{in any direction } \delta q \in T_q S(Q) \tag{7.31}$$

We set

$$\mathcal{S}(Q) = \{(q_1 \dots q_N) \,|\, q_i \in Q, q_1 = q_c, q_N = q_f\} \tag{7.32}$$

such that variations at the boundary are zero ($\delta q_1 = \delta q_N = 0$). In this case, we obtain the discrete Euler-Lagrange equations

$$\begin{aligned} P(q_i)^T \left(\frac{\partial W_{i-1}}{\partial q_i} + \frac{\partial W_i}{\partial q_i} \right) = 0 \qquad & i = 2 \dots N-1 \\ g(q_i) = 0 & \end{aligned} \tag{7.33}$$

which hold equivalently to (7.31). This system of equations serves as a basis for numerical algorithms. After introducing a reparametrisation $\phi : \mathbb{R}^6 \to Q$, we can reduce the number of unknowns to its theoretical minimum by solving the equivalent system $F(\phi(a_2) \dots \phi(a_{N-1})) = 0$ instead. An example of ϕ is $\phi(r, c) = (r, \exp(\hat{c})) = (r, R(c))$ i.e. SO(3)-matrices are parametrized by their rotation vectors.

Lemma 7.5.3 *Using the expressions* (7.25) *and* (7.26) *for the discrete forces and moments allows the discrete Euler-Lagrange equations* (7.33) *to be alternatively written as*

$$\begin{aligned} n_i - n_{i-1} + f_i &= 0 \\ m_i^- - m_{i-1}^- + (r_i - r_{i-1}) \times n_{i-1} + l_i &= 0 \\ m_i^+ - m_{i-1}^+ + (r_{i+1} - r_i) \times n_i + l_i &= 0 \end{aligned} \tag{7.34}$$

where $(7.34)_2$ *and* $(7.34)_3$ *are equivalent.*

Proof: The discrete Euler-Lagrange equations on $Q = \mathbb{R}^3 \times \mathrm{SO}(3)$ can be split in two components:

$$\frac{\partial W_{i-1}}{\partial r_i} - \frac{\partial W_i}{\partial r_i} = 0$$
$$\sum_{k=1}^{3} d_i^{(k)} \times \left(\frac{\partial W_{i-1}}{\partial d_i^{(k)}} - \frac{\partial W_i}{\partial d_i^{(k)}} \right) = 0$$

The claims follow by applying the definitions (7.25) and (7.26) and the identity (7.28). ∎
Already at this stage, we see that the discrete forces n_i are constant, if no external loads are applied ($W_i^{ext} = 0$).

7.5.2 Boundary conditions

By (7.32), the discrete Euler-Lagrange equations describe a configuration where both ends q_1, q_N are in fixed position (rod fully clamped at both ends). It is easy to extend the system of equations to the case where one end is free. For example if the end q_N is free, we have to consider the additional equations

$$P(q_N)^T \frac{\partial W_{N-1}}{\partial q_N} = 0, \qquad g(q_N) = 0$$

The meaning of these equations is that both the discrete force f_{N-1} and the discrete moment m_{N-1}^+ are zero. If r_N is fixed and R_N is free then the additional equations are

$$\sum_{k=1}^{3} d_N^{(k)} \times \frac{\partial W_{N-1}}{\partial d_N^{(k)}} = 0, \qquad g(q_N) = 0$$

which say that the discrete moment m_{N-1}^+ is zero. Discrete mechanics provides a most natural way to handle various boundary conditions. More sophisticated conditions involving external potentials at the boundary or single directors can also be handled, see [Bets 06, Leye 08a].

7.5.3 Discrete momentum maps

Let G be a Lie group acting on the manifold Q and let $\Phi : G \times Q \to Q$ denote the group action of G on Q, then Φ can be lifted canonically to $Q \times Q$.

$$\Phi^{Q\times Q} : G \times (Q \times Q) \to Q \times Q$$

An energy function $W_i : Q \times Q \to \mathbb{R}$ is said to be invariant under Φ if $W_i \circ \Phi_g^{Q\times Q} = W_i$ for all $g \in G$, $i = 1...N-1$. Again, Φ is called a symmetry action, and the discrete version of Noether's theorem states that there exists a discrete constant quantity (sequence of momentum maps) associated with Φ. A sequence of momentum maps $J_i^{\pm} : Q \times Q \to \mathfrak{g}^*$ is defined by

$$\langle J_i^+(q_i, q_{i+1}), \xi \rangle = \left\langle \frac{\partial W_i}{\partial q_{i+1}}(q_i, q_{i+1}), \xi_Q(q_{i+1}) \right\rangle, \qquad \xi \in \mathfrak{g},$$
$$\langle J_i^-(q_i, q_{i+1}), \xi \rangle = \left\langle -\frac{\partial W_i}{\partial q_i}(q_i, q_{i+1}), \xi_Q(q_i) \right\rangle, \qquad \xi \in \mathfrak{g}.$$

Remark 7.5.4 *When Noether's theorem applies, the two momentum maps J_i^- and J_i^+ coincide, and there is only one conserved quantity.*

Theorem 7.5.5 (Discrete Noether's theorem) *Consider a balanced configuration $(q_i)_{i=1}^N \in \mathcal{S}(Q)$ of a discrete rod. If its discrete energy functional is invariant under the action $\Phi : G \times Q \to Q$ then*

$$J_{i-1}^{\pm}(q_{i-1}, q_i) = J_i^{\pm}(q_i, q_{i+1}) \qquad \textit{for} \quad i = 2...N-1$$

i.e. the corresponding discrete momentum map is conserved.

For a proof, one can consult [Mars 01] again. Table 7.1 lists the momentum maps associated with the three symmetry actions for elastic rods. Their computations are omitted as they can be computed in exactly the same way as the continuous momentum maps.

symmetry action	momentum map
frame-indifference (a) rigid translation	n_i
(b) rigid rotation	$m_i^- + r_i \times n_i$ $= m_i^+ + r_{i+1} \times n_i$
isotropy	$\langle d_{i+1}^{(2)}, \frac{\partial W_i}{\partial d_{i+1}^{(1)}} \rangle - \langle d_{i+1}^{(1)}, \frac{\partial W_i}{\partial d_{i+1}^{(2)}} \rangle$ $= -\langle d_i^{(2)}, \frac{\partial W_i}{\partial d_i^{(1)}} \rangle + \langle d_i^{(1)}, \frac{\partial W_i}{\partial d_i^{(2)}} \rangle$

Table 7.1: Momentum maps of a discrete rod.

7.6 Discretisation

In all preceding developments, the discrete energy density of the rod has been presumed given. However, in practice discrete rods are often intended as approximations of continuous rods, and the question naturally arises of how to formulate discrete rod energy densities that are consistent with their continuous counterparts. Then, a result in [Mars 01] shows that the discrete equations of equilibrium are consistent in the sense of ordinary differential equations and the discrete rod configurations converge to the continuous limit by virtue of Gronwall's inequality. In this section, we present a specific discretisation strategy that is based on the formulation of discrete strain measures. We recall that the most general frame-indifferent energy density of a rod is of the form (7.9), i.e. it can be expressed in terms of the strain measures $\mathbf{u}$ and $\mathbf{v}$ defined in (7.7) and (7.8). Within this representation, the consistency condition (7.24) takes the form

$$W_i^{\text{int}}(q_i, q_{i+1}) = \int_{s_i}^{s_{i+1}} \overline{W}^{\text{int}}(\mathbf{u}, \mathbf{v}) \, \mathrm{d}s + \mathcal{O}(h_i^{\alpha+1}) \tag{7.36}$$

A family of discrete energy densities that is consistent in this sense is obtained by writing

$$W_i^{\text{int}}(q_i, q_{i+1}) = h_i \overline{W}^{\text{int}}(\mathbf{u}_i, \mathbf{v}_i) \tag{7.37}$$

where $\mathbf{u}_i$ and $\mathbf{v}_i$ are suitably chosen discrete strain measures that are frame-indifferent and consistent with $\mathbf{u}$ and $\mathbf{v}$ in the usual sense of numerical differentiation. It bears emphasis that the results of the general theory presented in the foregoing apply regardless of the choice of discrete strain measures. Considerable latitude therefore remains as regards that choice, which must be made based on considerations of stability, numerical accuracy and efficiency. A particular choice of discrete strain measures that is found to behave well in applications is presented next.

7.6.1 Discrete strain measures

From (7.7) it follows that the strain vector $\mathbf{u}$ satisfies the differential equation

$$\frac{\mathrm{d}}{\mathrm{d}s}R = R\,\hat{\mathbf{u}}\,. \tag{7.38}$$

If $R : [s_c, s_f] \to \mathrm{SO}(3)$ is a solution of (7.38) then the relation

$$R(s_{i+1}) = R(s_i)\exp(\Omega(s_{i+1})), \qquad \Omega(s_{i+1}) = \int_{s_i}^{s_{i+1}} \hat{\mathbf{u}}(s)\,\mathrm{d}s + \mathcal{O}(h_i^5) \tag{7.39}$$

holds. The proof of this statement as well as precise expressions for Ω can be found in [Hair 04], Chapter IV.7. The first step towards the discrete world is to assume that $\mathbf{u}$ is constant on $[s_i, s_{i+1}]$. In that case, (7.39) simplifies to

$$R(s_{i+1}) = R(s_i)\exp((s_{i+1} - s_i)\,\hat{\mathbf{u}}). \tag{7.40}$$

Next, the Cayley-transform which induces a map from $\mathfrak{so}(3)$ to $\mathrm{SO}(3)$ is introduced and its connection to the exponential map on $\mathfrak{so}(3)$ is shown. Finally, we use this knowledge to design discrete strain measures.

Lemma 7.6.1 *For $\hat{y} \in \mathfrak{so}(3)$, $R \in \mathrm{SO}(3), \mathrm{trace}(R) \neq -1$ the following identities hold:*

$$\begin{aligned} \mathbf{1}_3 + \frac{2}{1+\|y\|^2}(\hat{y} + \hat{y}^2) &= (\mathbf{1}_3 + \hat{y})(\mathbf{1}_3 - \hat{y})^{-1} \\ \frac{1}{1+\mathrm{trace}(R)}(R - R^T) &= (R + \mathbf{1}_3)^{-1}(R - \mathbf{1}_3) \end{aligned} \tag{7.41}$$

We recognise the Cayley-transform $\mathrm{cay}(\hat{y}) = (\mathbf{1}_3 + \hat{y})(\mathbf{1}_3 - \hat{y})^{-1}$ and its inverse $\mathrm{inv\,cay}(R) = (R + \mathbf{1}_3)^{-1}(R - \mathbf{1}_3)$ and Lemma 7.6.1 implies that the Cayley-transform gives a bijection

$$\mathrm{cay} : \mathfrak{so}(3) \xrightarrow{1:1} \{R \in \mathrm{SO}(3) | \,\mathrm{trace}(R) \neq -1\}.$$

The Cayley transform on $\mathfrak{so}(3)$ is interesting for applications in (computational) mechanics as can be seen in [Bets 98].

Lemma 7.6.2 *Let $R \in \mathrm{SO}(3)$ be a rotation with angle ϕ about the axis $n \in \mathbb{R}^3, \|n\| = 1$. Then the Cayley-transform is connected to the exponential map by the identity*

$$\exp(\phi\,\hat{n}) = \mathrm{cay}\left(\tan\left(\frac{\phi}{2}\right)\hat{n}\right) = R.$$

Since $2\tan(\phi/2) = \phi + \mathcal{O}(\phi^3)$, we obtain an approximation of the logarithm on SO(3) by (twice) the inverse Cayley-transform (7.41).
Note that whenever writing "$\log(R) \approx 2\,\mathrm{inv\,cay}(R)$" one has to consider the fact that the exponential map on $\mathfrak{so}(3)$ is not injective, so a logarithm can only be meant as a local inverse.
We apply this approximation property to the canonical (vertex based) discretisation of (7.7), assuming $\hat{\mathbf{u}}$ to be constant on the segment $[s_i, s_{i+1}]$ as in (7.40), and thus define the discrete strain measures $\hat{\mathbf{u}}_i$ to be

$$\begin{aligned}\hat{\mathbf{u}}_i(r_i, R_i, r_{i+1}, R_{i+1}) &= \frac{2}{h_i}\,\mathrm{inv\,cay}(R_i^T R_{i+1}) \\ &= \frac{1}{h_i}\frac{2}{1+\mathrm{trace}(R_i^T R_{i+1})}(R_i^T R_{i+1} - R_{i+1}^T R_i) \\ &= \frac{2}{h_i}\tan\left(\frac{\phi_i}{2}\right)\hat{n}_i, \qquad i = 1\ldots N-1\end{aligned} \tag{7.42}$$

where $\exp(\phi_i\,\hat{n}_i) = R_i^T R_{i+1}$ i.e. $\phi_i\,n_i$ is the rotation vector of the incremental rotation $R_i^T R_{i+1}$. In the special case, when ϕ_i measures pure bending, our curvature measure corresponds to the one proposed by Bergou et al. [Berg 08] (see also [Bobe 99], Section 6).
We define the discrete strain vectors $\mathbf{v}_i$ to be

$$\mathbf{v}_i(r_i, R_i, r_{i+1}, R_{i+1}) = \frac{1}{2}\frac{1}{s_{i+1}-s_i}(R_{i+1}^T + R_i^T)(r_{i+1} - r_i), \qquad i = 1\ldots N-1. \tag{7.43}$$

Remark 7.6.3 *At first glance, this discretisation seems to be very similar to the one obtained from a finite element method using linear finite elements and numerical integration via the midpoint rule, see e.g. [Bets 02b, Leye 06b]. The finite element method yields precisely the strain measures $\mathbf{v}_i$. Note the arithmetic averaging of the transposed frame variables in* (7.43)*, which corresponds to a non-orthogonal, yet second order accurate interpolation of the transposed frame evaluated at $(s_i + s_{i+1})/2$ that may be computed very efficiently. The bending strains* (7.42)*, however are different. Here, the finite element discretisation reads*

$$\hat{\mathbf{u}}_i(q_i, q_{i+1}) = \frac{1}{2h_i}(R_i^T R_{i+1} - R_{i+1}^T R_i) = \frac{1}{h_i}\sin(\phi_i)\,\hat{n}_i, \qquad i = 1\ldots N-1$$

Note the difference between $2\tan(\phi/2)$ and $\sin(\phi)$. The singularity for $|\phi_i| \to \pi$ and its positive effects are discussed further below. For $i = 1\ldots N-1$, the Taylor series expansions of the strain measures in the discrete mechanics and the linear finite element approach read

$$\hat{\mathbf{u}}_i^{disc\ mech}(q_i, q_{i+1}) = \left(1 + \mathcal{O}(h_i^2)\right)\left(\hat{\mathbf{u}}_i(q_i, q_i') + \frac{h}{4}(R_i^T R_i'' - (R_i'')^T R_i) + \mathcal{O}(h_i^2)\right)$$

$$\hat{\mathbf{u}}_i^{fem}(q_i, q_{i+1}) = \hat{\mathbf{u}}_i(q_i, q_i') + \frac{h}{4}(R_i^T R_i'' - (R_i'')^T R_i) + \mathcal{O}(h_i^2)$$

respectively. This shows that they only differ in terms of order $\mathcal{O}(h_i^2)$ and higher. Therefore, as long as deformation is rather small, the discrete mechanics approach yields the

same results as a linear finite element method. The comparison of load-displacement curves for the hinged frame in Figure 7.10 shows good agreement in the range of small displacements. However note, that quadratic finite elements have been used in [Bets 02b] while we use twice as many elements in the discrete mechanics approach. Naturally, the good agreement still holds for small deformation.

Using the quadrature rule (7.37) we obtain a discretisation of the energy integral ready for implementation. In the case of the small strain quadratic energy example (7.21) this yields

$$W_i^{\mathrm{int}}(q_i, q_{i+1}) = \frac{1}{2}\left(\langle \mathbf{u}_i - \mathbf{u}^0, C_1(\mathbf{u}_i - \mathbf{u}^0)\rangle + \langle \mathbf{v}_i - \mathbf{v}^0, C_2(\mathbf{v}_i - \mathbf{v}^0)\rangle\right) h_i\,. \tag{7.44}$$

Note that $\mathbf{u}_i$ and $\mathbf{v}_i$ inherit many properties from their continuous counterparts. In the context of symmetries, we would like to mention

$$\begin{aligned}\mathbf{u}_i \circ \Phi_{\mathrm{iso}}^{Y\times Y}(\alpha, \cdot\,) &= Q(\alpha)^T \mathbf{u}_i\\ \mathbf{v}_i \circ \Phi_{\mathrm{iso}}^{Y\times Y}(\alpha, \cdot\,) &= Q(\alpha)^T \mathbf{v}_i,\end{aligned}$$

which are the discrete equivalents to (7.20). Before going on, we elaborate on the properties of the energy defined above and explain why these properties are numerically favourable.

- Symmetries: the energy sum given by (7.44) is frame-indifferent and isotropic and uniform.
- Computational effort: (7.42) and (7.43) can be computed efficiently without evaluating trigonometric functions or matrix inverses.
- Growth of the elastic energy: as $\mathbf{v}_i$ is linear with respect to $r_{i+1} - r_i$, the discrete energy grows quadratically with respect to $r_{i+1} - r_i$. Growth with respect to ϕ_i is also important. Whereas, around $\phi_i = 0$, $\mathbf{u}_i$ is linear in ϕ_i, $\mathbf{u}_i$ exhibits a singularity for $|\phi_i| \to \pi$. Thus, in a admissible configuration, the angle between any pair $d_i^{(k)}$, $d_{i+1}^{(k)}$ of directors is strictly smaller than π. There is a stronger advantage of this singularity. In scenarios with large stresses it must be made sure that the discrete equilibrium equations $(7.34)_3$ still have a solution. This is achieved, for example by the choice of $\mathbf{u}_i$.
- Well-posedness: the large-strain behaviour resulting from the discrete strain measure (7.42) is also useful when studying well-posedness of certain problems, although this is generally a difficult issue (if e.g. buckling occurs).
- Consistency: we are going to show analytically and by numerical experiments that the energy sum given in (7.44) approximates the continuous integral with second-order consistency.

Remark 7.6.4 *While the discrete mechanics approach admits a certain freedom regarding the choice of discrete strain measures, the list of favourable properties of our specific choices* (7.42) *and* (7.43) *indicates that they are not arbitrary at all. From the*

viewpoint of the discrete differential geometry (DDG) of framed curves, the expression $\kappa_i = 2\tan(\phi_i/2)$ *provides the preferred definition of discrete curvature (see the contributions by T. Hoffmann and J.M. Sullivan in [Bobe 08]). It also appears as an essential part of the integrable discretisation of symmetric, inextensible Kirchhoff rods given in the work [Bobe 99] by Bobenko and Suris. The recent paper by Bergou et al. [Berg 08] provides a kinematical description of discrete, inextensible Kirchhoff rods of more general type (e.g. non-symmetric cross sections) as discrete curves with an adapted frame. These authors derive the discrete curvature* $\kappa_i = 2\tan(\phi_i/2)$ *using the DDG concepts of discrete parallel transport and discrete holonomy. In this sense, DDG confirms our definition* (7.42) *from a complementary viewpoint.*

7.6.2 Variational error analysis

In order to establish consistency of the discrete mechanics discretisation, variational error analysis is used, see [Mars 01]. There, it is shown that solutions of the discrete Euler-Lagrange equations converge to the continuous solution with order α if and only if the discrete Lagrangian approximates the continuous action with consistency order α and stability holds. Accordingly, the main task is to compute the order of consistency (7.36) for our discrete strain measures (7.42) and (7.43) in the vertex-based case, and (7.48) and (7.49) in the edge-based case, respectively.

For simplicity, only the case of additively separable energy densities is considered; as this is the case in (7.44). We start by rewriting (7.37) with $\overline{W}^{\mathrm{int}}(\mathbf{u},\mathbf{v}) = W^{\mathrm{u,int}}(\mathbf{u}) + W^{\mathrm{v,int}}(\mathbf{v})$ as

$$\begin{aligned} W_i^{\mathrm{int}}(q_i, q_{i+1}) &= W_i^{\mathrm{u,int}}(q_i, q_{i+1}) + W_i^{\mathrm{v,int}}(q_i, q_{i+1}) \\ &= h_i W^{\mathrm{u,int}}(\mathbf{u}_i(q_i, q_{i+1})) + h_i W^{\mathrm{v,int}}(\mathbf{v}_i(q_i, q_{i+1})) \end{aligned}$$

and we consider the contribution from axial and shear strains first. The Taylor series expansion

$$\begin{aligned} &\int_{s_i}^{s_{i+1}} W^{\mathrm{v,int}}\left(\mathbf{v}\left(q(s), \frac{\mathrm{d}}{\mathrm{d}s}q(s)\right)\right) \mathrm{d}s \\ &\quad = h_i W^{\mathrm{v,int}}(\mathbf{v}(q_i, q_i')) + \frac{h_i^2}{2}\left(\frac{\partial W^{\mathrm{v,int}}}{\partial q}(\mathbf{v}(q_i, q_i'))q_i' + \frac{\partial W^{\mathrm{v,int}}}{\partial q'}(\mathbf{v}(q_i, q_i'))q_i''\right) + \mathcal{O}(h_i^3) \end{aligned}$$

displays the lower order terms needed for comparison. Herein, the shorthand $q_i = q(s_i)$ has been extended to arbitrary derivatives of q. Note that the discrete strain measures (7.43) are given by

$$\mathbf{v}_i(q_i, q_{i+1}) = \mathbf{v}\left(\frac{q_i + q_{i+1}}{2}, \frac{q_{i+1} - q_i}{h_i}\right) \tag{7.45}$$

Before computing the derivatives $\dfrac{\partial^k W^{\mathrm{v,int}}}{\partial h_i^k}$ we make use of the Taylor series expansion

$q_{i+1} = q_i + h_i q_i' + \frac{h_i^2}{2} q_i'' + \mathcal{O}(h_i^3)$ of the configuration variable itself. This yields

$$\begin{aligned} &W_i^{\mathrm{v,int}}(q_i, q_{i+1}) \\ &= h_i W^{\mathrm{v,int}} \left(\mathbf{v} \left(q_i + \frac{h_i}{2} q_i' + \frac{h_i^2}{4} q_i'' + \mathcal{O}(h_i^3), q_i' + \frac{h_i}{2} q_i'' + \mathcal{O}(h_i^2) \right) \right) \\ &= h_i W^{\mathrm{v,int}} \left(\mathbf{v} \left(q_i, q_i' \right) \right) + \frac{h_i^2}{2} \left(\frac{\partial W^{\mathrm{v,int}}}{\partial q} (\mathbf{v}(q_i, q_i'))\, q_i' + \frac{\partial W^{\mathrm{v,int}}}{\partial q'} (\mathbf{v}(q_i, q_i'))\, q_i'' \right) + \mathcal{O}(h_i^3). \end{aligned} \tag{7.46}$$

Thus, $\int_{s_i}^{s_{i+1}} W^{\mathrm{v,int}}(\mathbf{v}(q, q'))\, \mathrm{d}s - W_i^{\mathrm{v,int}}(q_i, q_{i+1}) = \mathcal{O}(h_i^3)$ which means that $W_i^{\mathrm{v,int}}(q_i, q_{i+1})$ is second-order consistent.

The bending and torsional contribution takes a little more work, since the approximation (7.42) of the strain vector $\mathbf{u}$ involves the factor including the trace and is therefore not of the form (7.45). We perform this consistency order proof for discrete energies of the form

$$W_i^{\mathrm{u,int}}(q_i, q_{i+1}) = f(q_i, q_{i+1}) h_i W^{\mathrm{u,int}} \left(\mathbf{u} \left(\frac{q_i + q_{i+1}}{2}, \frac{q_{i+1} - q_i}{h_i} \right) \right)$$

with $f(q_i, q_{i+1}) = 1 + \mathcal{O}(h_i^2)$. The energy density in (7.44) together with the discrete strain measures (7.42) takes this form with

$$f(q_i, q_{i+1}) = \left(\frac{4}{1 + \operatorname{trace}(R_i^T R_{i+1})} \right)^2. \tag{7.47}$$

By the same arguments as used in (7.46), the expansion of $W_i^{\mathrm{u,int}}(q_i, q_{i+1})$ reads

$$\begin{aligned} &W_i^{\mathrm{u,int}}(q_i, q_{i+1}) = \\ &f(q_i, q_{i+1}) \left(h_i W^{\mathrm{u,int}} \left(\mathbf{u} \left(q_i, q_i' \right) \right) + \frac{h_i^2}{2} \left(\frac{\partial W^{\mathrm{u,int}}}{\partial q} (\mathbf{u}(q_i, q_i'))\, q_i' + \frac{\partial W^{\mathrm{u,int}}}{\partial q'} (\mathbf{u}(q_i, q_i'))\, q_i'' \right) + \mathcal{O}(h_i^3) \right) \end{aligned}$$

Accordingly,

$$\begin{aligned} &\int_{s_i}^{s_{i+1}} W^{\mathrm{u,int}}(\mathbf{u}(q, q'))\, \mathrm{d}s - W_i^{\mathrm{u,int}}(q_i, q_{i+1}) = \\ &(1 - f(q_i, q_{i+1})) \left(h_i W^{\mathrm{u,int}} \left(\mathbf{u} \left(q_i, q_i' \right) \right) + \frac{h_i^2}{2} \left(\frac{\partial W^{\mathrm{u,int}}}{\partial q} (\mathbf{u}(q_i, q_i'))\, q_i' + \frac{\partial W^{\mathrm{u,int}}}{\partial q'} (\mathbf{u}(q_i, q_i'))\, q_i'' \right) + \mathcal{O}(h_i^3) \right) \end{aligned}$$

Insertion of the expansion of q_{i+1} into (7.47) yields

$$f(q_i, q_{i+1}) = \left(\frac{1}{1 + \frac{h_i^2}{8} \operatorname{trace}(R_i^T R_i'') + \mathcal{O}(h_i^3)} \right)^2 = \left(1 - \frac{h_i^2}{8} \operatorname{trace}(R_i^T R_i'') + \mathcal{O}(h_i^3) \right)^2$$

since $R_i^T R_i = \mathbf{1}_3$ and $R_i^T R_i'$ is skew-symmetric. The last equality holds by the geometric series and the fact that $|\frac{h_i^2}{8} \operatorname{trace}(R_i^T R_i'') + \mathcal{O}(h_i^3)| < 1$ for sufficiently small elements. In summary, this yields $\int_{s_1}^{s_{i+1}} W^{\mathrm{u,int}}(\mathbf{u}(q, q'))\, \mathrm{d}s - W_i^{\mathrm{u,int}}(q_i, q_{i+1}) = \mathcal{O}(h_i^3)$. The total discrete energy $W_i^{\mathrm{int}}(q_i, q_{i+1})$ is therefore consistent of order 2 and solutions of the discrete Euler-Lagrange equations (7.33) converge quadratically.

7.6.3 Vertex-based and edge-based formulation

The underlying structure of a discrete beam is a one-dimensional simplicial complex consisting of N vertices (zero-simplices) $(v_1 \dots v_N)$ and $N-1$ edges (one-simplices) $(e_1 \dots e_{N-1})$, see Figure 7.3. The dual $*e_i$ of the edge e_i is simply its midpoint (a zero-simplex) while the dual $*v_i$ of the vertex v_i is given by the interval ranging from $*e_{i-1}$ to $*e_i$ (the convex hull of the midpoints of the adjacent edges). In the one-dimensional case, there is no difference between circumcentric and barycentric duals, see [Munk 84] for further details.

Figure 7.3: One-dimensional primal complex (bottom) and its dual (top).

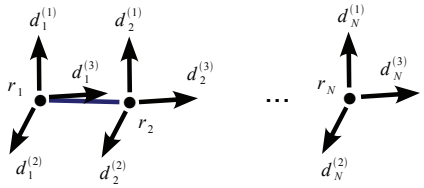

Figure 7.4: Vertex-based rod.

Vertex-based rod Specifying a discrete rod configuration $q = (q_1 \dots q_N) \in \mathcal{S}(Q)$ as defined in (7.32) with $q_i = (r_i, R_i) \in Q = \mathbb{R}^3 \times \mathrm{SO}(3)$, both the position vectors and the director frames are associated with (are functions defined on) the vertices and we call this the vertex-based approach (Figure 7.4). The discrete strain measures $\mathbf{u}_i, \mathbf{v}_i$ can take the form given in (7.42) and (7.43) and represent the strains in the edge e_i. Consequently, their dual quantities $m_i^{\pm}, n_i$ live on $*e_i$. Since the discrete Euler-Lagrange equations (7.33) involve derivatives of the discrete energy with respect to the primal quantities q_i living on v_i, they state an equilibrium condition on $*v_i$. Table 7.2 summarises the relevant quantities and their domains. Boundary conditions can be defined in a straightforward way in the vertex-based formulation by requiring e.g. q_1 and q_N to be equal to prescribed configurations.

Edge-based rod In their work, Bergou et al. [Berg 08] construct a discrete, inextensible Kirchhoff rod model, where the directors are associated with the edges. From the viewpoint of discrete differential geometry, this approach is more natural, as the definition of vertex tangents is ambiguous. We show that our formulation of discrete rods can

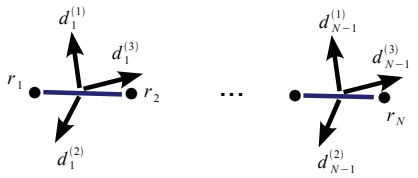

Figure 7.5: Edge-based rod.

easily be adapted to the edge-based concept. Thereby we also generalise the kinematical model of a discrete framed curve to the case of non-adapted frames. The position vectors $(r_1 \dots r_N)$ are again associated with the vertices whereas the director frames $(R_1 \dots R_{N-1})$ are associated with the edges (Figure 7.5). Thus, the i-th rod segment is specified by the position vectors r_i, r_{i+1} and the director frame R_i. Here, axial strains $\mathbf{v}_i$ are associated with the edges e_i while $\mathbf{u}_i$ represents the angular strains on the vertex v_i. This affects the approximation of the total deformation energy as follows

$$\overline{W} = \sum_{i=2}^{N-1} W^{\mathrm{u,int}}(\mathbf{u}_i)\, h_i^{(v)} + \sum_{i=1}^{N-1} W^{\mathrm{v,int}}(\mathbf{v}_i)\, h_i^{(e)}$$

where $h_i^{(e)}$ measures the length of e_i as in the vertex-based case and $h_i^{(v)}$ measures length of $*v_i$. The obvious edge-based analogue of (7.43) is given by

$$\mathbf{v}_i = \frac{1}{h_i^{(e)}} R_i^T (r_{i+1} - r_i), \qquad i = 1 \dots N-1. \tag{7.48}$$

Note that unlike in the vertex-based case, no interpolation of the frame variables is required for edge-based rods. We adapt the angular strains from (7.42)

$$\hat{\mathbf{u}}_i = \frac{1}{h_i^{(v)}} \frac{2}{1 + \mathrm{trace}(R_{i-1}^T R_i)} (R_{i-1}^T R_i - R_i^T R_{i-1}), \qquad i = 2 \dots N-1. \tag{7.49}$$

Note that our definition of edge-based frames (see Fig. 7.5) requires to shift indices backwards by one. Being dual to the angular strains, the bending and torsional moments $m_i^{\pm}$ live on $*v_i$, while the shear and stretch forces n_i are defined on $*e_i$ due to their duality to the axial strains. Consequently, the discrete Euler-Lagrange equations state equilibrium of forces on $*v_i$ and equilibrium of moments on $*e_i$, as summarised in Table 7.2. Special attention has to be given to boundary conditions specifying the orientation of the beam's ends. A naive approach would be to prescribe R_1 and R_{N-1}. However, this might lead to unnaturally large deformation between the first and the second, or the prelast and last beam element, respectively. Alternatively, the orientation of dummy-directors R_0, R_N sitting on the end-nodes v_1, v_N, respectively, can be prescribed. The contribution of the corresponding strains $\mathbf{u}_1, \mathbf{u}_N$ to the deformation energy involves the shorter interval lengths $h_1^{(v)}, h_N^{(v)}$. For both the vertex- and the edge-based rod, it is possible to associate the configuration variables, strains, forces and moments in a meaningful way with primal or dual mesh elements. This is done in Table 7.2. In the case of an edge-based discreti-

	vertex-based model	edge-based model
vertices (v_i)	$q_i = (r_i, R_i)$	r_i, $\mathbf{u}_i$
edges (e_i)	$\mathbf{u}_i, \mathbf{v}_i$	R_i, $\mathbf{v}_i$
dual vertices ($*v_i$)	f_i, l_i, DEL equations	$m_i^{\pm}$, f_i, DEL equations ($\frac{\partial}{\partial r_i}$-part)
dual edges ($*e_i$)	$m_i^{\pm}, n_i$	n_i, l_i, DEL equations ($\frac{\partial}{\partial d_i^{(k)}}$-part)

Table 7.2: Primal and dual rod variables.

sation, one has to take care of the more complicated, staggered grid structure. However, all steps of the variational error analysis can be carried out along the same lines as in the vertex based case, with the same results concerning consistency and convergence order.

7.7 Examples

7.7.1 Fully clamped three-dimensional rod

In the following, we treat a boundary value problem, where both ends of a straight rod are clamped. The main focus is on the spatial momentum maps and on convergence properties. We choose boundary data that result in a non-trivial deformation which exhibits non-zero twist, extension, flexure and shear:

$$\begin{aligned} r_c = \begin{bmatrix} 0 \\ -0.4 \\ 0 \end{bmatrix}, \quad r_f = \begin{bmatrix} 0 \\ 0.4 \\ 0 \end{bmatrix}, \quad d_c^{(3)} = d_f^{(3)} = \begin{bmatrix} -0.18070 \\ 0.89768 \\ 0.40187 \end{bmatrix} \\ d_c^{(1)} = -d_f^{(2)} = \begin{bmatrix} 0.21093 \\ -0.36372 \\ 0.90731 \end{bmatrix}, \quad d_c^{(2)} = d_f^{(1)} = \begin{bmatrix} 0.96065 \\ 0.24872 \\ -0.12363 \end{bmatrix} \end{aligned} \tag{7.50}$$

Practically any boundary data would work here because the actual shape of the deformation has no influence on the fact that momentum maps are conserved.
We first implement the model given by (7.42), (7.43) and (7.44) (i.e. the vertex-based model) involving diagonal stiffness matrices $C_1 = \mathrm{diag}(EI, EI, GJ)$, $C_2 = \mathrm{diag}(GA, GA, EA)$ and $\mathbf{u}^0 = (0,0,0)^T$, $\mathbf{v}^0 = (0,0,1)^T$, corresponding to an initially straight rod. The stiffness parameters are $EI = 1$, $GJ = 1$, $GA = 200$ and $EA = 200$. The rod of length $L = 1$ is equidistantly discretised into $N = 11$ material points; thus $h_i = 0.1$ for all i.
We compute the deformed configuration by solving the system (7.33) using a Gauss-Newton iteration (Matlab-function `fsolve`) and a finite-difference approximation of the Jacobi-matrix. The tolerance of the algorithm is set to 10^{-8}. The initial guess is simply a spline generated from the boundary data.
Figure 7.2 depicts the deformed configuration with the director frame at each node. The discrete forces $\mathbf{n}_i$ and moments $\mathbf{m}_i$ are shown in Figure 7.6. Since the stiffness matrices are diagonal, each component is associated to a specific component of strain. For example

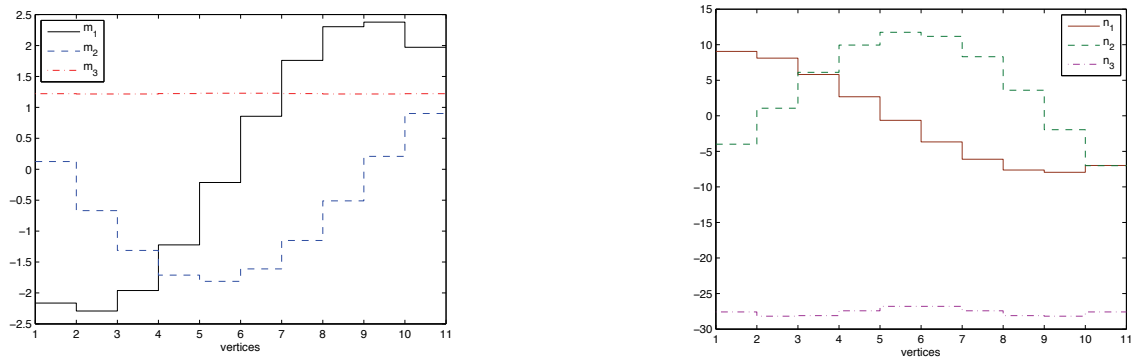

(a) (b)

Figure 7.6: (a) The three components $((\mathbf{m}_i)_1, (\mathbf{m}_i)_2, (\mathbf{m}_i)_3)$ of the stress-resultant moment in the material description, $(\mathbf{m}_i)_1$ and $(\mathbf{m}_i)_2$ being the bending moments, and $(\mathbf{m}_i)_3$ being the torsional moment. (b) The three components $((\mathbf{n}_i)_1, (\mathbf{n}_2), (\mathbf{n}_3))$ of the stress-resultant force in the material description, $(\mathbf{n}_i)_1$ and $(\mathbf{n}_i)_2$ being the shear-force and $(\mathbf{n}_i)_3$ being the stretch-force.

$(\mathbf{m}_i)_3$ is the twist moment. Note that in the discrete setting, $(\mathbf{m}_i)_3$ is not a momentum map, although it is 'almost' conserved, as we can see from Figure 7.6 (a). Figure 7.7 (a) shows the momentum maps associated with frame-indifference and isotropy (see Table 7.1). The momentum maps are constant up to a deviation of magnitude 10^{-6} to 10^{-7} as seen in Figure 7.7 (b). This number reflects the precision of the iteration algorithm. The components of the stress-resultant moment m_i^- in the spatial description are depicted in Figure 7.7 (c).

We analyse the convergence properties of discrete rod models and compare the two different approaches presented in Section 6.2 using the boundary value problem above. A fine discretisation with $N = 321$ material points is assumed to be sufficiently precise to serve as reference solution. We consider convergence of the discrete spacecurve $(r_1 \dots r_N)$ to the reference curve. Here, distances are measured with respect to the norm $\max\{\|r_i - r_i^{ref}\|_2, i = 1 \dots N\}$. In addition, convergence of the director field is analysed, distances being measured with respect to the norm $\max\{\|R_i - R_i^{ref}\|_F, i = 1 \dots N\}$ (and $i = 1 \dots N-1$ in the edge-based approach) using the Frobenius norm $\|\cdot\|_F$. The error plots obtained from the two-point boundary value problem (7.50) with $h \in \{\frac{1}{4}, \frac{1}{10}, \frac{1}{40}, \frac{1}{80}\}$ are shown in Figure 7.8. Both models converge quadratically to the same configuration as we have analytically determined in Section 7.6.2. Furthermore, we observe that the approximation properties of the edge-based model are slightly better, supposedly, because it does not employ a non-orthogonal SO(3)-interpolation.

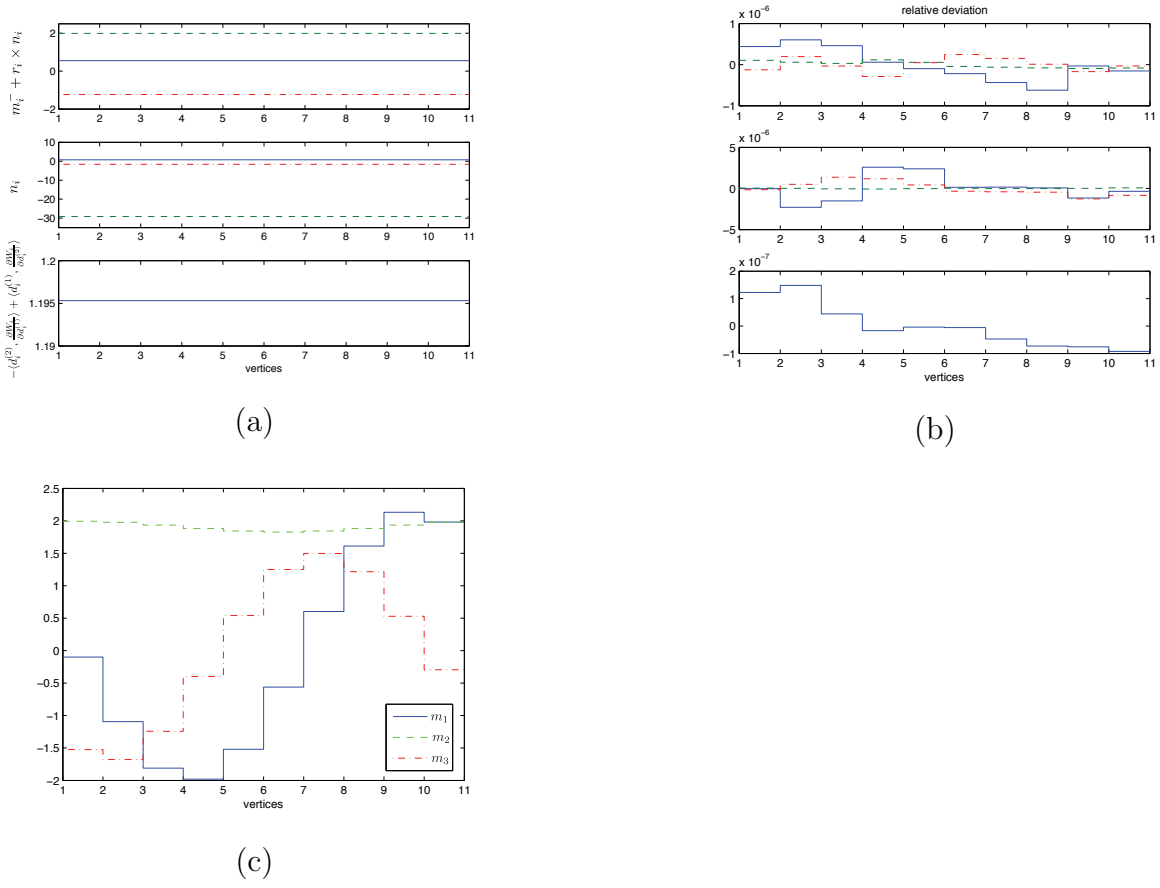

(a) (b) (c)

Figure 7.7: (a) The three momentum maps listed in Table 7.1. Top: $m_i^- + r_i \times n_i$. Middle: n_i. Bottom: $-\langle d_i^{(2)}, \frac{\partial W_i}{\partial d_i^{(1)}} \rangle + \langle d_i^{(1)}, \frac{\partial W_i}{\partial d_i^{(2)}} \rangle$. In each plot: blue = first component, green = second component, red = third component. (b) The relative deviation in the momentum maps, componentwise. (c) The components of the stress-resultant moment m_i^- in the spatial description.

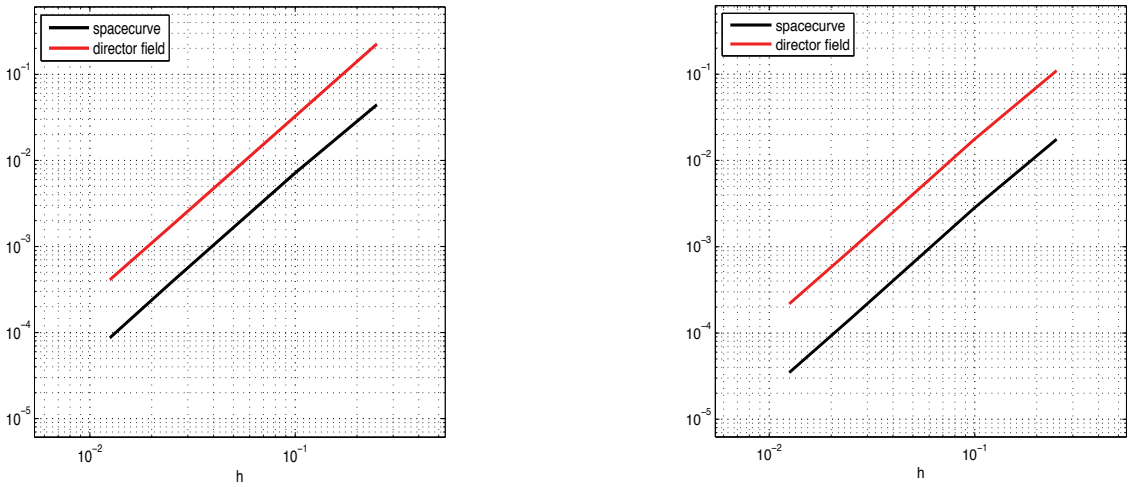

(a) (b)

Figure 7.8: Convergence analysis. (a) Vertex-based model. (b) Edge-based model.

7.7.2 Two-dimensional hinged frame

We consider the two-dimensional example of a hinged frame. An L-shaped extensible and shearable rod is attached at both endpoints such that the tangents are able to move freely (moment free support). This example has previously been discussed in the articles [Bets 02b, Simo 86] and all data are taken from there. The length of each leg is $\frac{1}{2}L = 120$ and the stiffness parameters are $GA = 16.62 \cdot 10^6$, $EA = 43.2 \cdot 10^6$, $EI = 14.4 \cdot 10^6$ and $GJ = 11.08 \cdot 10^6$. A vertical force $f = 10^3 \cdot (0, -\lambda)^T$ is applied at position 96 measured from the right upper end.
Here, the edge-based approach is used. As the problem is only two-dimensional, there are two translational degrees of freedom per node and only one rotational degree of freedom specifying the orientation of an edge. We employ the following reparametrisation

$$\begin{bmatrix} x \\ y \end{bmatrix} \mapsto r = \begin{bmatrix} x \\ y \\ 0 \end{bmatrix}$$

$$\alpha \mapsto R = \begin{bmatrix} 0 & \sin(\alpha) & \cos(\alpha) \\ 0 & -\cos(\alpha) & \sin(\alpha) \\ 1 & 0 & 0 \end{bmatrix}$$

and solve for $x_1 \dots x_N, y_1 \dots y_N, \alpha_1 \dots \alpha_{N-1}$. Note however, that the three-dimensional strains (7.42) and (7.48) are used to derive the discrete equilibrium equations. This buckling problem has multiple equilibria, the two stable equilibria are indicated in Figure 7.9 (a) by the dashed line. The equilibria can be used to create clever (deformed) initial configurations from which the configurations corresponding to the load-level parameters $\lambda_1 = 15$, $\lambda_2 = 18.495$, $\lambda_3 = -9.233$ and $\lambda_4 = 21.014$, depicted in Figure 7.9 (a), can be obtained directly by solving the discrete equilibrium equations iteratively (again Gauss-Newton iteration in the Matlab-function `fsolve` has been used). We compare the results from our discrete mechanics model using $N = 21$ vertices to those obtained by Betsch and Steinmann [Bets 02b] with ten quadratic finite elements and observe small differences in the configurations with high deformation which are probably due to the different factor used in the strains (7.42) and of course due to the different types of discretisation.
To compute the complete load-displacement curve for the node under load (see Figure 7.10), a standard arc length method described e.g. in [Cris 91] has been employed. Comparing the curve to that obtained in [Bets 02b] shows an overall good qualitative agreement and a very good agreement in the range of small displacements, see Remark 7.6.3 for an analysis of the different discrete strain measures in use.
The resulting material forces and moments are depicted in Figure 7.11. Due to the presence of loading, the problem is not frame-indifferent. However, the change in the discrete momentum maps in Figure 7.12 exactly represents the applied loading (up to the numerical tolerance used to solve the equilibrium equations). Note that this is guaranteed by the discrete mechanics approach independent of the number of nodes in the discrete grid.

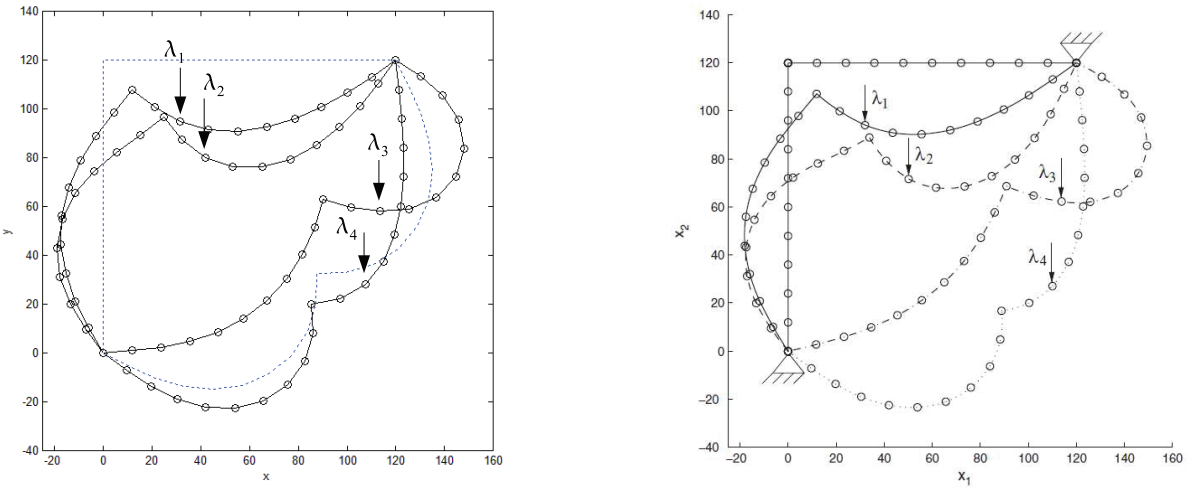

(a) (b)

Figure 7.9: (a) Deformation of the hinged L-frame corresponding to the load-level parameters $\lambda_1 = 15$, $\lambda_2 = 18.495$, $\lambda_3 = -9.233$ and $\lambda_4 = 21.014$. (b) The results obtained by Betsch and Steinmann [Bets 02b].

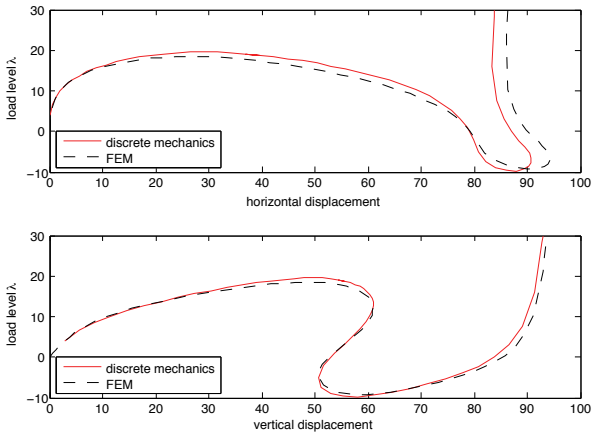

Figure 7.10: Load-displacement curve of the hinged L-frame.

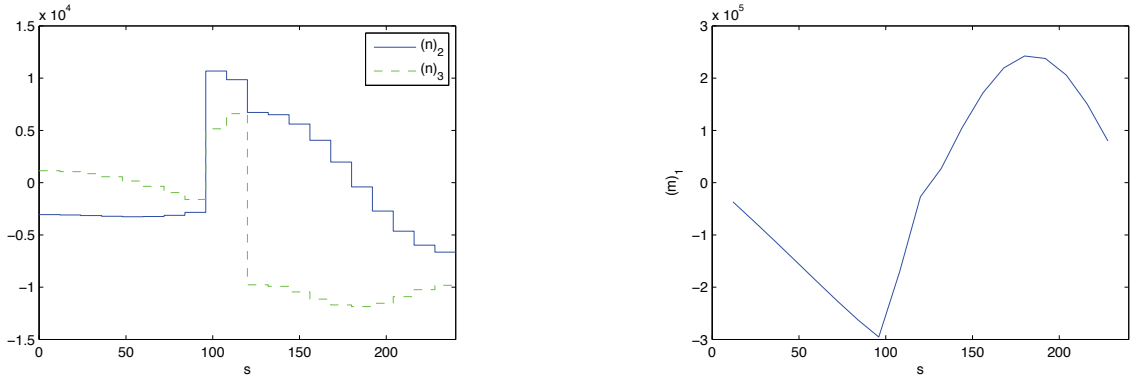

(a) (b)

Figure 7.11: (a) The discrete forces $\mathbf{n}_i$. (b) The discrete moments $\mathbf{m}_i$.

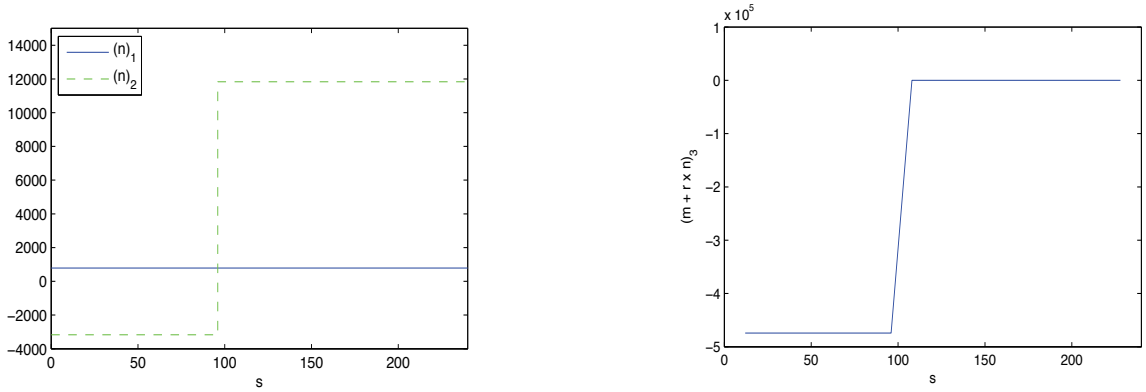

(a) (b)

Figure 7.12: The discrete momentum maps do change exactly according to the applied load.

7.8 Summary and conclusions

We have formulated a theory of discrete Cosserat rods that is analogous to discrete Lagrangian mechanics by exploiting Kirchhoff's kinetic analogy. In this analogy, the arc length along the rod plays the role of time in Lagrangian mechanics. The resulting theory of discrete Cosserat rods is a self-contained theory with a structure and scope identical to that of the classical theory of rods but where the arc length is a discrete variable ab initio. In particular, the discrete equilibrium equations are Euler-Lagrange equations and their structure is a consequence of frame-indifference. A discrete version of Noether's theorem identifies exact first integrals of the discrete equilibrium equations from the symmetries of the system. The symmetries relevant for rod mechanics are frame-indifference, isotropy and uniformity. The discrete Noether's theorem provides a constructive tool and a complete mathematical theory to identify the arc length wise first integrals of the equilibrium equations. This constructive tool is especially useful in the discrete setting where precise expressions for the forces and moments are not always evident. Numerical experiments based on a particular choice of discrete strain measures bear out the exact conservation of discrete momentum maps, exhibit a quadratic rate of convergence and illustrate the versatility of the approach, e.g. as regards the implementation of general material models, boundary conditions, as well as the handling of finite kinematics.
We close by pointing out limitations of the approach and opportunities for further development. As in the case of Lagrangian mechanics, the variational structure of the discrete theory and its exact conservation properties are no guarantee of good numerical performance, including accuracy and convergence. In practice, great care must be exercised in choosing a particular discrete energy density in order to ensure good numerical performance, which must be carefully assessed independently of geometrical considerations by means of standard tools of analysis. Specifically, the convergence properties of the discrete theory must be carefully established either by analytical tools or by way of numerical testing. A natural and straightforward extension of the theory to dynamics may be accomplished within the framework of multi-symplectic integrators [Lew 03a].

8 Structure preserving optimal control of three-dimensional compass gait

8.1 Introduction

When planning or predicting motion of multibody systems, one can pursue quite different strategies. One possibility is to rely purely on kinematic considerations. One can capture motion with a camera or simply prescribe certain desired poses for the motion. This information can be used as input for inverse kinematics, where a trajectory, meeting the prescribed conditions is reconstructed. However, thereby no forcing or dynamics is taken into account. If one is interested in the forces that cause real dynamics, then one is faced with a control problem. In this paper we consider the problem of determining an optimal controller that produces a walking gait for a three-dimensional compass biped model. This control task has been previously addressed with various biped models in the literature, for instance in [Chev 01, Rous 98]. However, this work is unique in the use of the DMOCC dynamic optimisation method, see Chapter 5 (see also [Leye 09b]), which exploits the geometric structure (see [Bull 98]) and variational dynamics of the biped model (see [Peka 08]) and yields a structure preserving simulation. DMOCC is a constrained version of the previously developed method called discrete mechanics and optimal control DMOC, see [Jung 05a, Ober 08, Ober 10].

The term structure preserving means that the approximate solution, i.e. the discrete trajectory, inherits certain characteristic properties of the continuous motion. For example, the evolution of the system's momentum maps (e.g. angular momentum is a momentum map for the biped) exactly represents externally applied forces, in particular they are conserved along the approximate motion of unforced systems. In addition to momentum maps, the symplectic structure underlying real dynamics is respected by certain mechanical integrators, and as a consequence, they also yield good energy behaviour, see e.g. [Mars 01, Hair 04]. Besides improving the fidelity of the approximate solution compared to standard methods, the preservation of these quantities stabilises the numerical integration and thus enables longterm simulation.

In contrast to many other works taking a rotation-based approach in minimal coordinates to multibody systems, (see e.g. [Schi 90,Gera 01]), here, the multibody system is described in terms of redundant coordinates subject to holonomic constraints. On the one hand, difficulties and in particular singularities associated with rotational parameters are circumvented in this way. On the other hand, the formulation of complex three-dimensional multibody systems is easily possible in a straight forward and intuitive way. The resulting equations of motion assume the form of index three DAEs for which structure preserving integration methods are well developed, see [Gonz 99, Wend 97]. Disadvantages like the large dimension and possible ill-conditioning of the resulting discrete nonlinear system due to the presence of the Lagrange multipliers can be remedied by using the discrete null space

method that eliminates the constraint forces. Details on the discrete null space method in the context of forward dynamic integration can be found in [Bets 05, Bets 06, Leye 08b]. An extension to the optimal control of multibody systems can be found in Chapter 5 (see also [Leye 09b]) on which this work here is relying heavily. However, no contact between bodies is considered there. In the context of the walker, the change between the stance and the swing leg during the double stance configuration imposes additional challenges, wherefore in this paper, the variational formulation of [Fete 03] is developed further to describe this transfer of contacts. While the variational theory for nonsmooth systems is just mentioned briefly in this paper, details can be found in [Peka 10].

Section 8.2 introduces the biped model and gives details on the constrained multibody formulation. The continuous optimal control problem for the walker is formulated in Section 8.3, while the corresponding problem in discrete time is described in Section 8.4. Finally, computational results are demonstrated in Section 8.5.

8.2 Compass gait walker model

In this work, a relatively simple model is used to illustrate the performance of the developed structure preserving numerical simulation method. The three-dimensional compass biped is modelled as a spherical kinematic pair in which the rigid legs are combined at the hip by a spherical joint, see Figure 8.1. A point mass in the hip represents the weight of the upper part of the body.

The contact between a foot and the ground is modelled as a perfectly plastic impact, constraining the foot to stay fixed on the ground during the other leg's swing phase. The contact is transferred instantaneously when the second foot hits the ground and the first one is released. During a swing phase, the walker has six degrees of freedom. However, only a three-dimensional torque acts in the hip joint yielding an underactuated system.

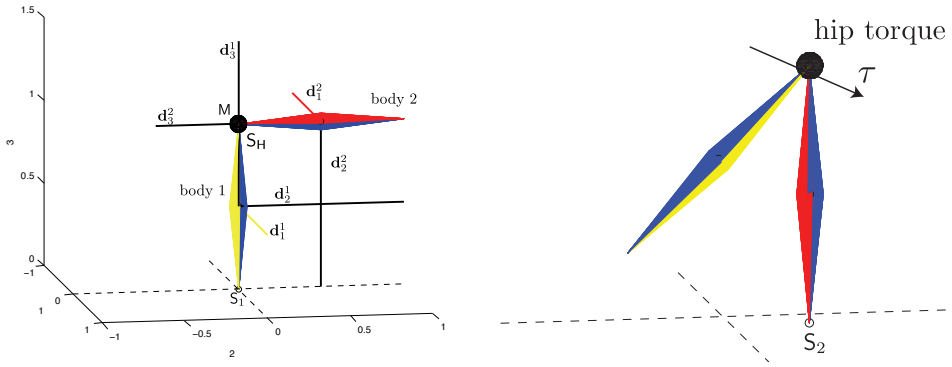

Figure 8.1: Compass biped model with directors (left) and with actuating torque in the hip joint (right).

8.2.1 Multibody configuration

A constrained formulation is used for dynamics of the complete multibody system as well as for a single rigid body (see e.g. [Antm 95, Bets 01b, Bets 06]). The $n = 27$-dimensional time dependent configuration variable of the walker $\boldsymbol{q}(t) \in Q = \mathbb{R}^{27}$ in the time interval $[t_0, t_N] \subset \mathbb{R}$ consists of the configurations of the two rigid bodies $\boldsymbol{q}^1$ and $\boldsymbol{q}^2$ and the placement $\boldsymbol{q}^M \in \mathbb{R}^3$ of the point mass M^M in the hip. It reads

$$\boldsymbol{q}(t) = \begin{bmatrix} \boldsymbol{q}^1(t) \\ \boldsymbol{q}^2(t) \\ \boldsymbol{q}^M(t) \end{bmatrix} \quad \text{with} \quad \boldsymbol{q}^\alpha(t) = \begin{bmatrix} \boldsymbol{\varphi}^\alpha(t) \\ \boldsymbol{d}_1^\alpha(t) \\ \boldsymbol{d}_2^\alpha(t) \\ \boldsymbol{d}_3^\alpha(t) \end{bmatrix} \quad \alpha = 1, 2$$

where $\boldsymbol{\varphi}^\alpha \in \mathbb{R}^3$ denotes the placement of the centre of mass and the directors $\boldsymbol{d}_I^\alpha \in \mathbb{R}^3, I = 1, 2, 3$ represent the orientation of the α-th body. Each director triad is constrained to stay orthonormal during the motion, see Figure 3.7.
The α-th body's Euler tensor with respect to the centre of mass can be related to the inertia tensor $\boldsymbol{J}^\alpha$ via $\boldsymbol{E}^\alpha = \frac{1}{2}(\mathrm{tr}\boldsymbol{J}^\alpha)\boldsymbol{I} - \boldsymbol{J}^\alpha$, where $\boldsymbol{I}$ denotes the 3×3 identity matrix. The principal values of the Euler tensor E_i^α together with the body's total mass M_φ^α are ingredients in the α-th rigid body's mass matrix. The constant symmetric positive definite mass matrix of the multibody system reads

$$\boldsymbol{M} = \mathrm{diag}(M_\varphi^1\boldsymbol{I} \quad E_1^1\boldsymbol{I} \quad E_2^1\boldsymbol{I} \quad E_3^1\boldsymbol{I} \quad M_\varphi^2\boldsymbol{I} \quad E_1^2\boldsymbol{I} \quad E_2^2\boldsymbol{I} \quad E_3^2\boldsymbol{I} \quad M^M\boldsymbol{I}).$$

8.2.2 Constraints

Rigidity of the two bodies gives rise to orthonormality constraints for the two director triads, thus there are $m_{int} = 12$ internal constraints.

$$\boldsymbol{g}_{int}(\boldsymbol{q}) = \begin{bmatrix} \boldsymbol{g}_{int}^1(\boldsymbol{q}) \\ \boldsymbol{g}_{int}^2(\boldsymbol{q}) \end{bmatrix} \quad \text{with} \quad \boldsymbol{g}_{int}^\alpha(\boldsymbol{q}^\alpha) = \frac{1}{2}\left((\boldsymbol{d}_j^\alpha)^T \cdot \boldsymbol{d}_k^\alpha - \delta_{jk}\right) = 0 \quad j, k = 1, 2, 3 \quad \alpha = 1, 2$$

During the second leg's swing phase, the first foot is fixed on the ground in x_{S_1} by a spherical joint S_1, see Figure 8.1. The corresponding constraint reads $\boldsymbol{g}_{S_1}(\boldsymbol{q}) = \boldsymbol{0}$. Furthermore, the spherical joint S_H connects the two legs in the hip via $\boldsymbol{g}_{S_H}(\boldsymbol{q}) = \boldsymbol{0}$ and the point mass is held in place by the condition $\boldsymbol{g}_M(\boldsymbol{q}) = \boldsymbol{0}$, thus the total number of external constraints is $m_{ext} = 9$.
It is assumed that a perfectly plastic impact with no sliding takes place, (see e.g. [Hurm 93]), when the second foot hits the ground, i.e. after hitting the contact surface in x_{S_2}, the foot is fully immobilised by the constraint $\boldsymbol{g}_{S_2}(\boldsymbol{q}) = \boldsymbol{0}$. Depending on the actual phase of the gait, the relevant constraints are collected in the $m = 21$-dimensional constraint function vector $\boldsymbol{g}_1$ or $\boldsymbol{g}_2$ given by

$$\boldsymbol{g}_1(\boldsymbol{q}) = \begin{bmatrix} \boldsymbol{g}_{int}(\boldsymbol{q}) \\ \boldsymbol{g}_{S_1}(\boldsymbol{q}) \\ \boldsymbol{g}_{S_H}(\boldsymbol{q}) \\ \boldsymbol{g}_M(\boldsymbol{q}) \end{bmatrix} \quad \text{or} \quad \boldsymbol{g}_2(\boldsymbol{q}) = \begin{bmatrix} \boldsymbol{g}_{int}(\boldsymbol{q}) \\ \boldsymbol{g}_{S_2}(\boldsymbol{q}) \\ \boldsymbol{g}_{S_H}(\boldsymbol{q}) \\ \boldsymbol{g}_M(\boldsymbol{q}) \end{bmatrix} \quad \text{with} \quad \begin{aligned} \boldsymbol{g}_{S_1}(\boldsymbol{q}) &= \boldsymbol{\varphi}^1 + \boldsymbol{\varrho}_{S_1}^1 - \boldsymbol{x}_{S_1} \\ \boldsymbol{g}_{S_2}(\boldsymbol{q}) &= \boldsymbol{\varphi}^2 + \boldsymbol{\varrho}_{S_2}^2 - \boldsymbol{x}_{S_2} \\ \boldsymbol{g}_{S_H}(\boldsymbol{q}) &= \boldsymbol{\varphi}^1 + \boldsymbol{\varrho}_{S_H}^1 - \boldsymbol{\varphi}^2 - \boldsymbol{\varrho}_{S_H}^2 \\ \boldsymbol{g}_M(\boldsymbol{q}) &= \boldsymbol{q}^M - \boldsymbol{\varrho}_{S_H}^1 - \boldsymbol{\varphi}^1 \end{aligned}$$

where the vectors $\boldsymbol{\varrho}_J^\alpha = (\varrho_J^\alpha)_I \boldsymbol{d}_I^\alpha$ point from the centre of mass of the α-th body to the specific joint $J \in \{S_1, S_2, S_H\}$.

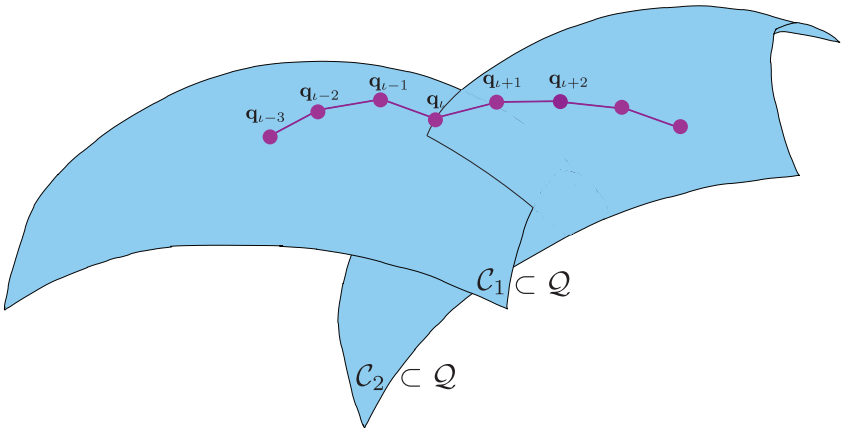

Figure 8.2: When the second foot hits the ground, the first foot is released, thus the system instantaneously leaves C_1 and enters C_2.

8.2.3 Transfer of contact

It is important to note that the placement of the second foot on the ground is not known a priori. The (scalar) contact condition for the second foot reads $g_c(\boldsymbol{q}) = (\boldsymbol{\varphi}^2 + \boldsymbol{\varrho}_{S_2}^2) \cdot \boldsymbol{e}_3 = 0$. In the instant the contact takes place, the point of contact $\boldsymbol{x}_{S_2}$ is determined which then defines the constraint function $\boldsymbol{g}_{S_2}$. The corresponding constraint manifolds are defined as $C_1 = \{\boldsymbol{q} \in \mathbb{R}^{27} | \boldsymbol{g}_1(\boldsymbol{q}) = \boldsymbol{0}\}$ and $C_2 = \{\boldsymbol{q} \in \mathbb{R}^{27} | \boldsymbol{g}_2(\boldsymbol{q}) = \boldsymbol{0}\}$, respectively. The transfer of contact is illustrated for the discrete trajectory in Figure 8.2.

In general, contact conditions are unilateral constraints. When modelling the transfer of contact as the concurrent release of the bilateral constraint $\boldsymbol{g}_1$ and the establishing of the new bilateral constraint $\boldsymbol{g}_2$, one has to verify for the resulting motion that the constraint forces point into the ground, thus they prevent the foot from penetrating the ground and do never prevent the lifting of the foot. Furthermore, the velocity of the previous point of contact (the just released previous stance foot) must have a positive component normal to the contact surface.

8.2.4 Null space matrix and nodal reparametrisation

In DMOCC, the system of discrete equations of motion (being subject to the kinematic constraints described in Section 8.2.2) serves as constraints for the optimisation. To reduce the system's dimension to the minimal possible number, the discrete null space method is used, see [Leye 08b, Leye 09b]. For each swing phase, the null space matrix and nodal reparametrisation used later in Section 8.4.1 are given here.

The $n \times (n-m)$ null space matrices $\boldsymbol{P}_1(\boldsymbol{q}) : \mathbb{R}^{n-m} \to T_{\boldsymbol{q}} C_1$ and $\boldsymbol{P}_2(\boldsymbol{q}) : \mathbb{R}^{n-m} \to T_{\boldsymbol{q}} C_2$

mapping to the tangent space of the constraint manifold in the specific gait phase read

$$\boldsymbol{P}_1(\boldsymbol{q}) = \begin{bmatrix} \widehat{\boldsymbol{\varrho}^1_{S_1}} & \mathbf{0} \\ -\widehat{\boldsymbol{d}^1_1} & \mathbf{0} \\ -\widehat{\boldsymbol{d}^1_2} & \mathbf{0} \\ -\widehat{\boldsymbol{d}^1_3} & \mathbf{0} \\ \widehat{\boldsymbol{\varrho}^1_{S_1} - \boldsymbol{\varrho}^1_{S_H}} & \widehat{\boldsymbol{\varrho}^2_{S_H}} \\ \mathbf{0} & -\widehat{\boldsymbol{d}^2_1} \\ \mathbf{0} & -\widehat{\boldsymbol{d}^2_2} \\ \mathbf{0} & -\widehat{\boldsymbol{d}^2_3} \\ \widehat{\boldsymbol{\varrho}^1_{S_1} - \boldsymbol{\varrho}^1_H} & \mathbf{0} \end{bmatrix}, \qquad \boldsymbol{P}_2(\boldsymbol{q}) = \begin{bmatrix} \widehat{\boldsymbol{\varrho}^1_{S_H}} & \widehat{\boldsymbol{\varrho}^2_{S_2} - \boldsymbol{\varrho}^2_{S_H}} \\ -\widehat{\boldsymbol{d}^1_1} & \mathbf{0} \\ -\widehat{\boldsymbol{d}^1_2} & \mathbf{0} \\ -\widehat{\boldsymbol{d}^1_3} & \mathbf{0} \\ \mathbf{0} & \widehat{\boldsymbol{\varrho}^2_{S_2}} \\ \mathbf{0} & -\widehat{\boldsymbol{d}^2_1} \\ \mathbf{0} & -\widehat{\boldsymbol{d}^2_2} \\ \mathbf{0} & -\widehat{\boldsymbol{d}^2_3} \\ \mathbf{0} & \widehat{\boldsymbol{\varrho}^2_{S_2} - \boldsymbol{\varrho}^2_{S_H}} \end{bmatrix}$$

The matrix $\boldsymbol{Q}(\boldsymbol{q}) : \mathbb{R}^n \to \eta(T^*_{\boldsymbol{q}}C)$ projects onto the embedding of $T^*_{\boldsymbol{q}}C$ in $\mathbb{R}^n$ and is canonical for regular Lagrangians. It is given by

$$\boldsymbol{Q}(\boldsymbol{q}) = \boldsymbol{I}_{n\times n} - \boldsymbol{G}^T \cdot \left[\boldsymbol{G} \cdot \boldsymbol{M} \cdot \boldsymbol{G}^T\right]^{-1} \cdot \boldsymbol{G} \cdot \boldsymbol{M}^{-1}$$

An equidistant time grid $\{t_0, t_0 + h, \ldots, t_0 + Nh = t_N\}$ is defined using the constant time step $h \in \mathbb{R}$ and the discrete approximation to the configuration at a time node reads $\boldsymbol{q}_n \approx \boldsymbol{q}(t_n)$. The discrete generalised coordinates $\boldsymbol{u}_{n+1} = \begin{bmatrix} \theta^1_{n+1} \\ \theta^2_{n+1} \end{bmatrix}$ consist of the incremental rotation vectors $\theta^1_{n+1}, \theta^2_{n+1} \in \mathbb{R}^3$ for the two bodies. With the corresponding rotation matrices obtained via the exponential map $\exp : so(3) \to SO(3)$, the nodal reparametrisations $\boldsymbol{q}_{n+1} = \boldsymbol{F}_1(\boldsymbol{u}_{n+1}, \boldsymbol{q}_n) \in C_1$ and $\boldsymbol{q}_{n+1} = \boldsymbol{F}_2(\boldsymbol{u}_{n+1}, \boldsymbol{q}_n) \in C_2$ in the specific gait phases read

$$\begin{aligned} (\boldsymbol{d}^\alpha_I)_{n+1} &= \exp\left(\widehat{\theta^\alpha_{n+1}}\right) \cdot (\boldsymbol{d}^\alpha_I)_n \qquad I = 1,2,3 \quad \alpha = 1,2 \\ \boldsymbol{\varphi}^\alpha_{n+1} &= x_{S_\alpha} - (\boldsymbol{\varrho}^\alpha_{S_\alpha})_{n+1} \\ \boldsymbol{\varphi}^\beta_{n+1} &= \boldsymbol{\varphi}^\alpha_{n+1} + (\boldsymbol{\varrho}^\alpha_H)_{n+1} - (\boldsymbol{\varrho}^\beta_H)_{n+1} \\ \boldsymbol{q}^M_{n+1} &= \boldsymbol{\varphi}^1_{n+1} + (\boldsymbol{\varrho}^1_H)_{n+1} \end{aligned}$$

In the last three equations, corresponding to $\boldsymbol{g}_1$ during stance phase of first foot, $(\alpha, \beta) = (1, 2)$. During the second stance phase, which is characterised by $\boldsymbol{g}_2$, $(\alpha, \beta) = (2, 1)$ holds.

8.2.5 Actuation

Although the system has six degrees of freedom, only a three-dimensional torque $\boldsymbol{\tau} \in \mathbb{R}^3$ acts in the hip joint, thus the system is underactuated. The generalised forces $\boldsymbol{\tau}$ are mapped to the redundant control force $\boldsymbol{f} \in \mathbb{R}^n$ (since the optimal control problem in Section 8.3 is formulated in terms of the n-dimensional redundant configuration and

control force) via the input transformation matrix

$$\boldsymbol{B} = \frac{1}{2}\begin{bmatrix} \mathbf{0} & -\widehat{\boldsymbol{d}_1^1} & -\widehat{\boldsymbol{d}_2^1} & -\widehat{\boldsymbol{d}_3^1} & \mathbf{0} & \widehat{\boldsymbol{d}_1^2} & \widehat{\boldsymbol{d}_2^2} & \widehat{\boldsymbol{d}_3^2} & \mathbf{0} \end{bmatrix}$$

To ensure regularity of the constrained optimisation problem in DMOCC, the discrete generalised forces $\boldsymbol{\tau}_n$ are defined in the interval $[t_n, t_{n+1}]$, then their effect is transformed to the nodes via $\boldsymbol{\tau}_{n-1}^+ = \frac{h}{2}\boldsymbol{\tau}_{n-1}$ and $\boldsymbol{\tau}_n^+ = \frac{h}{2}\boldsymbol{\tau}_n$ and finally the redundant forces at t_n are given by

$$\boldsymbol{f}_{n-1}^+ = \boldsymbol{B}^T(\boldsymbol{q}_n) \cdot \boldsymbol{\tau}_{n-1}^+, \qquad \boldsymbol{f}_n^- = \boldsymbol{B}^T(\boldsymbol{q}_n) \cdot \boldsymbol{\tau}_n^-$$

8.3 Optimal control of the walker

8.3.1 Objective functional

The objective functional $J(\boldsymbol{q}, \dot{\boldsymbol{q}}, \boldsymbol{f}) = \int_{t_0}^{t_N} C(\boldsymbol{q}, \dot{\boldsymbol{q}}, \boldsymbol{f})\, dt$ is to be minimised with respect to the state trajectory $(\boldsymbol{q}(t), \dot{\boldsymbol{q}}(t))$ and the control trajectory $\boldsymbol{f}(t)$. Motivated by the specific cost of transport used e.g. in [Diun 06], we consider the control effort per step length sl, i.e. $C(\boldsymbol{q}, \dot{\boldsymbol{q}}, \boldsymbol{f}) = \frac{\|\boldsymbol{f}\|}{sl}$ as a cost function. Although the walker is in principle free to move in any direction, the step length is measured as the projection of the distance between the feet in the double stance configuration onto a predefined walking direction, see Figure 8.3.

8.3.2 Boundary conditions

Let $\boldsymbol{q}_\iota$ denote the double stance configuration. It is assumed that the swing phases of the left and right leg of the walker are identical mirror images of each other, see Figure 8.3. Therefore, only half a gait cycle is optimised while the final state is requested to be a mirror image of the initial state that is translated by the step length into the

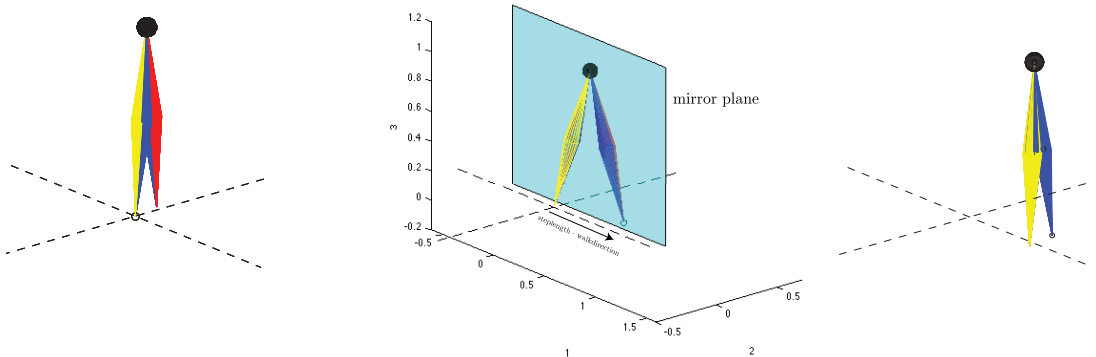

Figure 8.3: Initial and final configuration of half a gait cycle and mirror plane in the double stance configuration

walking direction. For the compass gait biped, this leads to 12 independent conditions. Another three conditions relate the torque in the first and last time interval to each other. These relations are described by the function $\boldsymbol{r}(\boldsymbol{q}_0, \boldsymbol{p}_0, \boldsymbol{q}_\iota, \boldsymbol{q}_N, \boldsymbol{p}_N, \boldsymbol{\tau}_0, \boldsymbol{\tau}_{N-1}) = \boldsymbol{0}$ involving the initial, impact and final configuration and conjugate momenta, respectively. Let $mirr : \mathbb{R}^3 \to \mathbb{R}^3$ denote the mirror function, then one possibility is to require alignment of

- the first leg's directors at t_0, i.e. $(\boldsymbol{d}_I^1)_0$, with the mirror image of the second leg's directors at t_N, i.e. $mirr((\boldsymbol{d}_I^2)_N)$ for $I = 1, 2, 3$ and
- the conjugate momenta $(\boldsymbol{p}_I^1)_0$ with $mirr((\boldsymbol{p}_I^2)_N)$ for $I = 1, 2, 3$ and
- the directors $(\boldsymbol{d}_I^2)_0$ with $mirr((\boldsymbol{d}_I^1)_N)$ for $I = 1, 2, 3$ and
- the conjugate momenta $(\boldsymbol{p}_I^2)_0$ with $mirr((\boldsymbol{p}_I^1)_N)$ for $I = 1, 2, 3$ and
- the torque $\boldsymbol{\tau}_0$ with $mirr(\boldsymbol{\tau}_{N-1})$.

Using the discrete Legendre transformation (8.4), these conditions can be transformed into relations between $\boldsymbol{q}_0$ and $\boldsymbol{q}_{N-1}$ and between $\boldsymbol{q}_1$ and $\boldsymbol{q}_N$, respectively, which simplifies their implementation in the framework of the discrete optimisation problem.
Furthermore, path constraints $h(\boldsymbol{q}) \geq 0$ depending on the geometry of the legs ensure that the walker does not penetrate itself during the gait.

8.3.3 Variational principles

Before and after the impact, the Lagrange-d'Alembert principle for constrained forced dynamics is used to derive the equations of motion from a variational principle. The Lagrangian $L : TQ \to \mathbb{R}$ with $L(\boldsymbol{q}, \dot{\boldsymbol{q}}) = \frac{1}{2}\dot{\boldsymbol{q}} \cdot \boldsymbol{M} \cdot \dot{\boldsymbol{q}} - V(\boldsymbol{q})$ represents the difference of kinetic and potential energy $V(\boldsymbol{q})$. In the case of the walker, the potential energy represents the influence of gravity. The Lagrange multipliers $\lambda_1, \lambda_2 \in \mathbb{R}^m$ correspond to the constraints active during the specific gait phases.
In the presence of a perfectly plastic impact, the dynamics takes place in a nonsmooth setting involving modifications to the path space such that one takes variations over curves with isolated points of diminished smoothness or continuity. In [Peka 10], a nonautonomous variational approach to nonsmooth dynamical problems is elaborated. While mentioning this here only very briefly, we refer to [Peka 10] for details. Essentially, we consider paths $c(s) = (c_t(s), c_q(s))$ in an extended configuration space $[t_0, t_N] \times Q$ parametrised in $s \in [0, 1]$. Now, the time reads $t = c_t(s)$ in $C^\infty([0, 1], [t_0, t_N])$ with strictly positive derivative and the configuration is given by the continuous function $\boldsymbol{q}(t) = c_q(c_t^{-1}(t))$ being (piecewise) twice continuously differentiable (away from the impact) and having a singularity at the impact configuration $\boldsymbol{q}(t_\iota) = c_q(s_\iota)$ due to which the action integral has to be split. With the variation $\delta c(s_\iota) = (\delta c_t(s_\iota), \delta c_q(s_\iota)) \in T_{\boldsymbol{q}_\iota}([t_0, t_N], C_2)$, it reads

$$\begin{aligned} &\delta\left(\int_{t_0}^{t_\iota^-} L(\boldsymbol{q}, \dot{\boldsymbol{q}}) - \boldsymbol{g}_1(\boldsymbol{q}) \cdot \boldsymbol{\lambda}_1 \, dt\right) + \int_{t_0}^{t_\iota^-} \boldsymbol{f} \cdot \delta\boldsymbol{q} \, dt + \boldsymbol{f}_t^c \cdot \delta c_t(s_\iota) + \boldsymbol{f}_q^c \cdot \delta c_q(s_\iota) + \\ &\delta\left(\int_{t_\iota^+}^{t_N} L(\boldsymbol{q}, \dot{\boldsymbol{q}}) - \boldsymbol{g}_2(\boldsymbol{q}) \cdot \boldsymbol{\lambda}_2 \, dt\right) + \int_{t_\iota^+}^{t_N} \boldsymbol{f} \cdot \delta\boldsymbol{q} \, dt = 0 \end{aligned} \tag{8.1}$$

Note that describing the transfer of contact, and in particular the perfectly plastic impact with no sliding, requires the joining of two variational principles at t_ι by incorporating the virtual work of the contact force $\boldsymbol{f}^c = (\boldsymbol{f}_t^c, \boldsymbol{f}_q^c) \in T^*_{\boldsymbol{q}_\iota}([t_0, t_N], C_2)$. In particular, it will be seen in the transition equations (8.2) below, that the configuration component $\boldsymbol{f}_q^c$ imposes a jump in the system's momentum tangential to the contact surface while $\boldsymbol{f}_t^c$ induces jump in the energy $E = \frac{\partial L}{\partial \dot{\boldsymbol{q}}} \cdot \dot{\boldsymbol{q}} - L$.

8.3.4 Optimal control problem

Deriving the differential-algebraic equations of motion from the variational formulation (8.1), results in the following optimal control problem in the time continuous setting.

$$\min_{\boldsymbol{q},\dot{\boldsymbol{q}},\boldsymbol{f}} J(\boldsymbol{q}, \dot{\boldsymbol{q}}, \boldsymbol{f})$$

subject to

constrained equations of motion in $[t_0, t_\iota[$

$$\begin{aligned} \tfrac{\partial L(\boldsymbol{q},\dot{\boldsymbol{q}})}{\partial \boldsymbol{q}} - \tfrac{d}{dt}\tfrac{\partial L(\boldsymbol{q},\dot{\boldsymbol{q}})}{\partial \dot{\boldsymbol{q}}} - \boldsymbol{G}_1^T(\boldsymbol{q}) \cdot \boldsymbol{\lambda}_1 + \boldsymbol{f} &= \boldsymbol{0} \\ \boldsymbol{g}_1(\boldsymbol{q}) &= \boldsymbol{0} \end{aligned}$$

constrained equations of motion in $]t_\iota, t_N]$

$$\begin{aligned} \tfrac{\partial L(\boldsymbol{q},\dot{\boldsymbol{q}})}{\partial \boldsymbol{q}} - \tfrac{d}{dt}\tfrac{\partial L(\boldsymbol{q},\dot{\boldsymbol{q}})}{\partial \dot{\boldsymbol{q}}} - \boldsymbol{G}_2^T(\boldsymbol{q}) \cdot \boldsymbol{\lambda}_2 + f &= \boldsymbol{0} \\ \boldsymbol{g}_2(\boldsymbol{q}) &= \boldsymbol{0} \end{aligned}$$

transition equations from $(\boldsymbol{q}(t_\iota^-), \dot{\boldsymbol{q}}(t_\iota^-)) \in TC_1$ to $(\boldsymbol{q}(t_\iota^+), \dot{\boldsymbol{q}}(t_\iota^+)) \in TC_2$

$$\frac{\partial L(\boldsymbol{q}, \dot{\boldsymbol{q}})}{\partial \dot{\boldsymbol{q}}}\Big|_{t_\iota^-}^{t_\iota^+} - \boldsymbol{f}_q^c = 0, \qquad E\Big|_{t_\iota^-}^{t_\iota^+} - \boldsymbol{f}_t^c = 0 \tag{8.2}$$

periodic boundary conditions

$$\boldsymbol{r}(\boldsymbol{q}_0, \boldsymbol{p}_0, \boldsymbol{q}_\iota, \boldsymbol{q}_N, \boldsymbol{p}_N, \boldsymbol{\tau}_0, \boldsymbol{\tau}_{N-1}) = \boldsymbol{0}$$

path constraints

$$h(\boldsymbol{q}) \geq 0$$

Here, $\boldsymbol{G}_1(\boldsymbol{q}) = D\boldsymbol{g}_1(\boldsymbol{q})$ and $\boldsymbol{G}_2(\boldsymbol{q}) = D\boldsymbol{g}_2(\boldsymbol{q})$ denote the Jacobians of the constraint functions. The transition equations (8.2) describe the change in momentum and energy due to the perfectly plastic impact that immobilises the foot.

8.4 Constrained discrete dynamics and optimal control of the walker

8.4.1 Discrete variational principles and equations of motion

Without loss of generality, it is assumed that the time of contact between a foot and the ground coincides with a time node t_ι. This is possible since periodic boundary conditions

are imposed on the initial and final states, see Section 8.3.2. Furthermore, it spares the necessity to consider variations with respect to time. Details on the discrete variational theory for nonsmooth systems with unknown collision time can be found in [Peka 10]. In analogy to the continuous variational principles (8.1), the joining of two discrete constrained Lagrange-d'Alembert principle at t_ι reads

$$\begin{aligned}
&\delta\left(\sum_{n=0}^{\iota-1} L_d(\boldsymbol{q}_n,\boldsymbol{q}_{n+1}) - \frac{h}{2}\,\boldsymbol{g}_1(\boldsymbol{q}_n)\cdot\boldsymbol{\lambda}_{1,n} - \frac{h}{2}\,\boldsymbol{g}_1(\boldsymbol{q}_{n+1})\cdot\boldsymbol{\lambda}_{1,n+1}\right) + \sum_{n=0}^{\iota-1}\big(\boldsymbol{f}_n^-\cdot\delta\boldsymbol{q}_n + \\
&\boldsymbol{f}_n^+\cdot\delta\boldsymbol{q}_{n+1}\big) + \boldsymbol{f}_q^c\cdot\delta\boldsymbol{q}_\iota + \delta\left(\sum_{n=\iota}^{N-1} L_d(\boldsymbol{q}_n,\boldsymbol{q}_{n+1}) - \frac{h}{2}\,\boldsymbol{g}_2(\boldsymbol{q}_n)\cdot\boldsymbol{\lambda}_{2,n} - \frac{h}{2}\,\boldsymbol{g}_2(\boldsymbol{q}_{n+1})\cdot\boldsymbol{\lambda}_{2,n+1}\right) \\
&+ \sum_{n=\iota}^{N-1}\big(\boldsymbol{f}_n^-\cdot\delta\boldsymbol{q}_n + \boldsymbol{f}_n^+\cdot\delta\boldsymbol{q}_{n+1}\big) = 0
\end{aligned} \tag{8.3}$$

with the variations $\delta\boldsymbol{q}_0,\ldots,\boldsymbol{q}_{\iota-1},\boldsymbol{q}_{\iota+1},\ldots,\delta\boldsymbol{q}_N \in TQ$, the constrained variation at the impact $\delta\boldsymbol{q}_\iota \in T_{\boldsymbol{q}_\iota}C_2$, the impact force $\boldsymbol{f}_q^c \in T^*_{\boldsymbol{q}_\iota}C_2$ and variations of the Lagrange multipliers $\delta\boldsymbol{\lambda}_{1,0},\ldots,\delta\boldsymbol{\lambda}_{1,\iota},\delta\boldsymbol{\lambda}_{2,\iota},\ldots,\delta\boldsymbol{\lambda}_{2,N} \in \mathbb{R}^m$. Here, the discrete Lagrangian L_d approximates the action of the continuous Lagrangian in one time interval. In this work, a midpoint approximation is used, i.e. $L_d(\boldsymbol{q}_n,\boldsymbol{q}_{n+1}) = L(\frac{\boldsymbol{q}_n+\boldsymbol{q}_{n+1}}{2},\frac{\boldsymbol{q}_{n+1}-\boldsymbol{q}_n}{h})$. Due to their derivation via a discrete variational principle, the discrete equations of motion resulting from (8.3), called discrete Euler-Lagrange equations, inherit the structure preserving properties from the real continuous dynamics. A discrete symplectic form as well as momentum maps arising from symmetries according to Noether's theorem are conserved exactly along the discrete trajectory, see [Mars 01].
The discrete equations of motion resulting from (8.3) involve configurations variables, forces and Lagrange multipliers only. However, in the context of boundary conditions as well as for post-processing and interpretation of the discrete equations of motion as balance of discrete momentum, the knowledge of the conjugate momenta is useful. At each time node, there exist two expressions for the conjugate momenta, taking into account the past or the following time interval. The constrained forced discrete Legendre transformation are given by

$$\begin{aligned}
\boldsymbol{p}_n^- &= -D_1L_d(\boldsymbol{q}_n,\boldsymbol{q}_{n+1}) + \tfrac{h}{2}\boldsymbol{G}^T(\boldsymbol{q}_n)\cdot\boldsymbol{\lambda}_n - \boldsymbol{f}_n^- \\
\boldsymbol{p}_n^+ &= D_2L_d(\boldsymbol{q}_{n-1},\boldsymbol{q}_n) - \tfrac{h}{2}\boldsymbol{G}^T(\boldsymbol{q}_n)\cdot\boldsymbol{\lambda}_n + \boldsymbol{f}_{n-1}^+
\end{aligned} \tag{8.4}$$

The projected discrete Legendre transforms, which still yield an n-dimensional conjugate momentum, read

$${}^Q\boldsymbol{p}_n^- = \boldsymbol{Q}(\boldsymbol{q}_n)\cdot\left[-D_1L_d(\boldsymbol{q}_n,\boldsymbol{q}_{n+1}) - \boldsymbol{f}_n^-\right], \quad {}^Q\boldsymbol{p}_n^+ = \boldsymbol{Q}(\boldsymbol{q}_n)\cdot\left[D_2L_d(\boldsymbol{q}_{n-1},\boldsymbol{q}_n) + \boldsymbol{f}_{n-1}^+\right]$$

Finally, the reduced discrete Legendre transforms are defined as

$${}^P\boldsymbol{p}_n^- = \boldsymbol{P}^T(\boldsymbol{q}_n)\cdot\left[-D_1L_d(\boldsymbol{q}_n,\boldsymbol{q}_{n+1}) - \boldsymbol{f}_n^-\right], \quad {}^P\boldsymbol{p}_n^+ = \boldsymbol{P}^T(\boldsymbol{q}_n)\cdot\left[D_2L_d(\boldsymbol{q}_{n-1},\boldsymbol{q}_n) + \boldsymbol{f}_{n-1}^+\right]$$

First swing phase For $n = 1, ..., \iota - 1$ the discrete variational principle (8.3) yields the following system which is to be solved for $\boldsymbol{q}_2, ..., \boldsymbol{q}_\iota, \boldsymbol{\lambda}_{1,1}, ..., \boldsymbol{\lambda}_{1,\iota-1}$.

$$\begin{aligned} D_2L_d(\boldsymbol{q}_{n-1}, \boldsymbol{q}_n) + D_1L_d(\boldsymbol{q}_n, \boldsymbol{q}_{n+1}) - h\boldsymbol{G}_1^T(\boldsymbol{q}_n) \cdot \boldsymbol{\lambda}_{1,n} + \boldsymbol{f}_{n-1}^+ + \boldsymbol{f}_n^- &= \boldsymbol{0} \\ \boldsymbol{g}_1(\boldsymbol{q}_{n+1}) &= \boldsymbol{0} \end{aligned} \tag{8.5}$$

Note that the first equation can be interpreted as balance of momentum $\boldsymbol{p}_n^+ = \boldsymbol{p}_n^-$. Equivalently, in reduced form using the null space matrix $\boldsymbol{P}_1$ and the discrete reparametrisation $\boldsymbol{q}_{n+1} = \boldsymbol{F}_1(\boldsymbol{u}_{n+1}, \boldsymbol{q}_n) \in C_1$, the balance of projected momentum ${}^P\boldsymbol{p}_n^+ = {}^P\boldsymbol{p}_n^-$ reading

$$\boldsymbol{P}_1^T(\boldsymbol{q}_n) \cdot \left[D_2L_d(\boldsymbol{q}_{n-1}, \boldsymbol{q}_n) + D_1L_d(\boldsymbol{q}_n, \boldsymbol{q}_{n+1}) + \boldsymbol{f}_{n-1}^+ + \boldsymbol{f}_n^- \right] = \boldsymbol{0} \tag{8.6}$$

is to be solved for $\boldsymbol{u}_2, ..., \boldsymbol{u}_\iota$. In contrast to the $(n+m)$-dimensional system (8.5), (8.6) is only $(n-m)$-dimensional.

Second swing phase The discrete variational principle (8.3) yields for $n = \iota+1, ..., N-1$ the system

$$\begin{aligned} D_2L_d(\boldsymbol{q}_{n-1}, \boldsymbol{q}_n) + D_1L_d(\boldsymbol{q}_n, \boldsymbol{q}_{n+1}) - h\boldsymbol{G}_2^T(\boldsymbol{q}_n) \cdot \boldsymbol{\lambda}_{2,n} + \boldsymbol{f}_{n-1}^+ + \boldsymbol{f}_n^- &= \boldsymbol{0} \\ \boldsymbol{g}_2(\boldsymbol{q}_{n+1}) &= \boldsymbol{0} \end{aligned}$$

which is o be solved for $\boldsymbol{q}_{\iota+2}, ..., \boldsymbol{q}_N, \boldsymbol{\lambda}_{2,\iota+1}, ..., \boldsymbol{\lambda}_{2,N-1}$. Equivalently using the null space matrix $\boldsymbol{P}_2$ and the discrete reparametrisation $\boldsymbol{q}_{n+1} = \boldsymbol{F}_2(\boldsymbol{u}_{n+1}, \boldsymbol{q}_n) \in C_2$ the reduced system

$$\boldsymbol{P}_2^T(\boldsymbol{q}_n) \cdot \left[D_2L_d(\boldsymbol{q}_{n-1}, \boldsymbol{q}_n) + D_1L_d(\boldsymbol{q}_n, \boldsymbol{q}_{n+1}) + \boldsymbol{f}_{n-1}^+ + \boldsymbol{f}_n^- \right] = \boldsymbol{0} \tag{8.7}$$

is to be solved for $\boldsymbol{u}_{\iota+2}, ..., \boldsymbol{u}_{N-1}$.

Transfer of contact As explained earlier, without loss of generality, it can be assumed that the impact of the second foot on the ground takes place at t_ι, thus $g_c(\boldsymbol{q}_\iota) = 0$. Then automatically $\boldsymbol{g}_2(\boldsymbol{q}_\iota) = \boldsymbol{0}$ follows, since the point of contact defines $\boldsymbol{g}_2$. Note that a contact force $\boldsymbol{f}_q^c \in T_{\boldsymbol{q}_\iota}^* C_2$ which immobilises the second foot in it's point of contact is normal to C_2, thus it is given by $\boldsymbol{f}_q^c = \boldsymbol{G}_2^T(\boldsymbol{q}_\iota) \cdot \boldsymbol{\lambda}_c$. Substituting this in the discrete form $\boldsymbol{p}_\iota^+ - \boldsymbol{p}_\iota^- + \boldsymbol{f}_q^c = \boldsymbol{0}$ of the transition equations (8.2) yields

$$\begin{aligned} D_2L_d(\boldsymbol{q}_{\iota-1}, \boldsymbol{q}_\iota) + D_1L_d(\boldsymbol{q}_\iota, \boldsymbol{q}_{\iota+1}) - \tfrac{h}{2}\boldsymbol{G}_1^T(\boldsymbol{q}_\iota) \cdot \boldsymbol{\lambda}_{1,\iota} - G_2^T(\boldsymbol{q}_\iota) \cdot (\tfrac{h}{2}\boldsymbol{\lambda}_{2,\iota} + \boldsymbol{\lambda}_c) + \\ \boldsymbol{f}_{\iota-1}^+ + \boldsymbol{f}_\iota^- = \boldsymbol{0} \\ \boldsymbol{g}_2(\boldsymbol{q}_{\iota+1}) = \boldsymbol{0} \end{aligned} \tag{8.8}$$

This is an underdetermined system. To solve for $\boldsymbol{q}_{\iota+1}, \boldsymbol{\lambda}_{1,\iota}, \boldsymbol{\lambda}_{2,\iota}, \lambda_c$, one possibility is to augment (8.8) by the constraints on momentum level $\boldsymbol{G}_1(\boldsymbol{q}) \cdot \boldsymbol{M}^{-1} \cdot \boldsymbol{p}_\iota^+ = \boldsymbol{0}$ and $\boldsymbol{G}_2(\boldsymbol{q}) \cdot \boldsymbol{M}^{-1} \cdot \boldsymbol{p}_\iota^- = \boldsymbol{0}$. However, since only constraints on the configuration variable are imposed elsewhere, this would be somewhat inconsequent. Therefore, the fact that ${}^Q\boldsymbol{p}_n^+ = \boldsymbol{p}_n^+$ holds is used and the transition equations read ${}^{Q_1}\boldsymbol{p}_\iota^+ - \boldsymbol{p}_\iota^- + \boldsymbol{f}_q^c = \boldsymbol{0}$. Next, projection with the second discrete null space matrix and insertion of the discrete reparametrisation $\boldsymbol{q}_{\iota+1} = \boldsymbol{F}_2(\boldsymbol{u}_{\iota+1}, \boldsymbol{q}_\iota) \in C_2$ yields

$$\boldsymbol{P}_2^T(\boldsymbol{q}_\iota) \cdot \left[\boldsymbol{Q}_1(\boldsymbol{q}_\iota) \cdot \left(D_2L_d(\boldsymbol{q}_{\iota-1}, \boldsymbol{q}_\iota) + \boldsymbol{f}_{\iota-1}^+ \right) + D_1L_d(\boldsymbol{q}_\iota, \boldsymbol{q}_{\iota+1}) + \boldsymbol{f}_\iota^- \right] = \boldsymbol{0} \tag{8.9}$$

to be solved for $\boldsymbol{u}_{\iota+1}$.

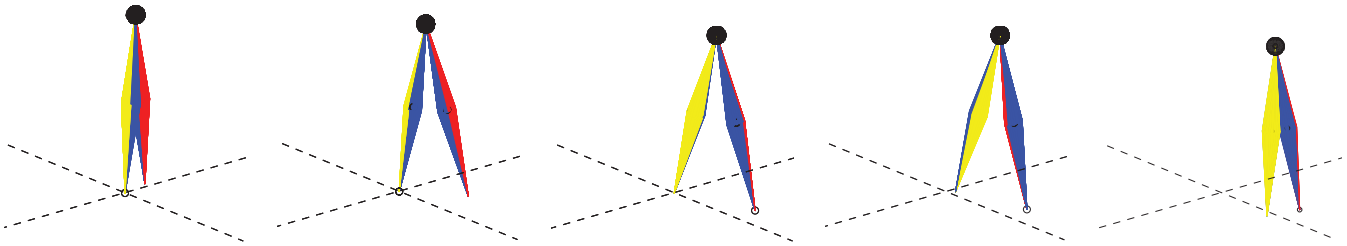

Figure 8.4: Snapshots of the compass biped gait.

8.4.2 Discrete constrained optimisation problem

As for the discrete Lagrangian in Section 8.4.1, the integral of the continuous cost function in one time interval is approximated by C_d. Furthermore, indicating the dependence on the discrete generalised coordinates $\boldsymbol{u}_d = \{\boldsymbol{u}_n\}_{n=1}^{N}$ and forces $\boldsymbol{\tau}_d = \{\boldsymbol{\tau}_n\}_{n=0}^{N-1}$ directly, the discrete objective function can be expressed as

$$J_d(\boldsymbol{u}_d, \boldsymbol{\tau}_d) = \sum_{n=0}^{N-1} C_d(\boldsymbol{u}_n, \boldsymbol{u}_{n+1}, \boldsymbol{\tau}_n)$$

The constrained optimisation problem reads

$$\min_{\boldsymbol{u}_d, \boldsymbol{\tau}_d} J_d(\boldsymbol{u}_d, \boldsymbol{\tau}_d)$$

subject to

reduced forced discrete equations of motion (8.6) for $n = 1, ..., \iota - 1$

$$\boldsymbol{P}_1^T(\boldsymbol{q}_n) \cdot \left[D_2 L_d(\boldsymbol{q}_{n-1}, \boldsymbol{q}_n) + D_1 L_d(\boldsymbol{q}_n, \boldsymbol{q}_{n+1}) + \boldsymbol{f}_{n-1}^{+} + \boldsymbol{f}_n^{-} \right] = \boldsymbol{0}$$

reduced forced discrete equations of motion (8.7) for $n = \iota + 1, ..., N - 1$

$$\boldsymbol{P}_2^T(\boldsymbol{q}_n) \cdot \left[D_2 L_d(\boldsymbol{q}_{n-1}, \boldsymbol{q}_n) + D_1 L_d(\boldsymbol{q}_n, \boldsymbol{q}_{n+1}) + \boldsymbol{f}_{n-1}^{+} + \boldsymbol{f}_n^{-} \right] = \boldsymbol{0}$$

transition equations (8.9)

$$\begin{aligned} \boldsymbol{g}_c(\boldsymbol{q}_\iota) &= \boldsymbol{0} \\ \boldsymbol{P}_2^T(\boldsymbol{q}_\iota) \cdot \left[\boldsymbol{Q}_1(\boldsymbol{q}_\iota) \cdot \left(D_2 L_d(\boldsymbol{q}_{\iota-1}, \boldsymbol{q}_\iota) + \boldsymbol{f}_{\iota-1}^{+} \right) + D_1 L_d(\boldsymbol{q}_\iota, \boldsymbol{q}_{\iota+1}) + \boldsymbol{f}_\iota^{-} \right] &= \boldsymbol{0} \end{aligned}$$

periodic boundary conditions

$$\boldsymbol{r}(\boldsymbol{q}_0, \boldsymbol{p}_0, \boldsymbol{q}_\iota, \boldsymbol{q}_N, \boldsymbol{p}_N, \boldsymbol{\tau}_0, \boldsymbol{\tau}_{N-1}) = \boldsymbol{0}$$

path constraints for $n = 1, ..., N$

$$h(\boldsymbol{q}_n) \geq 0$$

8.5 Results

In the walker model, the mass of the rigid legs is $M_\varphi^1 = M_\varphi^2 = 5$ while that of the point mass is $M^M = 10$. The legs are double cones of radius $r = 0.05$ and cone length $l = 0.5$.

Gravity points with an acceleration of $g = -9.81$ into the negative $\boldsymbol{e}_3$-direction. The simulation of the half step takes place in the time interval $[0, 0.7]$ and $N = 13$, i.e. 14 time nodes are used and the double stance configuration is assumed to be approximately in the middle of the interval, thus $\iota = 6$. Note that the periodic boundary conditions allow t_ι to be anywhere in the time interval. The restricted optimisation problem described in Section 8.4.2 is solved in Matlab using `fmincon` choosing an active-set algorithm and supplying user defined analytic gradients of the objective function and the constraints, respectively. The initial guess is quite rough and does not fulfil the discrete dynamics. At t_0, the biped stands in the $(\boldsymbol{e}_2, \boldsymbol{e}_3)$-plane, with the stance leg (yellow) rotated by the angle $\frac{\pi}{18}$ around the negative $\boldsymbol{e}_1$-axis and the swing leg (red) rotated by the same angle around the positive $\boldsymbol{e}_1$-axis. Then,

$$
\begin{array}{llll}
(\theta_1^1)_n = (\theta_1^2)_n = \frac{\pi}{18(N-1)} & & & n = 1, \dots, 12 \\
(\theta_2^1)_n = \frac{0.12}{\frac{N}{2}-1}, & (\theta_3^1)_n = (\theta_3^2)_n = -\frac{0.16}{\frac{N}{2}-1}, & (\theta_2^2)_n = \frac{0.25}{\frac{N}{2}} & n = 1, \dots, 6 \\
(\theta_2^1)_n = -\frac{0.12}{\frac{N}{2}-1}, & (\theta_3^1)_n = (\theta_3^2)_n = \frac{0.16}{\frac{N}{2}-1}, & (\theta_2^2)_n = -\frac{0.25}{\frac{N}{2}-2} & n = 7, \dots, 13
\end{array}
$$

and all discrete generalised forces are set to zero.
The gait resulting from the discrete objective function

$$J_d(\boldsymbol{u}_d, \boldsymbol{\tau}_d) = \frac{h}{sl} \sum_{n=0}^{N-1} \|\boldsymbol{\tau}_n\|$$

approximating $J(\boldsymbol{q}, \dot{\boldsymbol{q}}, \boldsymbol{f})$ introduced in Section 8.3.1 is computed. See Figure 8.4 for snapshots of the motion. Figure 8.5 shows the evolution of the feet trajectory coordinates (left) and projection of the feet and hip trajectories to the $(\boldsymbol{e}_1, \boldsymbol{e}_2)$-plane (right) during three steps. Only a half step has been simulated, however, the fulfilment of periodic boundary condition on configuration as well as on momentum level ensures the smooth transition between the steps. The vertical dotted lines in the left plot indicate the double stance configurations and the red and yellow circles in the right plot mark the placement $\boldsymbol{x}_{S_1}$ and $\boldsymbol{x}_{S_2}$ of the stancefoot during the specific gait phases, respectively. Due to the presence of gravity and the fixing of one foot on the ground, the only symmetry of the Lagrangian of the walker is rotation around the gravity axis trough the foot position. Figure 8.6 shows that during the specific gait phases, angular momentum with respect to the attachment point is conserved exactly. This illustrated the structure preservation guaranteed by the discrete Euler-Lagrange equations. From the discrete configuration and force trajectories, the step length for this gait is determined to be $sl = 0.1960$ and the value of the objective function is $J_d = 11.4020$.

8.6 Conclusion

A structure preserving method for the numerical simulation of the optimal control of a bipedal walker's compass gait has been developed and illustrated with an example. In the discrete formulation of the optimal control problem in Section 8.4.2, structure preservation is guaranteed by the derivation of the discrete equations of motion, and in particular the discrete transfer of contact equations, via a discrete variational principle.

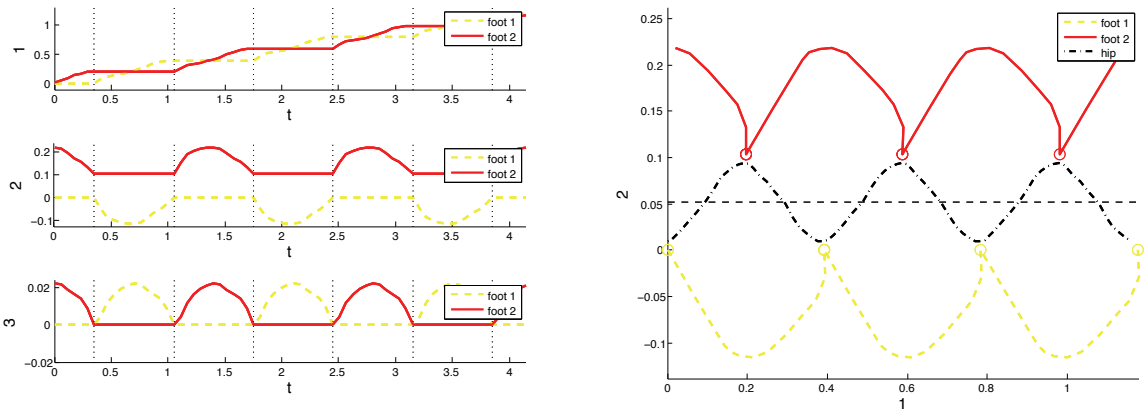

Figure 8.5: Evolution of the feet trajectory coordinates (left) and projection of the feet and hip trajectories to the (e_1, e_2)-plane (right).

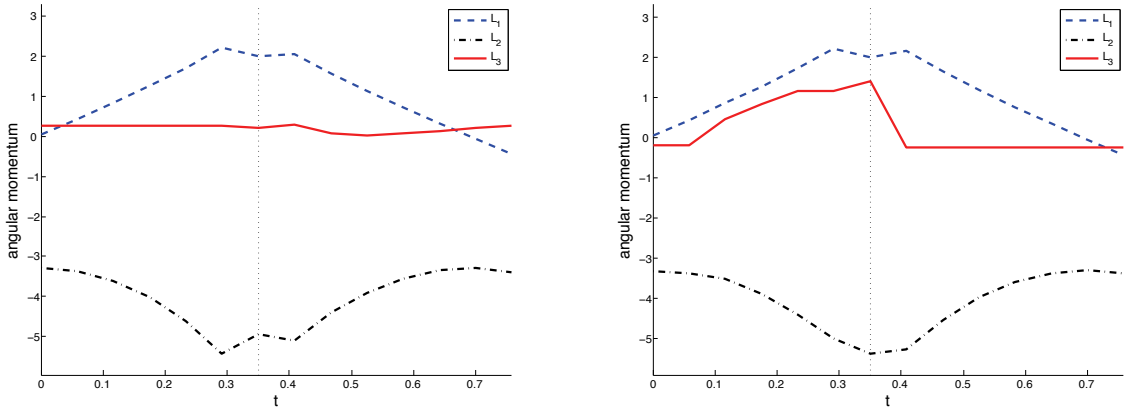

Figure 8.6: Angular momentum with respect to x_{S_1} (left) and with respect to x_{S_2} (right).

9 Summary and outlook

A robust, accurate and efficient simulation method for the optimal control of constrained multibody dynamics is developed in this work. This new numerical method meets the demand of structure preservation, i.e. the approximate numerical solution inherits certain characteristic properties like the consistency of momentum maps, symplecticity and good energy behaviour from the real dynamical process. Basic properties of the underlying discrete constrained dynamics like the correct initialisation and a discrete Legendre transform necessary to impose boundary conditions on momentum level are treated in Chapter 3. Then, Chapter 4 shows a convergence result for the constrained variational integrator using the theory of Γ-convergence. The most important piece of work, the contribution which takes all previously addressed structure preserving simulations of forward dynamical processes into a completely different problem setting, namely that of optimal control, where differential equation and inequality constrained optimisation problems with boundary values arise, is presented in Chapter 5. It combines the previously developed structure preserving method DMOC (discrete mechanics and optimal control) with a particular simulation technique of constrained multibody dynamics resulting in the proposed method called DMOCC (discrete mechanics and optimal control for constrained systems). This method is developed further to take the presence of uncertainty into account in Chapter 6. Here, COMOC (concentration-of-measure optimal control) seeks to minimise a concentration-of-measure upper bound on the probability of failure of a system. Chapter 7 presents a discrete mechanics approach to the computation of static equilibria for Cosserat rods. Here, the ideas used previously in the context of rigid multibody system dynamics are transferred into the context of a spatially distributed static system. Finally, a particular optimal control problem is investigated in Chapter 8, namely that of bipedal walking, where the contact between the foot and the ground imposes an additional challenge for the structure preserving simulation technique. All chapters consist on the one hand of theoretical sections where the proposed numerical methods are deduced from scratch as well as on the other hand of numerical results of their implementation.

There are many interesting and challenging research directions to be pursued on the basis of the developed optimal control simulation technique.

- Non-uniform and adaptive time grids: the variational integrator can deal with a prescribed series of time steps with varying size in a forward dynamical simulation. However, letting the algorithm itself pick time steps according to a specific goal is still an open question.
- Multirange integration: when the dynamics of different parts of a (multibody) system takes place on quite different time scales, a multirange time stepping scheme is required to cosimulate the parts of the system using different time steps. A big

challenge is to develop a structure preserving multirange integrator and to use it in the context of optimal control simulation.

- Design of objective functions – multiobjective optimisation: if multiple goals are to be met simultaneously by the motion, the simplest strategy is to define the objective function as a weighted sum of the different criteria. However, large differences in the order of magnitude of the different phenomena over time can blur the results substantially. Therefore, strategies for multiobjective optimisation subject to constraints have to be explored in combination with DMOCC.

- Initial guesses: if a method like SQP is used to find minima of the objective function, the algorithm needs an initial guess to start its search for local solutions. The computational costs are influenced substantially by the quality of this initial guess meaning the accuracy to which it fulfils the constraints and the value of the objective function. While creating initial trajectories via a purely forward dynamic simulation (with guessed forces) is a simple method to ensure that the initial guess fulfils the dynamics constraints, the resulting trajectory will probably not end in the desired final state. Another somewhat more expensive method is to choose a possible trajectory connecting the initial with the final state and to determine the corresponding forces in an inverse dynamics procedure. However, depending on the complexity of the problem this might be a difficult task.

- Optimal locomotion of submerged mutlibody systems: the dynamics and locomotion of a neutrally-buoyant deformable body that can undergo finite shape deformations and is immersed in a perfect and incompressible fluid has been studied already in a first work [Leye 09a]. Determining optimal actuations of the body with the goal to swim fast, or in an energy efficient way by combining [Leye 09a] with the optimal control simulation technique developed in this thesis is an interesting research topic.

- Optimal control of elastic multibody systems: so far, only rigid multibody systems are optimally controlled with DMOCC. The presence of (spatially discretised) elastic parts, for which by far not all degrees of freedom are actuated, introduces an internal dynamics into the system. Then the question arises whether this internal dynamics is stable and how a desired manoeuvre can be optimally controlled.

Bibliography

[Abra 88] R. Abraham, J. Marsden, and T. Ratiu. *Manifolds, Tensor Analysis, and Applications*. Vol. 75 of Applied Mathematical Sciences, Springer, 1988.

[Acke 07] M. Ackermann. "A novel optimization approach to generate physiological human walking patterms". In: *Proceedings of the 6th International Conference on Multibody Systems, Nonlinear Dynamics, and Control, ASME International Design Engineering Technical Conferences*, Las Vegas, Nevada, 4-7 September 2007.

[Allg 99] F. Allgöwer, T. Badgwell, T. Qin, J. Rawlings, and S. Wright. "Nonlinear predictive control and moving horizon estimation – an introductory overview". In: P. Frank, Ed., *Advances in control. Highlights of teh ECC'99*, 1999.

[Ande 83] H. Andersen. "RATTLE: A velocity version of the SHAKE algorithm for molecular dynamics calculations". *J. Comput. Physics*, Vol. 52, pp. 24–34, 1983.

[Ange 88] J. Angeles. *Rational Kinematics*. Springer, 1988.

[Ange 89] J. Angeles and S. Lee. "The modelling of holonomic mechanical systems using a natural orthogonal complement". *Trans. Canadian Society of Mechanical Engineers*, Vol. 13, No. 4, pp. 81–89, 1989.

[Antm 05] S. Antmann. *Nonlinear Problems in Elasticity, (2nd edn.)*. Springer, 2005.

[Antm 95] S. Antmann. *Nonlinear Problems in Elasticity*. Springer, 1995.

[Arme 01] F. Armero and I. Romero. "On the formulation of high-frequency dissipative time-stepping algorithms for nonlinear dynamics. Part I: low-order methods for two model problems and nonlinear elastodynamics". *Comput. Methods Appl. Mech. Engrg.*, Vol. 190, pp. 2603–2649, 2001.

[Arno 78] V. Arnold. *Mathematical Methods of Classical Mechanics*. Springer, 1978.

[Asch 79] U. Ascher, J. Christiansen, and R. Russell. "A collocation solver for mixed order systems of boundary value problems". *Math. Comp.*, Vol. 33, pp. 659–679, 1979.

[Asch 88] U. Ascher, R. Mattheij, and R. Russell. *Numerical solution of Boundary Value Problems for Differential Equations*. SIAM, 1988.

[Ast 06] A. Ast and P. Eberhard. "Flatness-based control of parallel kinematics using multibody systems – simulation and experimental results". *Archive of Applied Mechanics*, Vol. 76, No. 3-4, pp. 181–197, 2006.

[Barc 98] A. Barclay, P. Gill, and J. Rosen. "SQP methods and their application to numerical optimal control". In: W. Schmidt, K. Heier, L. Bittner, and R. Bulirsch, Eds., *Variational Calculus. Optimal Control and Application*, Birkhäuser, 1998.

[Bart 98] E. Barth, B. Leimkuhler, and S. Reich. "A Time-Reversible Variable-Stepsize Integrator for Constrained Dynamics". *Konrad-Zuse-Zentrum für Informationstechnik Berlin*, 1998.

[Bauc 03] O. Bauchau and L. Trainelli. "The Vectorial Parameterization of Rotation". *Nonlin. Dynamics*, Vol. 1, pp. 71–92, 2003.

[Bauc 95] O. Bauchau, G. Damilano, and N. Theron. "Numerical integration of non-linear elastic multibody systems". *Int. J. Numer. Methods Engng.*, Vol. 38, pp. 2727–2751, 1995.

[Bely 76] T. Belytschko and R. Mullen. "Mesh partitions of explicit-implicit time integrators". In: K. Bathe, J. Oden, and W. Wunderlich, Eds., *Formulations and Computational Algorithms in Finite Element Analysis*, pp. 673–690, MIT Press, Cambridge, MA, 1976.

[Bely 81] T. Belytschko. "Partitioned and adaptive algorithms for explicit time integration". In: W. Wunderlich, E. Stein, and K. Bathe, Eds., *Nonlinear Finite Element Analysis in Structural Mechanics*, pp. 572–584, Springer, New York, 1981.

[Benz 05] M. Benzi, G. Golub, and J. Liesen. "Numerical solution of saddle point problems". *Acta Numerica*, pp. 1–137, 2005.

[Berg 08] M. Bergou, M. Wardetzky, S. Robinson, B. Audoly, and E. Grinspun. "Discrete Elasic Rods". *ACM transaction on Graphic*, Vol. 27, No. 3, pp. 63:1–63:12, 2008.

[Bert 95] D. Bertsekas. *Nonlinear Programming.* Athena Scientific, Nashua, 1995.

[Bets 00a] P. Betsch and P. Steinmann. "Conserving properties of a time FE method – Part I: time-stepping schemes for N-body problems". *Int. J. Numer. Meth. Engng.*, Vol. 49, pp. 599–638, 2000.

[Bets 00b] P. Betsch and P. Steinmann. "Inherently Energy Conserving Time Finite Elements for Classical Mechanics". *J. Comput. Phys.*, Vol. 160, pp. 88–116, 2000.

[Bets 01a] P. Betsch and P. Steinmann. "Conserving properties of a time FE method – Part II: Time-stepping schemes for non-linear elastodynamics". *Int. J. Numer. Meth. Engng.*, Vol. 50, pp. 1931–1955, 2001.

[Bets 01b] P. Betsch and P. Steinmann. "Constrained integration of rigid body dynamics". *Comput. Methods Appl. Mech. Engrg.*, Vol. 191, pp. 467–488, 2001.

[Bets 02a] P. Betsch and P. Steinmann. "Conserving properties of a time FE method – Part III: Mechanical systems with holonomic constraints". *Int. J. Numer. Meth. Engng.*, Vol. 53, pp. 2271–2304, 2002.

[Bets 02b] P. Betsch and P. Steinmann. "Frame-indifferent beam finite elements based upon the geometrically exact beam theory". *Int. J. Numer. Meth. Engng.*, Vol. 54, pp. 1775–1788, 2002.

[Bets 03] P. Betsch and P. Steinmann. "Constrained dynamics of geometrically exact beams". *Comput. Mech.*, Vol. 31, pp. 49–59, 2003.

[Bets 05] P. Betsch. "The discrete null space method for the energy consistent integration of constrained mechanical systems. Part I: Holonomic constraints". *Comput. Methods Appl. Mech. Engrg.*, Vol. 194, No. 50-52, pp. 5159–5190, 2005.

[Bets 06] P. Betsch and S. Leyendecker. "The discrete null space method for the energy consistent integration of constrained mechanical systems. Part II: Multibody dynamics". *Int. J. Numer. Meth. Engng.*, Vol. 67, No. 4, pp. 499–552, 2006.

[Bets 07] P. Betsch, S. Uhlar, and M. Quasem. "On the incorporation of servo constraints into a rotationless formulation of flexible multibody dynamics". In: *Proceedings of the International Conference on Advances in Computational Multibody Dynamics, ECCOMAS Thematic Conference, CD-ROM, Milano, Italy, 25-28 June*, 2007.

[Bets 98] P. Betsch, A. Menzel, and E. Stein. "On the parametrization of finite rotations in computational mechanics; A classification of concepts with application to smooth shells". *Comput. Methods Appl. Mech. Engrg.*, Vol. 155, pp. 273–305, 1998.

[Bett 98] J. Betts. "Survey of numerical methods for trajectory optimization". *Journal of Guidance, Control, and Dynamics*, Vol. 21, No. 2, 1998.

[Bieg 84] L. Biegler. "Solution of dynamic optimization problems by successive quadratic programming and orthogonal collocation". *Comput. Chem. Engng.*, Vol. 8, pp. 243–248, 1984.

[Bind 01] T. Binder, L. Blank, H. Bock, R. Bulirsch, W. Dahmen, M. Diehl, T. Kronseder, W. Marquardt, J. Schlöder, and O. vonStryk. "Introduction to model based optimization of chemical processes on moving horizons". *Online Optimization of Large Scale Systems: State of the Art*, pp. 295–340, 2001. http://www.zib.de/dfg-echtzeit/Publikatio nen/Preprints/Preprint-01-15.html.

[Blaj 03] W. Blajer and A. Czaplicki. "Contact Modeling and Identification of Planar Somersaults on the Trampoline". *Multibody System Dynamics*, Vol. 10, pp. 289–312, 2003.

[Blaj 04] W. Blajer and K. Kolodziejczyk. "A Geometric Approach to Solving Problems of Control Constraints: Theory and a DAE Framework". *Multibody System Dynamics*, Vol. 11, pp. 343–364, 2004.

[Blaj 07] W. Blajer, K. Dziewiecki, and Z. Mazur. "Multibody modeling of human body for the inverse dynamics analysis of sagittal plane movements". *Multibody System Dynamics*, Vol. 18, No. 2, pp. 217–232, 2007.

[Bobe 08] A. Bobenko, P. Schröder, J. Sullivan, and G. e. Ziegler. *Discrete Differential Geometry*. Birkhäuser, 2008.

[Bobe 99] A. Bobenko and Y. Suris. "Discrete time Lagrangian mechanics on Lie groups, with an application on the Lagrange top". *Communications in Mathematical Physics*, Vol. 204, pp. 147–188, 1999.

[Bock 84] H. Bock and K. Plitt. "A multiple shooting algorithm for direct solution of optimal control problems". In: *Proc. 9th IFAC World Congress Budapest*, pp. 243–247, 1984.

[Bogg 95] P. Boggs and J. Tolle. “Sequential quadratic programming”. *Acta Numerica*, Vol. 4, pp. 1–50, 1995.

[Bott 04] C. Bottasso and A. Croce. “Optimal control of multibody systems using an energy preserving direct transcription method”. *Multibody system dynamics*, Vol. 12, pp. 17–45, 2004.

[Bott 05] C. Bottasso and O. Bauchau. “Time-step-size-independent conditioning and sensitivity to perturbations in the numerical solution of index three differential algebraic equations”. *preprint*, 2005.

[Bou 09] N. Bou-Rabee and J. Marsden. “Hamilton-Pontryagin Integrators on Lie Groups: Introduction and Structure-Preserving Properties”. *Found. Comput. Math.*, Vol. 9, No. 2, pp. 197–219, 2009.

[Bouc 04] S. Boucheron, O. Bousquet, and G. Lugosi. “Concentration inequalities”. In: O. Bousquet, U. Luxburg, and G. Rätsch, Eds., *Advanced Lectures in Machine Learning*, pp. 208–240, Springer, 2004.

[Bull 04] F. Bullo and A. Lewis. *Geometric Control of Mechanical Systems*. Springer, 2004.

[Bull 98] F. Bullo and M. Zefran. “On modeling and locomotion of hybrid mechanical systems with impacts”. In: *Proceedings of the 37th IEEE Conference on Decision & Control, Tampa, Florida, USA*, pp. 2633–2638, 1998.

[Busk 00] C. Büskens and M. Gerdts. “Numerical Solution of Optimal Control Problems with DAE Systems of Higher Index”. In: *Optimalsteuerungsprobleme in der Luft- und Raumfahrt, Workshop in Greifswald des Sonderforschungsbereichs 255: Transatmosphärische Flugsysteme*, pp. 27–38, 2000.

[Cauc 47] A. Cauchy. “Méthode générale pour la résolution systèmes déquations simultanées”. *Comp. rend. acad. sci.*, Vol. 25, pp. 536–538, 1847.

[Cell 03] E. Celledoni and N. Owren. “Efficient time-symmetric simulation of torqued rigid bodies using Jacobi elliptic functionsLie group methods for rigid body dynamics and time integration on manifolds”. *Comput. Methods Appl. Mech. Engrg.*, Vol. 192, pp. 421–438, 2003.

[Cerv 98] A. Cervantes and L. Biegler. “Large-scale DAE optimization using a simultaneous NLP formulation”. *AIChE Journal*, Vol. 44, No. 5, pp. 1038–1050, 1998.

[Cher 82] F. Chernousko and A. Luybushin. “Method of successive approximations for optimal control problems (survey paper)”. *Optimal Control, Applications and Methods*, Vol. 3, pp. 101–114, 1982.

[Chev 01] C. Chevallereau and Y. Aoustin. “Optimal reference trajectories for walking and running of a biped robot”. *Robotica*, Vol. 19, pp. 557–569, 2001.

[Chou 03] N. Chouaieb. *Kirchhoff’s problem of helical solutions of uniform rods and their stability properties*. PhD thesis, EPFL Lausanne, 2003.

[Chou 04] N. Chouaieb and J. Maddocks. “Kirchhoff’s problem of helical equilibria of uniform rods”. *Journal of Elasticity*, Vol. 77, pp. 221–247, 2004.

[Cris 91] M. Crisfield. *Non-linear Finite Element Analysis of Solids and Structures. Volume I: Essentials.* Wiley, 1991.

[Cris 96] M. Crisfield and J. Shi. "An Energy Conserving Co-Rotational Procedure for Non-Linear Dynamics with Finite Elements". *Nonlin. Dynamics*, Vol. 9, pp. 37–52, 1996.

[Cris 99] M. Crisfield and G. Jelenić. "Objectivity of strain measures in the geometrically exact three-dimensional beam theory and its finite-element implementation". *Proc. R. Soc. Lond. A*, Vol. 455, pp. 1125–1147, 1999.

[Dal 93] G. Dal Maso. *An Introduction to Γ-Convergence.* Birkhäuser, 1993.

[De S 06] V. De Sapio, O. Khatib, and S. Delp. "Task-level approaches for the control of constrained multibody systems". *Multibody System Dynamics*, Vol. 16, No. 1, pp. 73–102, 2006.

[Deuf 74] P. Deuflhard. "A modified Newton method for the solution of ill-conditioned systems of nonlinear equations with application to multiple shooting". *Numer. Math.*, Vol. 22, pp. 289–315, 1974.

[Dich 96] D. Dichmann, Y. Li, and J. Maddocks. "Hamiltonian Formulations and Symmetries in Rod Mechanics". *Mathematical Approaches to Biomolecular Structure and Dynamics, IMA Volumes in Mathematics and its Applications*, Vol. 82, pp. 71–113, 1996.

[Diun 06] V. Diundam. *Port-based modeling and control for efficient bipedal walking robots.* PhD thesis, University of Twente, 2006.

[Dixo 07] M. Dixon. *Geometric integrators for continuum dynamics.* PhD thesis, Imperial College, London, 2007.

[Du T 08] P. Du Toit, I. Mezić, and J. Marsden. "Actuated conformation change in biomolecules". *Proceedings of the National Academy of Sciences of the United States of America*, 2008. submitted for publication.

[Feat 87] R. Featherstone. *Robot Dynamics Algorithms.* Kluwer Academic Publishers, Norwell, 1987.

[Fete 03] R. Fetecau, J. Marsden, M. Ortiz, and M. West. "Nonsmooth Lagrangian Mechanics and Variational Collision Integrators". *Siam J. applied dynamical systems*, Vol. 2, No. 3, pp. 381–416, 2003.

[Fisc 97] G. Fischer. *Lineare Algebra.* Vieweg, 1997.

[Flem 77] W. Fleming. *Functions of Several Variables (2nd edn.).* Springer, 1977.

[Flet 84] C. Fletcher. *Computational Galerkin methods.* Springer, 1984.

[Fuhr 88] C. Führer. *Differential-algebraische-Gleichungssysteme in mechanischen Mehrkörpersystemen. Theorie, numerische Ansätze und Anwendungen.* PhD thesis, Technische Universität München, 1988.

[Ge 88] Z. Ge and J. Marsden. "Lie-Poisson Hamilton-Jacobi theory and Lie-Poisson integrators". *Physics Letters A*, Vol. 133, No. 3, pp. 134–139, 1988.

[Gera 01] M. Géradin and A. Cardona. *Flexible Multibody Dynamics – A Finite Element Approach*. John Wiley & Sons, 2001.

[Gerd 08a] M. Gerdts and M. Kunkel. "A globally convergent semi-smooth Newton method for control-state constrained DAE optimal control problems". *Comput Optim Appl*, Vol. DOI 10.1007/s10589-009-9275-0, 2008.

[Gerd 08b] M. Gerdts and M. Kunkel. "A Nonsmooth Newton's Method for Discretized Optimal Control Problems with State and Control Constraints". *Journal of Industrial and Management Optimization*, Vol. 4, No. 2, pp. 246–270, 2008.

[Gerd 09] M. Gerdts, S. Karrenberg, B. Mller-Beß ler, and G. Stock. "Generating Optimal Trajectories for an Automatically Driven Car". *Optimization and Engineering*, Vol. 10, No. 4, pp. 439–463, 2009.

[Gerd 10] M. Gerdts. *Optimale Steuerung*. Skript zur Vorlesung im WS 2009/2010 an der Universität Würzburg, 2010.

[Gill 97] P. Gill, W. Murray, and M. Saunders. "SNOPT: An SQP algorithm for large-scale constrained optimization". *Numerical Analysis Report, Department of Mathematics, University of California, San Diego, La Jolla, CA*, Vol. 97-2, 1997.

[Gold 02] H. Goldstein, C. Poole, and J. Safko. *Classical Mechanics*. Addison Wesley, 2002.

[Gonz 00] O. Gonzalez. "Exact Energy-Momentum Conserving Algorithms for General Models in Nonlinear Elasticity". *Comput. Methods Appl. Mech. Engrg.*, Vol. 190, pp. 1763–1783, 2000.

[Gonz 96] O. Gonzalez. "Time Integration and Discrete Hamiltonian Systems". *J. Nonlinear Sci.*, Vol. 6, pp. 449–467, 1996.

[Gonz 99] O. Gonzalez. "Mechanical Systems Subject to Holonomic Constraints: Differential-Algebraic Formulations and Conservative Integration". *Physica D*, Vol. 132, pp. 165–174, 1999.

[Gros 09] M. Großand P. Betsch. "Energy-Momentum Consistent Finite Element Discretisation of Dynamic Finite Viscoelasticity". *Int. J. Numer. Methods Engng.*, 2009. DOI 10.1002/nme.2729.

[Hage 00] W. Hager. "Runge-Kutta methods in optimal control and the transformed adjoint system". *Numer. Math.*, Vol. 87, No. DOI: 10.1007/s002110000178, pp. 247–282, 2000.

[Hair 04] E. Hairer, G. Wanner, and C. Lubich. *Geometric Numerical Integration: Structure-Preserving Algorithms for Ordinary Differential Equations*. Springer, 2004.

[Hair 89] E. Hairer, C. Lubich, and M. Roche. *The numerical solution of differential algebraic equations by Runge-Kutta methods*. Springer, 1989.

[Hart 95] R. Hartl, S. Sethi, and G. Vickson. "A Survey of the Maximum Principles for Optimal Control Problems with State Constraints". *SIAM Review*, Vol. 37, No. 2, p. 181218, 1995.

[Hest 66] M. Hestens. *Calculus of Variations and Optimal Control Theory*. John Wiley & Sons, 1966.

[Heus 92] H. Heuser. *Funktionalanalysis*. Teubner, 1992.

[Hick 71] G. Hicks and W. Ray. "Approximation methods for optimal control systems". *Can. J. Chem. Engng.*, Vol. 49, pp. 522–528, 1971.

[Hinz 09] M. Hinze, R. Pinnau, M. Ulbrich, and S. Ulbrich. *Optimization with PDE constraints*. Springer, Berlin, 2009.

[Hoef 63] W. Hoeffding. "Probability inequalities for sums of bounded random variables". *J. Amer. Statist. Assoc.*, Vol. 58, pp. 13–30, 1963.

[Hugh 00] T. Hughes. *The Finite Element Method. Linear Static and Dynamic Finite Element Analysis*. Dover, New York, 2000.

[Hugh 78] T. Hughes, T. Caughey, and W. Liu. "Finite-Element Methods for Nonlinear Elastodynamics Which Conserve Energy". *ASME J. Appl. Mech.*, Vol. 45, pp. 366–370, 1978.

[Hurm 93] Y. Hurmuzlu. "Dynamics of bipedal gait. Part I – objective functions and the contact event of a planar five-link biped. Part II – stability analysis of a planar five-link biped". *ASME Journal of Applied Mechanics*, Vol. 60, pp. 331–344, 1993.

[Ibra 02] A. Ibrahimbegović and S. Mamouri. "Energy consering/decaying implicit time-stepping scheme for nonlinear dynamics of three-dimensional beams undergoing finite rotations". *Comput. Methods Appl. Mech. Engrg.*, Vol. 191, pp. 4241–4258, 2002.

[Ibra 98] A. Ibrahimbegović and S. Mamouri. "Finite rotations in dynamics of beams and implicit time-stepping schemes". *Int. J. Numer. Meth. Engng.*, Vol. 41, pp. 781–814, 1998.

[Ibra 99] A. Ibrahimbegović and S. Mamouri. "Nonlinear dynamics of flexible beams in planar motion: formulation and time-stepping scheme for stiff problems". *Comput. Struct.*, Vol. 70, pp. 1–22, 1999.

[Isaa 65] R. Isaacs. *Differential Games: A Mathematical Theory with Applications to Warfare and Pursuit, Control and Optimization*. John Wiley & Sons, 1965.

[Jaco 71] D. Jacobson, M. Lele, and J. Speyer. "New Necessary Conditions of Optimality for Constrained Problems with State-Variable Inequality Constraints". *Journal of Mathematical Analysis and Applications*, Vol. 35, p. 255284, 1971.

[Jay 96] L. Jay. "Symplectic Partitioned Runge-Kutta Methods for Constrained Hamiltonian Systems". *SIAM J. Numer. Anal.*, Vol. 33, No. 1, pp. 368–387, 1996.

[Jay 98] L. O. Jay. "Structure Preservation for Constrained Dynamics with Super Partitioned Additive Runge–Kutta Methods". *SIAM Journal on Scientific Computing*, Vol. 20, No. 2, pp. 416–446, 1998.

[Jele 98] G. Jelenić and M. Crisfield. "Interpolation of rotational variables in non-linear dynamics of 3D beams". *Int. J. Numer. Meth. Engng.*, Vol. 43, pp. 1193–1222, 1998.

[Jele 99] G. Jelenić and M. Crisfield. "Geometrically exact 3D beam theory: implementation of a strain-invariant finite element for statics and dynamics". *Comput. Methods Appl. Mech. Engrg.*, Vol. 171, pp. 141–171, 1999.

[John 08] E. Johnson and T. Murphey. "Scalable variational integrators for constrained mechanical systems in generalized coordinates". *IEEE Transactions on Robotics*, 2008. submitted for publication.

[Jung 05a] O. Junge, J. Marsden, and S. Ober-Blöbaum. "Discrete mechanics and optimal control". In: *Proceedings of the 16th IFAC World Congress*, Prague, 2005.

[Jung 05b] O. Junge and S. Ober-Blöbaum. "Optimal Reconfiguration of Formation Flying Satellites". In: *IEEE Conference on Decision and Control and European Control Conference ECC*, Seville, Spain, 2005.

[Jung 06] O. Junge and S. Ober-Blöbaum. "Optimal Reconfiguration of Formation Flying Spacecraft – a decentralized approach". In: *Proceedings of the IEEE Conference on Decision and Control and European Control Conference ECC*, San Diego, USA, 2006.

[Jung 09] P. Jung. "A discrete mechanics approach to Cosserat rod theory – Static equilibria". 2009. Diplomarbeit, Universität Kaiserslautern.

[Jung 10] P. Jung, S. Leyendecker, J. Linn, and M. Ortiz. "A discrete mechanics approach to Cosserat rod theory. Part 1: static equilibria". *Int. J. Numer. Meth. Engng.*, 2010. in press.

[Kane 00] C. Kane, J. Marsden, M. Ortiz, and M. West. "Variational integrators and the Newmark algorithm for conservative and dissipative mechanical systems". *Int. J. Numer. Methods Engng.*, Vol. 49, No. 10, pp. 1295–1325, 2000.

[Kans 05] E. Kanso and J. Marsden. "Optimal motion of an articulated body in a perfect fluid". In: *IEEE Conference on Decision and Control and European Control Conference ECC 2005*, Seville, Spain, 2005.

[Kehr 97] S. Kehrbaum and J. Maddocks. "Elastic rods, rigid bodies, quaternions and the last quadrature". *Phil. Trans. R. Soc. Lond. A*, Vol. 355, No. 1732, pp. 2117–2136, 1997.

[Kim 86] S. Kim and M. Vanderploeg. "QR decomposition for state space representation of constrained mechanical dynamic systems". *J. Mech. Trans. Auto. Des.*, Vol. 108, pp. 183–188, 1986.

[Kirp 83] S. Kirpatrick, C. Gelatt Jr., and M. Vecchi. "Optimization by simulated annealing". *Science*, Vol. 220, pp. 671–680, 1983.

[Kobi 07a] M. Kobilarov, M. Desbrun, J. Marsden, and G. Sukhatme. "A discrete geometric optimal control framework for systems with symmetries". In: *Proc. of the Conference on Robotics: Science and Systems*, Atlanta, Georgia, 2007.

[Kobi 07b] M. Kobilarov and G. Sukhatme. "Optimal control using nonholonomic integrators". In: *IEEE International Conference on Robotics and Automation (ICRA)*, pp. 1832–1837, Rome, Italy, 2007.

[Kraf 85] D. Kraft. "On converting optimal control problems into nonlinear programming problems". *Computational Mathematical Programming*, Vol. F15, pp. 261–280, 1985.

[Krei 82] E. Kreindler. "Additional Necessary Conditions for Optimal Control with State-Variable Inequality Constraints". *Journal of Optimization Theory and Applications*, Vol. 38, No. 2, p. 241250, 1982.

[Kreu 79] E. Kreuzer. *Symbolische Berechnung der Bewegungsgleichungen von Mehrkörpersystemen*. Vol. 11, Fortschrittsbericht der VDI Zeitschriften, 1979.

[Krys 06] P. Krysl. "Direct time integration of rigid body motion with discrete-impulse mid-point approximation: explicit Newmark algorithms". *Comm. Numer. Methods Engrg.*, Vol. 22, No. 5, pp. 441–451, 2006.

[LaBu 76a] R. A. LaBudde and D. Greenspan. "Energy and Momentum Conserving Methods of Arbitrary Order for the Numerical Integration of Equations of Motion, I. Motion of a Single Particle". *Numer. Math.*, Vol. 25, pp. 323–346, 1976.

[LaBu 76b] R. A. LaBudde and D. Greenspan. "Energy and Momentum Conserving Methods of Arbitrary Order for the Numerical Integration of Equations of Motion, II. Motion of a System of Particles". *Numer. Math.*, Vol. 26, pp. 1–16, 1976.

[Lawr 04] C. Lawrence. "An introduction to stochastic differential equations". 2004. Technical report, University of California at Berkeley, available at math.berkely.edu/˜evans/SDEcourse.pdf.

[Ledo 01] M. Ledoux. *The Concentration of Measure Phenomenon*. American Mathematical Society, Providence, RI, 2001.

[Lee 09a] T. Lee, N. McClamroch, and M. Leok. "Attitude maneuvers of a rigid space-craft in a circular orbit". In: *American Control Conference*, pp. 1742–1747, Minneapolis, Minnesota, USA, 2009.

[Lee 09b] T. Lee, N. McClamroch, and M. Leok. "Optimal control of a rigid body using geometrically exact computations on SE(3)". In: *IEEE Conference on Decision and Control and European Control Conference ECC*, pp. 2710–2715, San Diego, California, USA, 2009.

[Leim 04] B. Leimkuhler and S. Reich. *Simulating Hamiltonian Dynamics*. Cambridge University Press, 2004.

[Leim 94] B. Leimkuhler and S. Reich. "Symplectic integration of constrained Hamiltonian systems". *Mathematics of Computations*, Vol. 63, pp. 589–605, 1994.

[Leim 96] B. Leimkuhler and G. Patrick. "A Sympletic Integrator for Riemannian Manifolds". *J. Nonlinear Sci.*, Vol. 6, pp. 367–384, 1996.

[Lerb 05] J. Lerbet. "Coordinate-free kinematic analysis of overconstrained mechanisms with mobility one". *ZAMM*, Vol. 85, No. 10, pp. 740–747, 2005.

[Lew 03a] A. Lew, J. Marsden, M. Ortiz, and M. West. "Asynchronous Variational Integrators". *Arch. Rational Mech. Anal.*, Vol. 167, pp. 85–146, 2003.

[Lew 03b] A. Lew, J. Marsden, M. Ortiz, and M. West. "An Overview of Variational Integrators". In: *Finite Element Methods: 1970's and beyond*, pp. 85–146, CIMNE, Barcelona, Spain, 2003.

[Lew 04] A. Lew, J. Marsden, M. Ortiz, and M. West. "Variational Time Integrators". *Int. J. Numer. Methods Engng.*, Vol. 60, pp. 153–212, 2004.

[Leye 04] S. Leyendecker, P. Betsch, and P. Steinmann. "Energy-conserving integration of constrained Hamiltonian systems – a comparison of approaches". *Comput. Mech.*, Vol. 33, pp. 174–185, 2004.

[Leye 06a] S. Leyendecker. *Mechanical integrators for constrained dynamical systems in flexible multibody dynamics*. PhD thesis, University of Kaiserslautern, 2006.

[Leye 06b] S. Leyendecker, P. Betsch, and P. Steinmann. "Objective energy-momentum conserving integration for the constrained dynamics of geometrically exact beams". *Comput. Methods Appl. Mech. Engrg.*, Vol. 195, pp. 2313–2333, 2006.

[Leye 07] S. Leyendecker, S. Ober-Blöbaum, J. Marsden, and M. Ortiz. "Discrete mechanics and optimal control for constrained multibody dynamics". In: *Proceedings of the 6th International Conference on Multibody Systems, Nonlinear Dynamics, and Control, ASME International Design Engineering Technical Conferences*, Las Vegas, Nevada, 4-7 September 2007.

[Leye 08a] S. Leyendecker, P. Betsch, and P. Steinmann. "The discrete null space method for the energy consistent integration of constrained mechanical systems. Part III: Flexible multibody dynamics". *Multibody System Dynamics*, Vol. 19, pp. 45–72, 2008.

[Leye 08b] S. Leyendecker, J. Marsden, and M. Ortiz. "Variational integrators for constrained dynamical systems". *ZAMM*, Vol. 88, No. 9, pp. 677–708, 2008.

[Leye 09a] S. Leyendecker and E. Kanso. "Locomotion of a submerged Cosserat beam". In: *Proceedings of the 7th International Conference on Multibody Systems, Nonlinear Dynamics, and Control, ASME International Design Engineering Technical Conferences*, San Diego, California, 30 August - 2 September 2009.

[Leye 09b] S. Leyendecker, S. Ober-Blöbaum, J. Marsden, and M. Ortiz. "Discrete mechanics and optimal control for constrained systems". *Optimal Control Applications & Methods*, 2009. DOI: 10.1002/oca.912.

[Leye 09c] S. Leyendecker, D. Pekarek, and J. Marsden. "Structure preserving optimal control of three-dimensional compass gait". In: *Workshop on Modeling, Simulation and Optimization of Bipedal Walking, 9th IEEE-RAS International Conference on Humanoid Robots (Humanoids09), submitted for publication*, Paris, France, 7-10 December 2009.

[Leye 10] S. Leyendecker, L. Luccas, H. Owhadi, and M. Ortiz. "Optimal control strategies for robust certification". *ASME Journal of Computational and Nonlinear Dynamics, special issue on Multi-disciplinary High-Performance Computational Multibody Dynamics, edited by Dan Negrut and Olivier Bauchau*, Vol. 5, No. 3, 2010. DOI: 10.1115/1.4001375.

[Love 27] E. Love. *A Treatise on the Mathematical Theory of Elasticity (4th edn.)*. Cambridge University Press, 1927.

[Luca 08] L. Lucas, H. Owhadi, and M. Ortiz. "Rigorous verification, validation, uncertainty quantification and certification through concentration-of-measure inequalities". *Computer Methods in Applied Mechanics and Engineering*, Vol. 197, pp. 4591–4609, 2008.

[Luen 84] D. Luenberger. *Linear and Nonlinear Programming*. Addison-Wesley, 1984.

[Madd 94] J. Maddocks and D. D.J. "Conservation laws in the dynamics of rods". *J. of Elasticity*, Vol. 34, pp. 83–96, 1994.

[Maed 81] S. Maeda. "Lagrangian formulation of discrete systems and concept of difference space". *Mathematica Japonica*, Vol. 27, pp. 345–356, 1981.

[Magg 04] F. Maggi and M. Morini. "A Γ-convergence result for variational integrators of Lagrangians with quadratic growth". *ESAIM Control Optim. Calc. Var.*, Vol. 10, pp. 656–665, 2004.

[Mars 01] J. Marsden and M. West. "Discrete mechanics and variational integrators". *Acta Numerica*, Vol. 10, pp. 357–514, 2001.

[Mars 94] J. Marsden and T. Ratiu. *Introduction to Mechanics and Symmetry. A Basic Exposition of Classical Mechanical Systems. Texts in Applied Mathematics 17*, Springer, 1994.

[Mars 98] J. Marsden, G. Patrick, and S. Shkoller. "Multisymplectic Geometry, Variational Integrators, and Nonlinear PDEs". *Commun. Math. Phys.*, Vol. 199, p. 351395, 1998.

[Mars 99] J. Marsden and S. Shkoller. "Multisymplectic geometry, covariant Hamiltonians, and water waves". *Math. Proc. Camb. Phil. Soc.*, Vol. 125, p. 553, 1999.

[McDi 89] C. McDiarmid. "On the method of bounded differences". In: *Surveys in combinatorics (Norwich, 1989), London Math. Soc. Lecture Note Ser.*, pp. 148–188, Cambridge Univ. Press, Cambridge, 1989.

[McLa 06a] R. McLachlan and M. Perlmutter. "Integrators for Nonholonomic Mechanical Systems". *J. Nonlinear Sci.*, Vol. 16, pp. 283–328, 2006.

[McLa 06b] R. McLachlan and G. Quispel. "Geometric integrators for ODEs". *J. Phys. A*, Vol. 39, No. 19, pp. 5251–5286, 2006.

[McLa 93] R. McLachlan. "Explicit Lie-Poisson integration and the Euler equations". *Physical Review Letters*, Vol. 71, pp. 3034–3046, 1993.

[Momb 05] K. Mombaur, H. Bock, J. Schlder, and R. Longman. "Open-loop stable solution of periodic optimal control problems". *ZAMM*, Vol. 85, No. 7, pp. 499–515, 2005.

[Momb 10] K. Mombaur, A. Truong, and L. J.P. "From human to humanoid locomotion – an inverse optimal control approach". *Autonomous Robots*, Vol. 28, No. 3, pp. 369–383, 2010.

[Moor 09] A. Moore, S. Ober-Blöbaum, and J. Marsden. "Optimization of spacecraft trajectories: A method combining invariant manifold techniques and discrete mechanics and optimal control". *AAS, 09-257,*, pp. 1–20, 2009.

[Mull 04] S. Müller and M. Ortiz. "On the Gamma-convergence of discrete dynamics and variational integrators". *J. Nonlinear Sci.*, Vol. 14, No. 4, pp. 153–212, 2004.

[Munk 84] J. Munkres. *Elements of Algebraic Topology*. Perseus Publishing, Cambridge, Massachusetts, 1984.

[Nagu 90] M. Nagurka and V. Yen. "Fourier-based optimal-control of nonlinear dynamic-systems". *Journal of Dynamic Systems Measurement and Control-Transactions of the ASME*, Vol. 112, No. 1, pp. 17–26, 1990.

[Neus 76] L. Neustadt. *Optimization: A Theory of Necessary Conditions*. Princeton, New Jersey, 1976.

[Nize 99] M. Nizette and A. Goriely. "Towards a classification of Euler–Kirchhoff filaments". *Journal of Mathematical Physics*, Vol. 40, No. 6, pp. 2830–2966, 1999.

[Noel 04] L. Noels, L. Stainier, and J. P. Ponthot. "An energy-momentum conserving algorithm for non-linear hypoelastic constitutive models". *Int. J. Numer. Meth. Engng.*, No. 59, pp. 83–114, 2004.

[Noet 18] E. Noether. "Invariante Variationsprobleme". *Kgl. Ges. Wiss. Nachr. Göttingen. Math. Physik*, Vol. 2, pp. 235–257, 1918.

[Ober 08] S. Ober-Blöbaum. *Discrete mechanics and optimal control*. PhD thesis, University of Paderborn, 2008.

[Ober 10] S. Ober-Blöbaum, O. Junge, and J. Marsden. "Discrete mechanics and optimal control: an analysis". *ESAIM: Control Optimisation and Calculus of Variations*, 2010. DOI: 10.1051/cocv/2010012.

[Peka 07] D. Pekarek, A. Aaron, and J. Marsden. "Discrete mechanics and optimal control applied to a compass gait biped". In: *Proceedings of the 46th IEEE International Conference on Decision and Control*, New Orleans, Lousiana, 12-14 December 2007.

[Peka 08] D. Pekarek and J. Marsden. "Variational collision integrators and optimal control". In: *Proc. of the 18th International Symposium on Mathematical Theory of Networks and Systems*, Blacksburg, Virginia, 2008.

[Peka 10] D. Pekarek. *Variational Methods for Control and Design of Bipedal Robot Models*. PhD thesis, California Institute of Technology Pasadena, California, 2010.

[Petz 86] L. Petzold and P. Lostedt. "Numerical Solution of Nonlinear Differential Equations with Algebraic Constraints II: Practical Implications". *SIAM J. Sci. Comput.*, Vol. 7, No. 3, pp. 720–733, 1986.

[Pont 62] L. Pontryagin, V. Boltyanski, R. Gamkrelidze, and E. Miscenko. *The Mathematical Theory of Optimal Processes*. John Wiley & Sons, 1962.

[Powe 78] M. Powell. "A fast algorithm for nonlinearly constrained optimization calculations". In: G. Watson, Ed., *Numerical Analysis, volume 630 of Lecture Notes in Mathematics*, pp. 261–280, Springer, 1878.

[Pytl 99] R. Pytlak. *Numerical methods for optimal control problems with state constraints*. Springer, 1999.

[Reic 94] S. Reich. "Momentum conserving symplectic integrations". *Physica D*, Vol. 76, No. 4, pp. 375–383, 1994.

[Reic 95] S. Reich. "Enhancing energy conserving methods". *BIT*, Vol. 36, pp. 122–134, 1995.

[Reic 96] S. Reich. "Symplectic integrators for systems of rigid bodies". *Fields Institute Commun.*, Vol. 10, pp. 181–191, 1996.

[Rene 01] J. Renegar. *Mathematical View of Interior Point Methods in Convex Optimization*. SIAM, Philadelphia, 2001.

[Rhei 97] W. Rheinboldt. "Solving Algebraically Explicit DAEs with the MANPAK-Manifold-Algorithms". *Computers Math. Applic.*, Vol. 33, No. 3, pp. 31–43, 1997.

[Rome 02] I. Romero and F. Armero. "An objective finite element approximation of the kinematics of geometrically exact rods and its use in the formulation of an energy-momentum scheme in dynamics". *Int. J. Numer. Meth. Engng.*, Vol. 54, pp. 1683–1716, 2002.

[Rome 04] I. Romero. "The interpolation of rotations and its application to finite element models of geometrically exact rods". *Comput. Mech.*, Vol. 34, No. 2, pp. 121–133, 2004.

[Rome 09] I. Romero. "Thermodynamically consistent time-stepping algorithms for non-linear thermomechanical systems". *Int. J. Numer. Meth. Engng.*, Vol. 79, pp. 706–732, 209.

[Ross 06] S. Ross. "Optimal flapping strokes for self-propulsion in a perfect fluid". In: *American Control Conference*, pp. 4118–4122, Minneapolis, Minnesota, 2006.

[Rous 98] L. Roussel, C. Canudas-de Wit, and A. Goswami. "Generation of energy optimal complete gait cycles for biped robots". In: *Proc. IEEE Conf. on Robotics and Automation*, 1998.

[Schi 80] K. Schittkowski. *Nonlinear programming codes, Lecture Notes in Economics and Mathematical Systems*. Vol. 183, viii+242, Springer, 1980.

[Schi 90] W. Schiehlen, Ed. *Multibody systems handbook*. Springer, 1990.

[Schm 09] B. Schmidt, S. Leyendecker, and M. Ortiz. "Γ-convergence of variational integrators for constrained systems". *J. Nonlinear Sci.*, Vol. 19, No. 2, pp. 1432–1467, 2009.

[Shin 01] H. Shin, J. Lee, S. Shin, and M. Gleicher. "Computer puppetry: An importance-based approach". *ACM Transactions on Graphics*, Vol. 20, No. 2, pp. 67–94, 2001.

[Simo 07] C. Simonidis, G. Stelzner, and W. Seemann. "A kinematic study of human torso motion". In: *Proceedings of the 6th International Conference on Multibody Systems, Nonlinear Dynamics, and Control, ASME International Design Engineering Technical Conferences*, Las Vegas, Nevada, 4-7 September 2007.

[Simo 85] J. Simo. "A finite strain beam formulation. The three-dimensional dynamic problem. Part I". *Comput. Methods Appl. Mech. Engrg.*, Vol. 49, pp. 55–70, 1985.

[Simo 86] J. Simo and L. Vu-Quoc. "A three-dimensional finite-strain rod model. Part II: Computational Aspects". *Comput. Methods Appl. Mech. Engrg.*, Vol. 58, pp. 79–116, 1986.

[Simo 88] J. Simo and L. Vu-Quoc. "On the dynamics in space of rods undergoing large motions – A geometrically exact approach". *Comput. Methods Appl. Mech. Engrg.*, Vol. 66, pp. 125–161, 1988.

[Simo 91a] J. Simo, D. Lewis, and J. Marsden. "Stability of Relative Equilibria. Part I: The Reduced Energy-Momentum Method". *Arch. Rational Mech. Anal.*, Vol. 115, pp. 15–59, 1991.

[Simo 91b] J. Simo and K. Wong. "Unconditionally Stable Algorithms For Rigid Body Dynamics That Exactly Preserve Energy and Momentum". *Int. J. Numer. Methods Engrg.*, Vol. 31, pp. 19–52 and 1321–1323, 1991.

[Simo 92] J. Simo and N. Tarnow. "The discrete energy-momentum method. Conserving algorithms for nonlinear elastodynamics". *ZAMP*, Vol. 43, 1992.

[Simo 93] J. Simo and O. Gonzalez. "Assessment of Energy-Momentum and Symplectic Schemes for Stiff Dynamical Systems". In: *proceedings of the ASME Winter Annual Meeting*, American Society of Mechanical Engineers, New Orleans, Louisiana, 1993.

[Simo 94] J. Simo and N. Tarnow. "A new energy and momentum conserving algorithm for the non-linear dynamics of shells". *Int. J. Numer. Meth. Engng.*, Vol. 37, pp. 2527–2549, 1994.

[Simo 95] J. Simo, N. Tarnow, and M. Doblare. "Non-linear dynamics of three-dimensional rods: Exact energy and momentum conserving algorithms". *Int. J. Numer. Meth. Engng.*, Vol. 38, pp. 1431–1473, 1995.

[Sten 94] R. Stengel. *Optimal control and estimation.* Dover, 1994.

[Stoe 02] J. Stoer and R. Bulirsch. *Introduction to numerical analysis.* Vol. 12, xvi+744, Springer, 2002.

[Stry 91] O. von Stryk. "Numerical solution of optimal control problems by direct collocation". *Optimal control (Freiburg, 1991), Internat. Ser. Numer. Math.*, pp. 129–143, 1991.

[Stry 92] O. Stryk and R. Bulirsch. "Direct and indirect methods for trajectory optimization". *Annals of Operations Research*, pp. 357–373, 1992.

[Stry 98] O. Stryk. "Optimal control of multibody systems in minimal coordinates". *ZAMM*, Vol. 78, pp. 1117–1120, 1998.

[Timm 08] J. Timmermann. "Die Nullraum-Methode in Kombination mit DMOC zur optimalen Steuerung mechanischer Systeme mit holonomen Zwangsbedingungen". 2008. Diplomarbeit, Universität Paderborn.

[Tola 00] D. Tolani, A. Goswami, and N. Badler. "Real-time inverse kinematics techniques for anthropomorphic limbs". *Graphical Models*, Vol. 62, No. 5, pp. 353–388, 2000.

[Toum 94] J. Touma and J. Wisdom. “Lie-Poisson integrators for rigid body dyanamics in the solar system”. *Astr. J.*, Vol. 107, pp. 1189–1202, 1994.

[True 65] C. Truesdell and W. Noll. “The non-linear field theories of mechanics”. In: *Handbuch der Physik III/3*, Springer, 1965.

[Uhla 09] S. Uhlar and P. Betsch. “A rotationless formulation of multibody dynamics: Modeling of screw joints and incorporation of control constraints”. *Multibody Syst. Dyn.*, Vol. 22, pp. 69–95, 2009.

[Uhla 10] S. Uhlar and P. Betsch. “On the derivation of energy consistent time stepping schemes for friction afflicted multibody systems”. *Computers and Structures*, Vol. 88, No. 11-12, pp. 737–754, 2010.

[Vese 88] A. Veseloc. “Integrable systems with discrete time and difference operators”. *Functional Analysis and its Applications*, Vol. 22, No. 2, pp. 83–93, 1988.

[Warb 76] G. Warburton. *The Dynamical Behaviour of Structures*. Pergamon, 1976.

[Wend 97] J. Wendlandt and J. Marsden. “Mechanical Integrators Derived from a Discrete Variational Principle”. *Physica D*, Vol. 106, pp. 223–246, 1997.

[Wirt 10] N. Wirth. “Optimal control of multibody systems in Lagrangian Mechanics: direct and indirect method”. 2010. Diplomarbeit, Technische Universität Kaiserslautern.

[Witt 77] J. Wittenburg. *Dynamics of systems of rigid bodies*. Teubner, 1977.

[Yosi 06] K. Yosida. *Functional analysis*. Springer, Berlin, 2006.

[Zeid 94] V. Zeidan. “The Riccati Equation for Optimal Control Problems with Mixed State-Control Constraints: Necessity and Sufficiency”. *SIAM Journal on Control and Optimization*, Vol. 32, No. 5, p. 12971321, 1994.

[Zhao 94] J. Zhao and N. Badler. “Inverse kinematics positioning using nonlinear-programming for highly articulated figures”. *ACM Transactions on Graphics*, Vol. 13, No. 4, pp. 313–336, 1994.